University of Southampton

Partial Discharge Monitoring of Power Transformers

By

Baojia HAN

A thesis submitted for the degree of

Doctor of Philosophy

In

The School of Electronics and Computer Science

January 2004

UNIVERSITY OF SOUTHAMPTON

ABSTRACT

FACULTY OF ENGINEERING, SCIENCE AND MATHEMATICS

SCHOOL OF ELECTRONICS AND COMPUTER SCIENCE

Doctor of Philosophy

PARTIAL DISCHARGE MONITORING OF POWER TRANSFORMERS

By Baojia HAN

This thesis is concerned with an approach to the monitoring and measurement of partial discharges within power transformers, including the classification and recognition of partial discharge signals in the both frequency and time domains from bushing tap points via RFCT (Radio Frequency Current Transducer), the propagation characteristics of high frequency signals and real partial discharge signals within a transformer model with a bandwidth of up to 200 MHz, and also the techniques of de-noising, diagnosis and localization of internal partial discharge.

The principle proposed based on the fact that an internal partial discharge signal of an oil-filled power transformer may propagate along a winding and its leads to reach a bushing core bar, the bushing acting like a capacitor can transfer the high frequency components of the partial discharge signal across to its tap point, using a sensor the transferred partial discharge signal can be detected. The developed technique allows the partial discharge monitoring and measurement of power transformers to be carried out by using a RFCT as a sensor at taps of transformer bushings. The obtained data was stored, displayed and analysed using digital equipment. This approach was applied to the auto-transformer SGT3A at Northfleet Substation, West London, and was also verified on the transformer model at the High Voltage Laboratory, UMIST.

Centred on this principle, the sensitivities of a 60kV transformer bushing, RFCTs, transformer oil, transformer windings and a transformer model with an interleaved disc winding and a plain disc winding were investigated by studying the propagation characteristics of high frequency signals within them. The classification and characteristics of partial discharges within power transformers and out of the 60kV bushing tap were also studied in both time and frequency domains. A major aspect of this work was the experimentally confirmed hypothesis that high frequency components of internal partial discharge signals pass through the winding and bushing with little attenuation and can be detected at the bushing tap point. The feasibility of software techniques required to realize de-noising from measured signals in the field was investigated. A transfer function has been developed for the transformer model based on its frequency response from 0-200 MHz. This linear model has a significantly wider bandwidth than previous published models and greatly improves the prospect of diagnosis and localization of partial discharges within power transformers.

Contents

List of Figures

List of photos

List of Tables

Acknowledgements

First and foremost, I would like to express my sincere thankfulness to my Ph.D supervisor, Dr Paul Lewin, for his trust, guidance and arrangement in all things throughout the last three years, this has given me the confidence, stimulation and freedom to develop the topics of this field upon which this thesis covers. And his kindly assistance, advice and encouragement have not only driven me to complete my project but also been helpful in overcoming my personal problems. I would like to dedicate this thesis to the memory of Professor Anthony (A.E.) Davies. Forever, I appreciate the Ph.D opportunity given to me by him and Dr Paul Lewin.

I would like to thank National Grid Company, the sponsor of the project. The financial support allowed the project progress smoothly, and reduced my living pressure in UK. I appreciate Dr Zhongdong Wang at H.V. laboratory, UMIST, for her continuous inspiritment and contribution to the testing at UMIST. Also thanks to H.V. laboratory, UMIST. I would like to thank High Voltage Laboratory of Southampton University, the highest level academic environment and the advanced equipment in the world have had me obtained the best academic nurture and training. And the thanks also to the technicians in the HV Lab; they are Neil, Brian, Mike and Roland; for their best contribution to the project. Furthermore, I would like to thank all of my colleagues in HV group for their help, advice and support when I encountered difficulties In addition, many thanks to my colleague Ping Wang for her help in the research and daily life. And thanks to Jason Tian for his help in the application of the PD detector and driving to UMIST Manchester.

I would like to thank my young brother Baohua and old brother Baofu as well as their families for their whole-heartedly looking after our parents, which has allowed me concentrate on the investigation. I would like to thank my family for their support. Last and not least, special thanks to my mother and father. They have given me their utmost support, care and concern that stimulate my determination to finish the investigation. As a best dedication to the memory of my mother, I offer the thesis and Ph.D degree to her and expect her forgiveness for my absence when she passed away in 5th September 2003,

Chapter 1

Introduction

Since large power transformers belong to the most expensive and strategically important components of any power generation and transmission system, their reliability is of crucial importance for the energy system operation. A serious failure of a large power transformer due to insulation breakdown can generate substantial costs for repair and financial loss due to any power outage. In order to guarantee supply, most power utilities are highly motivated to continually assess the actual condition of the insulation systems of their transformers. Meanwhile, with the increasing average age of the transformer population there is also an increasing need to understand the internal condition of transformers in order to estimate remaining lifetime and plan for maintenance outages.

As one of the most likely sources that may lead to insulation breakdown and finally result in an outage of a transformer, partial discharge (PD) activity has always been focused on by users and investigators. Previous investigations [17, 18] have revealed that partial discharge is due to imperfect insulation, which may cause a discharge with a partial breakdown under an electric stress. Furthermore the insulation will be degraded and finally cause an entire breakdown. In general, partial discharges occurring within a power transformer can be divided into internal and external discharges. The typical external discharge are corona and surface discharges, they may happen on bushing heads of a transformer. They usually belong to "glow discharges" that include low frequency current components and pulses with very small magnitudes and can be observed with pulse groups on the measured phase distribution. The partial discharges inside a transformer are mainly "pulse discharge". They can be observed with pulse groups on the measured phase

distribution too. The typical internal partial discharges include void discharge, floating discharge and corona in oil and usually, these discharge signals have wide bandwidths.

Modern techniques have made the diagnosing of the integrity of transformers through intrusive or non-intrusive tests possible in order to optimize the maintenance effort and to ensure maximum availability and reliability of supply. For this purpose on- and off-line methods and systems to monitor and detect transformer conditions have been developed in recent years. On-line monitoring can be used continuously during the operation of transformers and in that way offers a possibility to record different relevant stresses which can affect the life span of transformers. The automatic evaluation of the measured data allows the early detection of an oncoming fault. In comparison to this, off-line methods require disconnecting transformers from power networks and are mainly used during scheduled inspections or when transformers are already suspected of being faulty.

Several techniques to detect partial discharges within high voltage equipment have been developed and applied; they include, for example, VHF/UHF PD detection technique [1-5], the applications of acoustic sensors [11], UHF (antenna) sensors [6], Rogowski coils [7], but due to the complicated internal structure of a transformer, an internal partial discharge, especially if it occurs deep inside, may be attenuated and even disappear as it propagates. This may lead to incorrect or non-measurement. Some of above methods need modification to transformer walls or need to extend sensors into the transformer; these approaches must cause a re-consideration for the insulation design. The applications of these techniques are obviously difficult to apply to the transformers already connected to power networks.

Up until now, there has been little investigation into the use of transformer bushings for partial discharge measurement. The classification and characterization of partial discharges within oil-filed power transformers have not been detailed across a wide bandwidth up to 200 MHz in either the frequency or the time domain and there is little published information about partial discharge behaviour within oil-filled transformers.

Therefore it is important to investigate the classification and characterization of partial discharges within oil-filled power transformers in both the time and frequency domains and it is necessary to investigate the propagation characteristics of these partial discharges signals within bushings, windings and the oil-filled transformer itself.

Based on these investigations a technique, that does not require structural change to a transformer for on-line measurement and monitoring of partial discharge behaviour has been developed. The principle of the proposed technique is based on the fact that a power transformer body is connected to the power network via transformer bushings. The bushings support and lead the leads of the transformer windings out of the transformer using the bushing core bars which are connected to busbars or aerial cables of a power network. A partial discharge within the power transformer may

propagate along a winding and its lead to reach a bushing core bar and the bushing may transfer the high frequency components of the partial discharge signal across to its tap point. Thus, using a sensor at the bushing tap point to detect partial discharge signal is hypothetically possible. This approach is both convenient and economical due to the fact that no modification is required of the transformer.

1.1 Scope and Contribution of this Investigation

The investigation of partial discharge monitoring of power transformers was financially supported by the National Grid Company. Under this sponsorship a transformer winding model was purchased consisting of a plain disc winding and an interleaved disc winding, and was built at Alstom T&D Transformer Limited. The winding model was adapted to a transformer model with a core and tank and the transformer model was filled with transformer oil. The design and reconstruction of the transformer model was carried out by and at the High Voltage Engineering Laboratory, University of Southampton.

Based on the research on the winding model, the transformer model, a transformer bushing and RFCT (radio frequency current transducer), this thesis has introduced the investigation and application of partial discharge monitoring and measurement of power transformers at transformer bushing taps via clamp-type RFCTs. The contribution of this work includes the following aspects:

- Partial discharge recognition and classification from bushing taps via RFCTs by means of visual comparisons of pattern classifications and frequency spectra of different PD signals.
- Investigations into the propagation characteristics of high frequency signals and real partial discharge signals within a transformer model in both the time domain and frequency domain.
- Development of approaches to recognise and distinguish partial discharge signals on pattern charts in both time domain and frequency domain, and a preliminary transfer function for a whole transformer system.
- Development of a principle for partial discharge on-line measurement and monitoring of oil-filled power transformers.
- Completion of field trials on the auto-transformer SGT3A at Northfleet Substation West London and a transformer model at High Voltage laboratory, UMIST.

1.2 Thesis Organization

The remainder of this thesis consists of 8 chapters. Chapter 2 reviews previous research into partial discharge activity within power transformers, including the analysis used in the methods of recognition, diagnosis, monitoring, localization and measurement. Chapter 3 introduces an

investigation in the properties of high frequency signals within transformer bushings and RFCTs. In this chapter the frequency responses and impulse responses of a 60 kV bushing and a RFCT are discussed. Chapter 4 details the properties of partial discharge signals in both time domain and frequency domain from a 60 kV bushing via a RFCT. Chapter 5 presents an investigation into transformer windings and the transformer model. In this chapter the propagation characteristics of high frequency signals and real PD signals within transformer windings and the transformer model system are detailed. Chapter 6 suggests a new principle to realize PD on-line measurement and monitoring. A method to determine a transfer function for the whole transformer system and some software techniques for de-noising and recognising PD signals and localising PD are introduced. Chapter 7 describes the application of PD on-line measurement and monitoring of an oil-filled power transformer, the 500MVA 400kV/275kV auto-transformer SGT3A at Northfleet Substation South-East London. Chapter 8 describes verification tests undertaken on a transformer at the High Voltage Laboratory, UMIST. Finally, the conclusions and suggested future direction of this research are summarised in Chapter 9.

Chapter 2

Literature Review

2.1 Transformer Condition Monitoring

Diagnostic or monitoring techniques for oil-filled power transformers depend mainly on recognizing and understanding the condition of transformers; hence, the service efficiency of transformers and the ageing of their insulation systems need to be identified.

The condition classification of oil-filled power transformers includes [15]:

- Normal: In this case, there is no obvious problem with the transformer, and no remedial action will be applied. Transformers can remain normally in service for long periods of time.
- Defective: In this case, there may be a few problems, but there is no significant impact on short-term reliability, although the life of the transformer may be adversely affected over a long-term unless remedial action is taken.
- Faulty: In this case, the transformer can still remain in service, but short-term reliability may be reduced. It may or may not be possible to improve its condition by remedial action.
- Failed: In this case, the transformer cannot remain in service. Remedial action must be carried out before it is put into service again.

On the whole, if a transformer in operation is in "a normal condition", condition monitoring (including partial discharge condition monitoring) is necessary to detect any hidden troubles that may lead to future failure.

If it is in "a defective condition", the transformer may have developed a minor fault, such as insulation degradation. Thus, periodic inspection and monitoring of its condition, including partial discharge condition, are very useful in understanding and controlling the development of conditions (or insulation conditions) of the transformer.

If it is in "a faulty condition", in general it may remain in service for only about several hours, or days, or weeks, or months until it have to be removed due to failure, such as breakdown of the insulation system within the transformer. Hence, the monitoring of its condition (including partial discharge condition) is essential in order to estimate the degree of insulation degradation and ensure that the faulty transformer is removed from service whilst guaranteeing supply

If it is "a failed condition", the transformer must be removed from service immediately. The data obtained from the condition monitoring before the removal are still very valuable for forensic analysis and fault diagnosis.

Generally, the objectives of condition monitoring of oil-filled power transformers include:

- Hot spot monitoring both by direct and indirect (thermal model) methods
- Dissolved gas analysis (DGA) for hydrogen only or for up to ten different gases including acetylene, methane, hydrogen, carbon dioxide, ethylene, ethane, oxygen, nitrogen and carbon monoxide
- Partial discharge monitoring, including static electrification
- Bushing on-line power factor and capacitance measurement
- Cooling system
- Moisture in oil
- Transfer function analysis for both dielectric and dynamic defects
- Monitoring for clamping force
- On load tap changer (OLTC) monitoring

2.2 Partial Discharge Condition Monitoring of Power Transformers

All the aspects of condition monitoring of oil-filled power transformers are related to the reliability of the insulation systems of the transformer. In other words, any defects in the above aspects may cause or finally represent an insulation problem. For example, a local hot spot in a transformer can result in insulation ageing or degradation near to that point. It may therefore cause partial discharges and finally lead to a breakdown of the insulation system of the transformer. Therefore, partial discharge monitoring of the insulation system is the most important and final method for diagnosing and controlling the overall condition of oil-filled power transformers.

Partial discharge (PD) condition monitoring includes on-line collection and analysis of partial discharge data, detective sensor development and applications of on-line measurement and recognition techniques etc. To realize this, it is necessary to mount monitoring equipment on transformers and transmit measurement data over a safe working distance before analysis can be undertaken.

PD monitoring equipment mounted permanently on transformers should be reliable and convenient. Successful monitoring for partial discharges can bring the following benefits:

- Warning of impending failure, allowing corrective action to be taken.
- A switch from preventative to predictive maintenance techniques, giving major cost savings by freeing staff from routine inspection work and reducing plant outages.
- Operating a plant closer to its limits.
- Preventing long term outages, which may incur penalty payments
- Reducing the number of high voltage switching operations and leading to better quality of supply to customers.

2.3 Partial Discharge Characteristics and Classification within Power Transformers

Referring to IEC 270 [16], "a partial discharge (PD), within the term of this standard (IEC 270), is an electric discharge, which only partially bridges the insulation between conductors. Such discharge may, or may not, occur adjacent to the conductor. Partial discharge occurring in any test object under given conditions may be characterized by different measurable quantities such as charge, repetition rate, etc. Quantitative results of measurements are expressed in terms of one or more of the specified quantities."

Partial discharges are not the only factors that cause degradation, ageing and breakdown of high voltage insulation systems, but PD activity does indicate the actual state and condition of the insulation system. In an insulation system partial discharge is mainly caused by a local excessive intensity of electric field, which is due to the imperfections in the insulation or insulation system, for example a gas-filled inclusion such as a void or crack. During a partial discharge ionisation processes may occur, leading to increased discharge activity, increasing the likelihood of breakdown.

Generally, a single pulse of partial discharge has a very fast rise time and a short duration. It has been reported that for a corona discharge pulse the rise time can be as short as 0.1 ns, and its duration less than 1ns. Even for discharges in oil, the rise time is normally shorter than 5ns and the

duration under 20ns. The equivalent frequency bandwidth of a partial discharge can therefore range from several kHz to 2.5 GHz [17]. However, to detect PD activity is not an easy task, as it depends not only on the detection method and position of sensing equipment; but also on the transfer path from the PD source site to the detection point. Under ideal conditions (for example, an insulation construction, in which there is a low loss path for high frequency components of the PD signal), the PD signal will not be attenuated or dispersed during transfer. For a complex insulation system, such as the internal insulation system of a power transformer; as a result of large loss of high frequency components, PD signals may be significantly altered by the time they reached the measurement point. The shape and intensity of the detected signal at the measuring point depends on the following aspects [17, 18]:

- The energy of the original signal
- The complexity of the transfer path, including its length, construction
- The dielectric properties of the material
- The sensitivity of the detection method

Partial discharges damage insulation materials, such as oil, pressboard, etc., by causing local carbonisation. In general, the stronger the electric field stresses at the partial discharge site the more harmful the discharge. Depending on the kind of insulation material and the location of the discharge, the damaging mechanisms and the processes are very different. The following explanations of the mechanisms that cause insulation damage are commonly accepted [17]:

- Impacts of electric particles, accelerated due to the electric field, destroy the molecular construction of the insulation material and damage its fibres. This causes an increase of the temperature at the point of impact and may cause local carbonisation.
- O_2, NO, NO_2 created during partial discharge can damage insulation materials due to their active characteristics. This is especially a problem when the gases combine with water in the oil to produce nitric acid.
- When a partial discharge is developing, the products of oil electrolysis deposit themselves on the inter-turn insulation of windings or they combine with impurities on the surface of insulation construction. These deposits sharply increase the dielectric loss of insulation materials and decrease the ability of the insulation materials to radiate heat. This may lead to the breakdown of the insulation.

Although a high voltage oil-filled power transformer must pass routine tests during its manufacture, the hidden faults that can cause partial discharges within it may still exist or be created during its future operation. For an energized transformer partial discharge activities may still unavoidably occur. Partial discharge phenomena occurring within oil-filled power transformers can be summarized as one of following [19];

- Discharge in an oil gap that exists in oil-barrier insulation between windings
- Discharge in an oil gap at ends of windings
- Discharge in an oil gap between insulating conductor and insulating paper
- Discharge in an oil gap between discs
- Partial breakdown of inter-turn insulation
- Surface discharge of insulation material
- Discharge due to floating particles or impurities
- Discharge in voids existing in materials or constructions
- Discharge at protrusions of metal parts in strong electric fields or when floating with respect to earth.

2.4 Behaviour of Partial Discharge Signals within Transformers

Due to the complexity of oil-paper insulation systems of power transformers, the propagation of partial discharges within transformers is very diverse in form and paths. There are very different propagating functions between both of them.

In general, PD signals measured at transformer terminals have undergone change as they have travelled along transformer windings and leads. Actually the original sites of PD signals may or may not be located on some points of the windings or leads. They maybe located in any imperfection in the insulation system of the transformer. Due to the complexity of insulation construction (especially the winding structure), PD pulses suffer distortion and attenuation travelling from the PD source site to the measurement terminal. Since a partial discharge maybe located anywhere within a transformer, the deformation of its signal varies and is directly dependent on the properties of the dielectric materials providing propagation paths for the PD signals themselves.

So, the transfer of a partial discharge signal within a transformer attenuates and oscillates in magnitude. This is due to the function of the distributed parameters of the transformer windings. These parameters generally include capacitance to earth (tank and core), capacitance and inductance and mutual inductance amongst the turns and amongst the discs of the windings, frequency-dependent resistances and stray capacitance, etc. They are all very sensitive to high frequency signals. Furthermore, the parameters are all inter-coupled in a complicated way that also influences the PD signal transfer. The magnitude and phase properties of the above parameters depend on the construction and arrangement of windings. The complexity of transformer construction results in the propagation of PD pulses which is not only a complex attenuation process, but also an oscillating process [21].

2.5 PD Detection Methods for Oil-filled Power Transformers

2.5.1 Chemical Method (Dissolved Gas Analysis)

Dissolved Gas Analysis (DGA) is a typical application of chemical methods to detect PD activity within transformers. Partial discharges occurring within an oil-filled transformer naturally cause a change in the chemical composition of the oil. These manifest themselves in fault-generated gases in the oil and pressboard insulation degradation bi-products [18]. Oil samples for analysis can be taken on-line but the analysis is complex and should be performed under laboratory conditions.

Dissolved Gas Analysis has also been developed to identify potential defects in transformers. This is a simple and cheap available technique for on-line monitoring. Fault gases typically include acetylene, methane, hydrogen, carbon dioxide and ethylene plus ethane, oxygen, nitrogen and carbon monoxide. Many of these gases evolve logarithmically over the time of stressing. Different compositions of gases represent different levels of discharge energy. The composition analysis of gases can indicate the partial discharge situation within transformers. For example, with low level discharge activity only hydrogen and a few saturated hydrocarbons (principally methane) are generated. With high-energy discharges or arcing, acetylene is produced [18]. A chemical detection provides only an integrated measure of prevalent PD activity and provides little or no indication of its nature, intensity, extent or location.

2.5.2 Acoustic Methods

This method utilises the measurement of acoustic pressure waves which transfer from the discharge source and can be used to detect and locate the partial discharge activity in transformers. During discharge there are a lot of molecular impacts in the discharge area, the impacts generate pressure waves. Because of the discharge pulse the pressure wave is made up of a series of pulses containing various frequency components. In liquid materials, if discharges occur in bubbles, the process of a discharge is accompanied with explosions of the bubbles, the bubble splits into smaller bubbles, and the liquid may be disturbed. All these effects cause local pressure variations that combine each other to form acoustic waves. In solid materials discharge processes may be accompanied by small explosions and cause a subsequent change of local pressure, which may produce acoustic waves. In transformer oil the velocity of an acoustic wave depends on the temperature of the oil and can range between 1000 $ms^{-1}$and $1600ms^{-1}$. The higher the oil temperature the slower the acoustic velocity is. Because of spread, reflection and heat transfer the acoustic wave is inevitably attenuated during its propagation. Usually, if the PD source is regarded as a point source of sound, the propagation of an acoustic wave in a homogeneous medium should be considered as having the form of a spherical screen wave. The acoustic impedance between a PD source and a detection point is complicated as the acoustic wave propagates along multiple

pathways and is distorted by attenuation. The detection and interpretation of acoustic signals from partial discharge sources is both complex and often inaccurate. However, acoustic monitoring can be applied, but is not always successful and the measurement cannot always be effectively calibrated [25]. Using acoustic sensors PD may be detected on walls of a transformer tank [25]. A method has been introduced that use optical fibre interferometer sensors intruding into the inside of a transformer to collect acoustic signals of PDs [22].

2.5.3 Electrical Methods

Electrical Methods are those which directly or indirectly use transferred electric properties of partial discharge signals, such as voltages, charges etc., to detect PD signals within a transformer.

Electrical detection techniques for partial discharge activities are currently the most popular approach for on-line condition monitoring of power transformers. It is essentially based on the assessments of

- Apparent parameters of measured partial discharge signals, such as the quantity of partial discharges, the energy of partial discharges, the phases of partial discharges and the inception/ extinction voltages of partial discharges.
- Distribution of the frequency spectra of measured PD signals, such as discharge charge spectrum, discharge energy spectrum and discharge phase spectrum etc.
- Apparent trend parameters of measured PD signals over the measurement interval (days/weeks).

Correspondingly, an effective measurement of partial discharge waveforms in terms of their magnitude, number, peak and their frequency properties (all distinguished from background noise) is the most important factor when assessing partial discharge activities in transformers [26]. A typical application of above methods is the UHF/VHF technique. The UHF/VHF technique of detecting partial discharges within transformers is a practical application of an acoustic or electrical method or their combination on electrical apparatus and has been developed over several years [20].

A current pulse of a PD signal generally has a very short duration (a few nanoseconds), and can excite the dielectric of an insulation system of a transformer and be transferred through the insulation system to reach the measurement points. Their ultra high frequencies of up to 2.5GHz or more can be maintained. The signals reaching the UHF/VHF devices can be considered as multiple resonances that persist for several microseconds. The signals are readily picked up by the UHF/VHF devices fitted on tank walls or over dielectric apertures or at some other suitable places on a transformer. The collected signals can be amplified, analysed, stored and displayed using digital equipment. The transformer conditions can be assessed.

Attention to the following two aspects should be paid when using this technique: firstly, a pulse of partial discharge at the point of origin is extremely short; it radiates energy to the measurement points and sets up many modes of microwave resonance at the same time. The energy reaching the measurement points depends on the length of the PD current path, and also on its originating position and its radiating orientation within the transformer. Secondly, a UHF/VHF device (sensor) acts as an antenna producing a voltage at its output terminal in response to the UHF/VHF field incident upon it. The efficiency of the conversion, both in terms of sensitivity and bandwidth, must be measurable.

2.6 Recognition methods of partial discharge patterns

Most recognition methods of partial discharges within transformers are based on the analysis and observation of the behaviour and property of the signals measured during on-line monitoring or testing or laboratory experimentations. The measurement data can be represented in spectrum or waveform patterns in both time domain and frequency domain using two or three dimensional representations. The determination of properties or parameters that describe the characteristics of partial discharge signals and the extraction of true and reliable information from the coarse raw data are the key to acquiring and illustrating valuable waveforms or pattern charts or frequency spectra of partial discharge signals.

2.6.1 Evaluation of partial discharges

To entirely avoid partial discharge activities in high voltage transformers is impossible and uneconomic. The important thing is to limit partial discharge to an acceptable level to guarantee operation of the transformer over its design life. The status of a partial discharge depends on the defect level and the degree of ageing of the insulation materials or systems. It is possible to evaluate the degree of ageing of an insulation system by means of partial discharge status. Many parameters have been utilized which describe a partial discharge within an insulation system, but in practical engineering, only a few parameters and simpler methods are desirable and more available. It is therefore crucial to choose carefully the properties of partial discharges to be used in evaluating the nature of partial discharges. In recent years, the following methods of choosing parameters and recognizing patterns have been applied [17].

2.6.1.1 Apparent parameters evaluation of partial discharge signals

- Number of partial discharges

A discharge number can represent the damage degree and ageing velocity of insulation materials. Advantage can therefore be taken of this to evaluate the damage and ageing of the insulation system or material.

- Energy of partial discharges

A discharge process is certainly an energy exchange process. The more the energy exchange, the more the partial discharge energy. This means the damage degree of an insulation material is higher and the ageing velocity of the insulation material is faster.

- Average distribution of partial discharges in the 50 Hz cycle

For a strenuous partial discharge, it can be observed from a test voltage waveform that the discharge phase distribution has widened and even has spread beyond the zero crossing points of the 50 Hz voltage period. The value of the partial discharge group represents the severity of the degree of the discharge.

- Inception and extinction voltage of partial discharges

In general, for an insulation system it is necessary that the inception discharge voltage is higher than the operational voltage. In this case partial discharges should be seen in the insulation system. Under the same applied test voltage, the lower the inception voltage, the greater the discharge quantity, and the greater the discharge numbers

2.6.1.2 Pattern chart or spectrum of a partial discharge signal

In general, the above parameters are illustrated in chart and pattern form to permit PD recognition. In recent years, computer techniques have made this work easier. By using mathematical methods, the parameters can be expressed in the form of distribution spectra. The spectra can clearly represent the properties of a partial discharge.

- q-N spectrum (spectrum of discharge charge quantities and discharge times)

The apparent charge quantities of a partial discharge are arranged from large to small across equal divisions of a time domain and the discharge times for each unit time are counted. The illustration of them in a chart is a q-N spectrum. In general, any change of the q-N spectrum means that an obvious ageing is occurring in an insulation material or construction.

- W-N Spectrum (spectrum of discharge energy and discharge times)

By arranging the discharge energy for all collected signals from large to small across equal divisions of a time domain and counting discharge times for every time unit, a W-N spectrum can be constructed. In general, for an ageing insulation material the energy of both larger and smaller discharges all accompany an increase of discharge times.

- Φ-N spectrum (spectrum of phase and discharge times)

By dividing the test voltage of one cycle of the test voltage waveform into equal divisions and counting the discharge times for every time unit, a Φ-N spectrum can be made up. From this

spectrum we can observe whether there is a balance between the discharge pulse groups in the positive half cycle and those in the negative half cycle, and whether the discharge develops onto the zero phases between them. We can then judge the situation and type of the discharge.

In addition, in a partial discharge test on an insulation system, the discharge quantities are usually different between rising falling voltages. This forms a loop. The worse the property of the insulation system is, the larger the area of the loop. With the increase of test voltage, partial discharges become more severe. This property reflects the difference between inception voltage and extinction voltage. The larger the difference is, the worse the insulation property.

Electrical PD detection offers sophisticated approaches for obtaining real data of PD activities in power transformers. This includes PD magnitude (q), phase (Φ) and number (n) data as well as derived quantities or times from these parameters in a test voltage cycle (t). Research [27] has led to a better understanding of the acquisition, processing and analysis of PD phenomena to determine the nature of partial discharges. The Φ-q-n or Φ-q-t distribution histograms reveal the possibility of distinguishing PD signals from the different types of degradation conditions in power transformers. A resultant three-dimensional diagram can be used to visualize and interpret PD characteristics.

2.6.2 Algorithms of partial discharge signal recognition

To realise the recognition of partial discharge signals as described above, many signal processing methods have been investigated, developed and applied. These methods have obviously improved the capability of understanding partial discharge behaviour.

2.6.2.1 Artificial neural network (ANN)

The use of artificial neural networks (ANN) to analyse and judge discharge phenomena has been developed over several years. ANN, due to its ability to self-organize, self-learn the functions that it can realize and auto-process using non-linear mapping has become one of the most promising algorithms for partial discharge signal recognition. By means of learning from known discharge signals, ANN can develop the ability to diagnose real discharges.

This dynamic system consists of highly interconnected and parallel non-linear processing elements that create efficiency in computation. During the system training with a database of real partial discharge patterns from known types of detect, the links between layers (neurons) in ANN are automatically strengthened or weakened on the basis of the required output. Thus, the key parameters are finally recognised. Generally the Back Propagation Neural Network (BPNN) [28, 29] has been trained and used to recognize partial discharge behaviour in power apparatus.

2.6.2.2 Statistical parameter methods

In order to analyse and recognize a partial discharge pattern, the information contained in discharge distributions is usually utilized in a quantified style. The quantified distribution patterns may be described by statistical parameters such as skewness (*Sk*) and kurtosis (*Ku*) and Correlation factor (*CR*) and Cross-correlation factor (*CC*). These four parameters may be employed to describe PD phenomenon inside an insulation system. They are calculated from various patterns of phase-resolved and pC-resolved distributions. These can help to determine the type of discharge source and development of its activities. Therefore the results may be useful for the improvement of PD recognition. Additionally two-parameter and five-parameter Weibull distribution functions have been applied to describe the pulse-height distribution of partial discharge signals [28, 30, and 31].

2.6.1.3 Wavelet analysis method

If signals do not vary too much in the time domain, stationary signal Fourier analysis is useful. However, most PD signals contain numerous non-stationary or transitory characteristics: tendencies, abrupt changes, and variation of the start and end points of the signal. These characteristics are often the most important aspect of PD signal processing, and Fourier analysis does not allow them to be obtained due to its disadvantage, that when transforming to the frequency domain, temporal information is lost. It is impossible to look at a transformed Fourier signal and state when a particular event took place. A wavelet is a finite waveform with null average value. Fourier analysis consists of the decomposition of the original signal into sinusoid signals of several frequencies. In contrast, wavelet analysis decomposes the original signal into scaled signals of the original wavelet (or mother). It can be appreciated intuitively that signals with form changes, characteristic of those generated by partial discharges, can be better analysed with an irregular wavelet signal than with a uniform Fourier sinusoid.

One method of application of wavelet analysis is that of dividing partial discharge signal into two parts: the approximation and the detail. The approximation corresponds to the low-frequency components and the detail corresponds to high-frequency components of the measurement signal. The original signal passes through two filters and two signals emerge. These are the approximation signal (low frequency) and the detail signal (high frequency). This decomposition process can be iterated generating the decomposition wavelet tree [22].

2.6.1.4 Fuzzy Logic method

Fuzzy logic is a superset of conventional (Boolean) logic that has been extended to handle the concept of partial truth -- truth values between "completely true" and "completely false".

Procedure for application of fuzzy logic systems to the classification of partial discharge pulse

patterns in terms of PD source size have been described [32]. The features employed in the pattern recognition task are those related to the form or shape of the partial discharge pulses and its associated apparent charge transfer. Preliminary results, obtained with the fuzzy logic system on simple partial discharge sources, indicate a performance approaching that which is attainable using ANNs. The results obtained so far are of a very preliminary nature and further work is in progress with simple PD sources in order to determine in more detail the performance capability of fuzzy logic methods in the area of PD pattern recognition.

2.7 Location of partial discharge within power transformers

The locating of the source site of a partial discharge is of great importance in the monitoring of oil-filled power transformers, but it is very difficult to get an accurate PD location due to the complex construction of the insulation system within a transformer. In addition, the complexity (i.e. distortion, attenuation and oscillation) of the propagation characteristics of a PD signal within a transformer also making it very hard to judge and recognize the partial discharge source site by using the measured results from outside of a transformer. Two typical traditional detective approaches are the electric and supersonic location methods, and these have been widely applied in the electricity industry. Previous experience [21-23] has indicated the usefulness of using transfer functions describing the transformer winding relationship to localize PD. Most transfer functions are defined using combinations of the physical structure with the design parameters of the transformer windings and travelling wave theory. To determine and resolve these simulation mathematical functions, several methods have been developed as described in section 2.7.2.

2.7.1 Traditional Localization Methods

2.7.1.1 Electrical location methods

Electrical location methods include the multi-terminal location method, the travelling wave location method, the waveform comparison method and polarity location. Most of these are usually used by transformer manufacturers and on-site test engineers to look for partial discharge sources within transformers.

The practical methods recommended by IEC76-3 (1998) are the multi-terminal test method and the waveform comparison method. The principle of these two methods depends on the energy from the discharge signal reaching external terminals. The signals arriving at different terminals may be of different magnitude, waveform and spectrum due to their different propagating paths. When applying a calibrated pulse to two terminals, the pulse must propagate to all other terminals. Comparing and observing the magnitude and waveform of the measured signals can roughly infer the partial discharge source. Using this principle can only locate the "electric area" of a partial

discharge source; the real discharge source "geometry point" may not be so easily determined. In general, this method can only be utilized either when a transformer is off-line on a site or when a transformer is under test by a manufacturer.

2.7.1.2 Acoustic location method

The acoustic wave produced during a partial discharge inside a transformer may propagate through dielectric materials, like oil, pressboard, barriers and windings, etc., to reach the tank walls of the transformer. Acoustic sensors fitted on the wall can intercept the supersonic signals and convert them into electric signals. The latter can then be amplified and measured. Furthermore, the travel time can be measured and calculated by means of an oscilloscope combining the velocity of the supersonic wave and the distance between acoustic source (PD source) and sensor. Using several sensors mounted on different positions of tank walls, different calculation distances can be obtained. Consequently, the geometric position of acoustic source (PD source) may be estimated.

This method can be utilized either when a transformer is on site (off-line or on-line) or when a transformer is under test by a manufacturer.

2.7.2 Simulation Localization Methods

Partial discharge location methods based on a theoretical study of the system have been investigated [33-35], suggesting the possibilities of locating a partial discharge source by taking the characteristic behaviour of transformer coils into account using their transfer functions.

The infinitesimal homogenous winding model proposed by Wagner, where the series and parallel capacitances and the self-inductances are alone taken into account, greatly idealises the real conditions. For one thing, a real transformer winding is composed of a finite number of elements (e.g. disk, pairs of discs); therefore it is more appropriate to represent it by a model consisting of a finite number of elements than by an infinitesimal model. Thus in the case of disc type transformer windings, it is convenient to consider each disc, each pair of discs or each group of discs as a separate element. Further, real transformer windings are not homogenous in every case but generally different at the beginning and end of the winding. Very often the winding contains elements (discs) in which the number of turns, geometrical arrangement or shape deviates from the majority of elements constituting the winding. The Wagner model also simplifies the real condition by neglecting mutual inductances within the winding and the damping effect of eddy current losses on voltage oscillations. Finally, in the majority of cases, it is not a single winding that is to be investigated, but a transformer or a winding system consisting of two or more windings [36].

The following PD localization methods are all based on the Wagner model.

2.7.2.1 Analysis method of a lumped-element model for a multiple-windings transformer

The basic principle is to consider every single winding within a multiple-windings transformer as a ladder network-winding model. In general, a section (a pair of discs) is considered as an element. In a high frequency case, the ladder network consists of multiple inductances, capacitances, resistances and conductance. Figure 2.1 shows the illustration of a simplified ladder network model for a single winding ignoring winding loss; this model has only inductor and capacitor components.

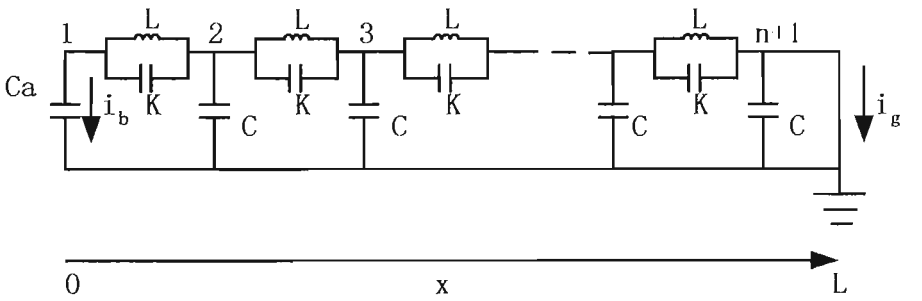

Figure 2.1, a simplified ladder network model of a transformer winding [33]

Wang, Crossley and Cornick [33] considered the multiple-windings of a transformer as a "lumped-element" model by considering the relationship of mutual inductances between windings. The system solutions were obtained by applying Kirchoff's voltage and current law (KVL and KCL) to the network. The authors postulated that the location of each pole on the Bode-plot depends on the overall properties of the winding. It is not affected by the location of the partial discharge. The location of each zero is an important parameter and may be essentially affected by the location of partial discharge. When the discharge occurs on the winding, the location of the zeros may change to different positions.

2.7.2.2 Using a linear time-invariant system to locate the partial discharge source on a transformer winding

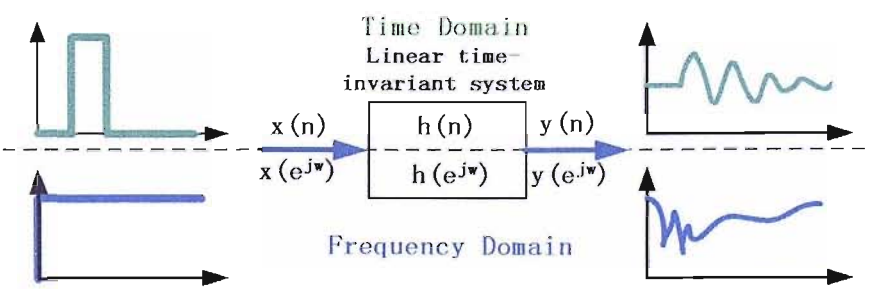

Figure 2.2 Linear time-invariant system [34]

Reference [34] introduced a method based on a linear time-invariant system theoretical approach.

The system can be described using its transfer function, and thus it can be visualized by a block diagram as shown in Figure 2.2.

For a linear time-invariant system, if the transfer function h[n] and any time discrete input signal x[n] are known, the output signal y[n] can be determined and vice versa by using the convolution theorem in the time domain. In a transformer winding, every section (a pair of discs) was considered as an element with a transfer function h[n].

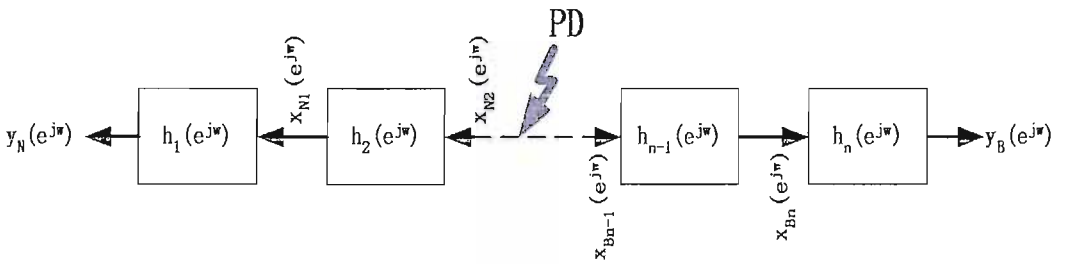

Figure 2.3 principle of PD location [34]

The transformer winding belongs without restrictions to the class of time invariant system, because it consists only of passive elements. Thus if an input signal has a delay, the output signal will have the same delay. So the PD location principle can be shown in Figure 2.3 using sub transfer functions.

2.7.2.3 Genetic Algorithms for Sectional Winding Transfer Function (SWTF)

This method is similar to neural network and fuzzy logic algorithms, which imitate the principles of natural creation. GAs (Genetic Algorithms) search for the solution of a function by simulation evolution, i.e., the survival of optimized individuals. At each generation a new set of approximations is created by selecting individuals according to their level of fitness and breeding them together using operators borrowed from natural genetics. This process leads to the evolution of populations of individuals they were created from. At the beginning of the computation a number of individuals are randomly initialized. The objective function is then evaluated for these individuals. The first generation is produced. If the optimization criteria are not met the creation of a new generation starts. Individuals are selected according to their fitness for the population of offspring, which is produced by recombination of the parents. All offspring will be mutated with a certain probability before the fitness of the offspring is computed. The offspring are inserted into the population replacing the parents, thus a new generation comes into being. This cycle is repeated until an optimization criterion is reached. Such a single population evolutionary algorithm is powerful and performs well on a widespread class of problems.

Akbari, Werle, Borsi and Grockenbach [37] introduced the genetic algorithm in the field of

identification and optimization to estimate parameters of the sectional winding transfer function (SWTF). In this application a small partial length along a winding is considered and a continuous circuit model is used to describe the partial differential equation of the winding structure. This equation determines the characteristics of the voltage wave propagation along the winding. Their simulated results of pulses indicated that the approach is limited to signals of less than 2 MHz bandwidth.

2.7.2.4 Transmission line method to build up a transfer function

In order to calculate the performance of transformer windings, a winding of N turns can be treated as a system of N transmission lines. This type of model represents the electrostatic and electromagnetic fields of the windings in a detailed manner. The study can be made with the model in which the PD pulse can be represented as a short-duration current pulse travelling through the multi-conductor transmission line network.

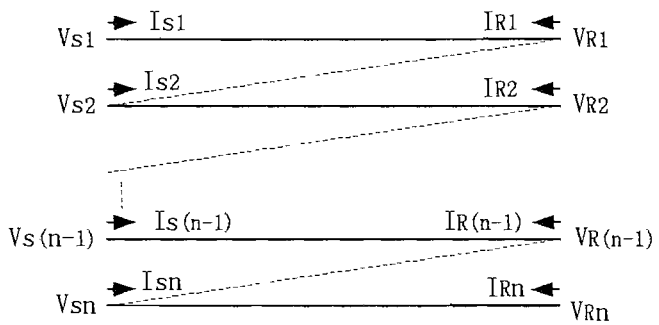

Figure 2.4, Multi-conductor transmission line model [38]

In the multi-conductor transmission line model each turn in the winding is imagined as a cut from the previous and following turns and then considered as a single conductor transmission line with a beginning and an end, as shown in Figure 2.4, this leads to a N transmission line system. Mathematically, the ends and beginnings of the N transmission lines need to be series connected, to give continuity of turns.

Hettiwatte, Crossley, Wang, Darwin and Edwards [38] have applied this method.

2.8 Conclusions

The literature survey indicates that there are some unavoidable defects or faults within a high voltage transformer. These defects or faults may cause the transformer damage and a power system outage, therefore lead to huge financial loss. Reliable techniques of monitoring and measurement on transformers may result in a great benefit. Some of these techniques have been developed and

applied by researchers and users. As one of the most important techniques, partial discharge monitoring and measurement of oil-filled transformers has been an area of continued development.

Previous investigations have revealed characteristics of partial discharges within an oil-filled power transformer from many aspects, such as origin, classification, behaviour and tendency. These investigations not only explain the partial discharge phenomena within transformers at molecular level, but also provide theoretical bases for researchers and users to develop techniques of monitoring and measurement of partial discharge activities within a transformer.

So far some methods of recognition and distinguishing of partial discharge signals within transformers have been investigated and developed. By means of the properties of pattern chart and spectra of partial discharge signals, researchers and users have developed the ability to recognize and distinguish partial discharge signals within transformers. These properties include valuable parameters and the relationships between them, such as quantity of partial discharges, energy of partial discharges, average distribution of partial discharges in a 50 Hz cycle and inception and extinction voltage of partial discharges. Mathematical methods have been applied, such as artificial neural networks (ANN), statistical parameter methods, the wavelet analysis method and fuzzy logic method.

Traditional measurement and localization methods for PD sources, within a transformer, such as dissolved gas analysis, electrical location and supersonic location have been investigated and applied. The simulation localization methods for PD sources have been developed as well. The development of these techniques indicates the feasibility of realizing PD location on a transformer winding. Typical examples of these methods include:

- Analysis method of a lumped-element model for a multiple-windings transformer
- Using a linear time-invariant system to locate the partial discharge source on a transformer winding
- Genetic Algorithms for Sectional Winding Transfer Function (SWTF)
- Transmission line method to build up a transfer function

All of these techniques have limits on the expression of measured signals in terms of their bandwidth or on the method of application of measurement equipment. A new technique utilising wide frequency measurements and a convenient method of application should be developed.

Chapter 3

Propagation Characteristics of High Frequency Signals within Bushings, RFCTs and Transformer Oil

A partial discharge is a wideband event (containing frequencies up to 2-3 GHz) and consequently this project has considered broadband PD defection using available external monitoring points of a large transformer. One possible monitoring point is the bushing tap point. Therefore, as part of the initial feasibility study a 60kV bushing (Photo 3.1) was assessed and its signal propagation characteristics experimentally determined.

The 60kV bushing, model 60HC755, has a 235pF capacitance, and is PD free under its standard application condition. As a sensor used in this investigation, the clamp-type RFCT EMCO model 93686-5, as shown in Photo 3.2, was also tested to determine its frequency response. The RFCT has a measurable frequency range from 10 kHz to 250 MHz. The transformer oil used in the investigation was produced by Stanlow Works, UK. The specification of the oil is BS148:1998 class 1. The main electric characteristic of the oil is: electric strength (breakdown, mm) : >30kV.

Photo 3.1, The 60kV Bushing

Photo 3.2, A clamp-type RFCT (Radio Frequency Current Transducer)

3.1 Bushing Sensitivities

The high voltage bushings mounted on an oil-filled power transformer are capacitive devices. A capacitive bushing generally has a power factor test tap on its installation flange. The test tap is connected to the ground layer of the capacitor core of the bushing. In its normal operation, a cap covers the insulated tap and grounds the tap to the flange (earth). Usually, for a power transformer, internal signals may transfer to the bushing core bar along windings and coil leads as well as external signals, such as corona and surface discharge and radio noise etc. The bushing, acting like a capacitor, passes the high frequency components of these signals from its core bar to its tap point.

3.1.1 Frequency Response of Bushings

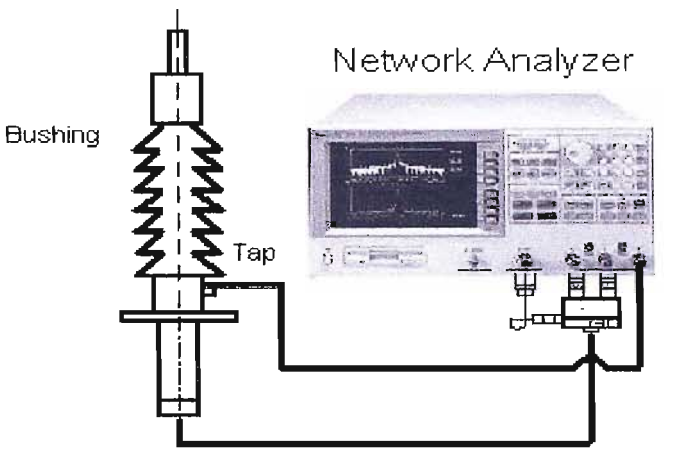

Figure 3.1 Frequency Measurement Circuit for a bushing

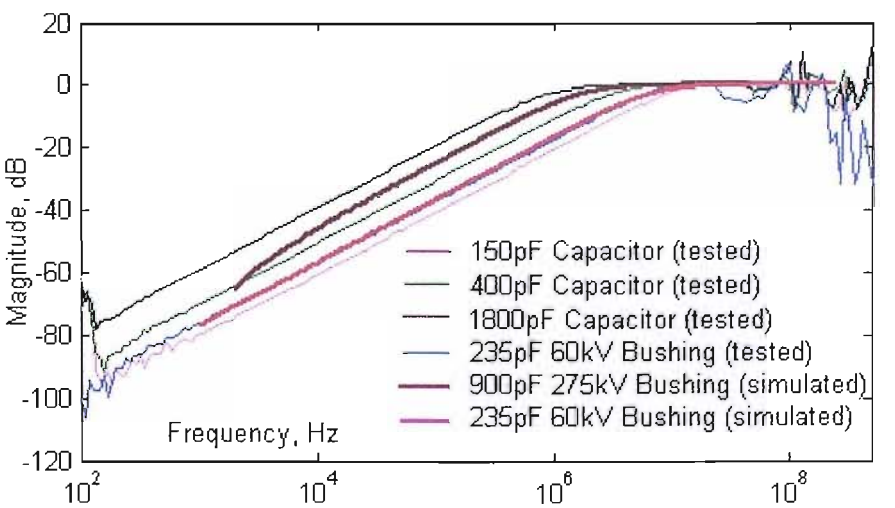

Figure 3.2 Frequency Responses of Bushings and Capacitors

Figure 3.1 shows the measurement circuit for the frequency response of the 60kV bushing between the bushing core bar and the bushing tap. Figure 3.2 shows a comparison of the measured

frequency responses of the 60kV transformer bushing and three pure capacitors, as well as simulated frequency responses of the 60kV bushing and a 275kV transformer bushing. The frequency responses represent the propagation of high frequency signals from the bushing core bars to the bushing taps. The 60kV bushing, model 60HC755, has a 235pF capacitance, and is PD free under its standard application condition. The 275kV bushing has a 900pF capacitance. The measured curves were obtained using the Agilent 4395A Network/Spectrum/Impedance Analyzer. The simulated results were generated using a simulation program compiled using MATLAB/Simulink. The oscillations on the experimental measured curves over 100 MHz were caused by the presence of stray inductance and capacitance.

3.1.2 Impulse Response of the 60kV Bushing

Using the circuit shown in Figure 3.3, a very fast pulse produced using an HP 8082A Pulse Generator was injected into the 60kV bushing core bar. A digital oscilloscope, LC684DXL, was used to display, analyse and store the input pulse and the output signal measured at the bushing tap.

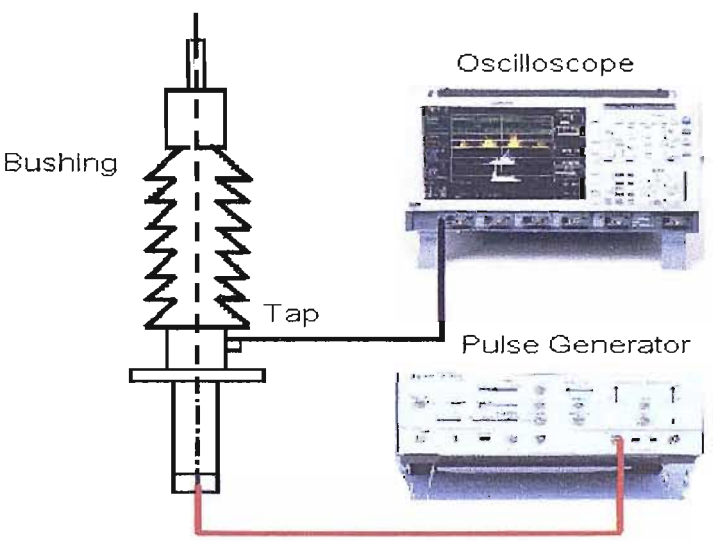

Figure 3.3 Schematic circuit of the measurement
for the impulse response of the 60kV bushing.

Figure 3.4 shows the waveforms of the both input and output signals. The input pulse travelled within the bushing. The bushing, acting like a capacitor, transferred the high frequency components of the input pulse across the insulation layers of the bushing to the bushing tap point. Therefore, the output signal was detected by the oscilloscope.

Figure 3.5 shows the frequency responses (FFTs) of the injected pulse and the output signal. From Figure 3.5, it is apparent that the bandwidth of the input pulse is greater than 500 MHz; and that of the output signal is below 200 MHz. For the output signal, the magnitudes of the signals below 200 MHz are attenuated to some degree.

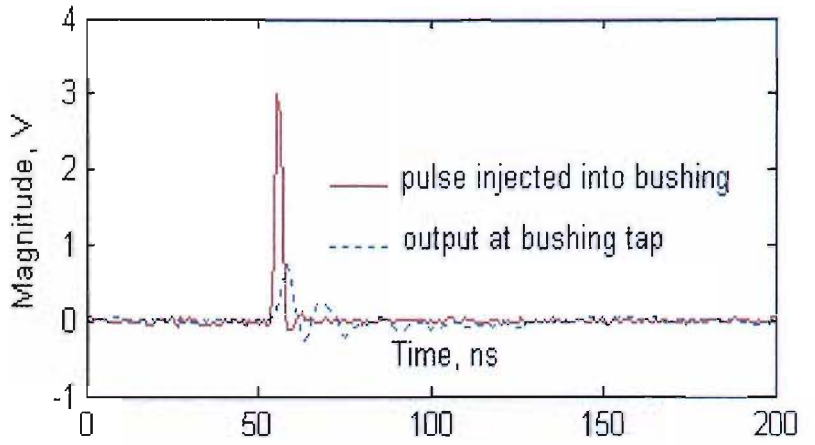

Figure 3.4, a pulse injected into the bushing and its output at the bushing tap

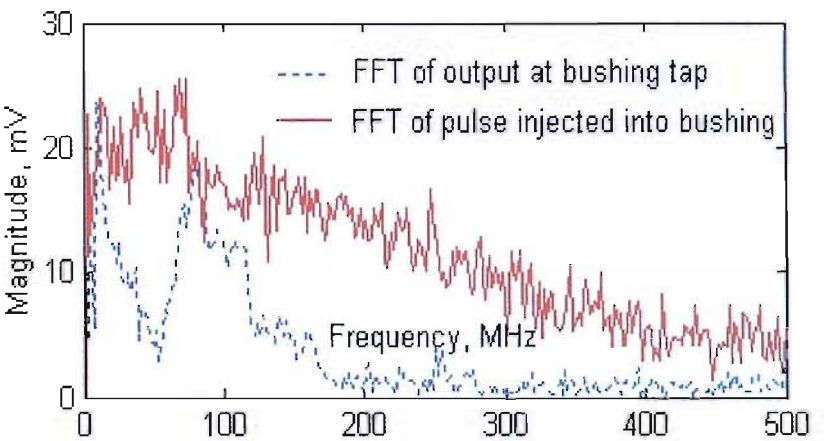

Figure 3.5 Frequency responses of the pulse and the output at the bushing tap

3.2 RFCT (Radio Frequency Current Transducer) Sensitivities

To improve the scalar gain of the RFCT, a wire of 3 turns was wrapped around it as the primary coil (input signal side). Figure 3.6 shows the measured frequency responses for the RFCT and the RFCT plus a 30 meter ethernet cable attached and a RFCT with a 1 turn primary coil. In the measurements an Agilent 4395A Network Analyzer was used and was set with frequency range from 10 kHz to 200 MHz, 20 sample average and 300 Hz bandwidth step.

The RFCT has a measurement gain of up to 200 MHz bandwidth. By using three turns on the primary side the frequency response is improved across the whole measurable frequency spectrum. The 30 meter cable reduced the sensitivity of the RFCT by 5dB.

The cable was included to simulate the conditions likely to be experienced when undertaking field measurements. In order to maintain safety it is important that measurement equipment and operators are a reasonable distance (30m say) from the on-line transformer under test.

With reference to Figure 3.6, there are three resonant peaks above 100 MHz for the 3 turns RFCT frequency response due to stray capacitance. However, the peaks are small (4-5dB) and will not substantially effect any measurement.

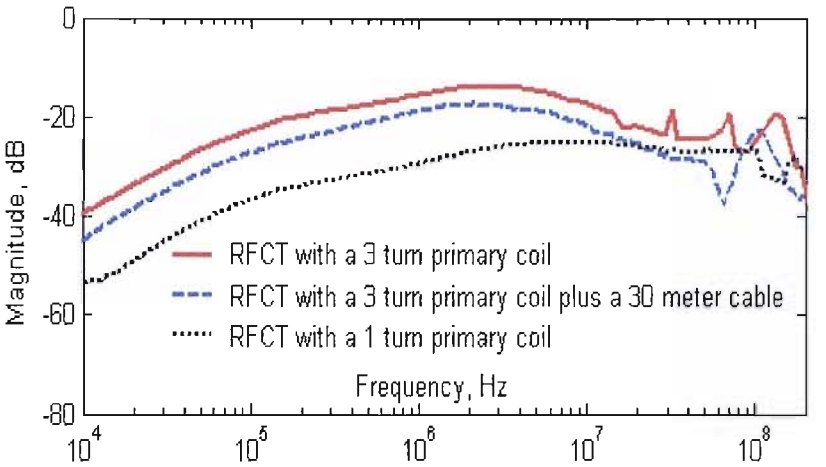

Figure 3.6 Frequency Responses of RFCTs

3.3 Sensitivity of Transformer Oil

As shown in Figure 3.7, a set of two parallel metal plates of diameter 130 mm was used to investigate the frequency response of transformer oil. The gap between the two plates was 3 mm. Before the set was placed inside the oil, the analyser was calibrated by short circuiting the measurement coaxial cables together in order to establish the frequency response due to the Analyzer input circuit and connection cabling. In the test the Agilent 4395A Network Analyzer was set with a frequency range from 1 kHz to 200 MHz and a bandwidth step of 300 Hz. The average numbers of samples were 20. Similar measurements were undertaken in air. Figure 3.8 shows the obtained frequency response for transformer oil normalised with respect to the air measurement.

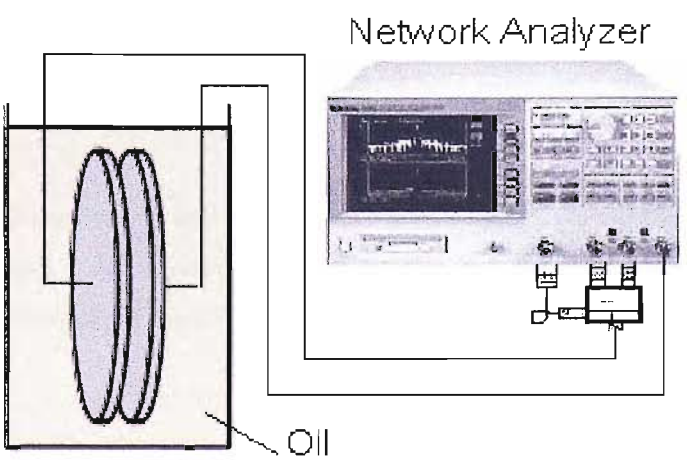

Figure 3.7 Measurement circuit for the frequency response of transformer oil

The measured curve shows that the below 25 MHz components of the signals can pass the oil-gap of the set more easily than the air-gap due to the presence of transformer oil. Beyond 25 MHz, the transformer oil hardly influenced the transfer of the signals compared with the air case. The behaviour of the response above 10 MHz (Figure 3.8) may be due to parasitic components present due to the measurement process itself.

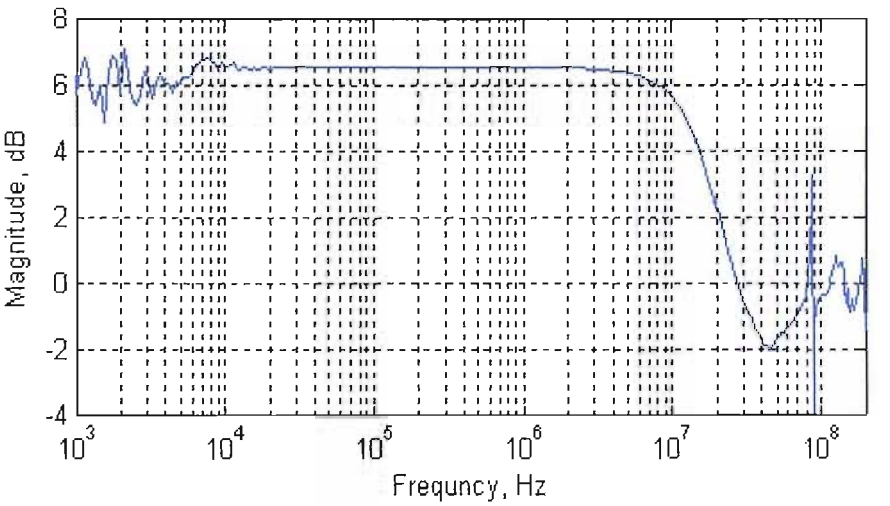

Figure 3.8 Normalised frequency response of transformer oil

3.4 Conclusion

The main property of the 60kV transformer bushing is that it is capacitive below 25 MHz. Beyond 100MHz the influence due to inductance reduced the ability of the bushing to transfer signals, but does not change its capacitive property. This feature determined that the output at the bushing tap must be an oscillating and declining pulse when a fast pulse passes through it from the bushing core bar to its tap. The test results also revealed that the detection of output signals might be maintained over a bandwidth of more than 180 MHz.

As sensors, RFCTs can transfer high frequency signals. A wire of three turns wrapped on a RFCT as a primary coil can improve the measurement gain. A long cable may attenuate the measurement signal by around 5dB.

The measured result shown in Figure 3.8 represents the ability of transformer oil to transfer high frequency signals. In fact it is a comparison with air and indicates the difference of the abilities between oil and air in transferring high frequency signals within the same construction.

Chapter 4

Discharge Signals from a 60kV Bushing via a RFCT

As described in Chapter 2, there may be many kinds of partial discharges within power transformers. They can be summarized as typical external corona, external surface discharge, internal void discharge, internal floating discharge and internal needle-plane discharge (corona in oil). In a power transformer if any discharges occur they will propagate and reach the bushing core bar, and the high frequency components of the signals can pass to earth via the bushing tap and therefore be detected using a RFCT. This chapter describes experiments undertaken to simulate PD signals and the measured propagation characteristics when they transfer through the 60kV bushing from its core bar to earth via the bushing tap point.

4.1 The Measurement Circuit and Discharge Sources

Figure 4.1 shows the schematic diagram of the circuit to measure PD signals from a 60kV bushing via a RFCT. A copper pipe having a sharp tip (needle point) was connected to the bushing core bar. The sharp tip of the copper pipe was used as an electrode of a discharge source. The diameter of the copper pipe was 15 mm and its length was 0.5 m. This ensured that the influence of stray capacitance and inductance was limited. During testing a 50Hz high voltage was applied to the core bar of the bushing. When the test voltage rises to a suitable value, a discharge or partial discharge was produced at the discharge source. The discharge signals then transfer to the bushing core bar from the copper bar and the high frequency components of the discharge signals pass

through the bushing to reach the bushing tap. A RFCT, as a sensor, was used to detect the output signals at the bushing tap. In the test the RFCT was wrapped with a wire of three turns to improve it measurement gain, the wire was connected between the bushing tap and ground. The frequency response of the RFCT is as shown earlier in Figure 3.5. Digital equipment, consisting of an oscilloscope and a Network/Spectrum Analyzer were used to display, store and analyse the collected waveforms and data. In addition, a PD detector, Robinson Model 5, was also used to detect the discharge in order to provide a calibrated measurement of the apparent charge and obtain the original PD signal waveform. A test in which the PD source was disconnected was carried out by applying a 45kV Voltage to the bushing core bar. No PD was detected either by the oscilloscope or the PD detector. This infers that for the voltages up to 45kV the whole measurement system was PD free.

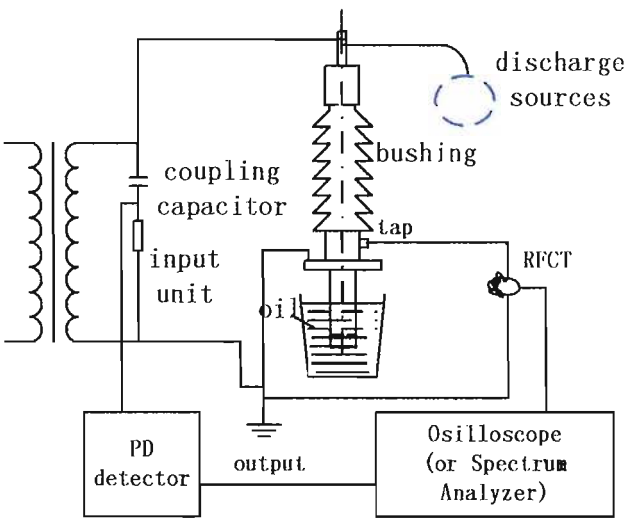

Figure 4.1 Schematic diagram of the measurement circuit

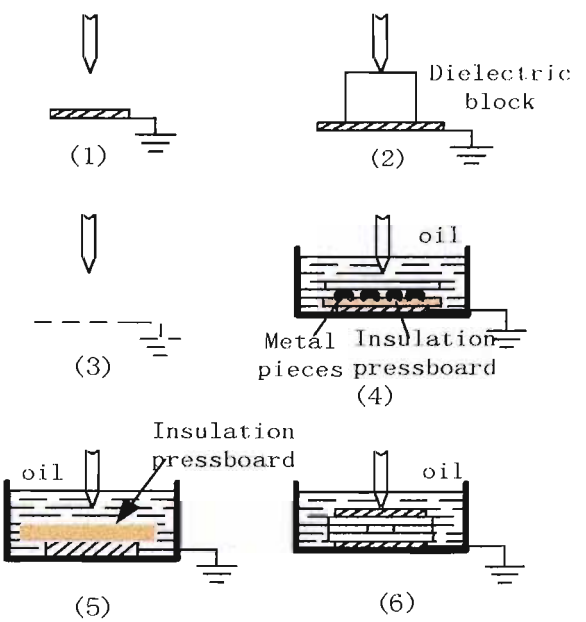

Figure 4.2 Discharge sources

Figure 4.2 illustrates the six typical discharge sources that were investigated in the test. These PD sources can reflect the majority of the PD phenomena within a power transformer. They are:

- Corona discharge source with near the ground electrode in air ((1) in Figure 4.2)
- Surface discharge source in air ((2) in Figure 4.2)
- Corona discharge source with remote earth in air ((3) in Figure 4.2)
- Floating partial discharge source in oil ((4) in Figure 4.2)
- Partial discharge from a needle point to earth plane arrangement in oil ((5) in Figure 4.2)
- Partial discharge from a void source ((6) in Figure 4.2)

The transformer oil used in the test was produced in Stanlow Works, UK. The specification of the oil is BS148:1998 class I. The main electric characteristics of the oil is: electric strength (breakdown, mm) : >30kV.

4.2 Corona Discharges in Air

Generally, corona occurs on operational transformer bushings or the equipment connected to them and is caused by high potentials, which can be seen under normal operating conditions.

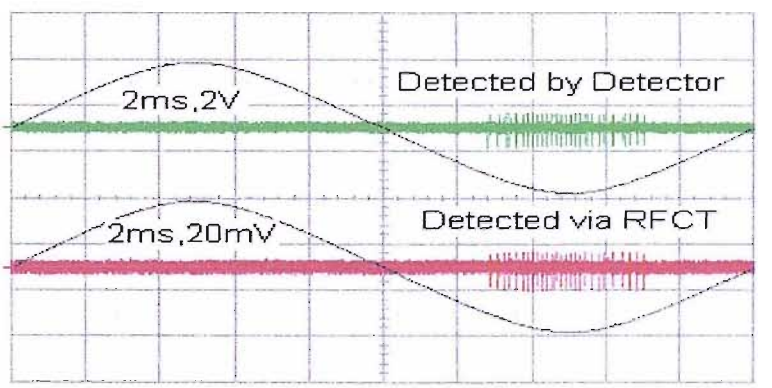

Figure 4.3 Corona with remote earth at 10.5kV

Figures 4.3 and 4.4 show the corona waveforms obtained using the measurement system in Figure 4.1 and the discharge source (3) shown in Figure 4.2. The waveforms represent a single period of the 50Hz applied voltage. In the test the distance from the needle point to the earth was kept as great as possible. Thus the discharge system had a remote earth electrode (the ground). The inception corona occurred at around 4kV with some pulses of almost equal magnitude situated in the middle of the negative half cycle of the test voltage waveform. With increasing test voltage, the number of pulses increased rapidly and spread out over a greater range of phase, but there was no increase in pulse magnitude compared to that measured at inception. The waveform in Figure 4.3 was obtained for an applied voltage of 10.5kV. Raising the test voltage to around 17kV, the generated waveform shown in Figure 4.4 was obtained. The number of pulses kept increasing, as

did their spread. However, in the middle of the negative half cycle of the test voltage waveform, the pulse magnitudes were reduced, but there was an increase in pulse density. The pulse magnitudes of the edge of the corona pulse group were still similar to that measured at inception (Figure 4.3).

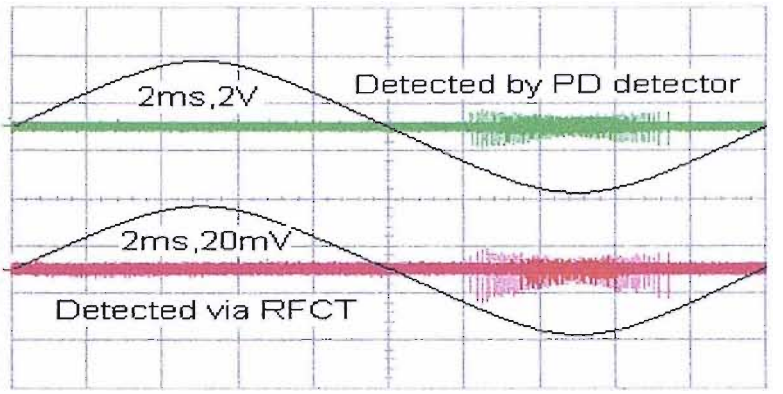

Figure 4.4, Corona with remote earth at 17kV

A metal earth plate to reduce the distance from the needle point to earth to around 100mm was then used (this formed the discharge source (1) as shown in Figure 4.2). When the test voltage was raised to around 4 - 7kV, a similar corona discharge pattern occurred as that described for the system with a remote earth. When the voltage was increased to 11.2kV, a different corona waveform was obtained. This waveform is shown in Figure 4.5.

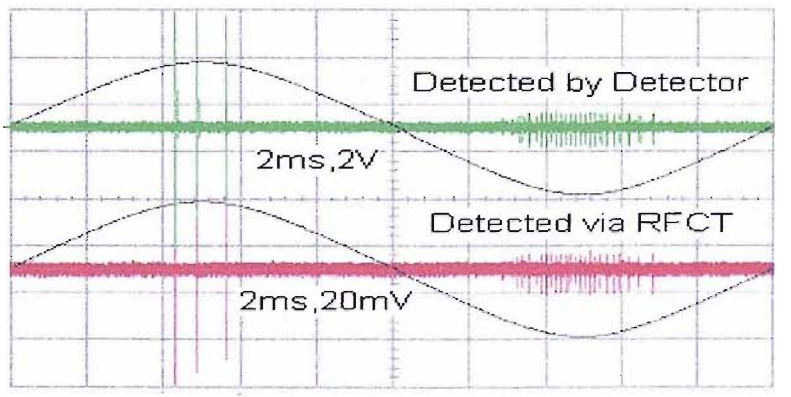

Figure 4.5, Corona with near earth

This result shows corona occurring not only in the negative half cycle but also in the positive half cycle of the test voltage waveform. The pulse magnitudes of the corona in the negative half cycle are almost equal; but the number of pulses is greater. In the positive half cycle of the test waveform the pulse magnitudes are greater; but there are fewer pulses. All of the corona discharge activities are centred on the peaks of the test waveform.

Generally, corona occurs around a metal needle electrode in air. Whether it discharges or not depends on the electric field intensity around the needle point which is dependent on the applied

test voltage. It increases as the test voltage is increased. When it reaches the inception discharge intensity, discharges start to occur. For a metal electrode it is easier to emit electrons when it has negative polarity, so discharge always occurs at the needle point around when the needle electrode is at peak negative polarity. Thus, corona always initially appears in the negative half cycle of the test voltage waveform. Meanwhile, due to the electric field, neutral molecules are ionised into positive and negative ions and these ions move towards the opposite polarity electrodes. When the positive ions combine with electrons near to the negative electrode there is a reduction in the local electric field intensity and discharge ceases. As soon as the negative ions reach the earth electrode, or the value of the ascending phase voltage continues to rise, the electric field intensity reaches the inception discharge intensity level and new discharge activity commences. In addition, the impact of positive ions on the negative electrode causes secondary electron emission, causing an increase in discharge number and a reduction in discharge magnitude. So, for the PD sources in Figure 4.2 (1) and (3), when the test voltage is not too high corona discharge pulses appear around the peak of the negative half cycle of the test waveform and are uniformly distributed about the peak, whilst their pulse magnitudes are almost equal.

If the test voltage is further increased then the number of discharge pulses increase and the spread of the across the peak of the applied voltage also increases. The rapid increase in the number of discharges creates a great deal of electrons (negative ions) between the earth and the electrode. This is due to the slower movement of electrons attached to neutral molecules travelling to earth compared to the positive ions attracted towards the negative electrode. Meanwhile, positive ions combine with the negative electrode (needle electrode) causing secondary electron emission. This leads to a rapid increase in the numbers of discharges and the magnitudes of the discharge pulses are reduced. This phenomenon occurs around the peak voltage, and therefore at the peak voltage there are far smaller magnitude discharge pulses compared to the situation when the voltage was around the inception level (Figure 4.5).

Consider now the discharge system with a near earth (Figure 4.2 (1)). Under suitable test voltage and when the needle electrode is of negative polarity, discharge occurs around the needle point and this causes electron emission and ionization of air molecules. The physics of the discharge event are similar to that described above. When the needle electrode is of positive polarity, discharges also occur near the needle point and cause ionization of air molecules.

Due to the short distance between the two electrodes the electric field intensity is high enough to reach the inception discharge intensity causing discharge and ionisation. Thus, as shown in Figure 4.5, corona discharge also occurs when the needle electrode is of positive polarity. As there are no positive ions combining with the needle electrode, there is no secondary electron emission in this half cycle. Hence, the magnitudes and number of positive discharges are not greatly influenced by the magnitude of the applied voltage. Thus the discharge signals occurring during the positive half

cycle of the test waveform have a greater magnitude and are less numerous than those occurring during the negative half cycle of the test waveform [17].

Using two discharge sources with a remote earth (Figure 4.2 (3)), comprising of copper bars with different sharp tips, the corona discharge waveforms shown in Figure 4.6 were produced when the applied test voltage was 8kV.

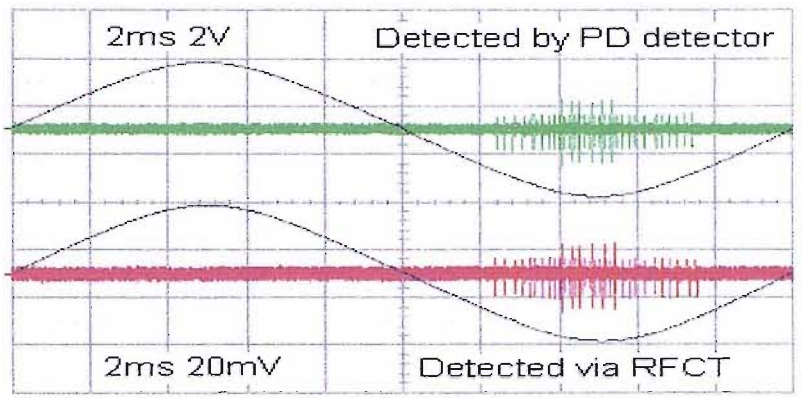

Figure 4.6 Corona with remote earth and two sources

The time-based signal and its frequency spectrum of a single pulse of corona are shown in Figures 4.7 and 4.8. The single pulse was sampled from the pulse group in Figure 4.3.

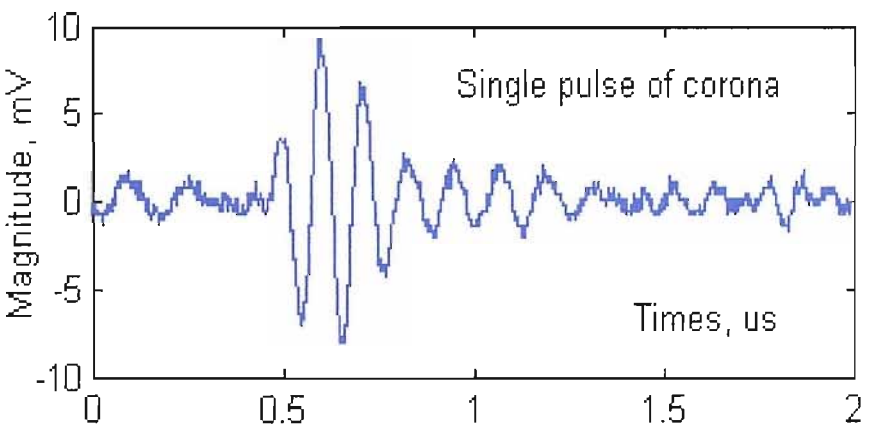

Figure 4.7 a single pulse of corona discharge shown in Figure 4.4

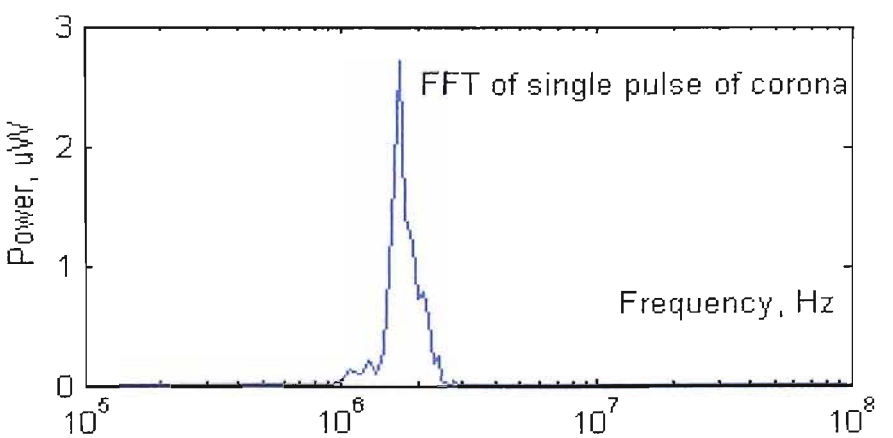

Figure 4.8 Frequency spectrum of the single pulse in Figure 4.7

For comparison the frequency spectra of the background noise and corona signals measured using the Spectrum Analyzer are shown in Figure 4.9. In this test the bandwidth of corona did not exceed 10 MHz.

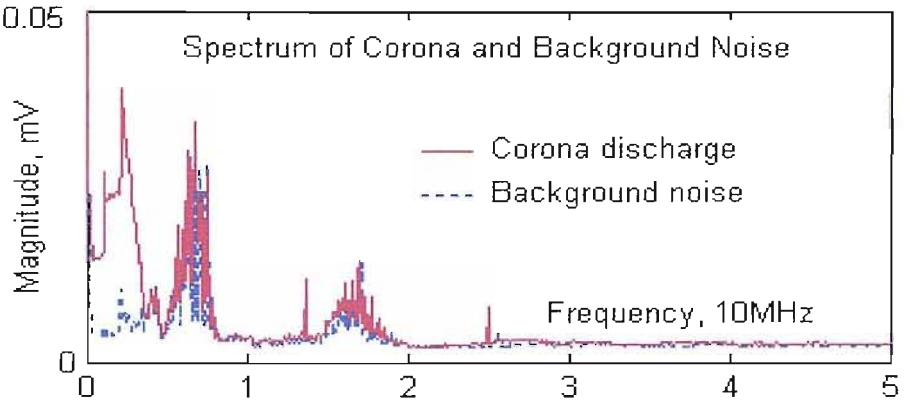

Figure 4.9 Frequency spectra of background noise and the corona discharge shown in Figure 4.4

A persistence figure for the corona discharge signal in Figure 4.5 is shown in Figure 4.10. The measurement period of the persistence figure is over 1000 cycles of the 50 Hz test voltage. This figure shows that the discharge is steady and strong.

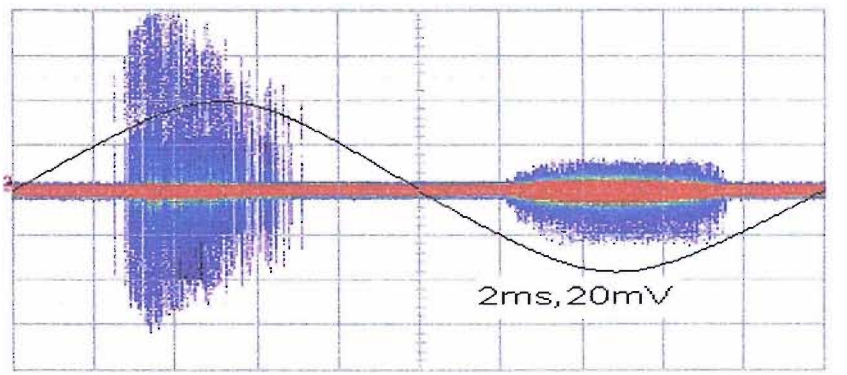

Figure 4.10, Persistence for Corona Discharges Shown in Figure 4.5

4.3 Surface Discharge

Figure 4.11 shows the phase resolved surface discharges, which was obtained using the measurement system shown in Figure 4.1 and the discharge source (2) shown in Figure 4.2. From Figure 4.11, the following can be surmised:

- Surface discharges (pulse groups) occur in the advance of each half cycle of the test voltage waveform.
- The surface discharges occurring in the positive half cycle of the test voltage waveform are slightly greater in magnitude and slightly smaller in number than those occurring in the negative half cycle of the test voltage waveform.

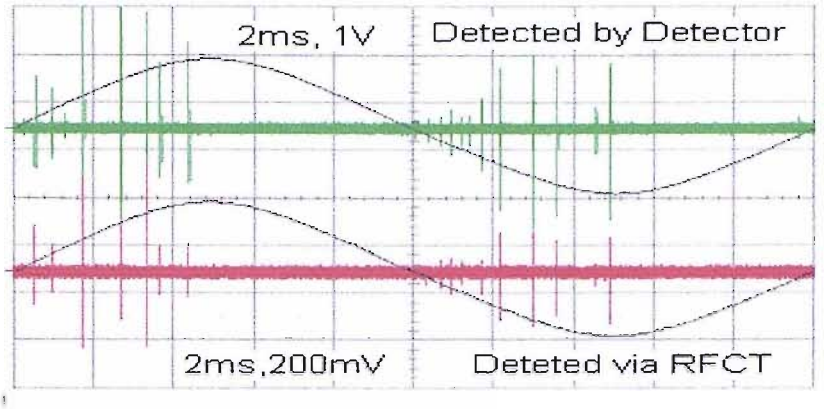

Figure 4.11 Surface discharge

Figure 4.2 (2) suggests that the experiment contains an unbalanced discharge system because the discharge source is an electrode with a dielectric block resting on an earthed metal plate. The needle electrode is at high potential with reference to the earthed metal plate. The small air gap between the needle tip and the dielectric block is easily ionised and discharge activity commences at a very low inception voltage. When the electrode is of positive polarity, the positive ions move and accumulate on the dielectric surface, and there is very little charge in the air gap. When the electric field is reversed the total field strength reduces and as soon as the field strength is less than the inception discharge intensity the discharge activity ceases. As the reversed field strength then continues to increase in magnitude the inception discharge intensity is re-achieved, and discharge occurs once more. This process repeats until the test voltage rises to around the peak of the test voltage. After the peak, due to the existence of the reverse electric field and the descending phase voltage, the electric field intensity may not reach the inception intensity until the voltage falls to zero. Thus, during the descending phase of the absolute value of the test voltage waveform, there are very few surface discharges. When the electrode is of negative polarity, the field is reversed and discharge activity commences once the inception voltage is reached. There is secondary electron emission, but its effect is fairly limited due to the discharge source arrangement. Once the applied voltage has reached the negative peak value, discharge activity ceases until the applied voltage is again positive [15].

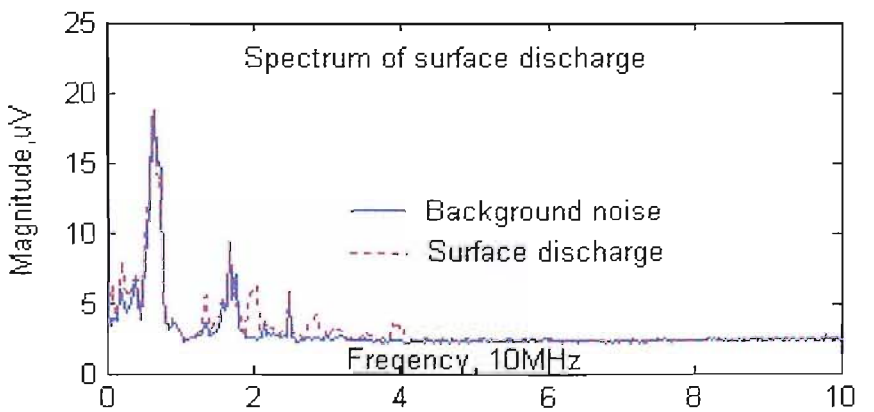

Figure 4.12 Frequency spectra of surface discharge and background noise

Figure 4.12 compares the frequency spectrum of the surface discharge signal with background noise. In this test, the frequency spectrum of the surface discharge contains very few components over 40MHz. The two spectra share several common features however the surface discharge signal also has additional components around 20, 30 and 40 MHz.

Figure 4.13 shows a single pulse of the surface discharge and its corresponding frequency spectrum is shown in Figure 4.14. Analysis of a single pulse using a different time based window (2μs as opposed 20ms) also confirms that a surface discharge detected in this experiment contains frequency components at 20, 30, 40 MHz. Figure 4.15 shows a persistence figure over 1000 cycles of 50Hz test voltage waveform. This figure shows that the surface discharge is steady and there is a balanced pulse group in both half cycles.

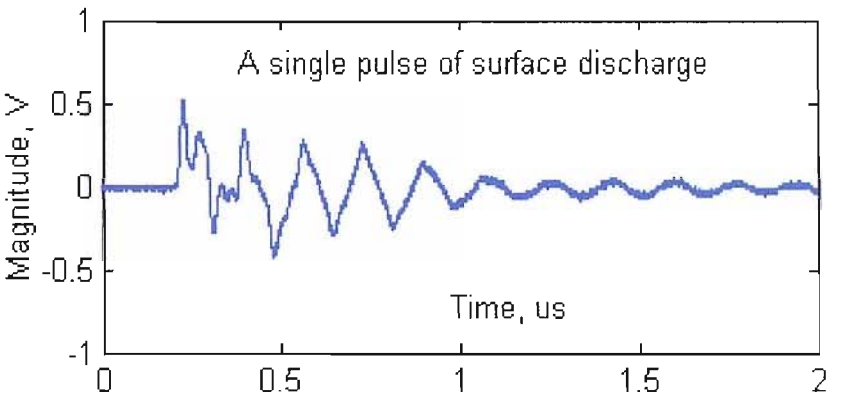

Figure 4.13 A single pulse of surface discharge

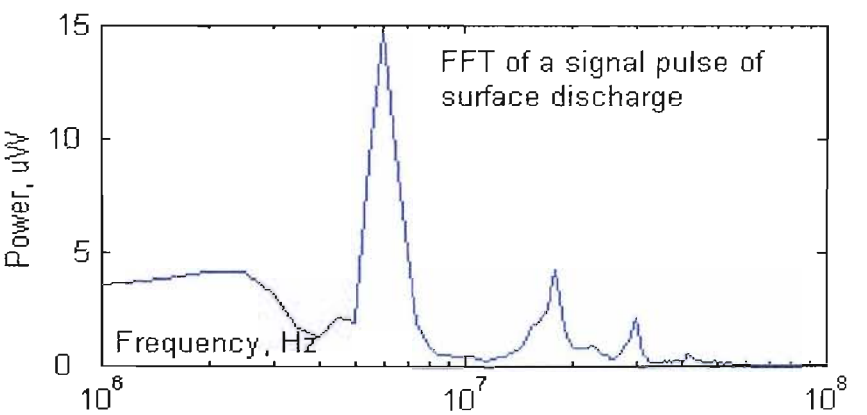

Figure 4.14 Frequency spectrum of the single pulse shown in Figure 4.13

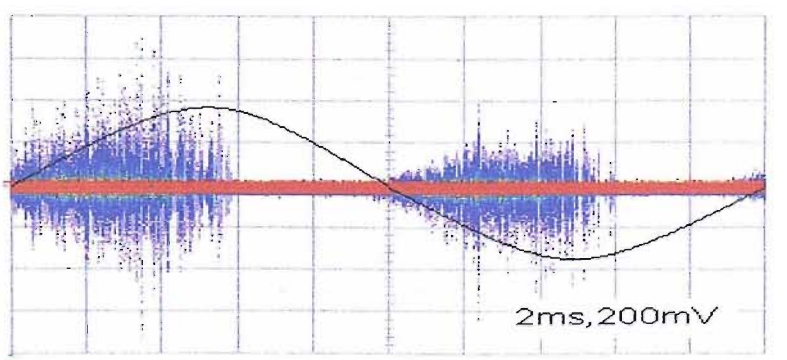

Figure 4.15 Persistence of Surface Discharge

4.4 Floating Discharge in Oil

To produce floating partial discharges, the test system shown in Figure 4.1 plus the discharge sources shown in Figure 4.2 (4) were used; a 50Hz ac high voltage of 17kV was applied to the 60kV bushing. The floating discharge signal is shown in Figure 4.16. The floating partial discharge occurred in the advance of each half cycle of the test voltage waveform. The persistence figure of the floating discharge is shown in Figure 4.17, which was collected over 1000 cycles of the 50 Hz test voltage

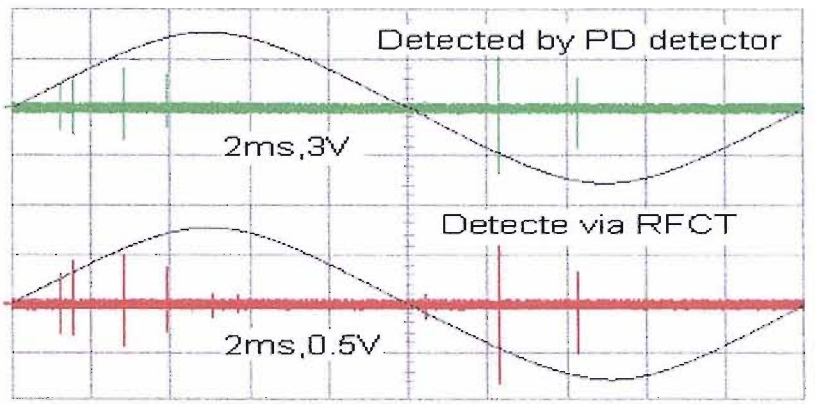

Figure 4.16 Floating discharge

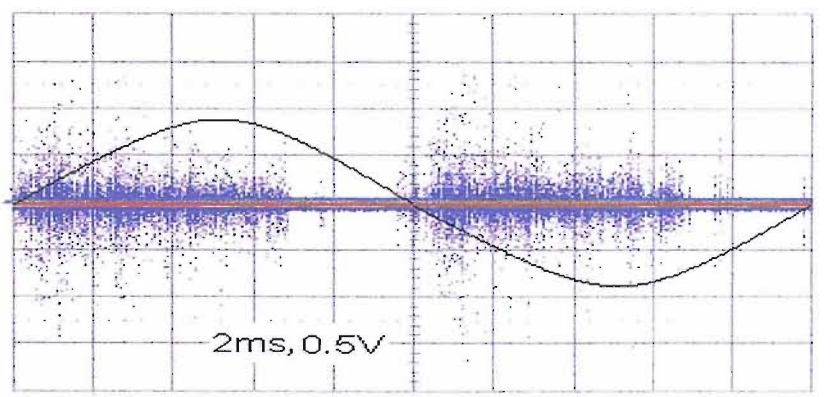

Figure 4.17 persistence figures of floating discharge

The above two figures indicate that floating discharge mainly occurs on the advanced half cycle of the 50 Hz test voltage waveform; there is a balance. The pulse group even cross over the peaks of each half cycle.

The frequency spectrum of the floating partial discharge signal and the frequency spectrum of background noise under identical experimental conditions were obtained using the Spectrum Analyzer. Figure 4.18 shows the comparison between them. The bandwidth of the floating partial discharge signal is quite wide, up to 170MHz. But the magnitudes of the signals over 60MHz are very small compared to those below 60MHz.

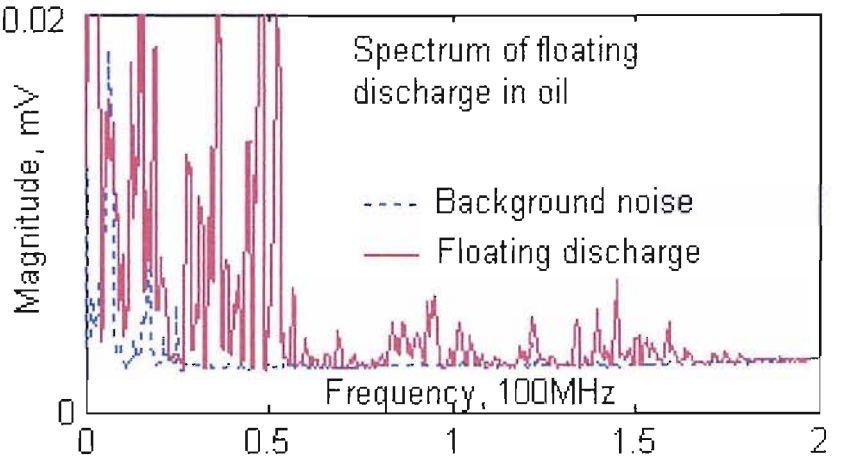

Figure 4.18 Frequency spectra of floating discharge and background noise

Figure 4.19 shows a single pulse of the floating partial discharge and its corresponding frequency spectrum is shown in Figure 4.20. The obvious feature of the floating discharge is that its signal bandwidth is over 170 MHz. This is also indicated by these two figures.

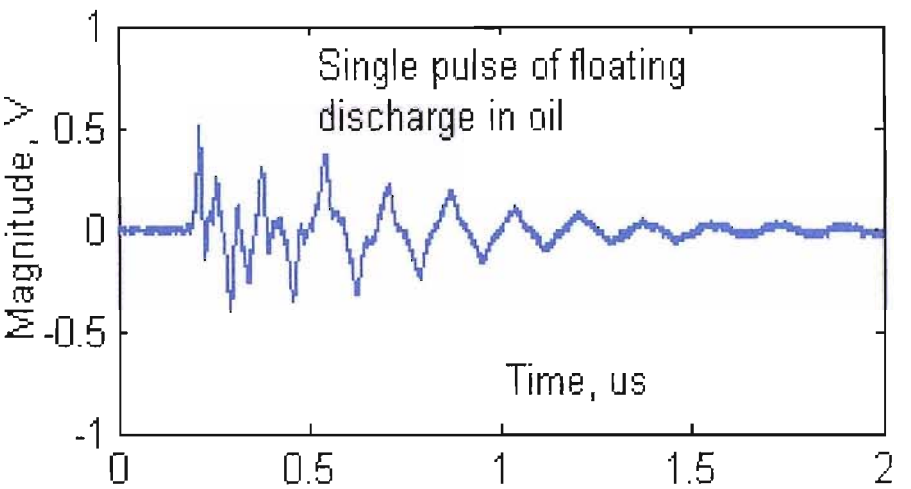

Figure 4.19 a single pulse of floating discharge

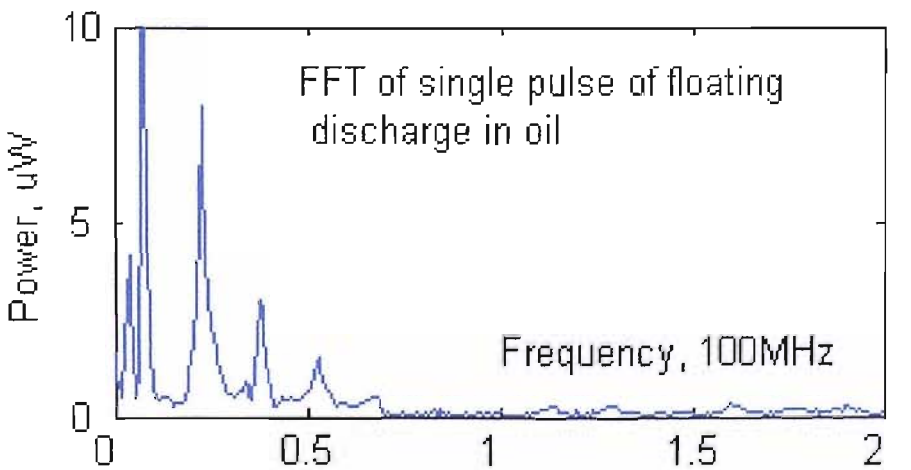

Figure 4.20 Frequency spectrum of the single pulse shown in Figure 4.19

4.5 Void Discharge

As shown in Figure 4.2 (6), a void discharge can be simulated using a sandwich of insulation films. The central film has a 10 mm hole punched into it. The films are manufactured from Low Density Polyethylene and are 0.2 mm thick. When a 7.7 kV voltage was applied onto the bushing a discharge was generated as shown in Figure 4.21. The discharge occurred in the advance of each half cycle of the test waveform. Due to the position of the void between the two electrodes, the magnitudes and numbers of detected pulses in the positive half cycle and negative half cycle of the applied test voltage are similar.

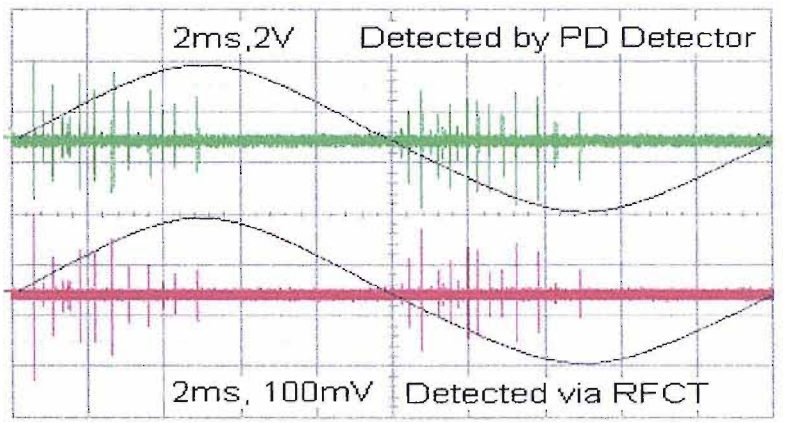

Figure 4.21 Void partial discharges

When the applied test voltage is high enough, the voltage across the void reaches its breakdown value causing discharges to occur. Because the void size is small in the test, the inception discharge voltage is low. Thus, the discharges occur at a low voltage in the first and third quarters of the applied test voltage. During the discharge, the gas in the void is ionized producing positive and negative ions; and these space charges fill the void. Due to the external electric field they move towards the void walls. When they reach the void walls an electric field acting against the external electric field is produced. Due to ionic movement the voltage across the void decreases below that of the inception voltage and discharge activity temporarily ceases. With the increase of external voltage, the voltage across the void reaches its inception value again, causing a new discharge. During discharge activity the internal electric field is increased due to each discharge. The process continues until the applied voltage peaks. After this, the voltage across the void is less than the inception voltage, and discharges do not generally occur until the external applied voltage reaches zero. During this period, an internal voltage within the void is maintained. On passing through zero volts the external voltage is in the same direction as the internal voltage within the void and consequently the inception voltage is achieved causing discharges to reoccur. This process continues until the voltage reaches the peak value of the half cycle. After the peak, the discharge activity ceases until the external voltage reaches its zero point. This process creates the void partial discharge waveforms shown in Figure 4.21.

The persistence figure of the void partial discharge is shown in Figure 4.22, which was collected over 1000 cycles of the 50 Hz test voltage.

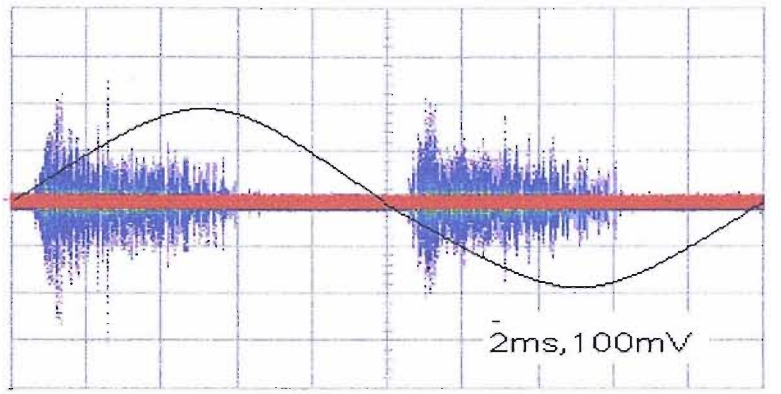

Figure 4.22, Persistence figure of void partial discharge

The frequency spectrum of the void partial discharge signal and the frequency spectrum of background noise under identical experimental conditions were obtained using the Spectrum Analyzer. Figure 4.23 shows the comparison between them. In this test the frequency range of the void discharge is up to 30MHz.

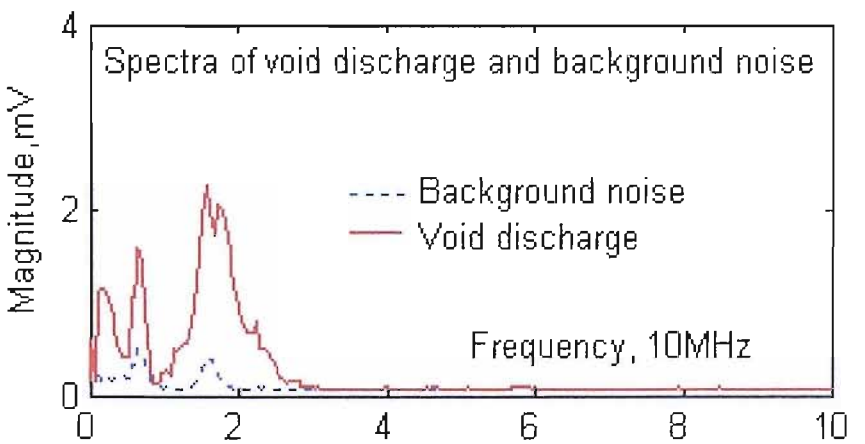

Figure 4.23, Frequency spectra of void partial discharge and background noise

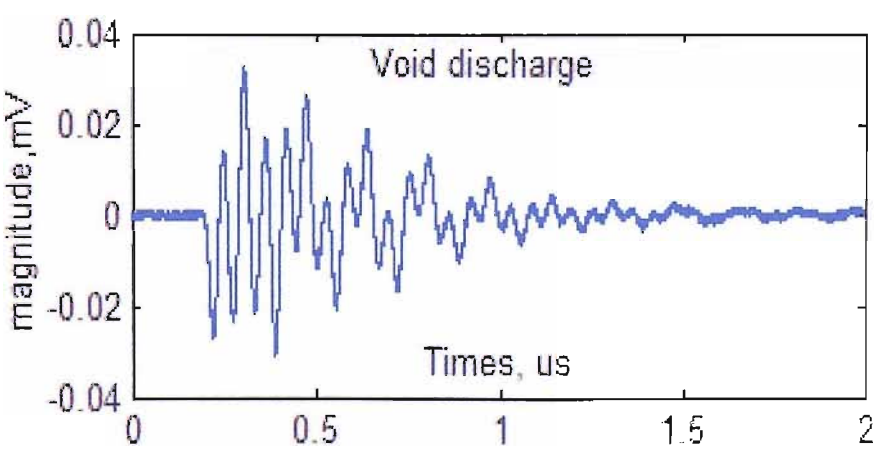

Figure 4.24, A single pulse of void partial discharge

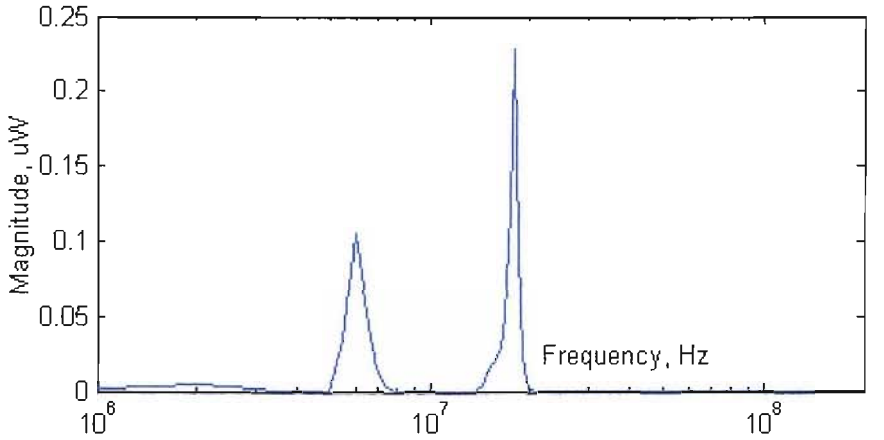

Figure 4.25 Frequency spectrum of the single pulse of void partial discharge

Figure 4.24, shows a single pulse of the void partial discharge and its frequency spectrum is shown in Figure 4.25.

From above figures, the void discharges are seen to occur mainly on the advanced half cycle of the 50 Hz test voltage waveform. There is a balance in both the positive and negative half cycles. The pulse groups even extend across the peak in the middle of each half cycle.

4.6 Needle-plane Discharges in oil

Using the PD source (5) as shown in Figure 4.2, needle-plane discharges in oil were obtained. The PD source placed in transformer oil had an electrode with a needle tip and a grounded metal plane; an insulation pressboard of 1.5mm thick was placed between them; the distance from the needle tip to the pressboard was around 2mm. The measurement circuit was similar to that shown in Figure 4.1, but the PD detector was not used in the test. A zero crossing detector was used as an external trigger in the test; the trigger is synchronous to the 50 Hz test voltage.

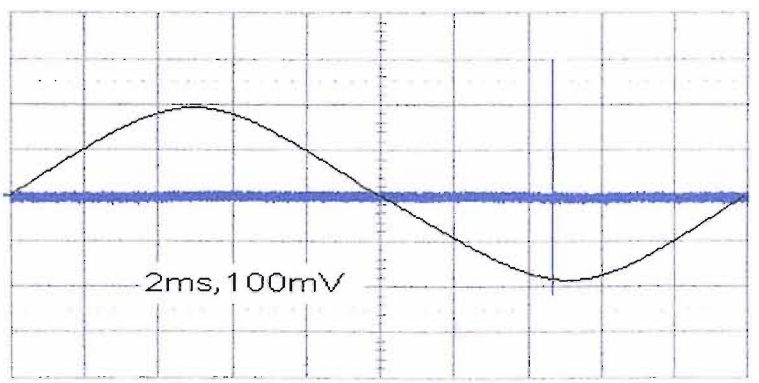

Figure 4.26 a needle- plane partial discharge pulse occurring
at the negative half cycle of the 50 Hz (20ms) test voltage waveform

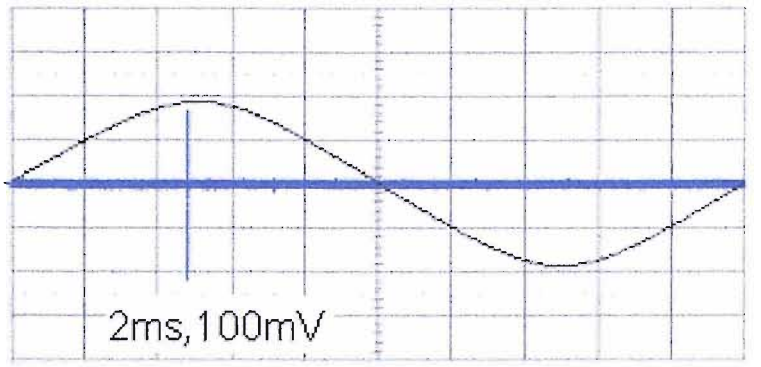

Figure 4.27 a needle- plane partial discharge pulse occurring
at the positive half cycle of the 50 Hz (20ms) test voltage waveform

When a 24kV voltage was applied to the PD source a discharge pulse as shown in Figure 4.26 or Figure 4.27 was captured using the oscilloscope. The pulse was sporadic and occurred with occasional jumps around the peak middle of the positive and negative half cycles of the 50Hz (20ms) test voltage waveform. As the test voltage increased to 29kv, a new type of discharge waveform was obtained as shown in Figure 4.28. The pulse groups appeared unsteady near the middles of both half cycles of the 50 Hz test voltage waveform. The magnitudes of the pulses were also always irregular. Figure 4.29 is the persistence figure of over 1000 cycles of the test voltage.

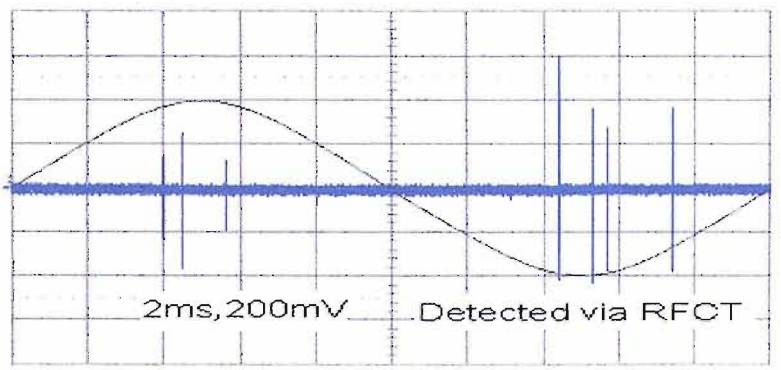

Figure 4.28, Needle-plane partial discharges in a 50Hz test voltage waveform

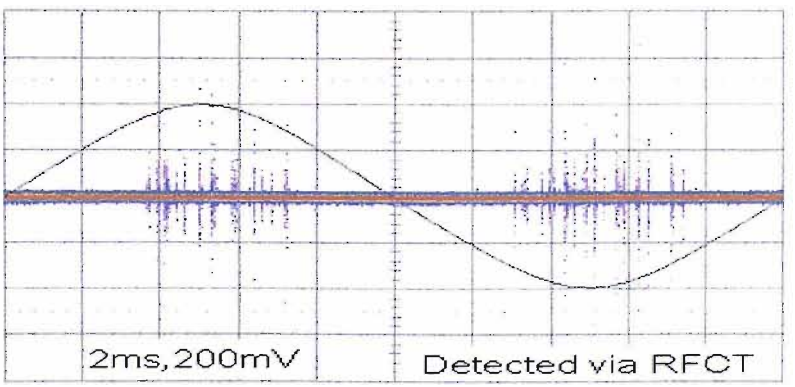

Figure 4.29, Persistence figure of needle-plane partial discharges
in a 50Hz test voltage waveform

For the insulation system used in this investigation (the PD source (5)), a partial discharge depends on the inception discharge stress between the needle electrode and the grounded metal plate. Due to the existence of the insulation oil and the oil-immersed insulation pressboard, the inception discharge voltage might be higher. The partial discharge therefore generally occurred at a higher voltage, around the middle of both half cycles of the test voltage.

Using the Spectrum Analyzer, the frequency spectra of the needle-plane partial discharge and the background noise were measured. The results are shown in Figure 4.30. In this test the frequency spectrum of the needle-plane partial discharge was found to extend up to 130MHz. In Figure 4.30 the blue curve is the background noise that was measured when the PD source was de-energized.

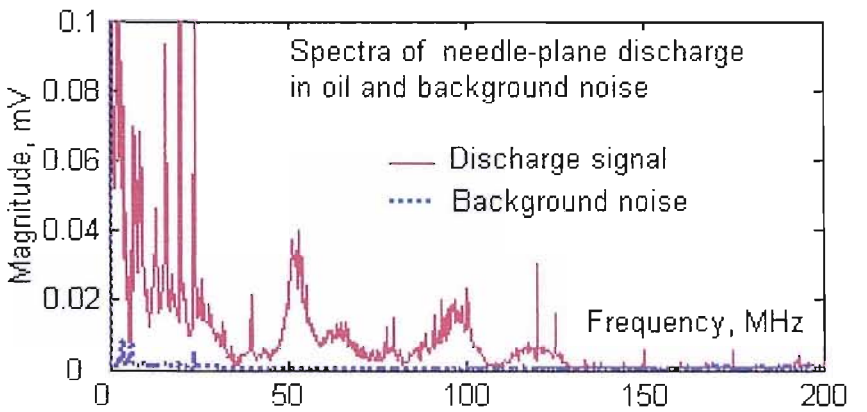

Figure 4.30 Frequency spectra of needle-plane partial discharge in oil and background noise

The time record of a single pulse of the needle-plane partial discharge in oil is shown in Figure 4.31, which was obtained using the oscilloscope when the test voltage was kept on 29kV. In the test the oscilloscope was set with 1000 sample points at 500 MHz/s. The power spectrum of the single pulse is shown in Figure 4.32. This was obtained from a FFT calculation using Matlab. From Figure 4.32, one deduces that the majority of the energy of the pulse occurs below 70MHz.

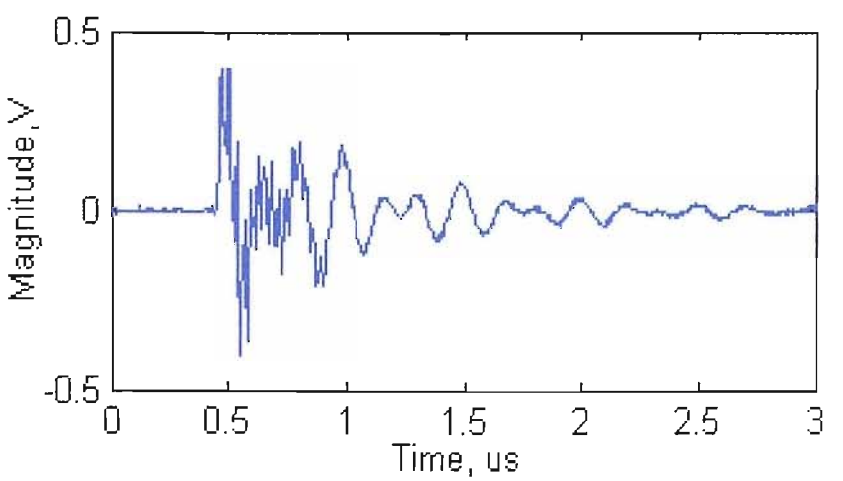

Figure 4.31 a single pulse of the needle-plane partial discharge in oil

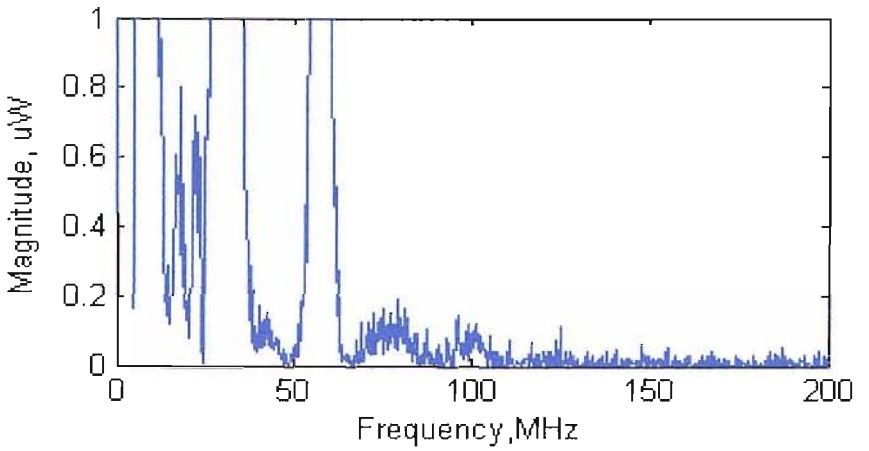

Figure 4.32 Power spectrum of the single pulse

4.7 Conclusions

The waveforms measured using the PD detector reflected the situations and distribution of partial discharges in the time domain and in magnitude. The resulting patterns from the bushing tap via the RFCT are similar to that on the PD detector. This shows that the measured time domain waveforms at the bushing tap using the RFCT can represent the partial discharge distribution at the bushing core bar. The classification of the partial discharges from bushing top measurements can be concluded as the following:

- Corona discharges in air have obvious properties in the shape of pulse groups and phase positions on a 50Hz cycle time of the test voltage. They occurred at the middle of each half cycle. In this test its bandwidth was only up to 3-4 MHz.
- The pulse groups of the surface discharge in air occurred at the advance of each half cycle of the test voltage. Its frequency range is up to 40MHz in this test.
- The magnitudes of the pulses of the void discharge are small when the void is small. Its pulse groups occur at the advance of each half cycle of the test voltage. Its bandwidth is only up to 30MHz in this test.
- Floating discharge has a wider bandwidth of up to 170MHz. Its pulse groups occurred at the advance of each half cycle of the test voltage.
- The needle-plane discharge in oil is complex. It occurred at the middle of each half cycle of the test voltage. But depending on the test voltage, its pulses could be sporadic with occasional jumps, unsteady in magnitude. The positions of the pulses could be variable. Its bandwidth is over 130MHz in this measurement.

Table 4.1 shows the comparison of the above PD signals for their location in the half cycles, their frequency bandwidth and other characteristics.

Discharge type	Phase position	Frequency Bandwidth	Other characteristics
Corona with remote earth	In the middle of the negative half cycle	Up to 3-4 MHz	Steady in magnitude and phase position
Corona with near earth	In the middle of each half cycle	Up to 3-4 MHz	The magnitude of the pulses on positive half cycle are bigger
Surface discharge in air	At the advance of each half cycle	Up to 40 MHz	
Void discharge	At the advance of each half cycle	Up to 30 MHz	Small when void is small
Floating discharge in oil	At the advance of each half cycle	Over 170 MHz	Unsteady in magnitude and phase position
Needle-plate discharge in oil	In the middle of each negative half cycle	Over 130 MHz	Sporadic, unsteady in magnitude; variable in phase position

Table 4.1 Comparison of the different discharges

Chapter 5

Propagation characteristics of high frequency signals within a transformer model

In recent years, the propagation characteristics of partial discharge signals within power transformers have been used to realize diagnosis and monitoring of power transformer condition. The techniques developed have all been based on PD measurements either for the narrow band or using wide band PD signals. These approaches are usually used for offline measurements, in which the apparent charges of partial discharges can be detected. However the localization of the discharges which is indispensable for good maintenance cannot usually be performed [37]. In these techniques the parameters, such as charge magnitude, phase of the pulse relative to power frequency waveforms, repetition rate and the energy of each pulse are more important and useful in the judgements for the condition of transformers. IEC60270 [16] gives useful guidance of application of the above mentioned techniques and parameters.

As described before, partial discharge localization can be made by analyzing the shape of partial discharge signals in the time domain and by analysing the components in the frequency domain. Partial discharge signals are usually distorted as they are transmitted. The amount of distortion depends on the following factors: the distance from the discharge source to the detection point; the media material of the paths through which the PD signal is travelling. Previous researchers have identified that a sensor bandwidth greater than 10 MHz is appropriate for analysis of PD data [39].

This chapter introduces the investigations into a practical transformer model system, and the propagation characteristics of high frequency signals of up to 200MHz within the model. It has focused on measurement and analysis of the frequency responses, the impulse responses, and the responses to real PD signals. All these are respectively carried out on the model in the following conditions: the windings in air; the windings in an earthed tank without oil; the windings in an earthed tank with oil and the 60kV bushing plus the windings in the oil-filled earthed tank.

5.1 Transformer Model and its Windings

The windings of the transformer model were provided by Alstom, including an interleaved disc winding and a plain disc winding. The transformer model was further developed by the Electrical Power Engineering Group of Southampton University. Photo 5.1 shows the transformer model. After some necessary tests without oil the transformer model was filled with transformer oil. The oil used was made in Stanlow Works, UK. Its specification is BS148:1998 class 1. Its main electric characteristics is: the electric strength (breakdown, mm) : >30kV.

Photo 5.1 Transformer Model

5.1.1 Essential Structure of the Transformer Model

Figure 5.1 is the cross-section view of its internal construction. The construction sizes are given in Appendix A.

The transformer model consists of two windings, as shown in Figure 5.1. The upper winding has a

type of interleaved disc winding; the lower one is a plain disc winding. The two windings have the same construction size and use identical materials. Every pair of discs of the both windings provides a terminal as a measurement point. A metal cylinder connected to earth was placed inside the windings as an iron core for the model.

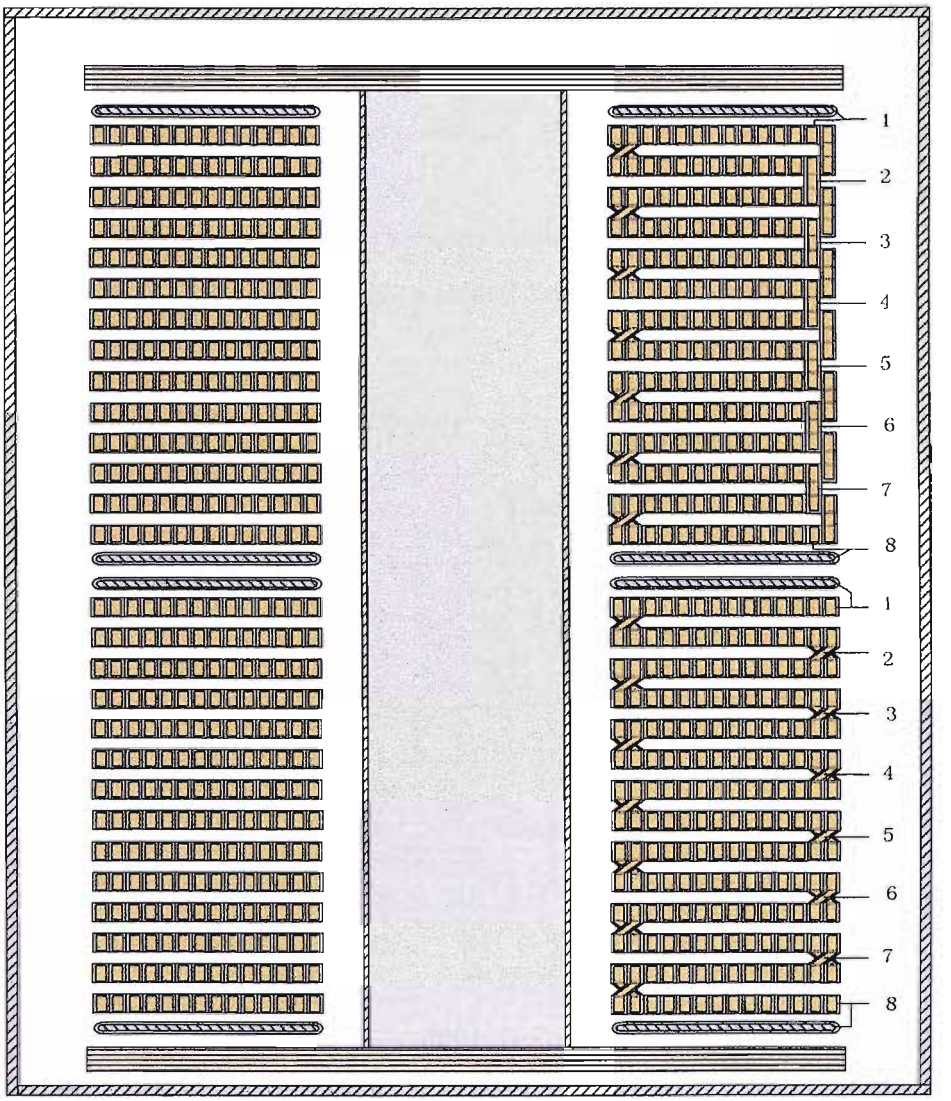

Figure 5.1 the cross-section view of the transformer model

5.1.2 General Electrical Parameters of the Transformer Model

The electrical parameters of a transformer model are required for computerised modelling and simulation leading to an explanation of the propagation characteristics of high frequency signals within a transformer winding.

In the transformer simulation model, both windings are disc-type and each winding includes 14 discs. By dividing each winding into 7 sections (pairs) and regarding each section as having individual elements (parameters) of itself, and based on the mathematical model for a transformer

winding proposed by Wagner [72], the mathematical model of the model transformer was constructed as shown in Figure 5.2 (only four sections are illustrated in the figure). The main parameters are:

- K, series capacitance between immediate sections
- Cg, capacitance to ground (tank and core)
- L, self-inductance of the section
- Mi, mutual inductance with all other sections
- Rs, frequency-dependent resistance
- G, conductance of insulation loss between immediate sections
- Gg, conductance of insulation loss to ground (tank and core)

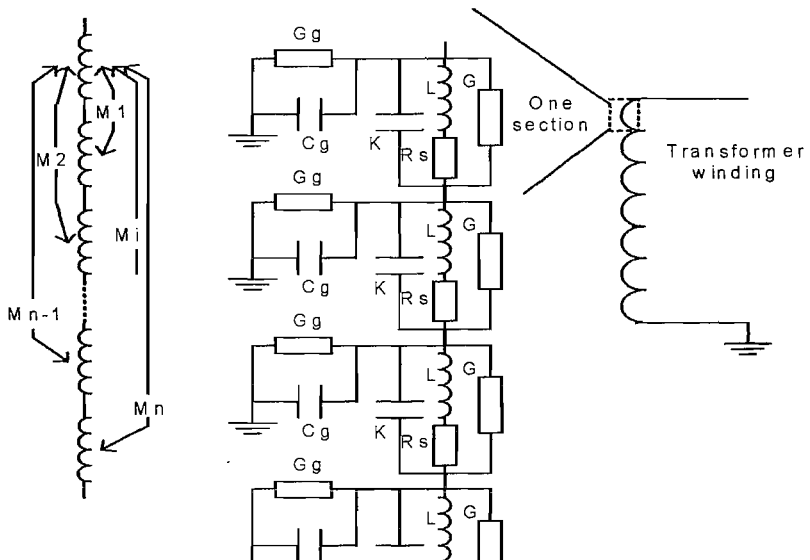

Figure 5.2 Parameter construction of the transformer model

The constructional electrical parameters of the transformer model are very complex. The propagation process of high frequency signals within the transformer model is the result of these parameters functioning together and therefore this is a complicated problem. The simulation model ignores non-linearities of the system, whereas the experimental model allows us to practically investigate signal propagation.

5.2 Frequency Responses of Windings and Transformer Model

As described above, the construction of the transformer simulation model was very complicated. It includes many physical parameters, such as capacitance, inductance, conductance and resistance

etc. These make the propagation of high frequency signals within the transformer model very complex. Previous research [37] on the frequency response of high frequency signals within transformers has concentrated on a bandwidth of up to 10MHz. But PD signals within a real transformer may include even higher frequency components, so it is important to practically investigate the behaviour of higher frequency signals within the windings of the transformer model.

In order to understand the propagation characteristics of the high frequency signals within the transformer model, the bandwidth in this investigation was extended up to 200MHz.

5.2.1 Frequency Responses of the Interleaved Disc Winding

5.2.1.1 Frequency Responses of the Interleaved Disc Winding in Air

Before the windings were installed within the tank and core, measurements of frequency response on the interleaved disc winding in air were carried out using the network analyzer, Agilent 4395A. In the test the measurement frequency range was set from 100 Hz to 200MHz; the sample average was 20 and sample bandwidth was 30Hz. The measurement circuit is shown in Figure 5.3. Due to the absence of the tank and core during this test the mathematical model of the interleaved disc winding can be regarded as without Cg and Gg in the lumped parameter circuit of Figure 5.2.

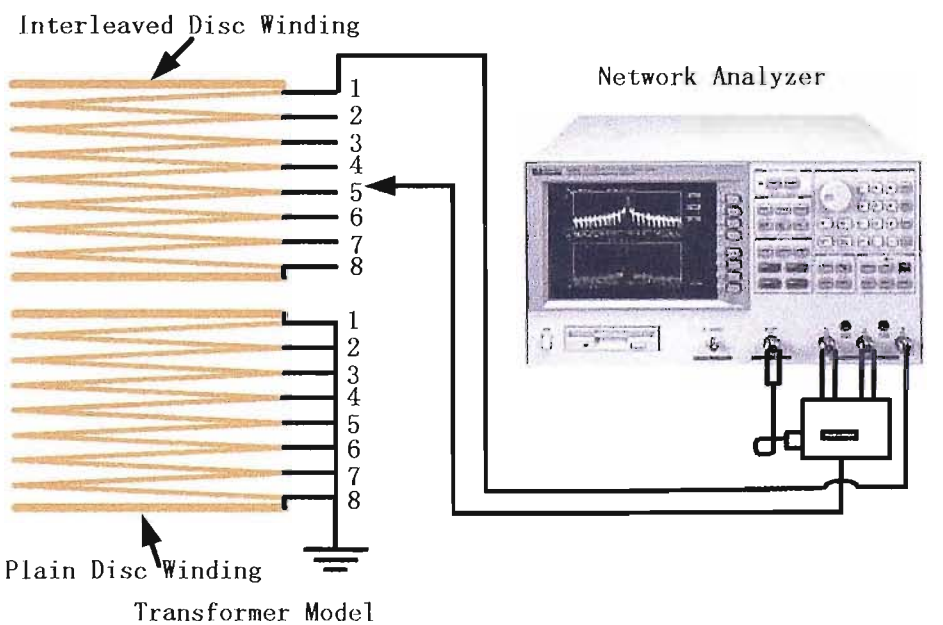

Figure 5.3 Frequency response measurement circuit
for the interleaved disc winding in air

In the test a calibration signal was in turn injected into the interleaved disc winding from the 2nd to the 8th terminals; while the measurement point was at terminal 1. The frequency responses of the interleaved disc winding in air are shown in Figure 5.4.

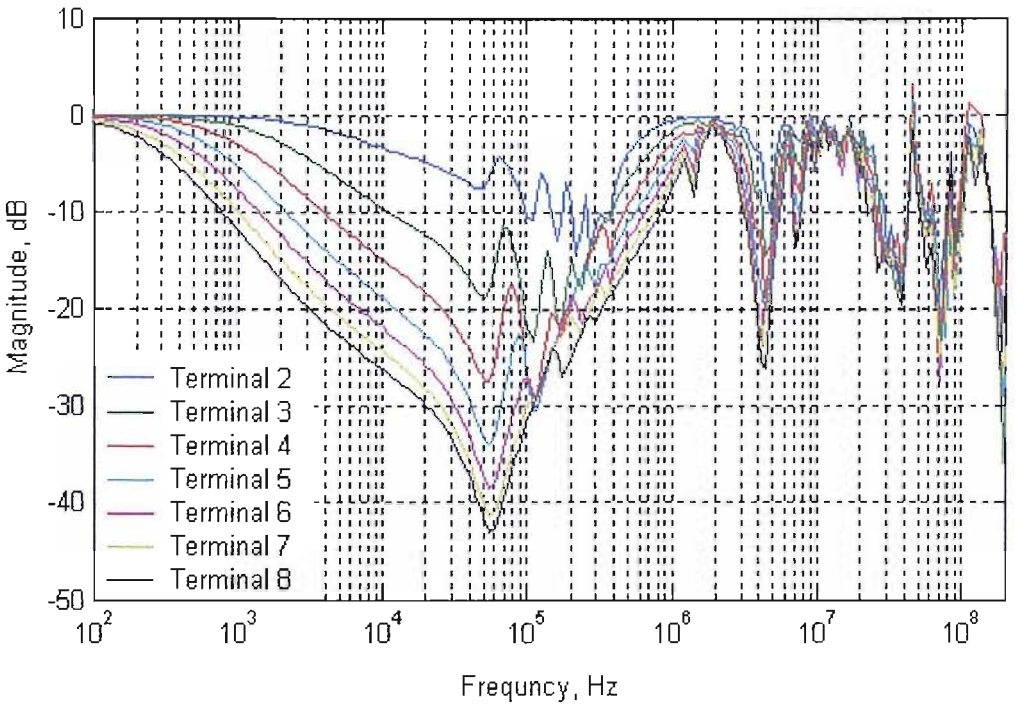

Figure 5.4 Frequency responses of the interleaved disc winding in air

The measured results indicate that in every case for the interleaved disc winding in air, the first peak resonance is at around 60 kHz. As the number of sections involved in the measurement were increased the first peak resonance moves across the low frequency range towards 100 kHz. Across the bandwidth from 1MHz to 200 MHz, the frequency responses are similar. This means that during the high frequency range the attenuation per section of the winding is small. The frequency spectrum of the winding shows that at frequencies above 20 MHz the inter-winding capacitance dominates, and consequently, there is little attenuation as the number of winding discs between the PD source and measurement point increases. Below 20 MHz signals propagate through the winding and are attenuated by each additional winding disc

5.2.1.2 Frequency Responses of the Interleaved Disc Winding in the Tank without Oil

After placing the winding into a grounded tank with a grounded core, but without oil, the frequency responses were measured again. This time the mathematical model can be regarded as the same as the circuit in Figure 5.2. The measurement circuit is shown in Figure 5.5. The Aligent 4395A Network Analyzer used to detect the frequency response of the model was set with a frequency range from 100 Hz to 200MHz; the sample average was 20 and sample bandwidth was 30Hz. The order of injection signal is from the 2^{nd} to the 8^{th} terminals. Figure 5.6 illustrate the results and a comparison between the different terminals.

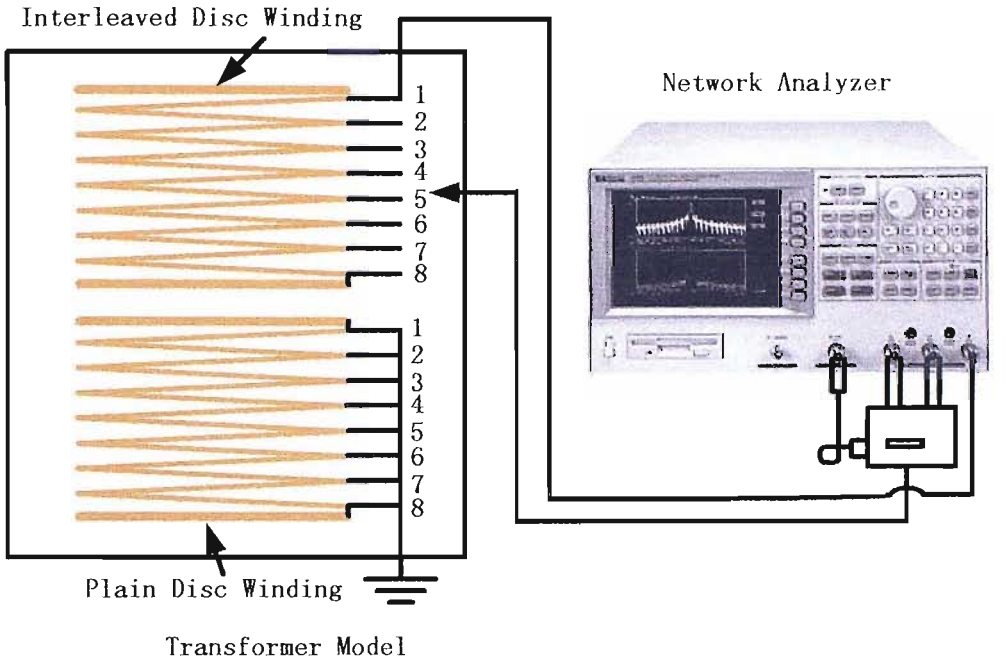

Figure 5.5 Frequency response measurement circuit
for the model with the interleaved disc winding without oil

Analysing the figure 5.6, the resonance peaks of the winding model increase across whole frequency range with the increase in the number of sections involved in the measurement. A remarkable characteristic is that the peak resonances of different sections occur at similar frequency break points. Another feature is that the frequency spectra of all sections have a similar shape from 1MHz to 200 MHz, which means that during this frequency range the attenuation per section of the winding is small.

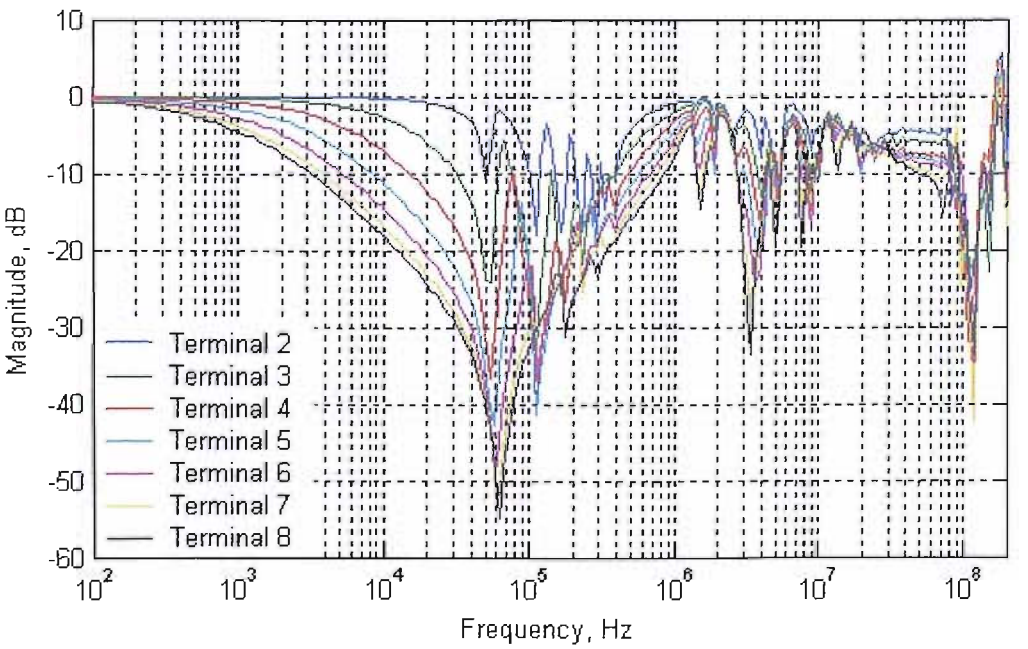

Figure 5.6 Frequency response of the interleaved disc winding in the tank without oil

By comparing Figure 5.6 with Figure 5.4, the impedance across the whole frequency range is seen increase. This is due to the influence from Cg and Gg. Cg and Gg attenuate the injected calibration signal, so the outputs at the measuring terminals are reduced. But the positions of the peak resonances are not greatly influenced.

5.2.1.3 Frequency Responses of the Interleaved Disc Winding in the Oil-filled Tank

After filling the transformer model with transformer oil, the frequency responses of the interleaved disc winding were measured again using the measurement circuit shown in Figure 5.5. The Aligent 4395A Network Analyzer was set with the same parameters as the description in section 5.2.1.2. The results are shown in Figure 5.7.

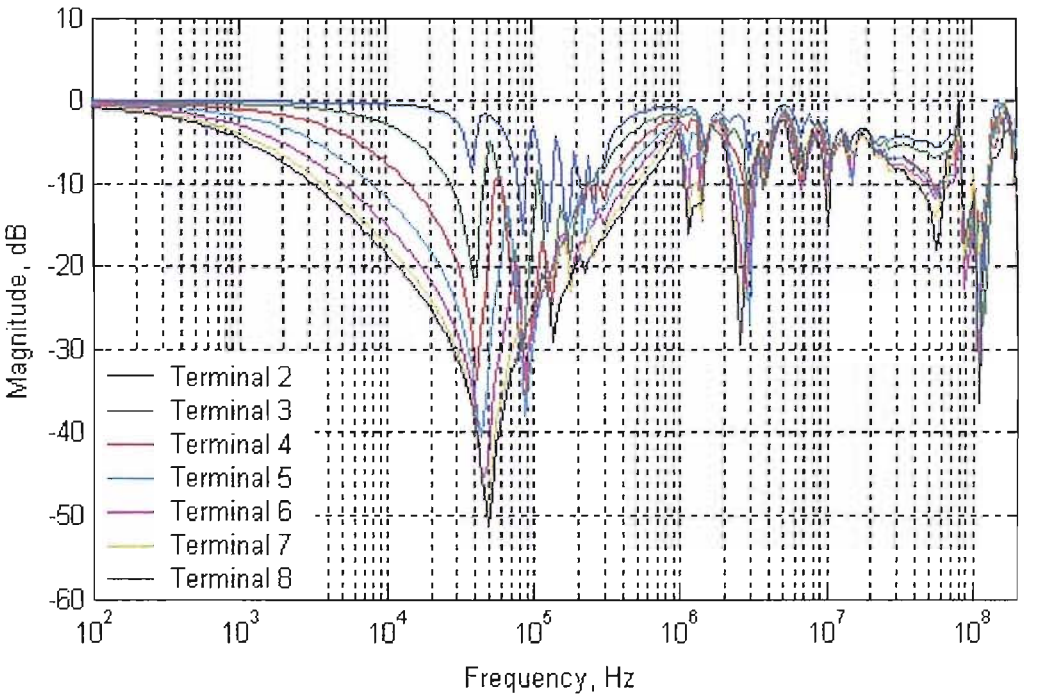

Figure 5.7 Frequency responses of the interleaved disc winding in the oil-filled tank with oil

Comparing Figures 5.4, 5.6 with 5.7, the following changes due to filling with oil were found: the resonance break points below 20 MHz altered, becoming lower; and the magnitudes of the peak resonances were reduced. This is due to the functions of the capacitance and conductance parameters (see Figure 5.2). From Figure 3.8, across the frequency range of up to 25MHz, the ability of oil to pass signals is higher than air. This led to increases in the capacitance parameters, and furthermore caused the movement of the resonance peaks towards lower frequencies (see Figure 3.2). It also resulted in the reductions of resonant magnitudes across the frequency range up to 25MHz.

5.2.1.4 Frequency Responses of the Non-oil Transformer Model System with an Interleaved Disc Winding

The transformer model system used here includes the transformer model and the 60kV bushing. Before being filled with oil, the frequency responses of the interleaved disc winding transformer model system were measured at the bushing tap of the connected bushing via a RFCT. Figure 5.8 shows the measurement circuit. The 60kV bushing, model 60HC755, was connected to the 1st terminal of the interleaved disc winding. The bushing's frequency spectrum is shown in Figure 3.1. The RFCT was wrapped three turns of wire to improve the measurement gain. Its frequency spectrum is shown in Figure 3.5. The Agilent network analyzer was set with a measurement range from 10 kHz to 200 MHz, 20 average sample and 3 kHz sample bandwidth. During measurement the calibration signals were injected in turn into the interleaved disc winding from the 1st terminal to the 8th terminal and the measurement was carried out at the bushing tap via the RFCT. Figure 5.9 show the results.

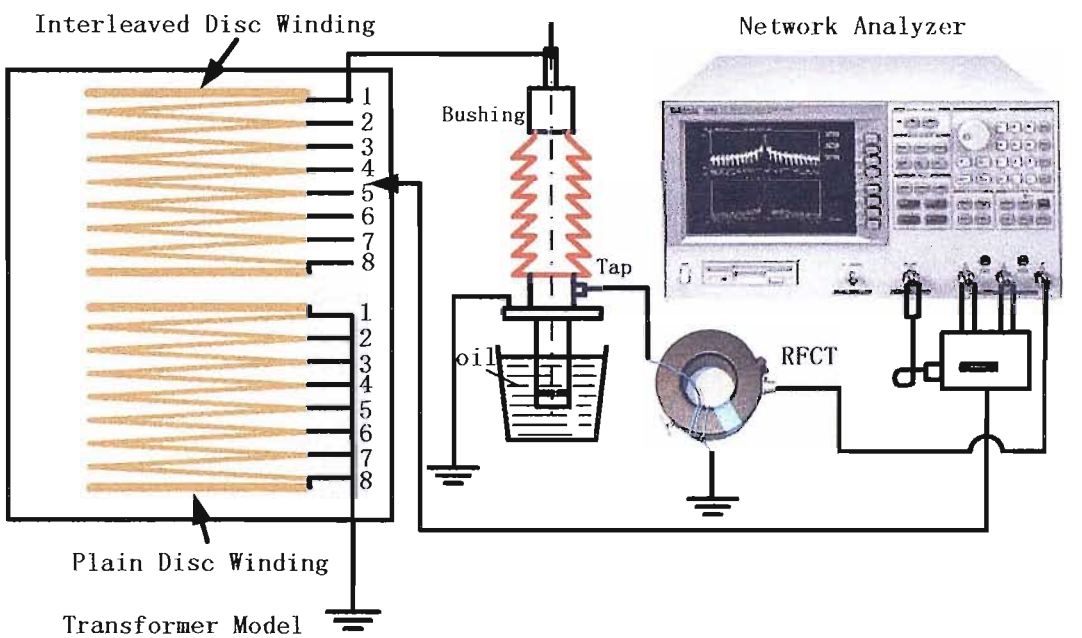

Figure 5.8 Frequency response measurement circuit

Analysing Figures 5.9 and 5.6, and referring to the frequency spectra of the 60 kV bushing and RFCT shown in Figures 3.2 and 3.5, the following conclusions were drawn:

The influence of the bushing on the propagation characteristics of the high frequency signals within the whole transformer model system was very apparent. This is due to the bushing having the property of a high frequency pass filter (see Figure 3.2). Across the low frequency range (up to 25 MHz), with an increase of frequency the ability of the transformer model system to pass the signals also increases. The ability of the RFCT to pass signals also influenced the responses across

the whole of the measurement range from 10 kHz to 200 MHz. At low frequencies, the peak resonance points due to the winding are still visible. Their corner frequencies are similar to those for the frequency response curves of the interleaved disc winding (Figure 5.6). The peak magnitudes are reduced because of the attenuation due to the bushing and RFCT. Furthermore, additional high frequency resonances exist due to the combination of the winding, bushing and RFCT. Above 1 MHz the attenuation per section of the winding is small.

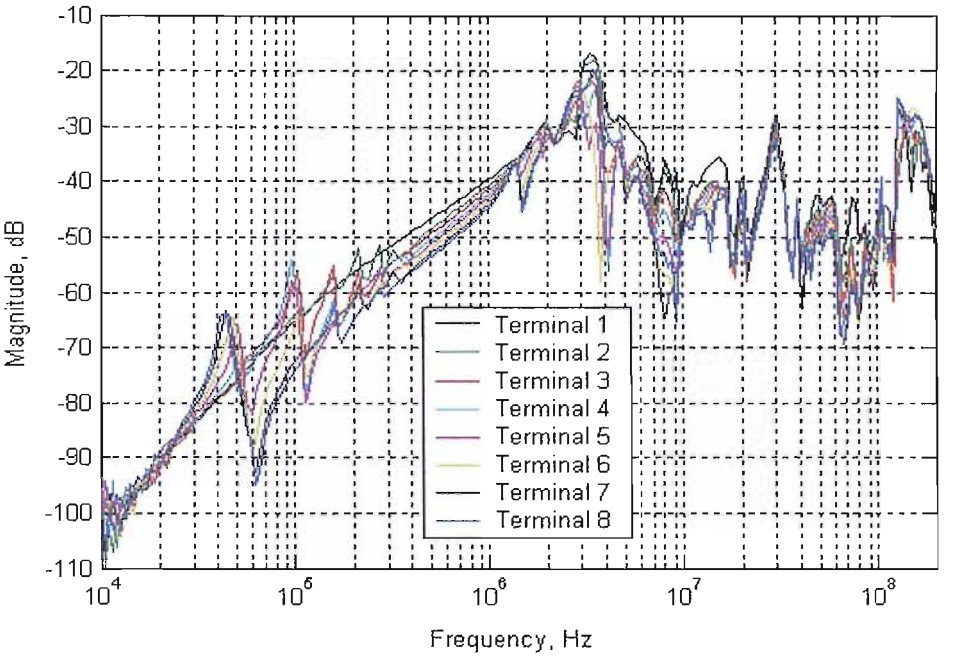

Figure 5.9 Frequency response of the interleaved disc winding transformer model system without oil, measured at the 60kV bushing tap via a RFCT

5.2.1.5 Frequency Responses of the Oil-filled Transformer Model System with an Interleaved Disc Winding

Using the same measurement circuit as shown in Figure 5.8 but with the transformer model filled with oil, the frequency responses of the interleaved disc winding transformer model system as shown in Figure 5.10 were obtained. The devices were set with the same parameters as those of section 5.2.1.4.

Comparing Figure 5.10 with Figure 5.9, the following features are found:

There are reductions in magnitudes of all curves below 25MHz; and in this frequency range all the corner frequency of peak resonances decreased. This is due to the increases in the capacitance parameter values caused by the presence of oil (see Figures 5.2 and Figure 3.8). From Figure 5.10, above 5 MHz the resonances are almost similar. Above 1 MHz the attenuation per section of the winding is small.

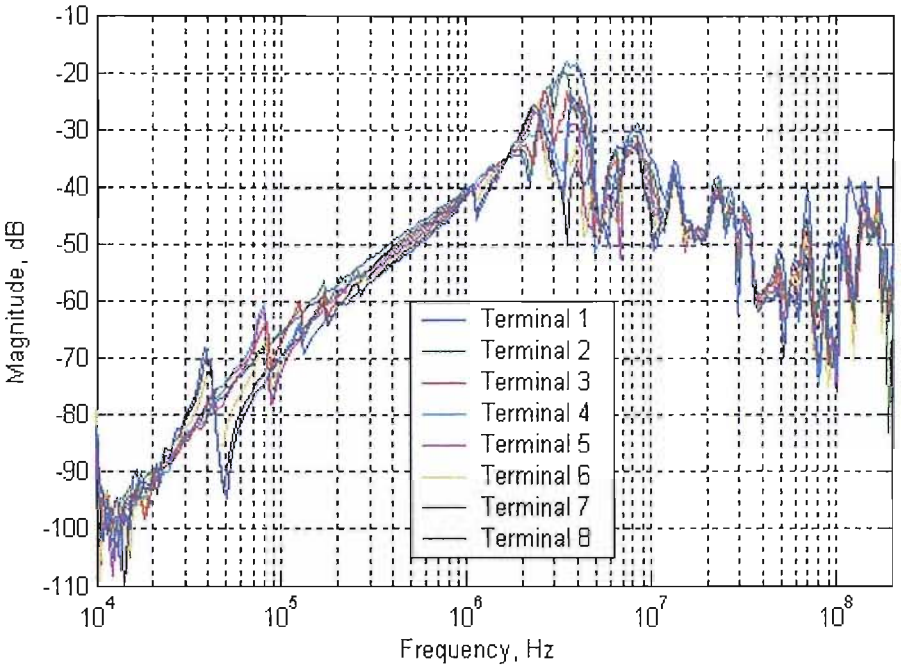

Figure 5.10 Frequency response of the interleaved disc winding transformer model system with oil, measured at the 60kV bushing tap via a RFCT

5.2.2 Frequency Responses of the Plain Disc Winding

The plain disc winding has the same geometry sizes as the interleaved disc winding (Figure 5.1). The difference between them is that there are different connections between each disc. This reduces the inter-turn capacitance and inter-disc capacitance compared to the interleaved disc winding. Thus, the frequency response of the plain disc winding is different from the interleaved disc winding. Consequently, the measurements of section 5.2.1 were repeated for the different winding arrangement.

5.2.2.1 Frequency Responses of the Plain Disc Winding in the Tank without Oil

The measurement circuit as shown in Figure 5.11, connected to the plain disc winding arrangement, was set up for this test. The frequency range of the Aligent 4395A Network Analyzer was set from 100 Hz to 200MHz; the sample average is 20 and the sample bandwidth is 30Hz. The measurement was carried out without oil in the model tank. The calibration signals from the network analyzer were injected into the plain disc winding in turn from 2^{nd} to 8^{th} terminals. The output signals were collected at the 1^{st} terminal using the network analyzer. Figure 5.12 give the measured results at different terminals and a comparison between them.

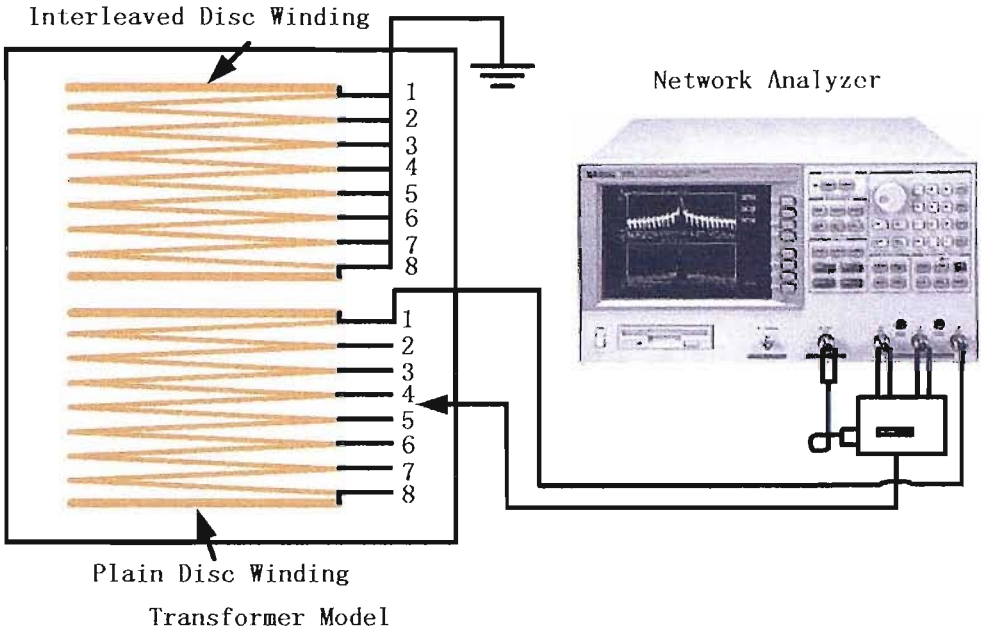

Figure 5.11 Frequency spectrum measurement circuit
for the plain disc winding transformer model

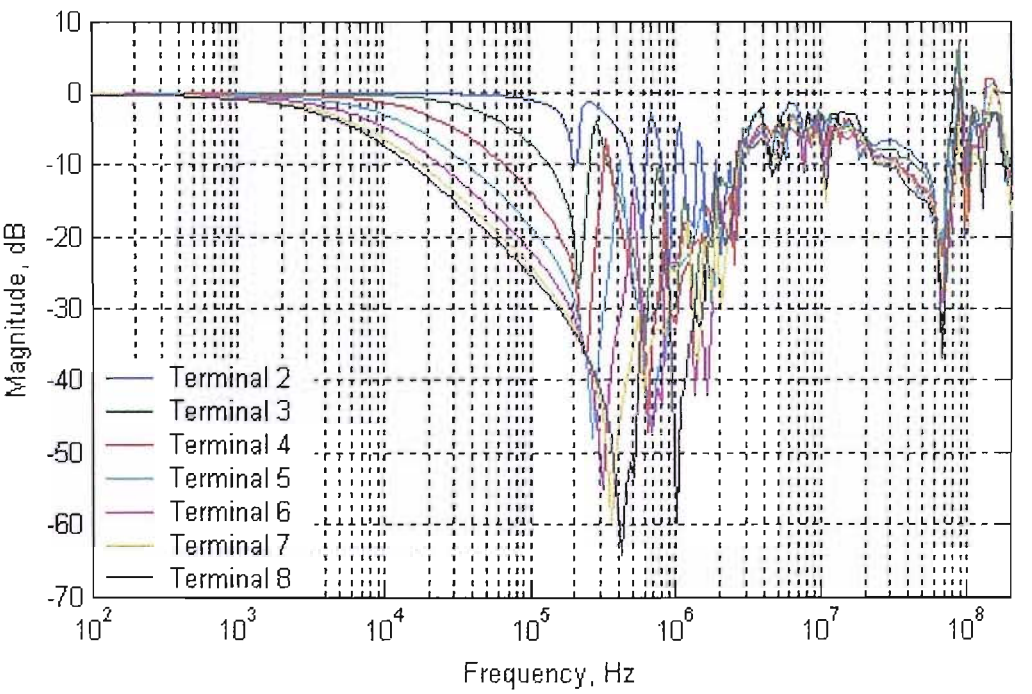

Figure 5.12 Frequency responses of the plain disc winding in the tank without oil

By analysing the above two figures, it is seen that with an increase of discs involved in the measurement, the magnitudes of the resonances of the model increase across whole frequency range; the lower the frequency, the more the increase is. The first peak resonance had a marked increase. A characteristic is that the peak resonances of different sections have similar frequency break points. Another property is that the frequency spectra shapes are similar in high frequency region (over 20MHz), which means the attenuation per section of the winding is small.

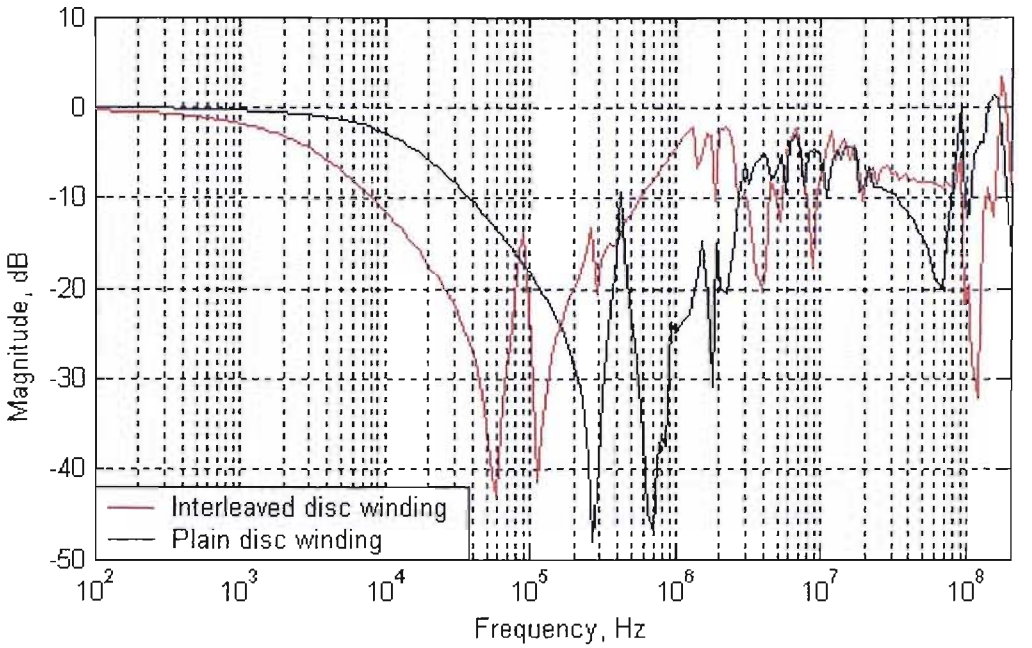

Figure 5.13 the comparison of the frequency responses of the both inter leaved disc winding and plain disc winding in the non-oil tank; the signals were injected at terminal 5

Figure 5.13 shows the frequency responses for terminal 5 of the both interleaved disc winding and plain disc winding in the non-oil tank. The first peak resonance corner frequencies of the plain disc winding are at higher frequencies, compared to those of the interleaved disc winding by approximately around 300 kHz.

5.2.2.2 Frequency Responses of the Plain Disc Winding in the Oil-filled Tank

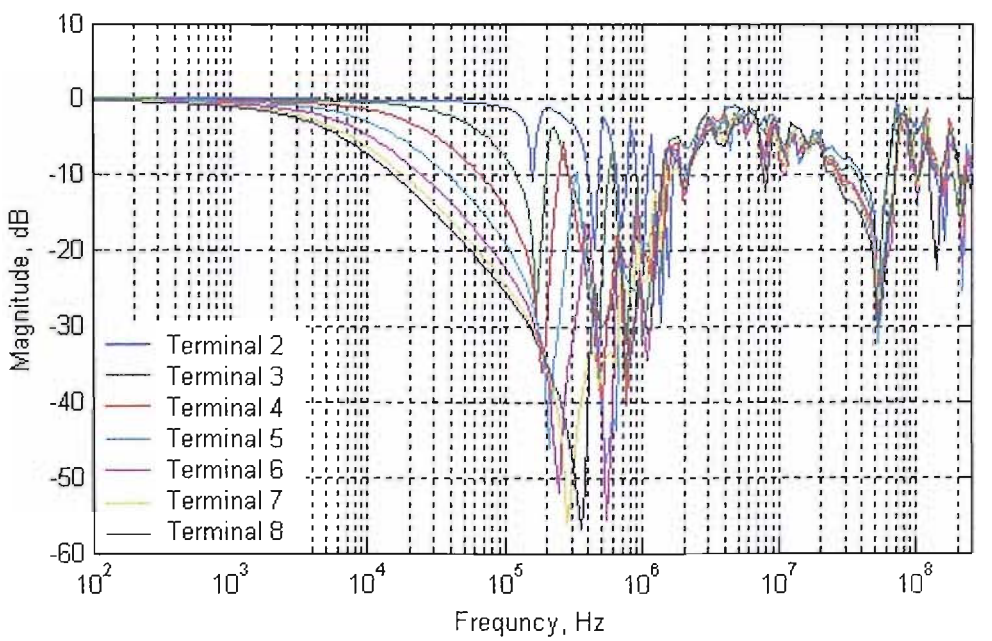

Figure 5.14, Frequency responses of the plain disc winding in the oil-filled tank

Using the same measurement circuit as shown in Figure 5.11, under the same experimental conditions as described in 5.2.2.1, the frequency response of the plain disc winding in the oil-filled tank was obtained. Figure 5.14 show the measured results.

Comparing Figure 5.14 with Figure 5.12, there is a reduction in magnitude of the resonant peaks below 20 MHz and the frequencies are at lower values. This is due to the presence of oil (see section 5.2.1.3)

5.2.2.3 Frequency Responses of the Non-oil Transformer Model System with a Plain Disc Winding

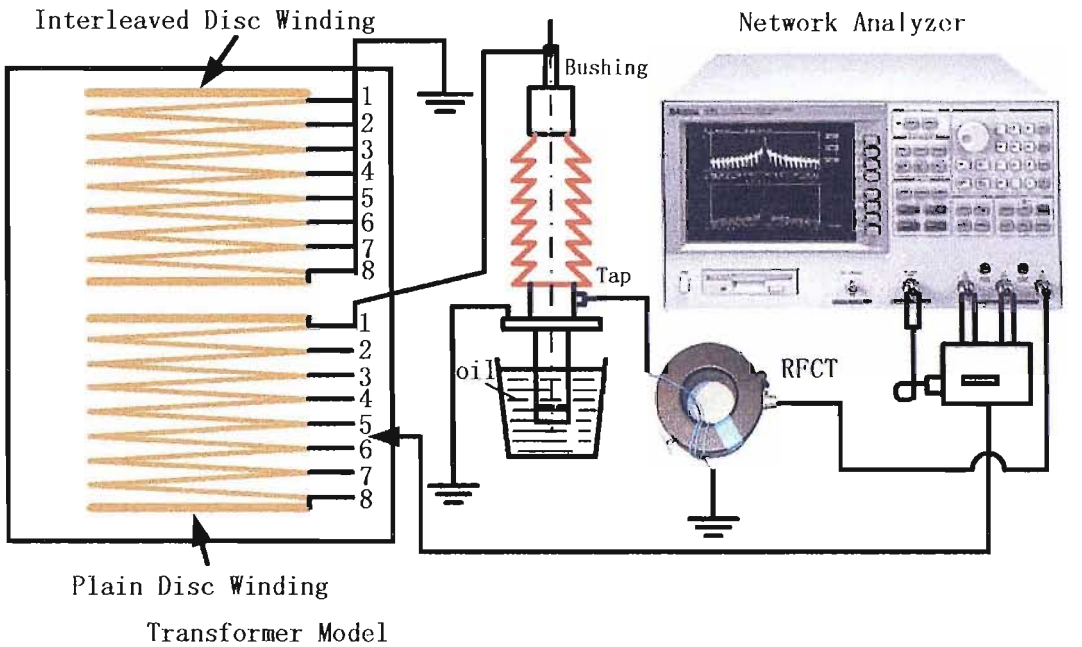

Figure 5.15 the frequency response measurement circuit

Figure 5.15 is the frequency response measurement circuit for the plain disc winding transformer model system. The frequency range of the Aligent 4395A Network Analyzer was set from 100 Hz to 200MHz; the sample average was 20 and the sample bandwidth was 30Hz. The measurement was carried out at the bushing tap via a RFCT when the transformer model was not filled with oil. The calibration signals from the network analyzer were injected into the plain disc winding in turn from the 2nd to the 8th terminals. The 60kV bushing, model 60HC755, was connected to the 1st terminal of the plain disc winding; its frequency spectrum is illustrated in Figure 3.22.

The RFCT was wrapped with a wire of three turns to improve the measurement gain; its frequency spectrum as shown in Figure 3.6. The obtained results are illustrated in Figure 5.16. Analysing the curves on Figure 5.16 and comparing them with that of Figure 5.14, the following conclusions can be drawn:

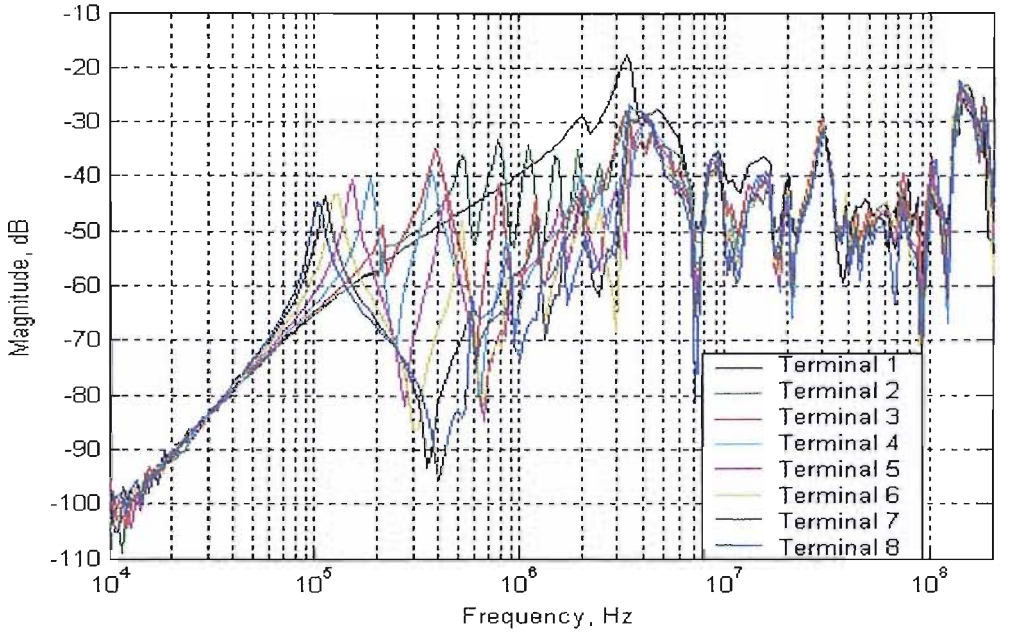

Figure 5.16, Frequency response of the interleaved disc winding transformer model system without oil, measured at the 60kV bushing tap via a RFCT

Due to the capacitive characteristic of the 60kV bushing the low frequency components of the injected signals were attenuated when passing through the transformer model system. The obvious range of influence was up to 3MHz. The ability of the RFCT in detecting signals influenced the model across the whole measurement range from 10 kHz to 200 MHz, and reduced the measurement magnitudes. In the low frequency region, the peak resonance points due to the winding were still visible. Their positions did not change but their magnitudes are reduced because of attenuation due to the bushing and RFCT detector. Meanwhile, some additional resonances were observed due to the combined influence of the winding, bushing and RFCT. Above 1 MHz the attenuation of per section of the winding is small.

5.2.2.4 Frequency Responses of the Oil-filled Transformer Model System with a Plain Disc Winding

Using the same measurement circuit as shown in Figure 5.15, but with the transformer model filled with oil, the frequency responses of the plain disc winding transformer model system as shown in Figure 5.17 were obtained. During the measurement the settings of the Network Analyzer were as described in 5.2.2.3, and the same measurement method was also used.

Comparing Figure 5.17 with Figure 5.16, the following was observed: the frequency response is reduced in magnitude below 25 MHz. Across this frequency range all the positions of peak resonance occur at lower frequencies. This is because the capacitance parameter values increase due to the presence of oil (see Figures 5.2 and Figure 3.8). From Figure 5.17, the frequency

responses above 300 kHz are similar; this indicates that above 1 MHz the attenuation per section of the winding is small.

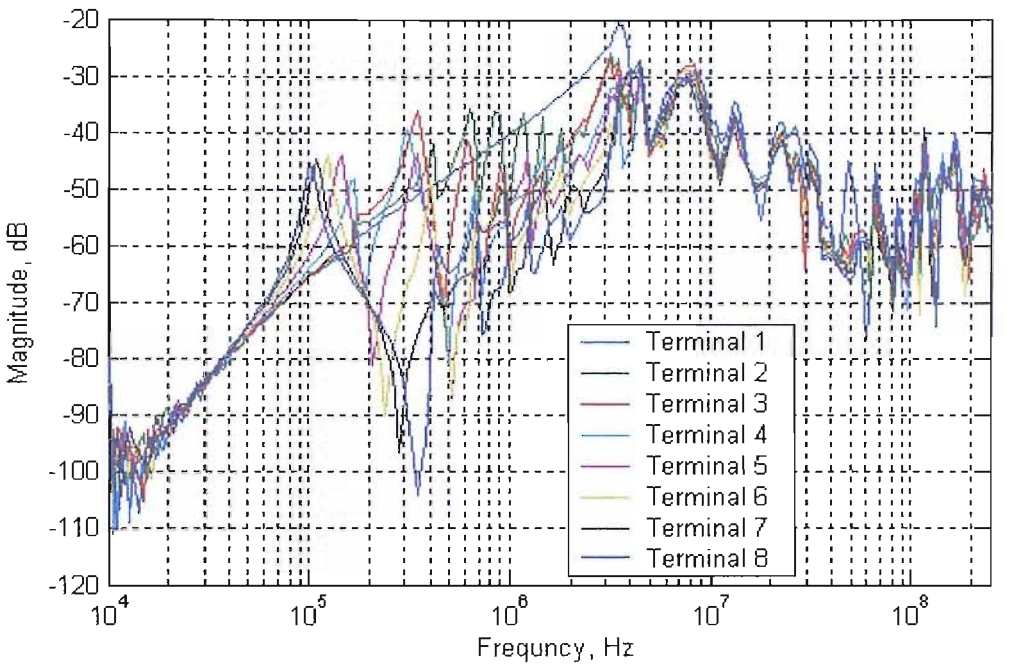

Figure 5.17 Frequency response of the plain disc winding transformer model system with oil, measured at the 60kV bushing tap via a RFCT

5.3 Impulse Responses of Windings and Transformer Model

An investigation into the impulse responses of the windings and the transformer model has been completed. A pulse generated using a HP 8082A pulse generator as shown in Figure 5.18 was injected into the terminals of the windings of the transformer model during the measurements. Figure 5.19 shows the FFT of the pulse calculated using a Matlab program. The purpose of this experiment was to establish if the proposed measurement approach was capable of detecting PD type pulses, given that the system significantly attenuates lower frequency components of any detected signal

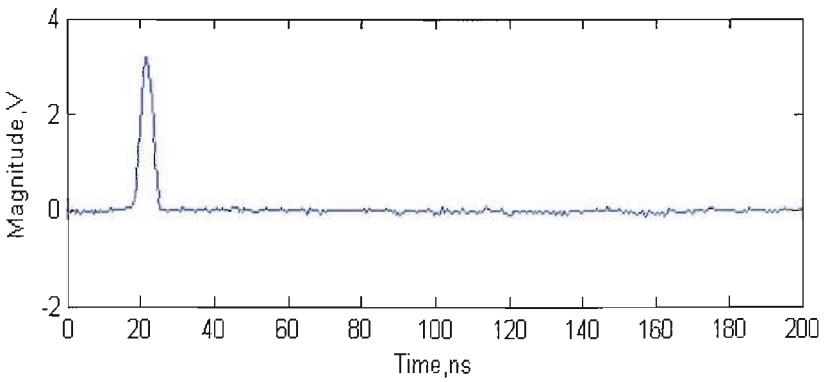

Figure 5.18, A test pulse

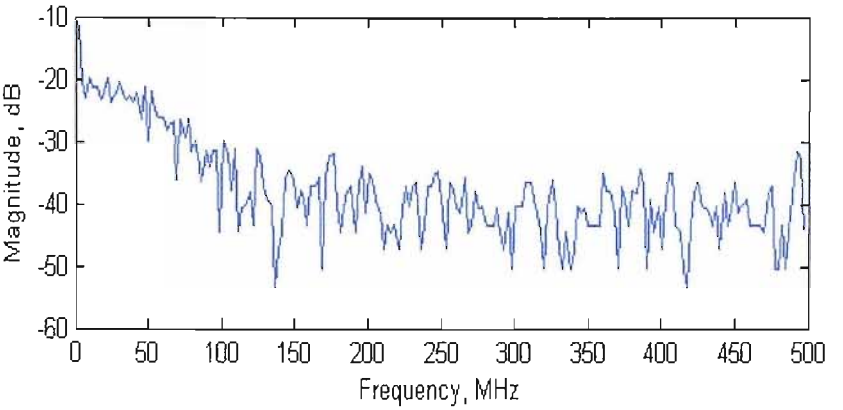

Figure 5.19, Frequency spectrum of the pulse shown in Figure 5.18

5.3.1 Impulse Responses of the Interleaved Disc Winding in the Tank without Oil

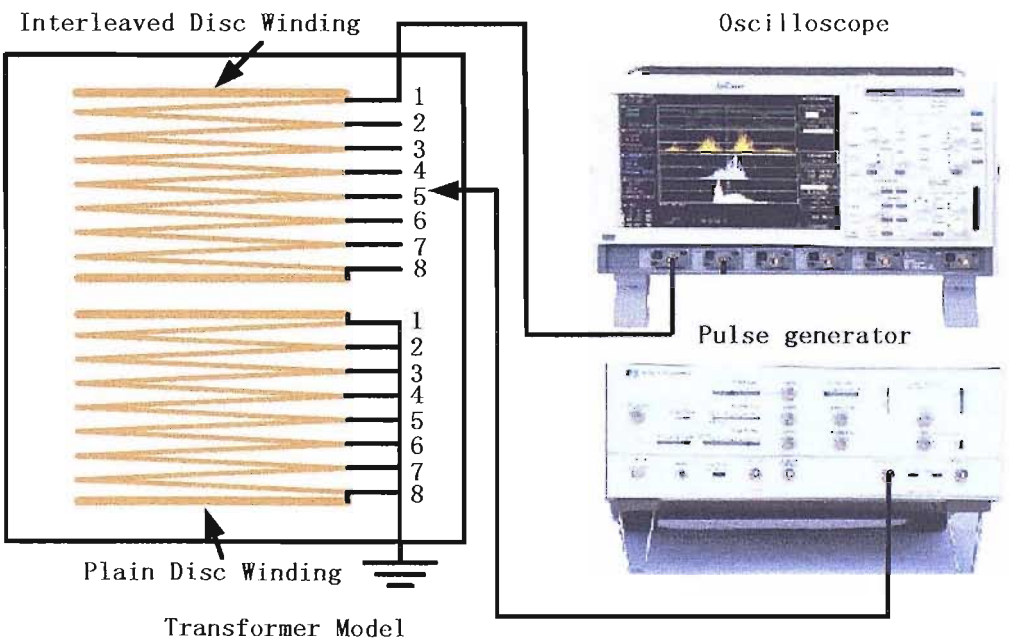

Figure 5.20 Impulse response measurement circuit

Figure 5.20 shows the measurement circuit for the interleaved disc winding transformer model without oil. A pulse shown in Figure 5.18 was injected into the model in turn from the 1st to the 8th terminals, and a digital oscilloscope, LC684DXL, was used to measure the response pulses at the 1st terminal. The oscilloscope was set with 1000 samples at 500Ms/s for 2.0us

Figure 5.21 illustrates the response pulses at the first terminal. The response pulse when the injection pulse was injected at terminal 1 is obviously different from the injected pulse shown in Figure 5.18, although the coax cable for the injected pulse was directly connected to the

oscilloscope. This is due to the influence of the interleaved disc winding, which attenuates the injected pulse signal. Some of which propagates to earth rather than pass to bushing tap point. With an increasing the number sections involved in the measurement, the magnitude of the response signal is correspondingly reduced. This was caused by increased impedance across the low frequency range (Figure 5.7).

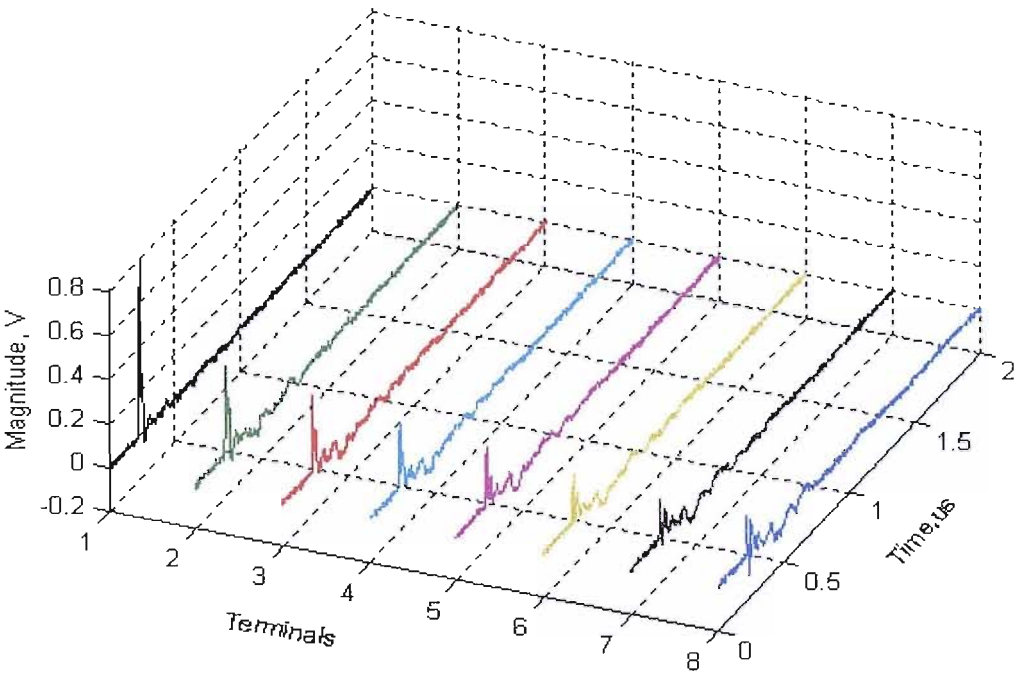

Figure 5.21 Measured pulses at the terminals

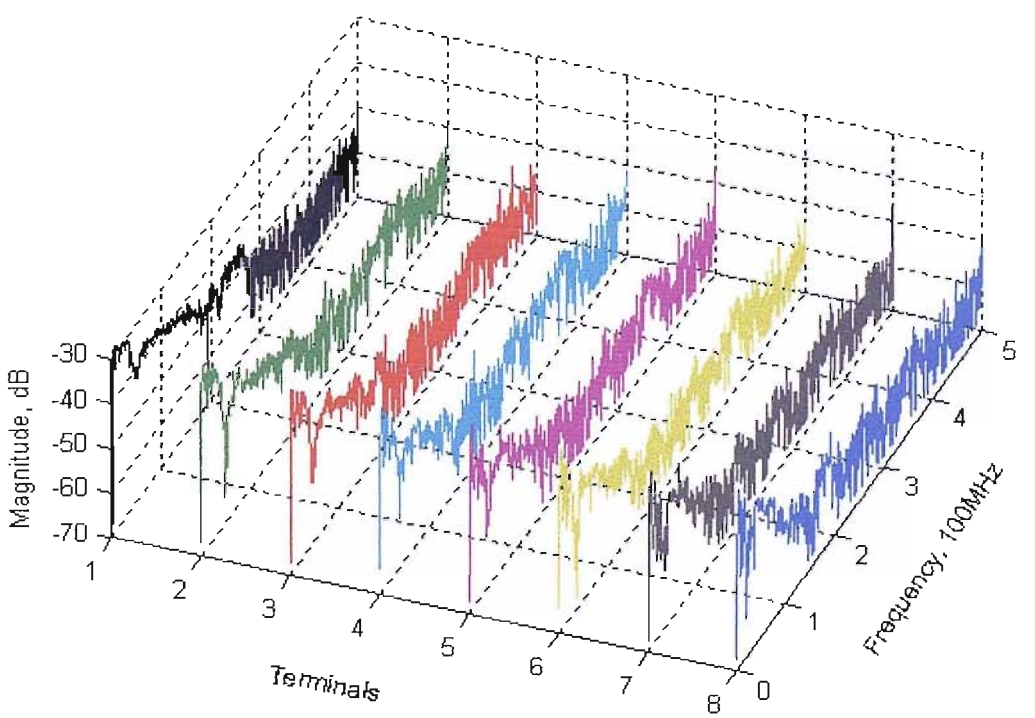

Figure 5.22 Frequency spectra of the measured pulses at the terminals

Figure 5.22 shows the frequency spectra of the response pulses, and gives a similar indication, which is that the high frequency components of the injected pulses can pass through the whole winding, but across low frequency ranges the response magnitudes are reduced as the number of the disc sections increases between the signal source and the measurement point.

5.3.2 Impulse Responses of the Interleaved Disc Winding Transformer Model without Oil

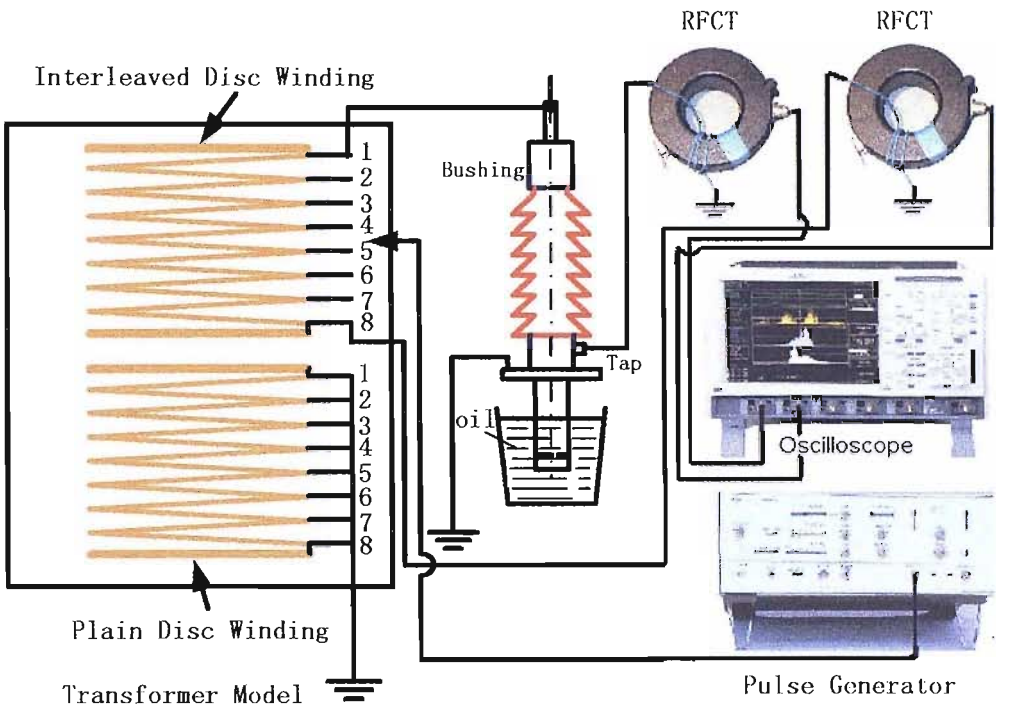

Figure 5.23 Impulse response measurement circuit

Using the measurement circuit as shown in Figure 5.23, the pulse, generated using a HP 8082A pulse generator as shown in Figure 5.18, was injected into the interleaved disc winding model in turn from the 1st to the 8th terminals, and a digital oscilloscope, LC684DXL, was used to measure impulse responses at the 60kV bushing tap point and at the earthed end of the interleaved disc winding via RFCTs. The oscilloscope was set with 1000 samples at 500Ms/s for 2.0us. In order to improve the measurement gain of the both RFCTs, the primary wires were wrapped around the RFCT core three turns. The bushing core bar was connected to the 1st terminal of the interleaved disc winding.

Figure 5.24 shows the pulses measured at the bushing tap via the RFCT. Figure 5.25 is the frequency spectra of these output pulses.

The results indicate that with an increase of the number of disc sections involved in the measurement, the magnitudes of the output pulses are increasingly attenuated. This is due to the attenuation of low frequency components of the injected pulse as it passes through the winding

(refer to Figure 5.9). All signals appear to oscillate and by comparison with earlier results (Figure 5.21) it can be concluded that these oscillations are caused by the electrical properties of the bushing. The frequency characteristics of the measured pulses shown in Figure 5.25 suggest a similar conclusion as drawn from earlier experiments (Figure 5.9), which is that the high frequency components of a signal can pass through the system to the bushing tap point.

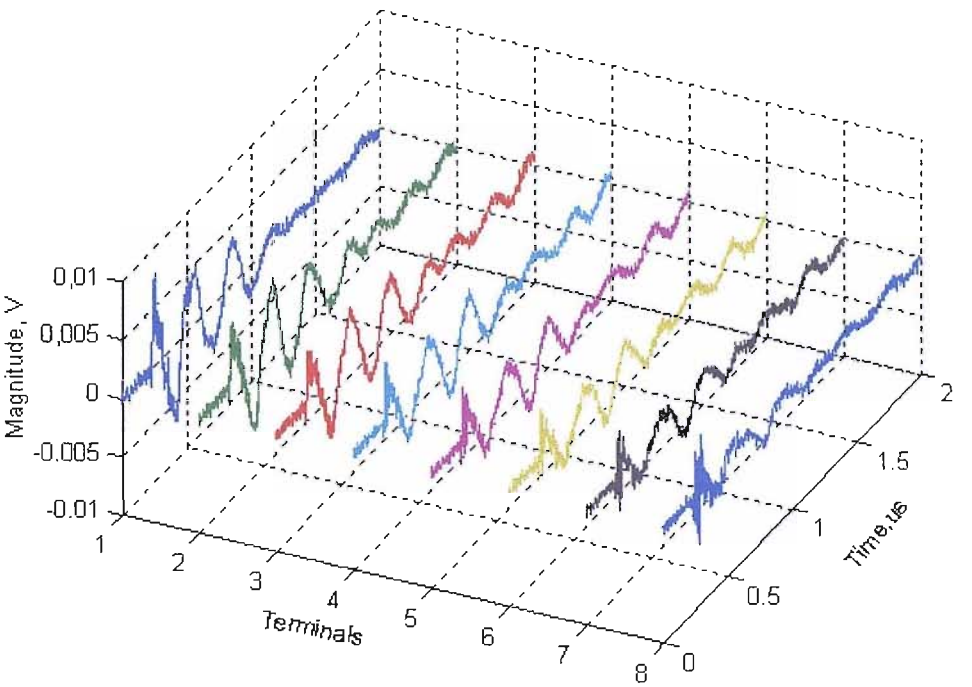

Figure 5.24 Impulse responses at the bushing tap via the RFCT

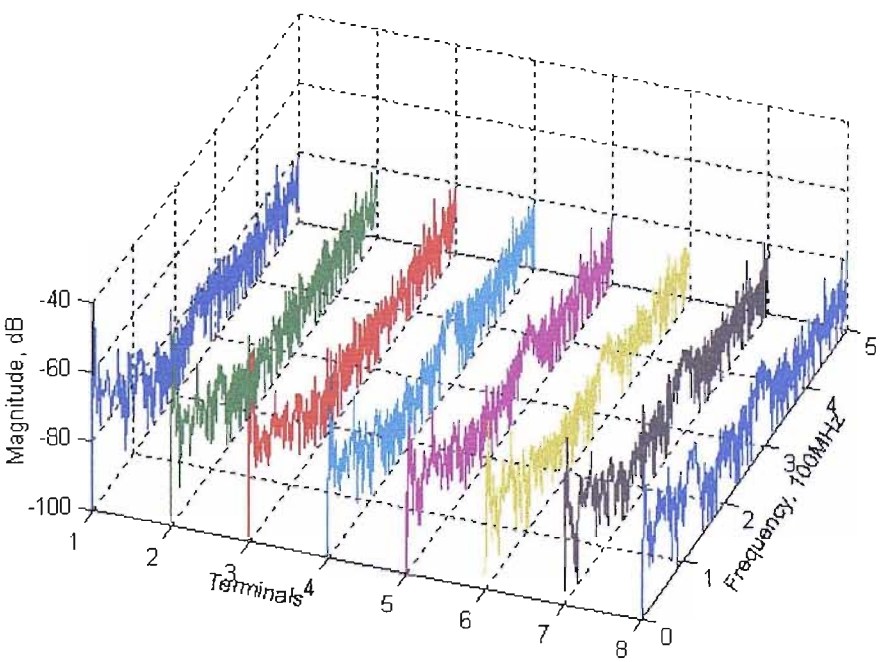

Figure 5.25 Frequency spectra of response pulses at the bushing tap via a RFCT

Figure 5.26 shows the pulses measured at the end of the interleaved winding via the RFCT, and Figure 5.27 shows their frequency spectra. Referring to Figure 5.24 when the injection point was at the 1st terminal, the magnitude of the output pulse in Figure 5.24 was greatest and that in Figure 5.26 smallest. When the injection point was at the 8th terminal, the magnitude of the output in Figure 5.24 was smallest and that in Figure 5.26 greatest.

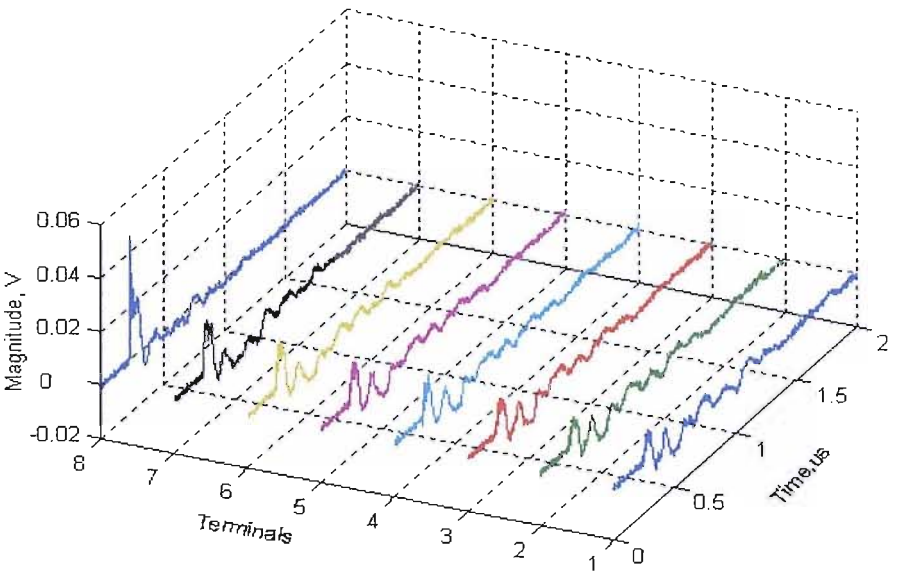

Figure 5.26 Impulse responses at the end of the interleaved winding via a RFCT

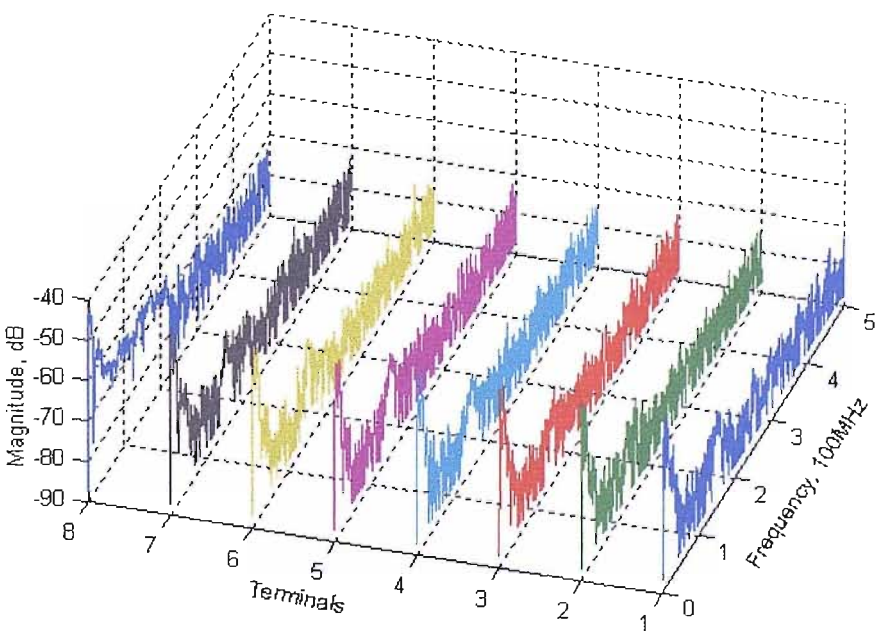

Figure 5.27 Frequency spectra of response pulses at the end of the interleaved winding via a RFCT

The results indicate that by monitoring both the bushing tap point and the other end of the winding it may be possible to obtain an indication of the location of the discharge source within a winding. Figures 5.24 and 5.26 show that the low frequency components of the pulses dominate the pulse

shapes and form oscillating waves. The high frequency components of the outputs are small in magnitude and are superimposed on the main waves of low frequency.

5.3.3 Impulse Responses of the Oil-filled Transformer Model with an Interleaved Disc Winding

Using the circuit in Figure 5.23, after the transformer model was filled with transformer oil the pulse response measurements were carried out on the interleaved disc winding model. The same circuit and procedure and instrument settings were used as in section 5.3.2.

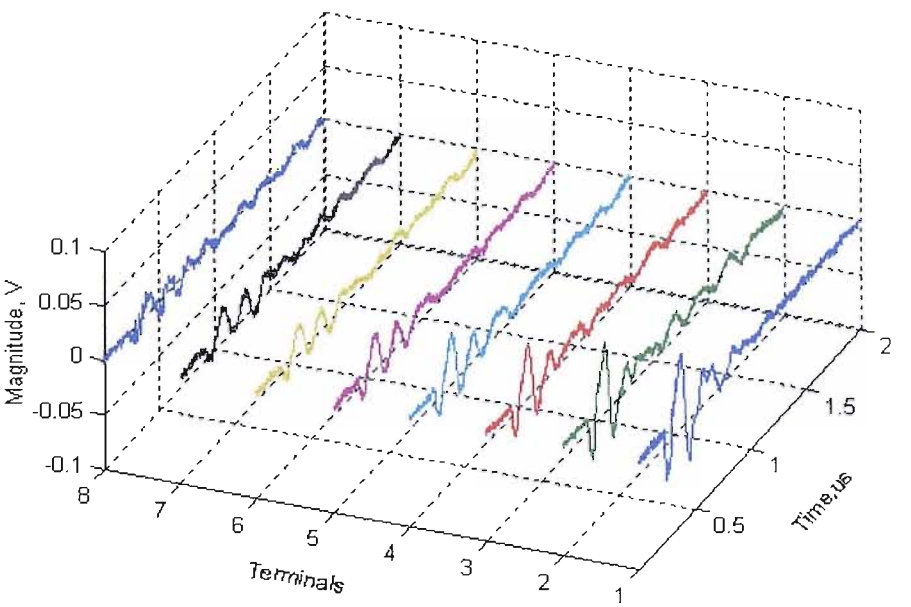

Figure 5.28 Impulse responses at the bushing tap via a RFCT

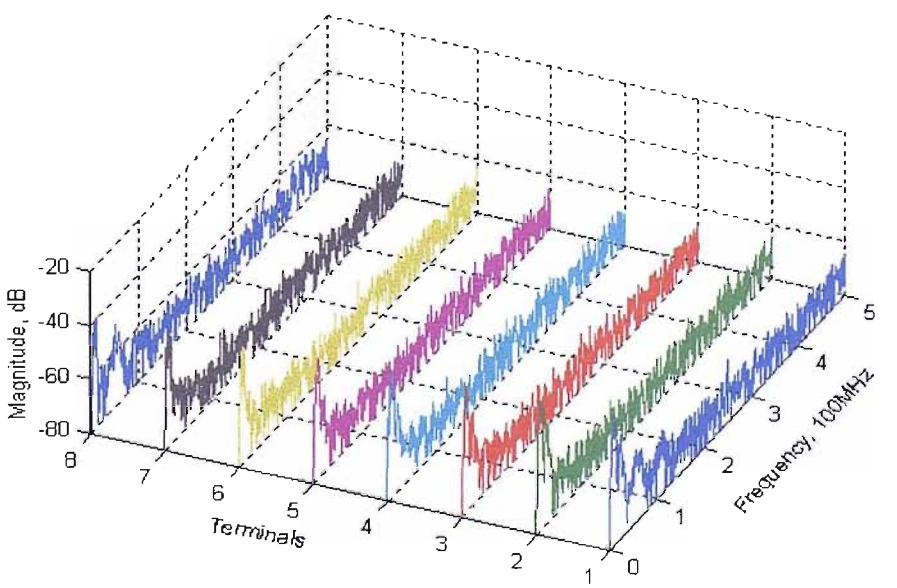

Figure 5.29 Frequency responses of the impulse response at the bushing tap via a RFCT

Figures 5.28 and 5.30 are respectively the time-based waveforms measured via RFCTs at the bushing tap and at the end of the interleaved disc winding. Figures 5.29 and 5.31 show the FFT calculation of the waveforms, obtained from the oscilloscope traces.

Consider Figure 5.28. When the triangular pulse was injected into the winding at the first terminal, the magnitude of the output pulse at the bushing tap is bigger than the others. As the number of the disc sections involved increased, the response magnitudes gradually reduced. This is because the increasing number of the disc sections caused the impedance to increase in the low frequency region (several 10 kHz, see Figure 5.10).

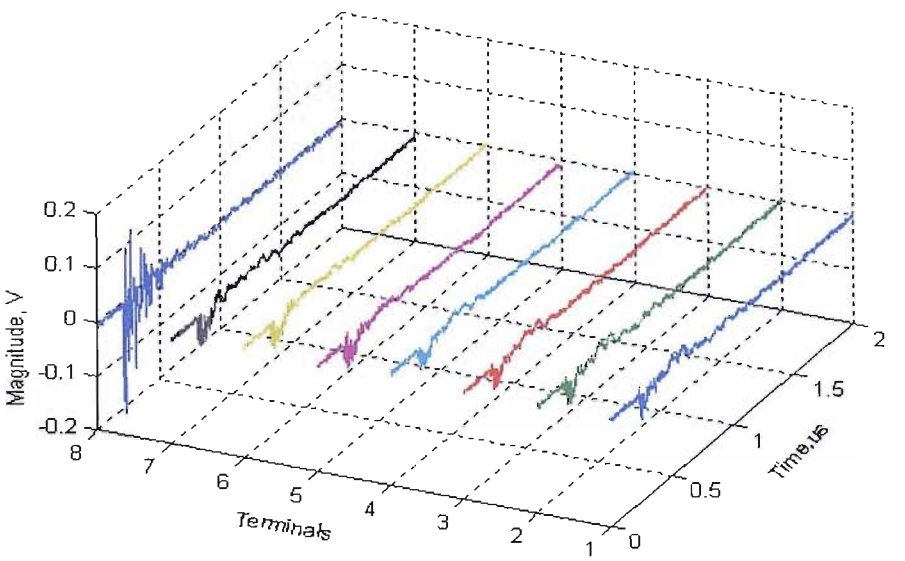

Figure 5.30 Impulse responses at the end of the winding via a RFCT

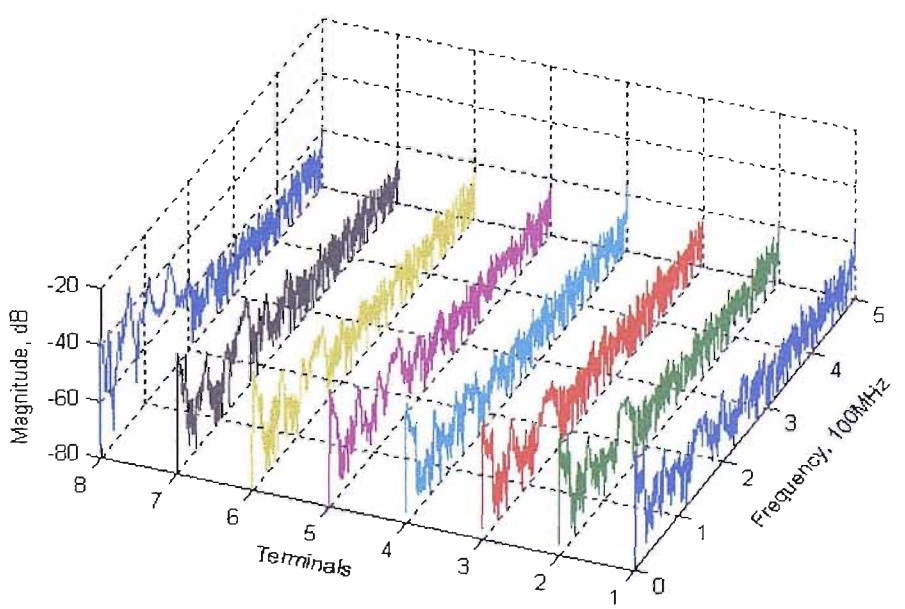

Figure 5.31 Frequency responses at the end of the winding via a RFCT

In Figure 5.30, with the triangular pulse injected into the winding at the first terminal, the magnitude of the output pulse at the end of the winding is smallest. This is because the transmission path is longest and has the biggest impedance across the low frequency range. Comparing Figure 5.29 with Figure 5.31, more high frequency components in the outputs at the winding end (Figure 5.31) are found. This is because of attenuation of high frequency components by the bushing.

5.4 Propagation Characteristics of Real PD Signals within the Transformer Model

Section 5.3 considered some propagation characteristics of pulse signals within the interleaved disc winding. However, the injected signal was only a simulation of a partial discharge single pulse. Its behaviour within the transformer model is not necessarily representative of a real PD signal. As described in Chapter 4, real PD signals may be made up of pulse groups within a 50 Hz cycle of the test voltage waveform. This kind of PD signal was next used in this investigation to understand the behaviour of real PD signals within the transformer model.

5.4.1 PD Signals from the Non-oil Transformer Model with the Interleaved Disc Winding

Using the circuit shown in Figure 5.32, some real PD signals were generated by applying a high voltage to the PD source (5) (needle-plane PD source) as shown in figure 4.2. The real PD pulses were injected into the interleaved disc winding of the transformer model in turn from terminal 1 to terminal 8..

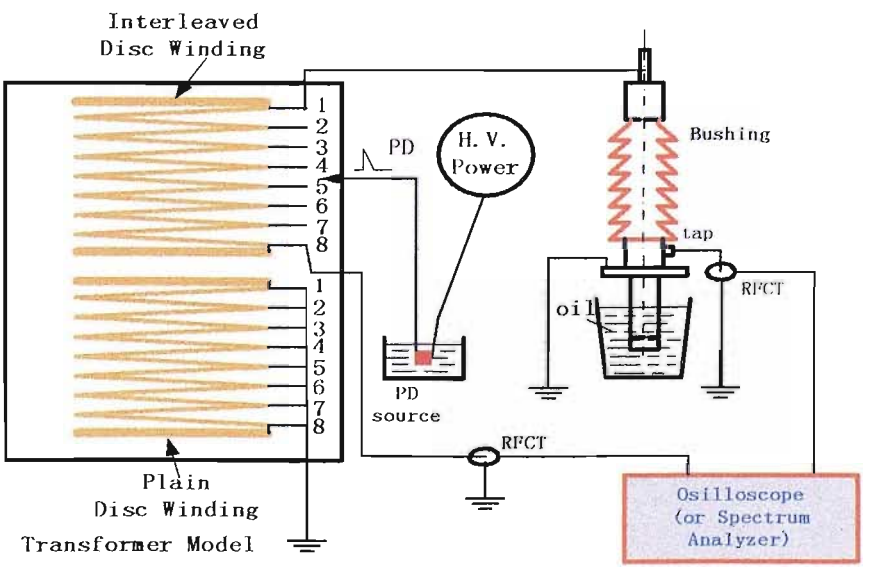

Figure 5.32 Measurement circuit of injecting real PD signals into the transformer model system

For these tests the distance from the needle tip to the insulation pressboard of the PD source was 1.5 mm Before the PD source was connected to the measurement system a 40kV voltage was applied to the bushing core bar, no evidence of PD activity was found and this means that below 40kV the measurement system was PD free.

When a high voltage is applied to the PD source, a partial discharge is generated and the corresponding voltage pulse travels to and is directly injected into the interleaved disc winding. One part of the PD signal will travel along the winding to reach the bushing core bar, and then pass out of the bushing tap. It finally arrives at the digital measuring equipment via a RFCT. Another part of the PD signal travels along the winding to reach the end of the winding and is finally detected by the digital measuring equipment via another RFCT. The digital equipment, including a digital oscilloscope, LC684DXL and an Agilent spectrum analyser, stores, analyses and displays the measured data to form frequency spectra and time domain waveforms.

In this measurement the oscilloscope was set with 2M samples at 200MHz/s for 20ms (one cycle period of a 50Hz test voltage). The spectrum analyzer was set with a sweeping range from 10 kHz to 200 MHz, and 20 average samples. The 60kV bushing is model 60HC755. The RFCTs were respectively wrapped with a wire of three turns to improve their measurement gain. During the test a zero crossing detector was used as an external trigger, the trigger was synchronized to the 50 Hz test voltage. The test voltage was kept at 16kV and the transformer model was not filled with oil.

- **Time domain waveforms**

Figures 5.33 to 5.40 show the persistence figures over 1000 cycles of 50 Hz test voltage waveform. They were captured by using the oscilloscope. In each figure the upper waveform was obtained at the bushing tap via a RFCT and the lower waveform was obtained at the end of the interleaved winding via another RFCT. In all cases the two RFCTs detected the injected PD pulses at either end of the winding.

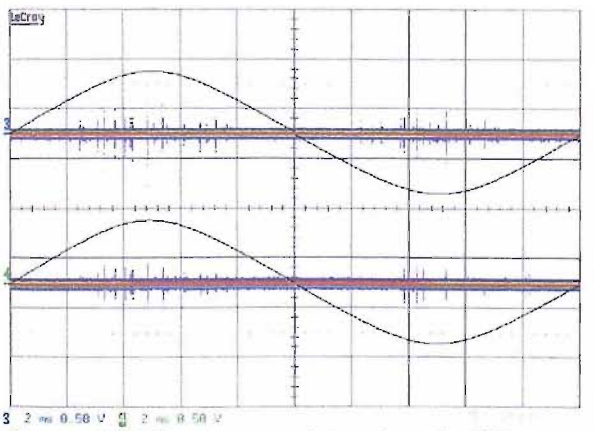

Figure 5.33 Persistence plots when the PD was injected at terminal 1

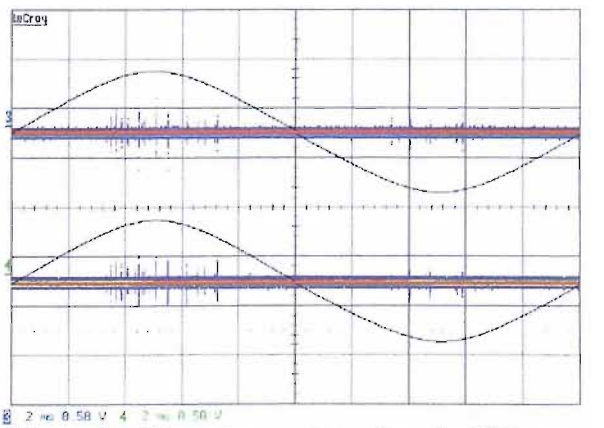

Figure 5.34 Persistence plots when the PD was injected at terminal 2

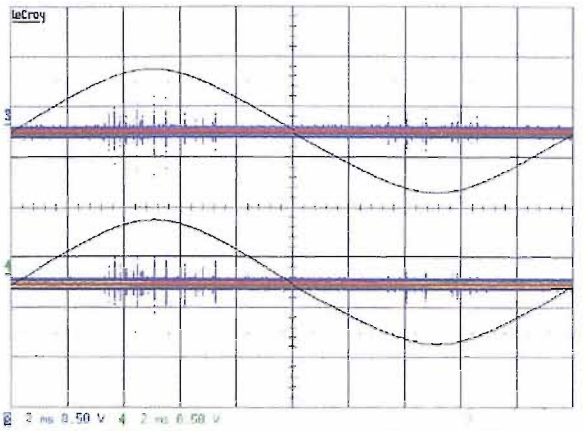

Figure 5.35 Persistence plots when the PD was injected at terminal 3

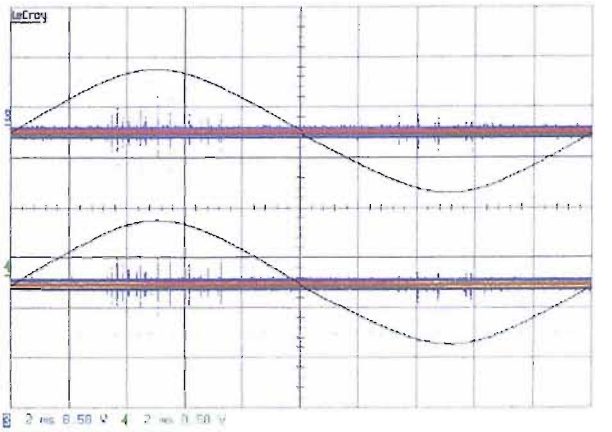

Figure 5.36 Persistence plots when the PD was injected at terminal 4

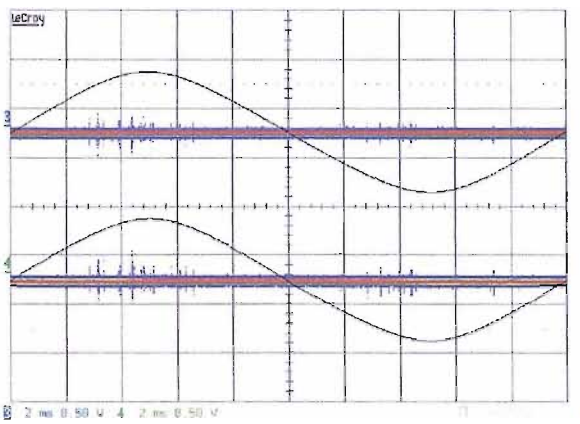

Figure 5.37 Persistence plots when the PD was injected at terminal 5

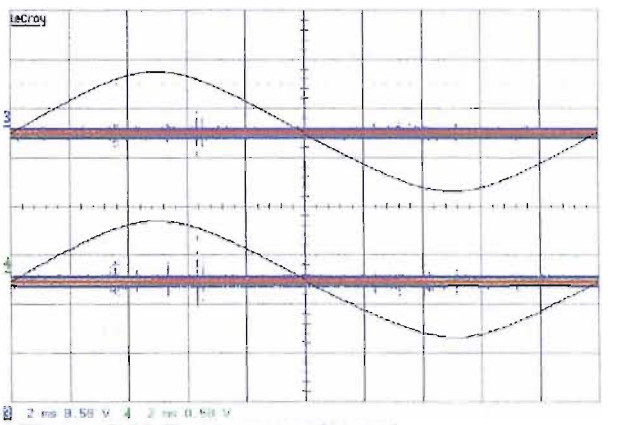

Figure 5.38 Persistence plots when the PD was injected at terminal 6

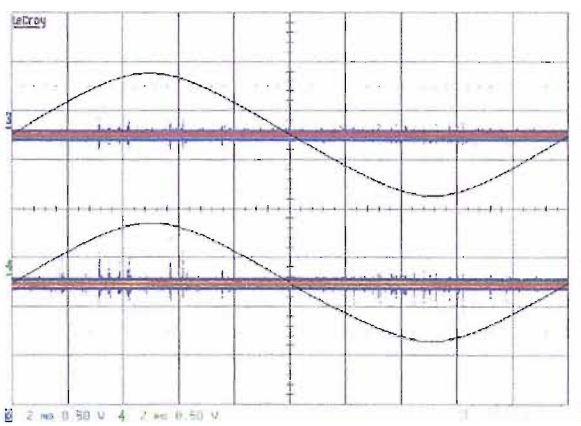

Figure 5.39 Persistence plots when the PD was injected at terminal 7

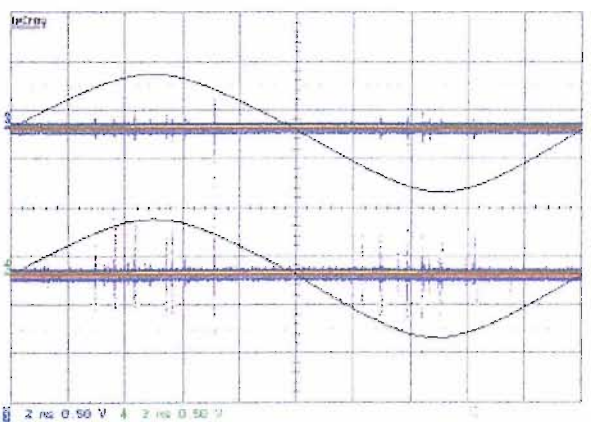

Figure 5.40 Persistence plots when the PD was injected at terminal 8

Observations from Figures 5.33 to 5.40 are as follows. When the real PD was injected at the 1st terminal, the magnitudes of the measured PD pulses at the bushing tap were bigger, but at the end of the interleaved disc winding the measured PD pulses were smaller. When the PD was injected at the 8th terminal, the magnitudes at the bushing tap were smaller; and at the end of the interleaved disc winding the magnitudes were bigger.

- **Frequency spectra**

Figure 5.41 shows the frequency spectra measured using the Spectrum Analyzer at the bushing tap via a RFCT. Figure 5.42 is the frequency spectra measured using the Spectrum Analyzer at the end of the interleaved disc winding via a RFCT. They all correspond to the signals in Figures 5.33 to 5.40. The spectrum at the each "0 position" on the both terminal axis is the frequency spectrum of background noise. They were measured separately at the bushing tap and at the end of the interleaved disc winding via RFCTs when the PD source was not energized.

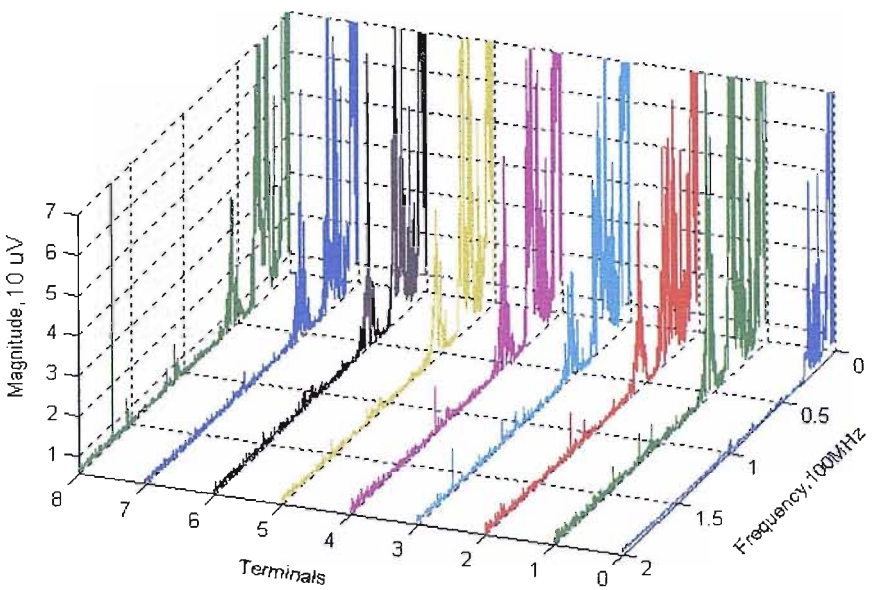

Figure 5.41 Frequency spectra at the bushing tap via a RFCT

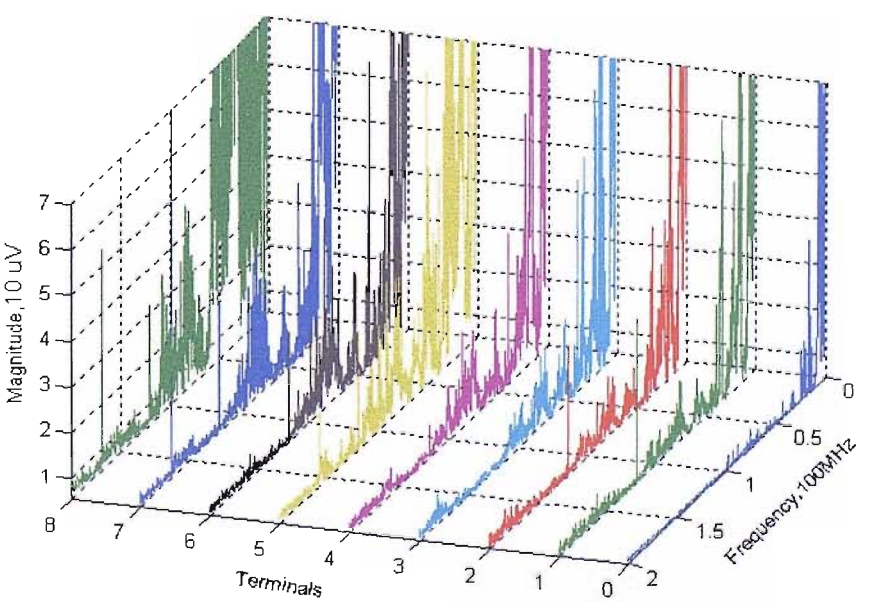

Figure 5.42 Frequency spectra at the end of the interleaved disc winding via a RFCT

Figures 5.41 and 5.42 show that the bandwidth of the transferred PD signals were up to 200 MHz corresponding to the bandwidth of the RFCT sensor. The majority of the transferred components of the PD signals had bandwidths of up to 50 MHz, but the signals over 50 MHz could still pass through the winding and the bushing. By comparing the two figures, one sees that the more components of high frequency over 50MHz were detected at the end of the winding. This is because the bushing attenuates the PD signals passing through it.

5.4.2 PD Signals from the Oil-filled Transformer Model with the Interleaved Disc Winding

In the test the same measurement circuit and procedure and instrument settings were used as the described in section 5.4.1, but with the transformer model filled with transformer oil and the test voltage was maintained at 20kV.

- **Time domain waveforms**

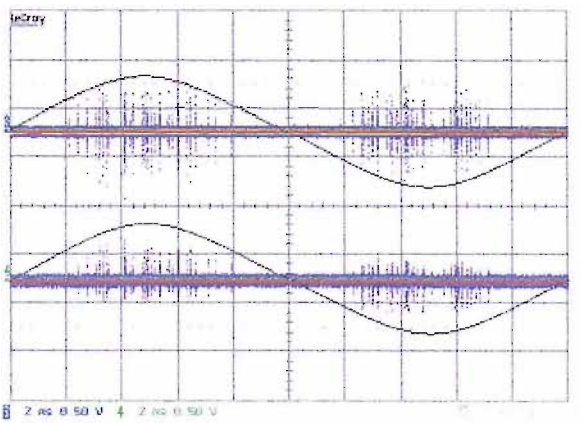

Figure 5.43 Persistence plots when the PD was injected at 1st terminal

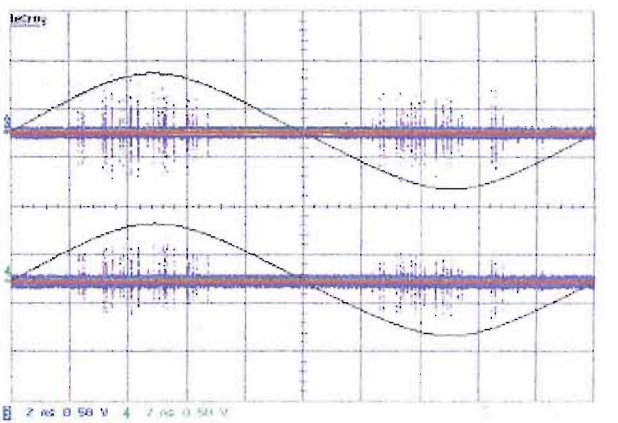

Figure 5.44 Persistence plots when the PD was injected at 2nd terminal

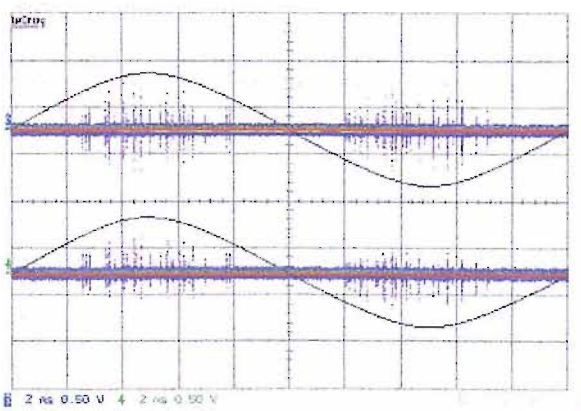

Figure 5.45 Persistence plots when the PD was injected at 3rd terminal

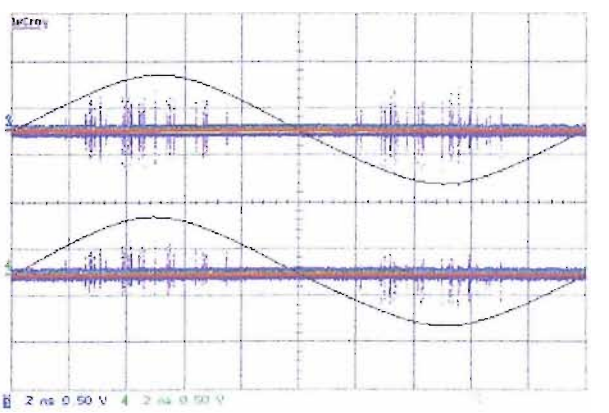

Figure 5.46 Persistence plots when the PD was injected at 4th terminal

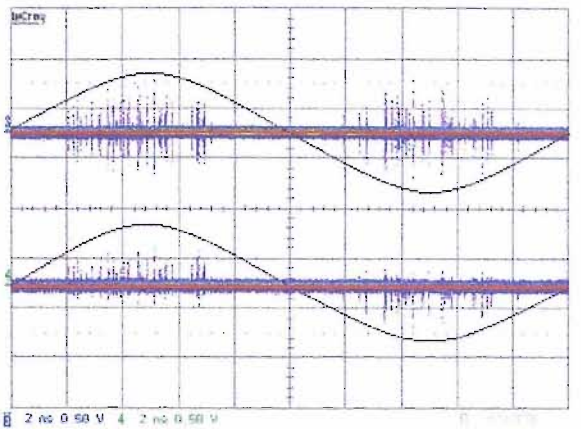

Figure 5.47 Persistence plots when the PD was injected at 5th terminal

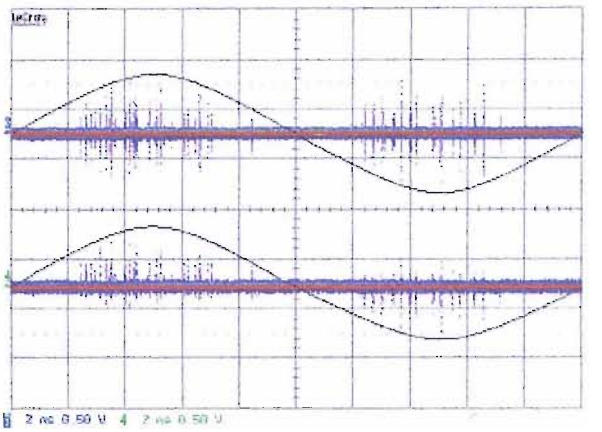

Figure 5.48 Persistence plots when the PD was injected at 6th terminal

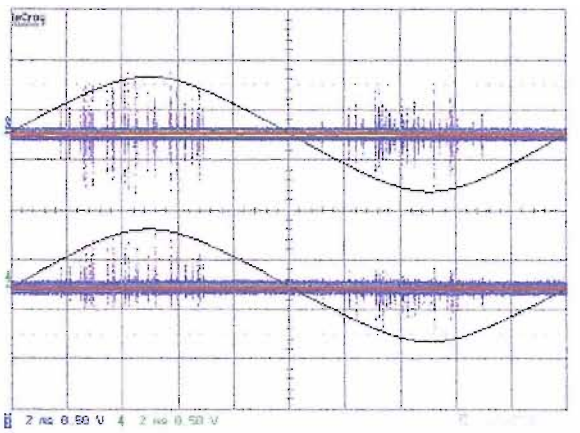

Figure 5.49 Persistence plots when the PD was injected at 7th terminal

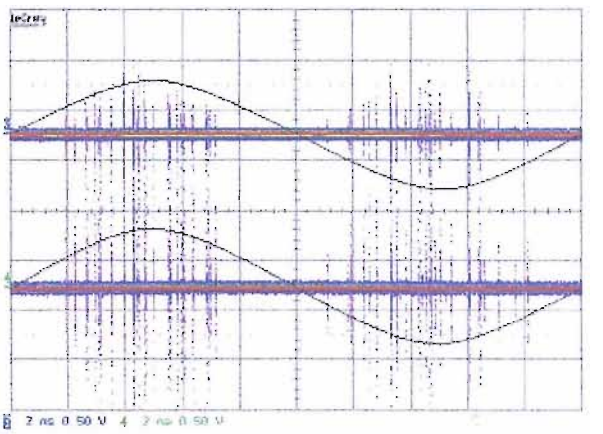

Figure 5.50 Persistence plots when the PD was injected at 8th terminal

Figures 5.43 to 5.50 were measured using the oscilloscope. They are persistence figures over 1000 cycles of 50Hz test voltage. The upper waveform in each figure was obtained at the bushing tap via a RFCT and the lower waveform was obtained at the end of the interleaved winding via another RFCT. From these plots, it can be seen that when the PD was injected at the 1st terminal, the magnitudes of measured PD pulses at the bushing tap were greater, but at the end of the interleaved disc winding the magnitudes were smaller. When the PD was injected at the 8th terminal the magnitudes of measured PD pulses at the bushing tap were smaller, but the magnitudes at the end of the interleaved disc winding were greater.

- **Frequency spectra**

Figure 5.51 shows the frequency spectra measured using the Spectrum Analyzer at the bushing tap via a RFCT. Figure 5.52 shows the frequency spectra measured at the end of the interleaved disc winding via another RFCT. The waveforms at the "0 position" on each terminal axis are the

frequency spectra of the background noise, which were measured separately at the bushing tap and the end of the interleaved disc winding via RFCTs when the PD source was not energized.

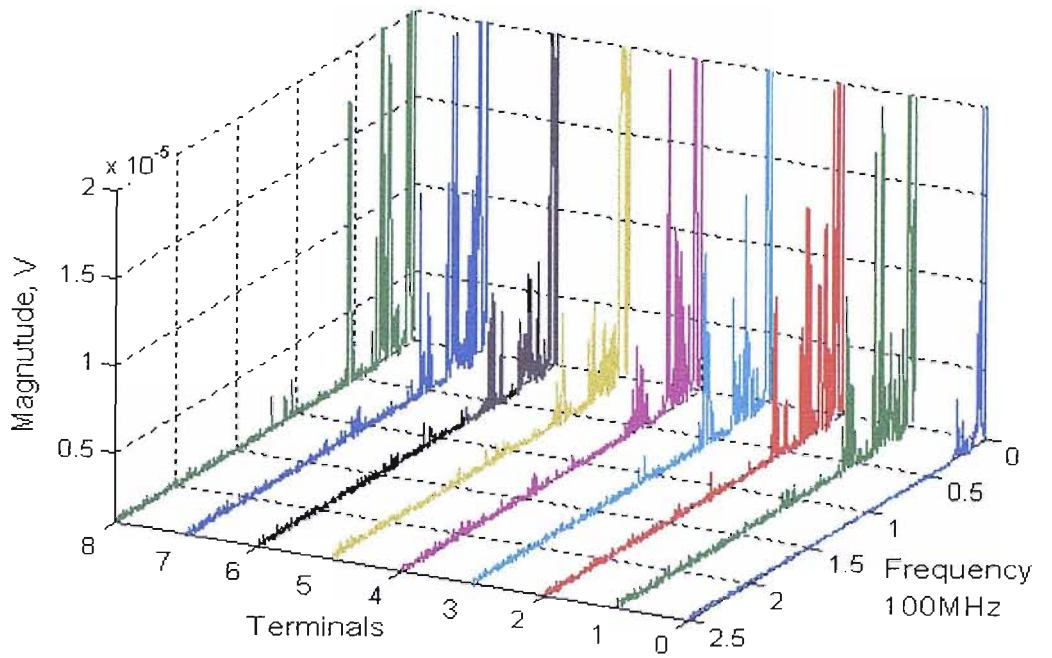

Figure 5.51 Frequency spectra at the bushing tap via a RFCT

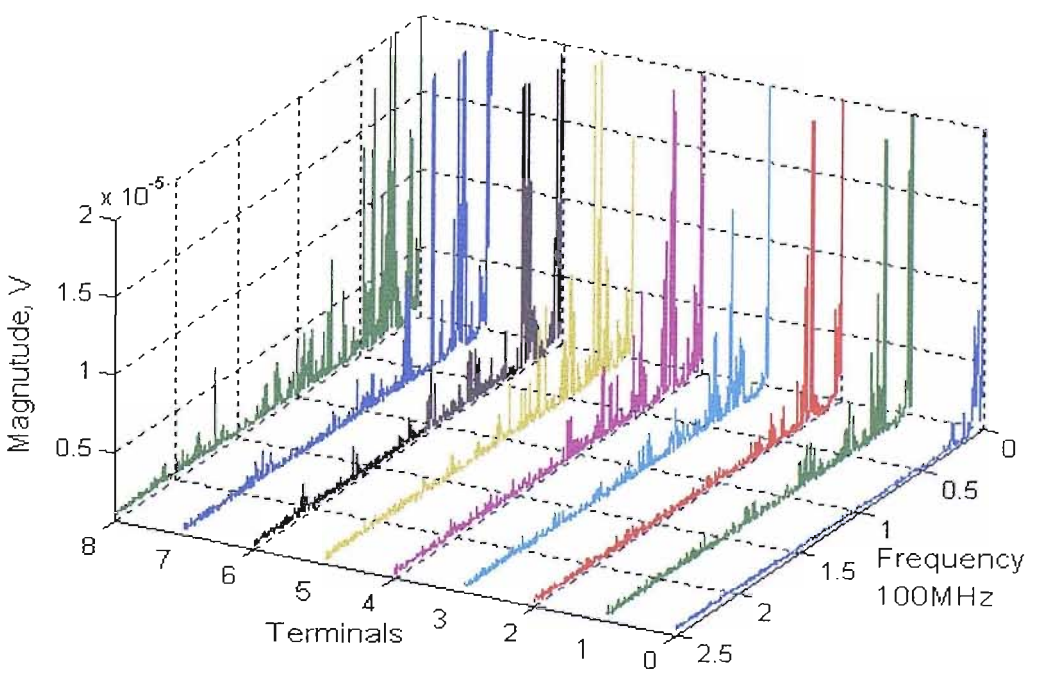

Figure 5.52 Frequency spectra at the end of the winding

The majority of the transferred components of the PD signals have a bandwidth of up to 50 MHz, but the signals over 50 MHz could still pass through the winding and the bushing. By comparing the

both figures, 5.51 and 5.52, again it is apparent that high frequency components over 50MHz are transmitted to the end of the winding, but are then attenuated by the bushing when passing to the bushing tap point

5.4.3 Single Pulses of the Transferred PD Signals from the Oil-filled Transformer Model

Using the same measurement circuit and procedure and instrument settings as described in section 5.4.1, but with the transformer model oil-filled and the oscilloscope set to 2500 sample points at 500Ms/s, single pulses of the PD responses at the bushing tap and the end of the interleaved disc winding were captured via the RFCTs.

Figure 5.53 shows the single pulses measured at the bushing tap via a RFCT; Figure 5.54 show their frequency spectra calculated directly by the oscilloscope. The single pulses measured at the end of the winding are shown in Figure 5.55, and their frequency spectra are shown in Figure 5.56.

From Figure 5.53 and Figure 5.54, it can be seen that the single pulses at the bushing tap have similar time domain properties. These are formed due to the function of the bushing working together with the interleaved disc winding. The majority of the oscillating waves have low frequency components of several ten kHz. The higher frequency components are all superimposed on the low frequency waves.

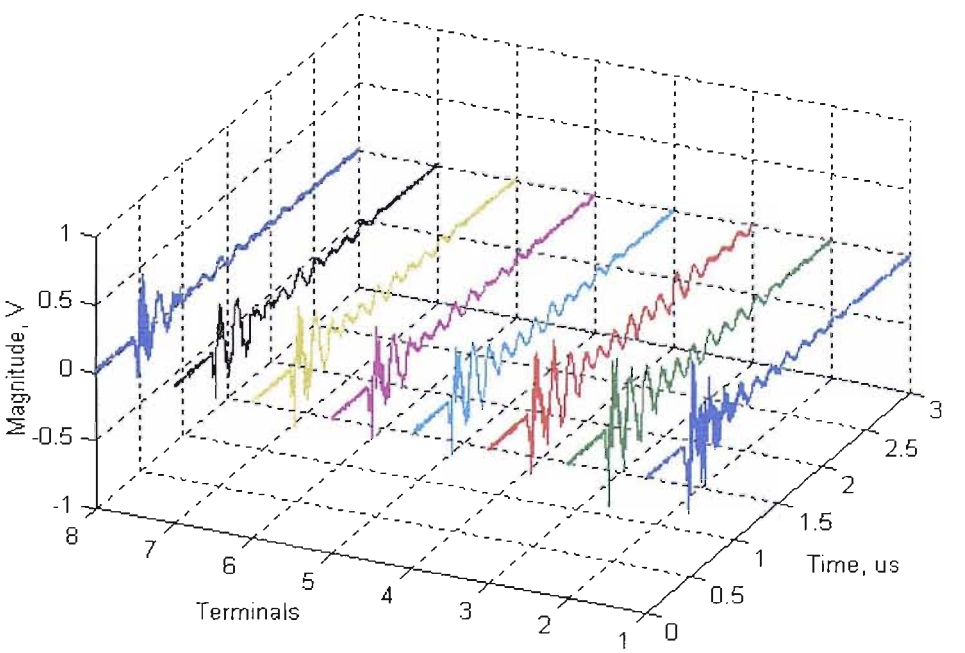

Figure 5.53 Single pulses at the bushing tap via a RFCT when the PD signal was injected into the winding from 1st to 8th terminals

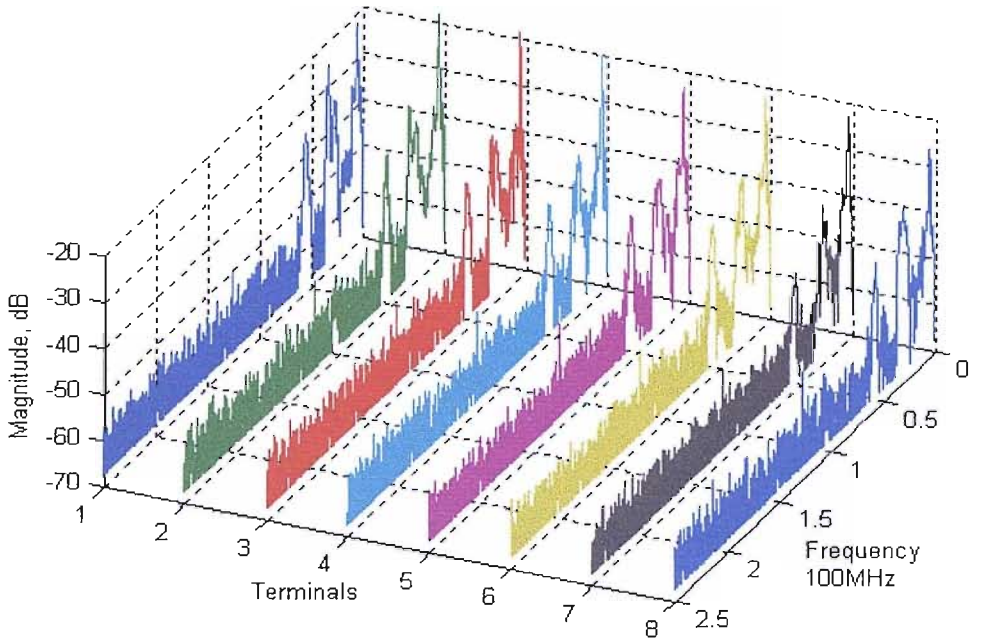

Figure 5.54 Frequency spectra of the single pulses at the bushing tap via a RFCT when the PD signal was injected into the winding from 1st to 8th terminals

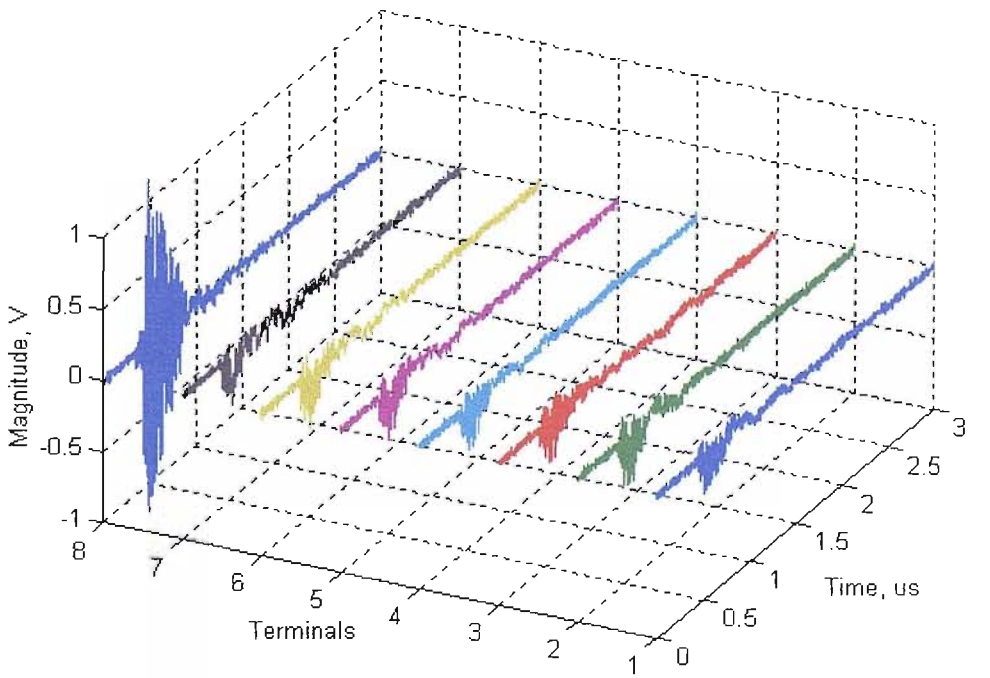

Figure 5.55 Single pulses at the winding end via a RFCT when the PD signal was injected into the winding from 1st to 8th terminals

Figure 5.55 and Figure 5.56 show that in the absence of the 60kV bushing, the output signals at the end of the interleaved disc winding were very different from those at the bushing tap. The majority of their components are low frequency oscillations.

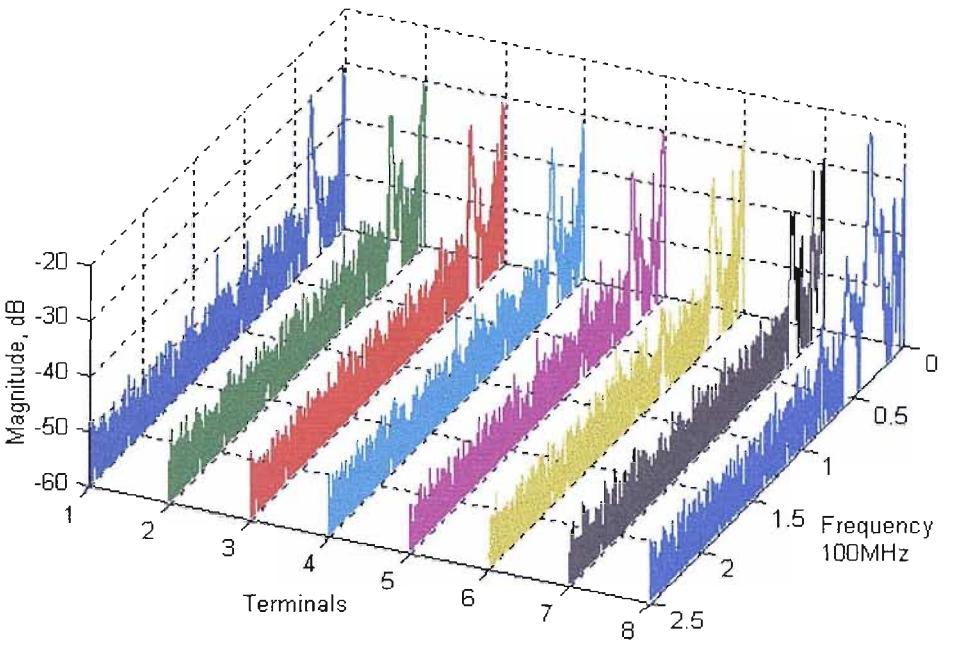

Figure 5.56 Frequency spectra of the single pulses at the winding end via a RFCT when the PD signal was injected into the winding from 1st to 8th terminals

5.5 Conclusions

A disc type winding of a high voltage transformer has a frequency characteristic that shows an increase of the number of discs involved increases the attenuation at low frequencies. In this investigation this property was separately shown from 200Hz to 1MHz for the interleaved disc winding and from 3 kHz to 2 MHz for the plain disc winding.

The results for the both interleaved disc winding and plain disc winding showed that the frequency break points of peak resonances of the interleaved disc winding are lower than those of the plain disc winding, although both windings have identifical geometric sizes. For both windings, an increase of the number of the discs involved led to an increase in the magnitudes of their peak resonances, but in high frequency range the attenuation per section of each winding is small.

Figure 5.57 shows a comparison of the frequency responses of the interleaved disc winding in both air and the non-oil tank when the calibration signals were in injected at terminal 5. The measurements were carried out separately using the measurement circuits as shown in Figures 5.3 and 5.5.

From Figure 5.57, it can be seen that the existence of Cg, (the capacitance to ground tank and core), and Gg (conductance of insulation loss to ground tank and core) causes attenuation of the injection signal at the first lowest resonance point.

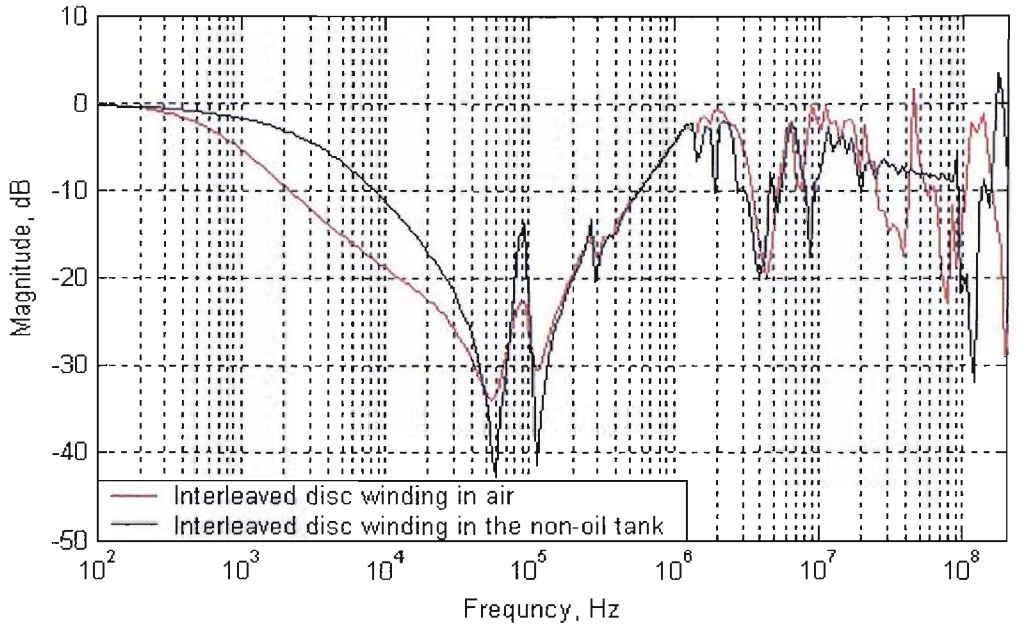

Figure 5.57 A comparison of the frequency responses of the interleaved disc winding in air and in the non-oil tank, the signals were injected at terminal 5

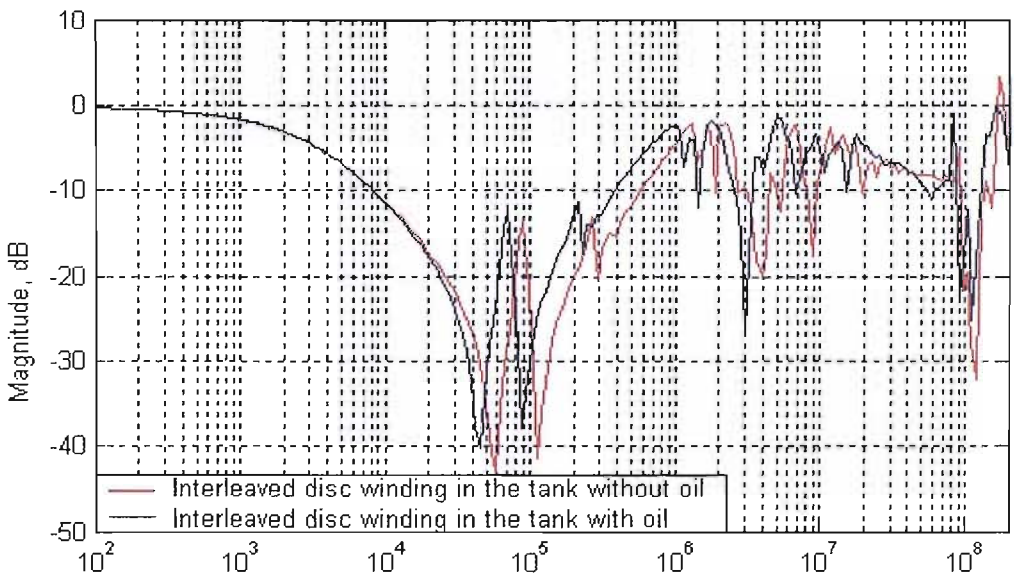

Figure 5.58 A comparison of the frequency responses of the interleaved disc winding in the tank with and without oil, the signals were injected at terminal 5

Transformer oil can improve signal transmission over the frequency range 20 kHz to 25 MHz. This can be deduced by comparing frequency responses measurements of the interleaved disc winding in the tank with and without oil (Figure 5.58). These measurement were carried out using the measurement circuit in Figure 5.5.

In the transformer model system, the function of the bushing is obvious. Over the low frequency range it significantly attenuated the transfer of signals from its core bar to its tap point. But over the high frequency range the attenuation is limited.

PD signals can be transferred within the transformer model from a point on a winding to the bushing core bar. The higher frequency components of the PD signal can then pass through the bushing and be detected at the bushing tap. Furthermore, they can be captured using digital equipment via a RFCT. Although there must be some information loss during the PD signal transfer, the frequency components at several tens of MHz and up to 200 MHz can still be seen. The property of pulse groups superimposed on a 50 Hz cycle of a test voltage waveform can be preserved.

The use of RFCTs as a sensor to detect internal PD activity within high voltage transformers has been validated. Additionally, the broad band signals generated by a internal discharge may be detected. It might be possible to determine discharge location each winding requires using at least two RFCTs – one at the bushing tap point and the other at the neutral-earth point, this conclusion is based on results shown in Figures 5.43-5.50.

Chapter 6

Methods of Measuring, Monitoring, Recognizing and Locating Partial Discharges

The properties of six typical PD signals which may occur within power transformers and their propagation characteristics from the bushing core bar to its tap point have been investigated. The frequency response, the impulse response and the real PD response of the transformer components, including a transformer bushing, RFCTs, transformer oil, an interleaved disc winding, a plain disc winding and a transformer model, have also been determined. Based on these results this chapter details a method to realize online measurement and monitoring of power transformers. Several software techniques to recognize and locate PD have been investigated.

6.1 Measurement and Monitoring Principles

Figure 6.1 shows a schematic diagram of a circuit for measuring partial discharge within an oil-filled power transformer. PD signals occurring near to or on a winding in a transformer must propagate along the winding or its lead to the core bar of a bushing connected to a winding phase. Of course this assumes that the discharge has enough energy to overcome attenuation due to the impedance of the coil. The bushing, as a capacitive component, passes the high frequency components of the PD signals without significant attenuation across to the bushing tap. As a sensor, a RFCT detects the high frequency signals of partial discharges via a primary coil connected to the

bushing tap. Measurement data are transferred via cable to a shielded box containing a penetrator wall to an oscilloscope, spectrum analyzer and computer. The filter box contains passive filters that are used to attenuate noise from FM, AM radio and mobile phones etc.

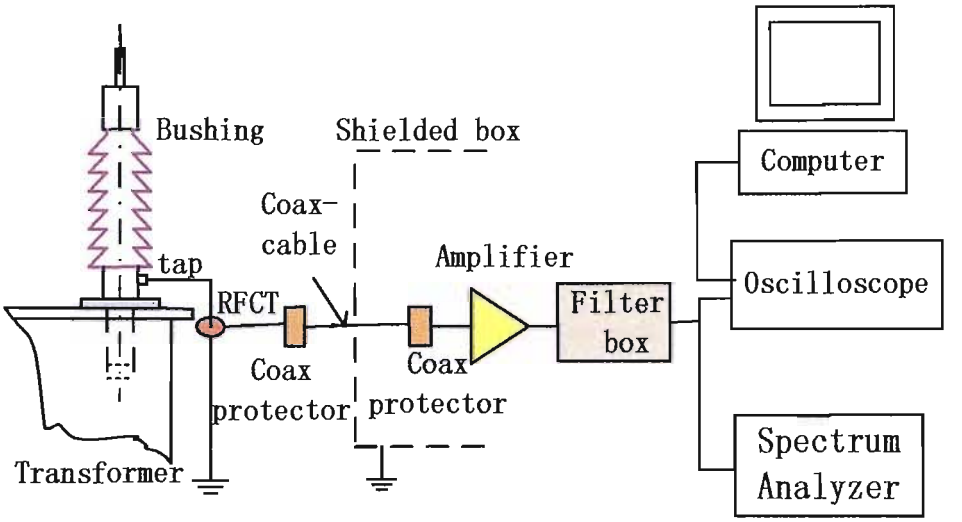

Figure 6.1, Schematic diagram of measurement circuit

An Agilent 4395A Network/Spectrum/Impedance Analyzer is used to analyze the frequency spectrum of the signals obtained using the RFCT. The analyzer can determine the frequency spectrum from 10Hz to 500MHz. A signal amplifier with a frequency range from 0.01 to 1000MHz and an amplification gain of 20dB is used to amplify the obtained measurement signals. A digital Oscilloscope, LC684DXL, is used to display time-based waveforms and store raw data. A computer is used to process measured data.

6.2 PD Recognition and Location from Patterns

Chapters 3 and 4 have shown that PD signals have their own characteristics in both the time and frequency domains. These characteristics are, respectively, the positions of PD pulse groups on a 50 Hz test voltage waveform and the bandwidth of the PD signals.

For example, corona in air generally occurs at the peaks of the 50Hz test voltage waveform and have very regular pulse distributions and differences in magnitude in the two half cycles. Surface discharges in air normally occur in the advance peak of each half cycle of the 50Hz test voltage waveform and have frequency ranges up to 40MHz only. For oil-filled power transformers these are external partial discharges. They can be distinguished from other discharges according to their property patterns.

Typical internal partial discharges are floating discharge and corona in oil (needle-plane discharge in oil). Floating discharge signals appear in the advance of the two peak half cycles of a 50 Hz test voltage waveform with the magnitudes of the pulses being almost equal in both half cycles. Corona

in oil (needle-plan discharge in oil) generally occurs near the middle of the peak of each half cycle of a 50 Hz test voltage waveform, and the pulse groups in the two half cycles are similar in magnitude and shape. Their common characteristics are that their bandwidths are more than 50MHz. They are also easy to be observed on the pattern of a 50 Hz test voltage waveform and can be distinguished from others using bandwidth analysis.

6.2.1 The Band-pass and High-pass Filters

In general, captured PD signals from an energized high voltage transformer will not only include internal partial discharges but external partial discharges as well. It is necessary to decompose or filter the cross-linked signals and to preserve internal signals. Based on the differences between the frequency properties of internal and external PD signals, two software filters to recognize PD signals from a measurement on a time domain waveform pattern have been designed. The filter programmes were compiled in the Matlab environment and process stored measurement data. This work was completed as a feasibility study, prior to taking actual field measurements.

- The band-pass filter

Band pass filter can be used to remove both low frequency and unwanted high frequency signals from the captured data. This allows suppression of AM-FM signals. Figure 6.2 is the principal pattern of a band-pass filter which was made up using an elliptic algorithm. The elliptic algorithm offers steeper roll off characteristics, but equiripple in both the pass- and stop-bands.

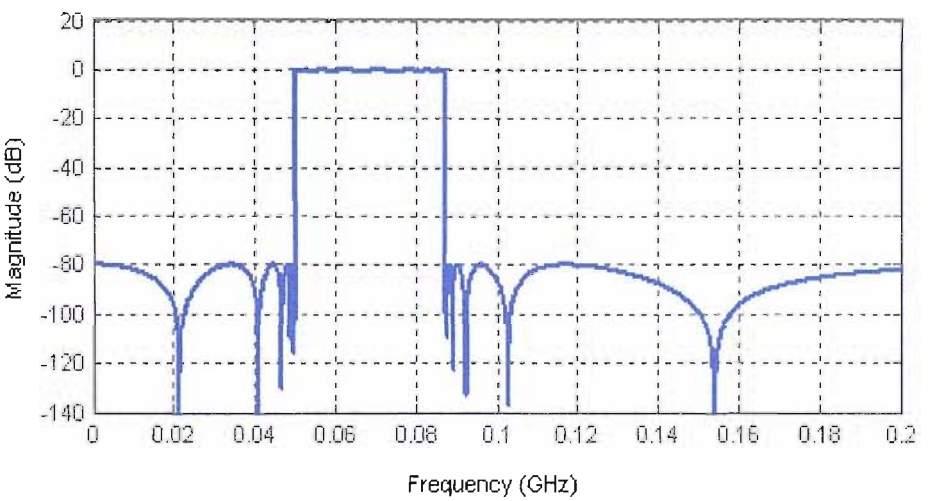

Figure 6.2 A band-pass filter (50 MHz-87MHz) [93]

The Matlab command of the elliptic filter is [93].: [b,a] = ellip(n,Rp,Rs, [w1 w2]) This returns an order 2*n band-pass filter with pass-band between w1 and w2 and Rp dB of ripple in the pass-band, and a stop-band Rs dB down from the peak value in the pass-band. It returns the filter coefficients in

the length n+1 row vectors b and a, with coefficients in descending powers of z. The filter transfer function is

$$H(Z)=\frac{B(z)}{A(z)}=\frac{b(1)+b(2)z^{-1}+\cdots+b(n+1)z^{-n}}{1+a(2)z^{-1}+\cdots+a(n+1)z^{-n}} \tag{6.1}$$

The normalized cut--off frequency is the edge of the pass-band, at which the magnitude response of the filter is -Rp dB. For this filter, the normalized cut-off frequency w1 or w2 is a number between 0 and 1, where 1 corresponds to half the sampling frequency (Nyquist frequency). Smaller values of pass-band ripple Rp and larger values of stop-band attenuation Rs both lead to wider transition widths (shallower roll-off characteristics).

In general, elliptic filters meet given performance specifications with the lowest order of any filter type. For this example, the data sampled at 500MHz, an eighth-order band-pass elliptic filter with a cut off frequency below 50MHz and over 87MHz was designed, which corresponds to a normalized value of 0.6, 3 dB of ripple in the pass-band, and 80 dB of attenuation in the stop-band. An application example of the software filter is described in Chapter 7.

- The high-pass filter

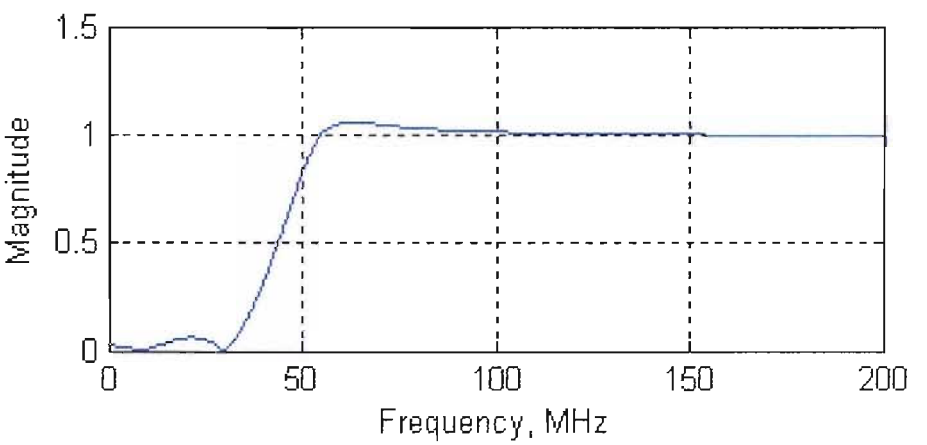

Figure 6.3 A high-pass filter

High pass filters can be applied in field measurements to remove external lower frequency discharge signals, such as corona at the bushing heads. Figure 6.3 is a high-pass filter using the yulewalk function of the Matlab Signal Processing Toolbox [93]. The eighth-order digital filters provide a least-squares fit to a specified frequency response. In the application of the filter the band edge frequency parameter is a vector of frequency points in the range 0 to 1, where 1 corresponds to half the sampling frequency (the Nyquist frequency). The first element of this vector must be 0 and the last element 1, and intermediate points must appear in ascending order. The magnitude parameter is a vector containing the desired magnitude response at the points specified in the band edge

frequency vector. The designed filter was eighth-order 50MHz high-pass.

Figure 6.4 shows a discharge signal on a time domain waveform of a half cycle of a 50 Hz test voltage, which was measured using an oscilloscope at the tap of the 60kV bushing via a RFCT according to the circuit in Figure 4.1. The sample rate was set at 500ms/s. The outstanding pulse is a PD signal produced within the PD source of a needle-plane in oil (PD source 5 in Figure 4.2) when a 21kV voltage was applied.

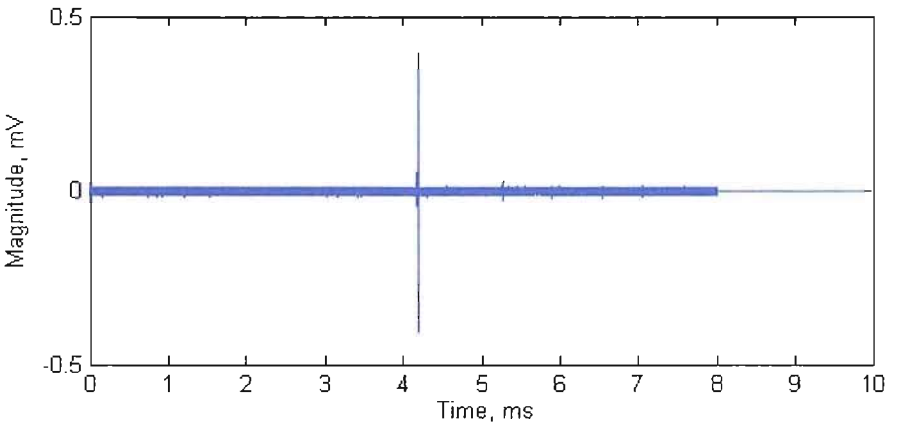

Figure 6.4 A waveform of a half cycle of a 50 Hz test voltage

The single pulse is also shown in Figure 6.5. From this Figure, many high frequency pulses appear on the low frequency fundamental waveform. Figure 6.6 shows the frequency spectrum of the single pulse calculated using a Fast Fourier Transform in the Matlab programming environment.

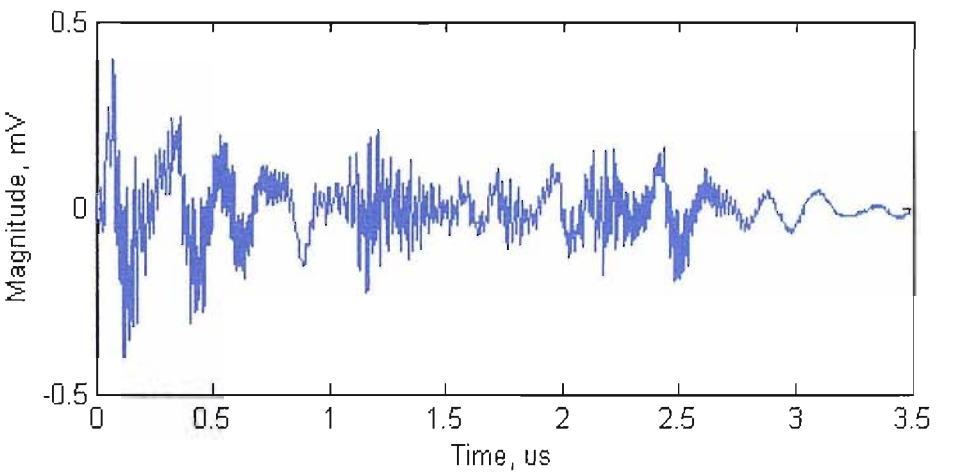

Figure 6.5 The single pulse in Figure 6.4

Figure 6.7 shows the result after the waveform in Figure 6.4 was filtered through the software filter shown in Figure 6.3. The magnitude of the outstanding pulse (PD signal) was much reduced due to its low frequency components being filtered out.

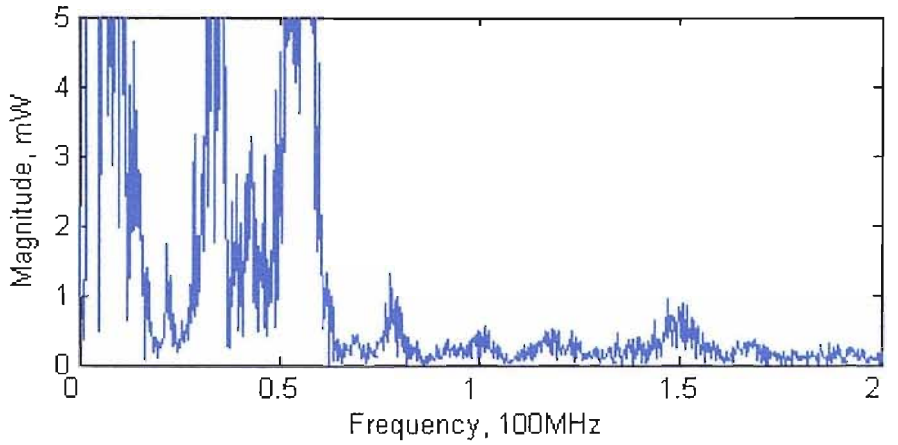

Figure 6.6 Frequency spectrum of the single pulse in Figure 6.5

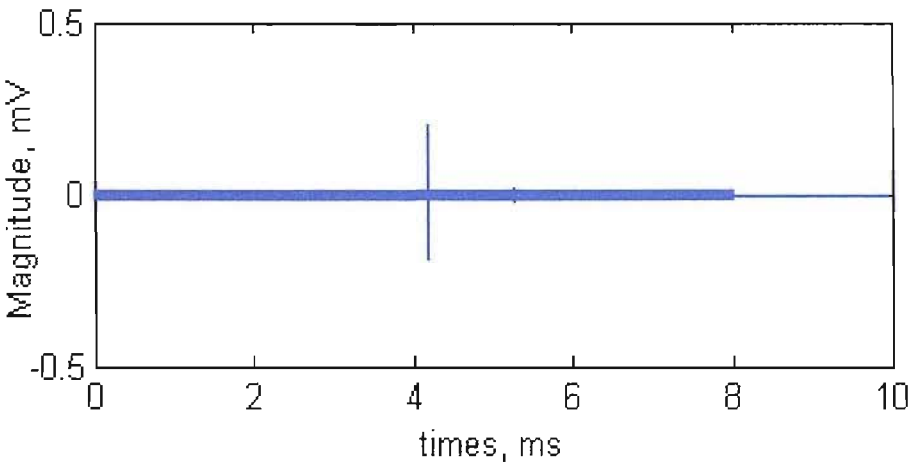

Figure 6.7 The filtered result for the waveform in Figure 6.4

The spread of the single pulse (PD after filter) is shown in Figure 6.8. This is a division of a pulse group of high frequency components. Figure 6.9 illustrates the frequency spectrum of the single pulse from a Matlab FFT calculation.

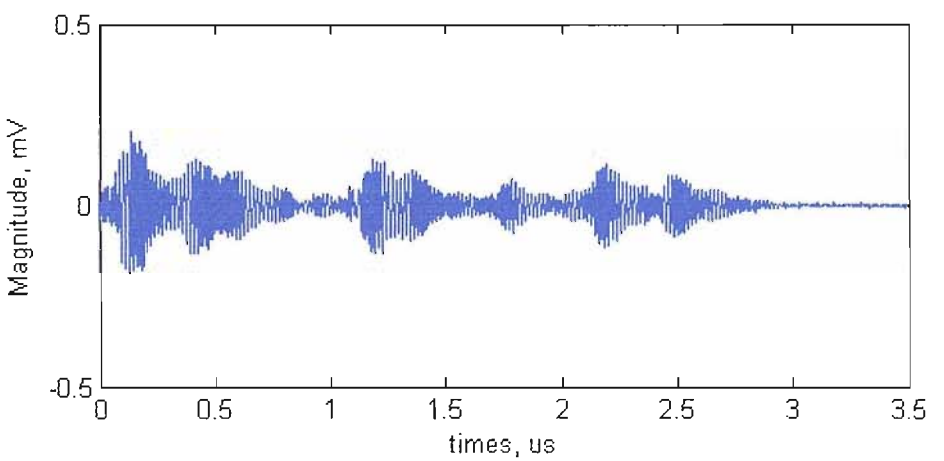

Figure 6.8 The single pulse in Figure 6.7

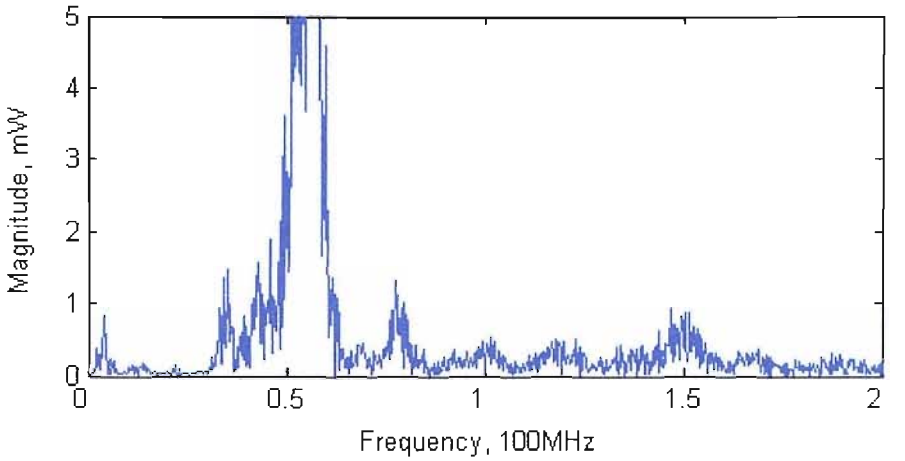

Figure 6.9 The frequency spectrum of the single pulse in Figure 6.8

The efficiency of the software filter is that the higher frequency components above 50MHz were preserved. This conclusion can be drawn by comparing Figure 6.9 with Figure 6.6.

6.2.2 The filter for PD in Frequency Domain Patterns

As described before, typical internal partial discharges, such as corona in oil (needle-plane discharge in oil) and floating discharge have higher bandwidths. This property can be used to recognise and locate PD signals. For example, if higher frequency components (e.g. above 40MHz) were directly obtained at a measurement point of a-phase, an internal PD can be considered to have occurred.

A software filter compiled in the Matlab environment for filtering frequency domain signals has been developed. Figure 6.10 shows one result of the use of this filter to obtain the PD signal as shown in Figure 6.6 in frequency domain.

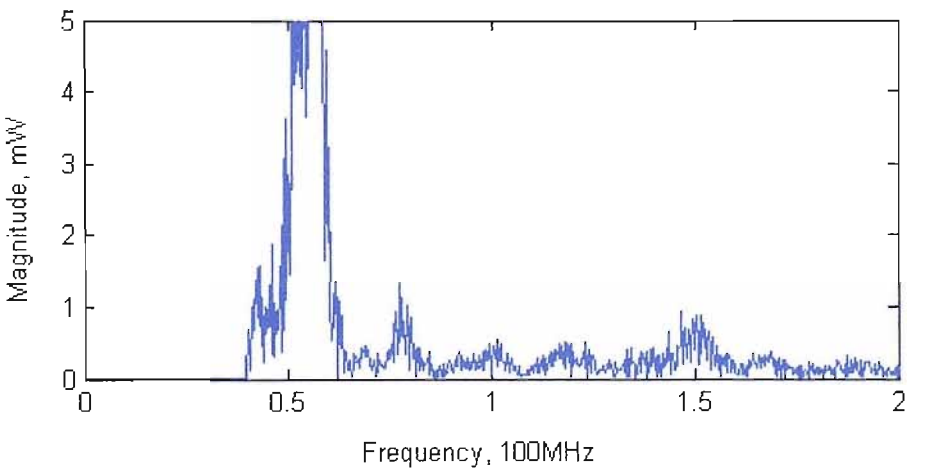

Figure 6.10 A frequency spectrum for the PD signal in Figure 6.6

6.3 Wavelet Analysis for Recognizing PD [93, 95].

In the signal decomposition by wavelet analysis the approximations A and details D are often mentioned when the signal is separated into low and high-frequency components. The approximations are the large-scale, low-frequency components of the signal. The details are the small-scale, high-frequency components of the signal. An example of a basic filtering process to achieve this decomposition is shown in Figure 6.11, where the signal, S, is passed through two *complementary-power* filters and emerges at two signals.

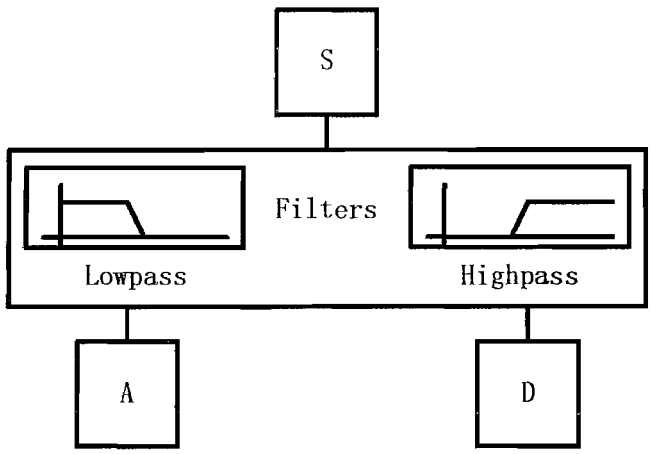

Figure 6.11 The wavelet analysis as a low and high-pass filtering process.

This decomposition process can be iterated, with successive approximations being decomposed in turn, so that the signal is broken down into many lower resolution components. This is called the wavelet decomposition tree. In this version of the tree, the detail signals are not decomposed further. In the example of Figure 12, three levels of approximations are computed, each with a factor of the two less bandwidths than the one above. At each level, a detail signal is also extracted, containing the high-frequency components of the approximation above it.

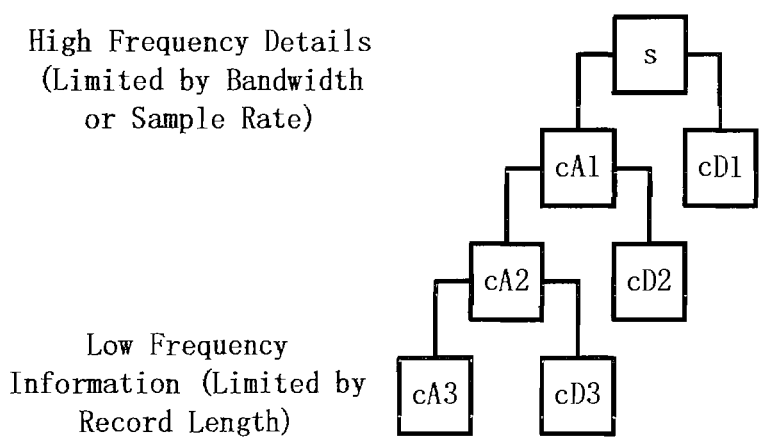

Figure 6.12 Analysis of a signal by a wavelet decomposition tree.[93]

A complete set of coefficients, in terms of reconstruction ability, consists of the set of all termination branches of the decomposition tree, *e.g. A*3; *D*3; *D*2 and *D*1.

The process can be reversed, reuniting the signal into its original form. The encoding process can be applied to the signal more than once, analyzing the trend waveform with the wavelet in the same manner as the original signal. In essence it uses the wavelet function to redistribute the information in the signal, over multiple resolutions. This redistribution is the key to the usefulness of wavelet analysis. The analysis by wavelets can effectively perform what is thought of as a Fourier-type function resolving a signal into constituent waves of different frequencies [93].

The wavelet analysis application in the following two sections quotes the method of Daubechies Wavelets: dbN. The dbN are the names of the Daubechies family wavelets, where N is the order, and db the "surname" of the wavelet [93].

A wavelet analysis programme based on the Daubechies Wavelets: db10, leading to the detail of the decomposed signal into the Level 1, 2, 3 and 4, was used to decompose a PD signal. The software was compiled under Matlab programming environment. Figure 6.13 and Figure 6.14 show the results of using the software to deal with the PD signal shown in Figure 6.4. Where signals in Figure 6.14 are the spread of the outstanding single pulses in Figure 6.13.

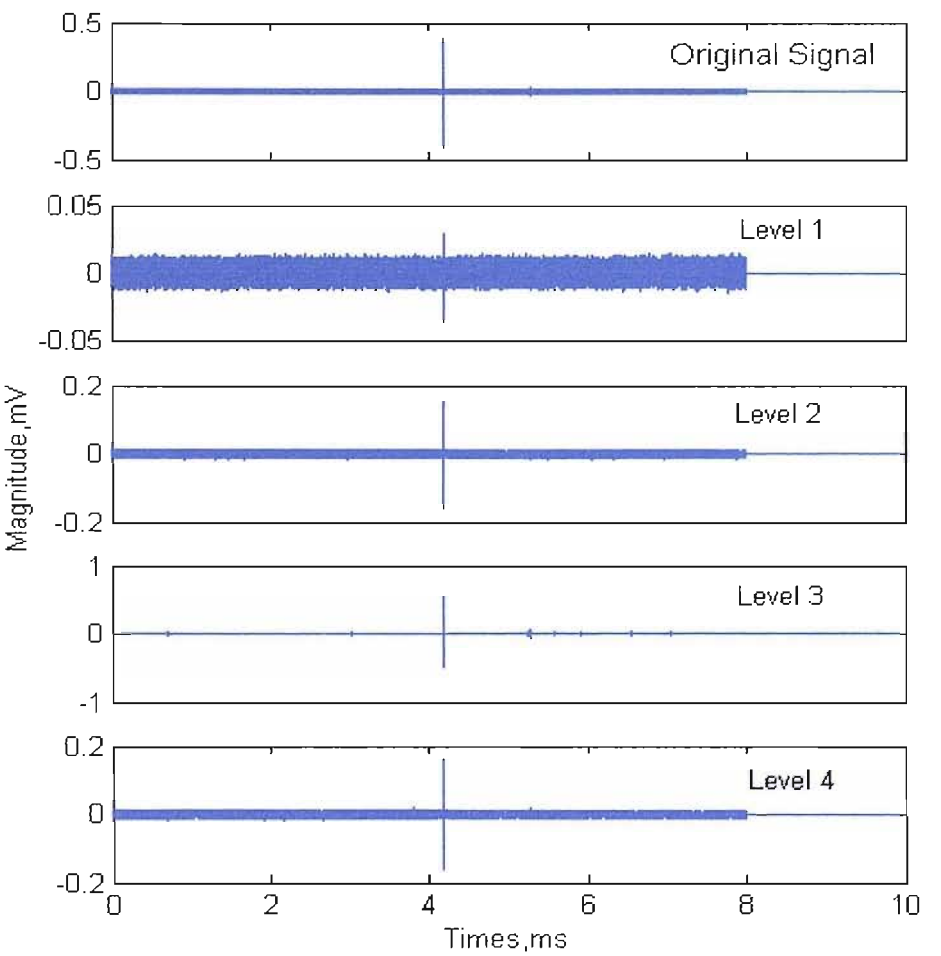

Figure 6.13 The wavelet analysis for the signal on a half cycle of a 50 Hz test voltage

In Figures 6.13 and 6.14 the decomposed approximations are neglected, the decomposed details of the PD are shown. These are the high frequency components decomposed by the wavelet analysis. This indicates that the PD signal consists of different frequency components. So the wavelet analysis can clearly determine the components of a measured signal, and can be considered as a software tool for the PD online analysis.

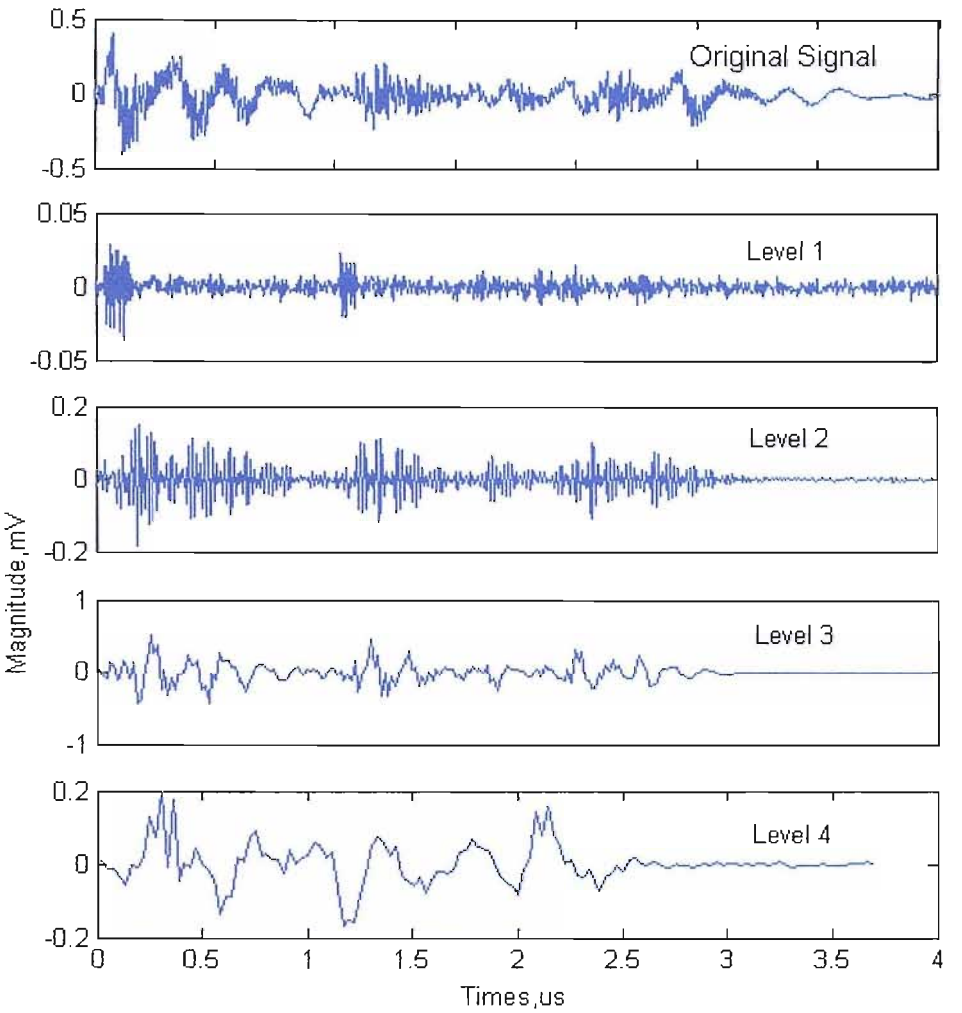

Figure 6.14, Spread single pulses for the outstanding pulses in Figure 6.11

6.4 Distinguishing PD from a Multi-PD waveform

Figure 6.15 shows the multi-PD measurement circuit. A corona discharge source as shown in Figure 4.2 (1) was used. Its metal plate electrode was connected to the 60 kV bushing core bar. A PD source of the needle-plate in oil (as shown in Figure 4.2 (6)) was connected to the bushing core bar. When 26 kV was applied to the two PD sources, the discharge signal occurring at the corona discharge source and the PD source of the needle-plate in oil were directly injected into the bushing at the same time, and then are detected by the RFCT. The time-based waveform across a 50 Hz cycle (20 ms) of the test voltage shown in Figure 6.16 was obtained using the oscilloscope. The sample rate was set with 250 ms/s.

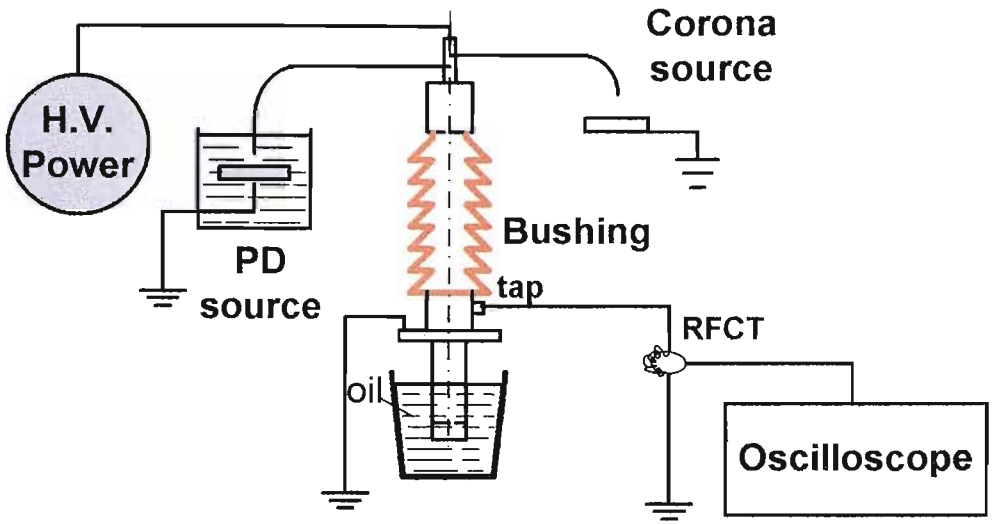

Figure 6.15 A multi-PD waveform measurement circuit

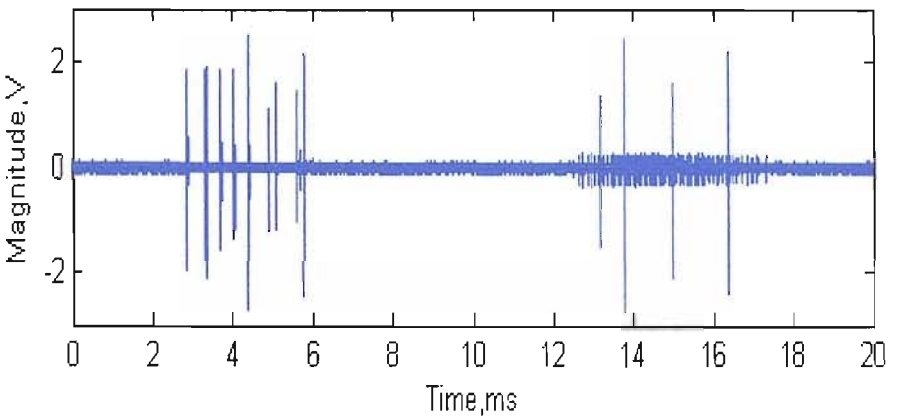

Figure 6.16 A multi-PD waveform

In Figure 6.16, the corona discharge group on the negative half cycle can be recognized by observation. The bigger magnitude pulses on the middle of the positive half cycle may include the positive corona discharge signals and the discharge signals from the needle-plate discharge source. The bigger magnitude pulses on the middle of the negative half cycle may also be the signals from the needle-plate discharge source.

6.4.1 The Application of a Band-pass Filter

Using the band-pass filter described in the section 6.2.1, the measured signal shown in Figure 6.16 was filtered with the bandwidth between 40 MHz and 100MHz. The result is shown in Figure 6.17. Referring to the properties of the partial discharges for a needle-plate PD source (Chapter 4), the preserved pulses might be PD signals from the needle-plate discharge source. From the results obtained the feasibility of this approach is questionable. The filter does remove external corona signals, but also compromises the measurement of internal discharge.

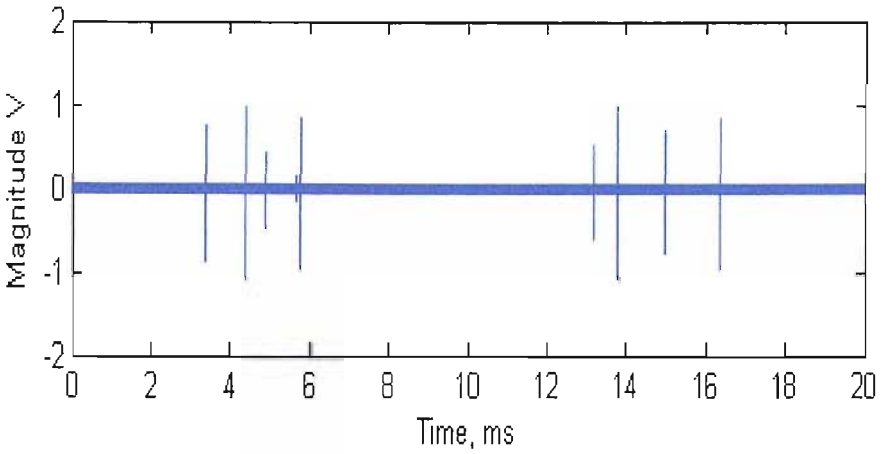

Figure 6.17 The filtered waveform for the Multi-PD waveform

6.4.2 The Application of Wavelet Analysis

The same wavelet analysis method as described in the section 6.3.1 was used again to analyse the multi-PD signal shown in Figure 6.16. The result is shown in Figure 6.18.

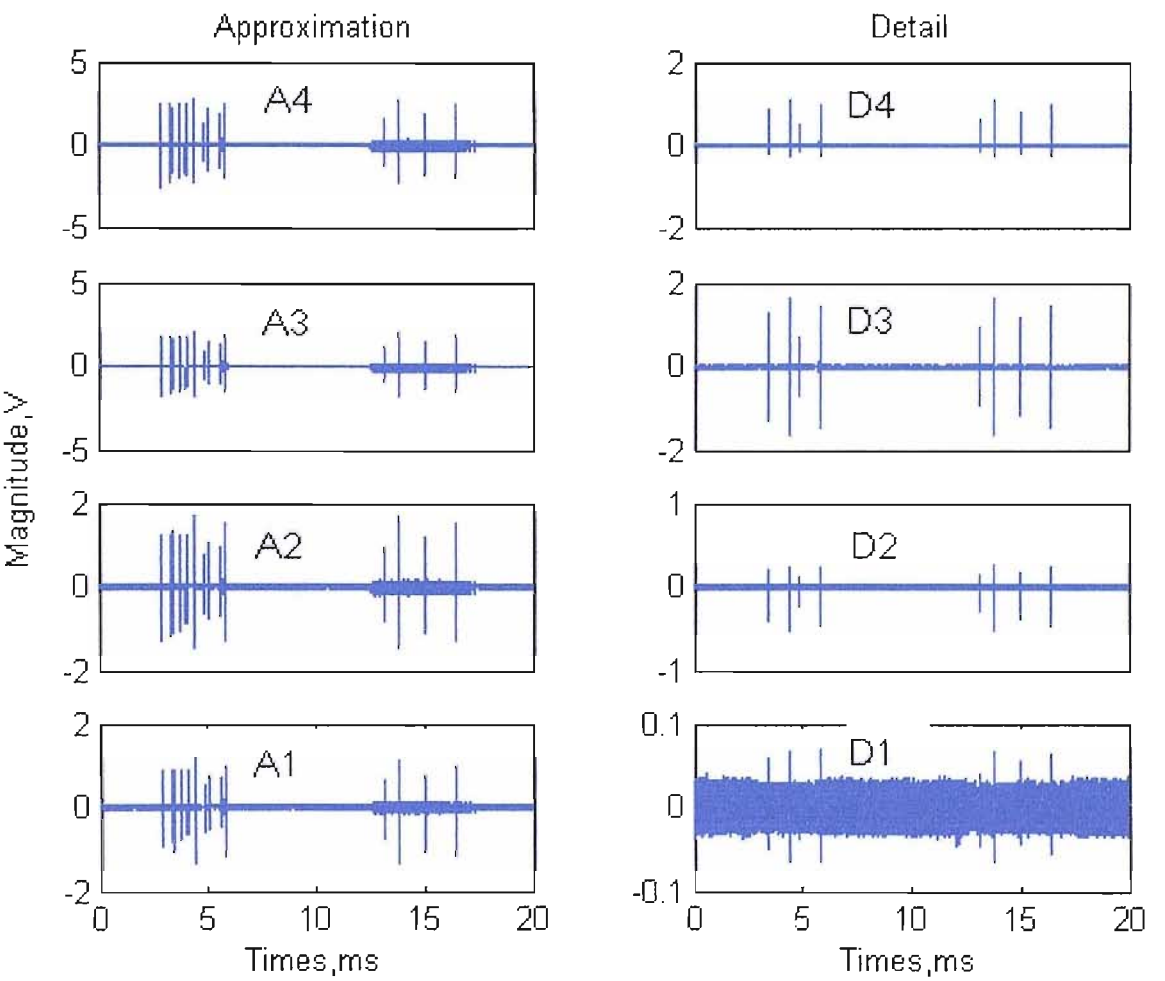

Figure 6.18 The wavelet analysis for a multi-PD waveform

The analysed results show that the bandwidth of the corona discharge has the components of the lowest frequency, so they always appear in the approximation figures. The pulses on all the detail figures correspond to high frequency signals that are decomposed from the approximations. Referring to the properties of the needle-plate discharge in oil as described in Chapter 4, the pulses on the detail figures should be the PD signals from the needle-plate PD source.

6.5 Software Compensator in the frequency Domain

The signals presented on Figure 6.6 were transferred from bushing core bar via a RFCT. The frequency response properties of the bushing and RFCT are shown in Figures 3.2 and 3.5, and indicate the attenuation degree when signals propagate between the bushing core bar and RFCT. Based on analysis for the data of the frequency spectra of the bushing and the RFCT, a software compensator was designed using Matlab. Using this software compensator the measured frequency domain signals at the bushing tap via a RFCT were amplified by the compensator, thereby compensating for the attenuation caused by the bushing and RFCT and reduced background noise signals. Thus, the frequency spectrum situation of the real signals at bushing core bar can be approximated.

Figure 6.19 shows the efficiency of the software compensator is shown. The red curve is the compensated measurement from Figure 6.6. The blue curve is the background noise. The results disclose the "real" frequency content of the PD signals occurring at the bushing core bar.

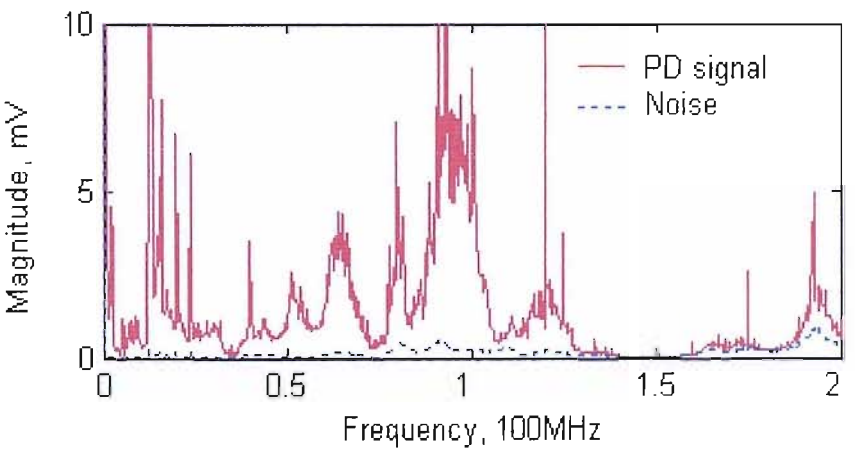

Figure 6.19 An efficiency of the software compensator

6.6 Transformer Models for PD Location and Characterisation

Mathematical models based on the physical properties of a transformer do exist [34, 37]. However, they are only applicable over a reduced frequency range (up to 10 MHz). The RFCT sensor can

detect discharge signal frequencies up to 200 MHz and there is no suitable physical-based model to simulate this process. Based on the assumption that a transformer has linear-time invariant properties, it is feasible to describe it using a transfer function. The transfer function may be obtained from frequency response measurements.

Knowledge of the transfer function combined with measurements at more than one point may be used to develop tools for locating and quantifying a discharge source within the transformer itself.

Due to different sources, PD signals have very different modes and propagation characterisations within a transformer or transformer winding. To trace and analyse PD characteristics within transformer windings and establish the relationship between PD propagation patterns and the PD location, some simulation methods have been investigated. Previous research has focused on transformer windings and neglected the influence of sensors and measurement positions, furthermore, the frequency ranges of these investigations are limited to around 2 MHz.

In this section a Black Box Model method, based on frequency domain signal measurements and mathematical analysis using Matlab/Simulink programming, is introduced.

6.6.1 Computation Principle [96]

Without reference to the internal structure of a transformer, the complicated frequency response of the transformer system can be expressed in general as in following a fractional polynomial of the Laplace operator, s, or the assumption that $s \equiv j\omega$. This is based on the assumption that the transformers characteristic is linear time-invariant in the frequency domain [88, 96].

A complex transfer function with first and second order's zeros and poles can be determined using formula6.2. In this formula, K is the system gain, and ω_i is the break-frequency of the zeros and poles. e^{-sT} allows for the effect of a time delay. The value of the time delay can be determined by plotting phase against frequency (not log of frequency), and measuring the negative slope of the resulting straight line.

$$G(s) = \frac{Z(S)}{P(S)} = \frac{\prod_{i=1}^{n_1} Z_i(s) \prod_{i=1}^{n_2} Z_i(s) e^{-sT}}{\prod_{i=1}^{m_1} P_j(s) \prod_{i=1}^{m_2} P_j(s)} = \frac{K \prod_{i=1}^{n_1} (s+\omega_{1i}) \prod_{i=1}^{n_2} (s^2 + \xi_1 \omega_{2i} s + \omega_{2i}{}^2) e^{-sT}}{\prod_{i=1}^{m_1} (s+\omega_{1j}) \prod_{i=1}^{m_2} (s^2 + \xi_2 \omega_{2j} + \omega_{2j}{}^2)} \quad (6.2)$$

Where, *Z(s)* is the fractional polynomial of *s* for zeros; and *P(s)* is the fractional polynomial of *s* for poles.

If *s* is equal to $j\omega$, then

$$e^{-sT} = e^{-j\omega T} = 1 \arg(-\omega T)$$

If *X(s)* is an impulse voltage waveform, the response waveform is computed in the polynomial form.

$$Y(s) = G(s)\,X(s) \qquad (6.3)$$

Where *Y(s)*, *G(s)* and *X(s)* form an open loop system.
The above equation can be transformed into a time domain analytical function, therefore, a response of the injected impulse can be obtained.

The gain $K(\omega)$ and phase $\theta(\omega)$ of the overall transfer function can be written as sums of the gains, or phases respectively for the individual terms:

$$K(\omega) = \sum K_{Zi}(\omega) + \sum K_{Pj}(\omega),\quad K_{Zi}(\omega) = 20\log|Z_i(j\omega)|,\quad K_{Pj}(\omega) = 20\log\left|\frac{1}{P_J(j\omega)}\right|$$

$$\theta(\omega) = \sum \theta_{Zi}(\omega) + \sum \theta_{Pj}(\omega),\quad \theta_{Zi}(\omega) = \angle(Z_I(j\omega)),\quad \theta_{Pj} = \angle\left(\frac{1}{P_j(j\omega)}\right)$$

To derive the transfer function, the following rules were used:

- First order zeros and poles transfer function

Zero transfer function

$$T(s) = \frac{s+\omega_0}{\omega_0}$$

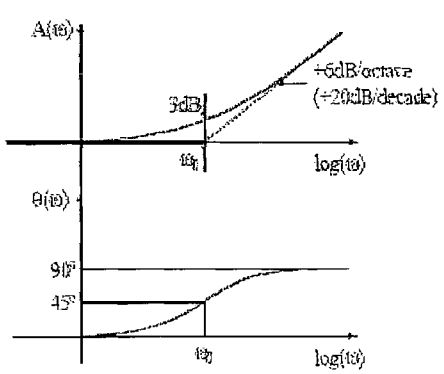

Figure 6.20 Bode plot of first order zero transfer function [96]

Pole transfer function

$$T(s) = \frac{\omega_0}{s+\omega_0}$$

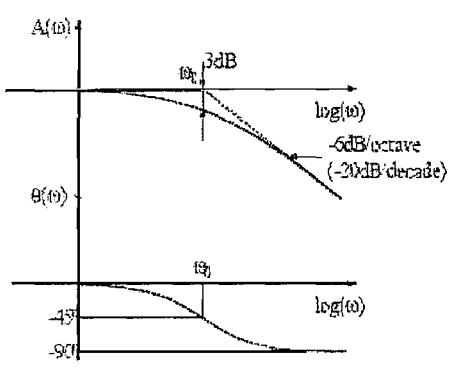

Figure 6.21 Bode plot of first order pole transfer function [96]

- Second order zeros and poles transfer function

Zero transfer function

$$T(s) = \frac{s^2 + s\frac{\omega_0}{Q} + \omega_0^{\,2}}{\omega_0^{\,2}}$$

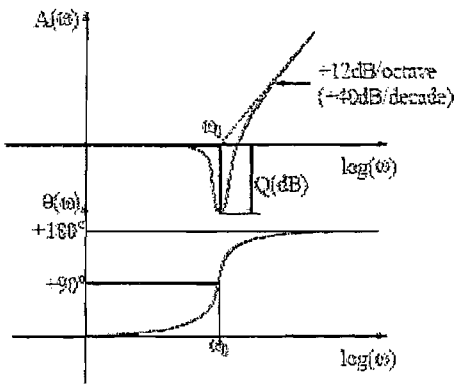

Figure 6.22 Bode plot of second order zero transfer function [96]

Pole transfer function

$$T(s) = \frac{\omega_0^{\,2}}{s^2 + s\frac{\omega_0}{Q} + \omega_0^{\,2}}$$

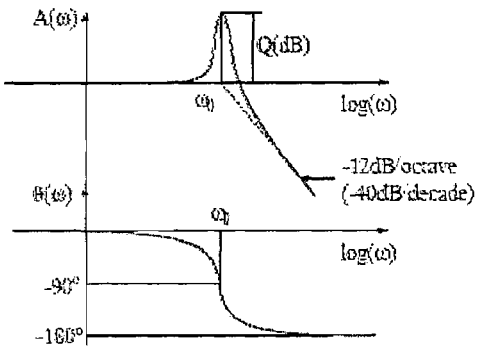

Figure 6.23 Bode plot of second order pole transfer function [96]

In the Figures 6.20-6.23, ω_0 is the break frequency of the zero or pole. The plots are drawn for a positive ω_0. If ω_0 is negative, the gain plots remain the same, but the phase will be decreasing for the left side plot and increasing for the right side one. Rules for drawing high-order Bode plots are [94, 96]:

- Compute $T(0)$ and, based on the obtained value, determine $K(0)$ and $\theta(0)$.
- Decompose the transfer function into first and second order terms. Represent on the frequency axis the critical values where the Bode plots will change.
- The changes in the Bode plots are:
  (1) Each first order term at the numerator (zero) will increase the slope of the gain plot with 20dB/decade, while each first order term at the denominator (pole) will decrease the slope of the gain plot with 20dB/decade.
  (2) Each second order term at the numerator (complex conjugate zeros) will cause a drop of Q dB at ω_0 and an increase in the slope of the gain plot of 40dB/decade, while each second order term at the denominator (complex conjugate poles) will introduce a peak of Q dB at ω_0 and a decrease in the slope of the gain plot of 40dB/decade.
  (3) Each zero located in the left half plane will introduce an increase in the phase of 90°, while each pole located in the left half plane will decrease the phase by 90°. If the zero is located in the right half plane, it will decrease the phase. If the pole is in the right half plane it will increase the phase.
- If there are one or more singularities (poles or zeros) located at ω=0, the initial value of

the gain $K(0)$ will be $\pm\infty$ and the initial slope of the gain plot is not 0dB/decade, but is set by the number of poles or zeros at $\omega=0$.

6.6.2 Transfer Function of the Transformer model

Based on the above theory, using a Matlab program to calculate and analyze the frequency spectrum data measured on the interleaved disc winding transformer model system without oil (Figure 5.8), a transfer function, Formula 6.4, for the interleaved disc winding transformer model without oil was derived. Figures 6.24 and 6.25 compare the simulated and measured spectra of the transformer model system in magnitude and phase.

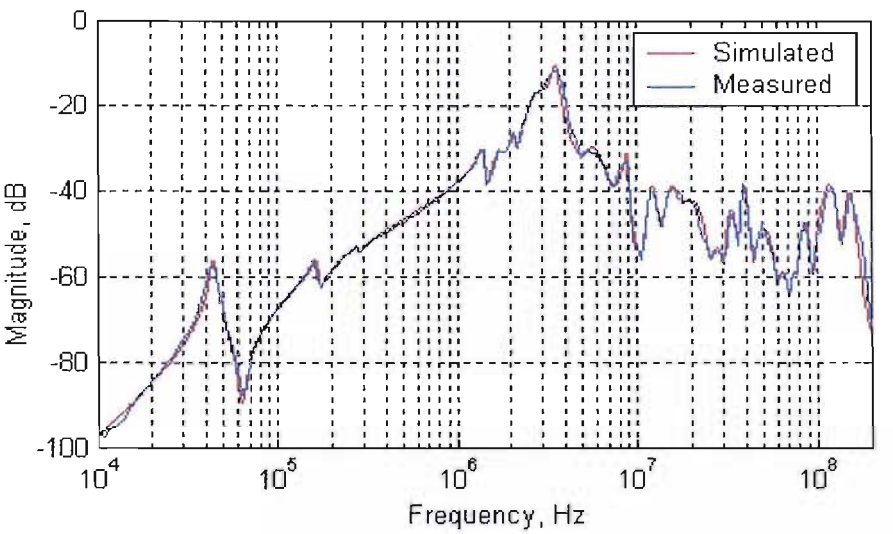

Figure 6.24 Magnitudes of the simulated and measured frequency spectra of the transformer model

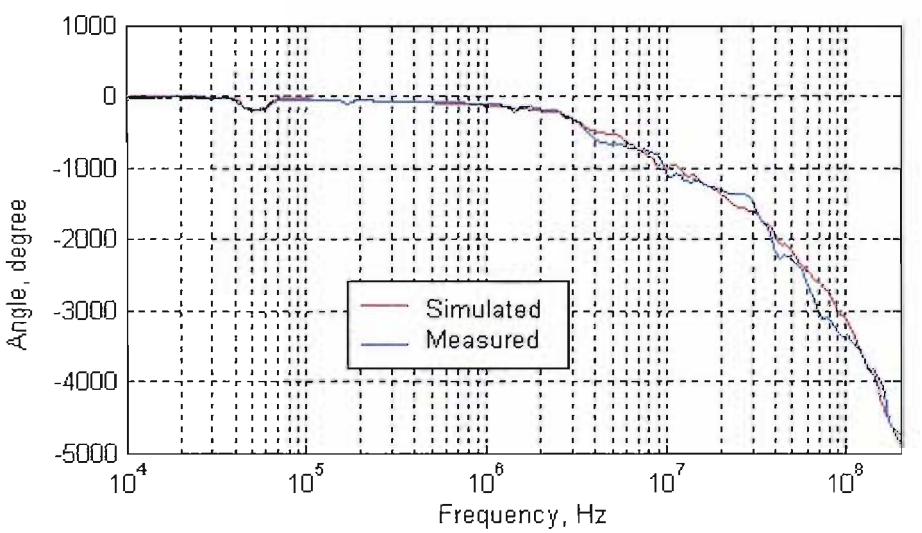

Figure 6.25 Phases of the simulated and measured frequency spectra of the transformer model

In this investigation, the measurement was at the bushing tap via a RFCT and the injection point was at terminal 8. The cables were considered as parts of the system and not excluded by calibration. The Agilent network analyzer was set with a measurement range from 10 kHz to 200

MHz, 20 average sample and 3 kHz sample bandwidth.

In Figures 6.24 and 6.25, the blue curves are the measured magnitude and phase responses of the transformer model system. The red curves are the simulated magnitude and phase responses that were calculated and simulated using the transfer function of Equation 6.4. The calculation and the derivation of the transfer function were all under the Matlab programming environment.

$$
\begin{aligned}
F(s) = \\
&(3.631e\text{-}224\, s^{64} - 2.869e\text{-}214\, s^{63} + 1.136e\text{-}204\, s^{62} \\
&- 3.099e\text{-}195\, s^{61} + 6.602e\text{-}186\, s^{60} - 1.162e\text{-}176\, s^{59} \\
&+ 1.737e\text{-}167\, s^{58} - 2.249e\text{-}158\, s^{57} + 2.557e\text{-}149\, s^{56} \\
&- 2.577e\text{-}140\, s^{55} + 2.32e\text{-}131\, s^{54} - 1.878e\text{-}122\, s^{53} \\
&+ 1.373e\text{-}113\, s^{52} - 9.101e\text{-}105\, s^{51} + 5.492e\text{-}096\, s^{50} \\
&- 3.024e\text{-}087\, s^{49} + 1.523e\text{-}078\, s^{48} - 7.023e\text{-}070\, s^{47} \\
&+ 2.97e\text{-}061\, s^{46} - 1.152e\text{-}052\, s^{45} + 4.104e\text{-}044\, s^{44} \\
&- 1.342e\text{-}035\, s^{43} + 4.028e\text{-}027\, s^{42} - 1.109e\text{-}018\, s^{41} \\
&+ 2.8e\text{-}010\, s^{40} - 0.06477\, s^{39} + 1.371e007\, s^{38} \\
&- 2.653e015\, s^{37} + 4.685e023\, s^{36} - 7.539e031\, s^{35} \\
&+ 1.104e040\, s^{34} - 1.467e048\, s^{33} + 1.765e056\, s^{32} \\
&- 1.926e064\, s^{31} + 1.885e072\, s^{30} - 1.674e080\, s^{29} \\
&+ 1.341e088\, s^{28} - 9.191e095\, s^{27} + 6.563e103\, s^{26} \\
&- 2.814e111\, s^{25} + 2.362e119\, s^{24} - 2.8e126\, s^{23} \\
&+ 6.355e134\, s^{22} + 7.686e141\, s^{21} + 1.138e150\, s^{20} \\
&+ 2.296e157\, s^{19} + 1.115e165\, s^{18} + 1.941e172\, s^{17} \\
&+ 5.065e179\, s^{16} + 6.053e186\, s^{15} + 1.05e194\, s^{14} \\
&+ 8.07e200\, s^{13} + 9.821e207\, s^{12} + 4.403e214\, s^{11} \\
&+ 3.502e221\, s^{10} + 7.218e227\, s^{9} + 1.562e234\, s^{8} \\
&+ 2.513e240\, s^{7} + 1.668e246\, s^{6} + 2.211e252\, s^{5} \\
&+ 2.667e257\, s^{4} + 2.814e263\, s^{3} - 2.533e264\, s^{2}) * e^{-sT} / \\
&(3.002e\text{-}277\, s^{69} + 2.93e\text{-}267\, s^{68} + 1.474e\text{-}257\, s^{67} \\
&+ 5.105e\text{-}248\, s^{66} + 1.362e\text{-}238\, s^{65} + 2.97e\text{-}229\, s^{64} \\
&+ 5.481e\text{-}220\, s^{63} + 8.765e\text{-}211\, s^{62} + 1.234e\text{-}201\, s^{61} \\
&+ 1.548e\text{-}192\, s^{60} + 1.745e\text{-}183\, s^{59} + 1.78e\text{-}174\, s^{58} \\
&+ 1.651e\text{-}165\, s^{57} + 1.399e\text{-}156\, s^{56} + 1.086e\text{-}147\, s^{55} \\
&+ 7.75e\text{-}139\, s^{54} + 5.09e\text{-}130\, s^{53} + 3.083e\text{-}121\, s^{52} \\
&+ 1.724e\text{-}112\, s^{51} + 8.912e\text{-}104\, s^{50} + 4.26e\text{-}095\, s^{49} \\
&+ 1.885e\text{-}086\, s^{48} + 7.717e\text{-}078\, s^{47} + 2.925e\text{-}069\, s^{46} \\
&+ 1.026e\text{-}060\, s^{45} + 3.332e\text{-}052\, s^{44} + 1.001e\text{-}043\, s^{43} \\
&+ 2.779e\text{-}035\, s^{42} + 7.129e\text{-}027\, s^{41} + 1.689e\text{-}018\, s^{40} \\
&+ 3.689e\text{-}010\, s^{39} + 0.07426\, s^{38} + 1.375e007\, s^{37} \\
&+ 2.34e015\, s^{36} + 3.654e023\, s^{35} + 5.223e031\, s^{34} \\
&+ 6.826e039\, s^{33} + 8.139e047\, s^{32} + 8.838e055\, s^{31} \\
&+ 8.722e063\, s^{30} + 7.805e071\, s^{29} + 6.319e079\, s^{28} \\
&+ 4.617e087\, s^{27} + 3.035e095\, s^{26} + 1.79e103\, s^{25} \\
&+ 9.432e110\, s^{24} + 4.426e118\, s^{23} + 1.841e126\, s^{22} \\
&+ 6.763e133\, s^{21} + 2.182e141\, s^{20} + 6.168e148\, s^{19} \\
&+ 1.525e156\, s^{18} + 3.263e163\, s^{17} + 6.201e170\, s^{16} \\
&+ 9.838e177\, s^{15} + 1.445e185\, s^{14} + 1.655e192\, s^{13} \\
&+ 1.874e199\, s^{12} + 1.48e206\, s^{11} + 1.254e213\, s^{10} \\
&+ 6.257e219\, s^{9} + 3.558e226\, s^{8} + 9.311e232\, s^{7} \\
&+ 1.884e239\, s^{6} + 3.168e245\, s^{5} + 3.114e251\, s^{4} \\
&+ 2.621e257\, s^{3} + 1.577e263\, s^{2} + 2.071e268\, s + 1e274) \qquad (6.3)
\end{aligned}
$$

Where T= 2.6432e-008

6.6.3 Verification for the Transfer Function

A very fast pulse as shown in Figure 6.26, generated using the HP 8082A pulse Generator, was injected the transformer model system at the terminal 8. The output at the bushing tap was measured and is shown in Figure 6.27 (blue curve) using an oscilloscope. The condition of the transformer model system was the same as described in section 6.6.2. The measurement circuit was the same as shown in Figure 5.20. The corresponding frequency response of the model system including cables is shown in Figure 6.24.

The same pulse data as in Figure 6.26 was used as the input, *X(s)* in Equation 6.3 to compute the output *Y(s)* of the Function described by Equation 6.4. A simulated output was obtained and is shown in Figure 6.27 (red curve). The simulation procedure was carried out under the Matlab/Simulink programming environment. Figure 6.26 obviously shows that the transfer function produces and output estimate that is very similar to the measured signal.

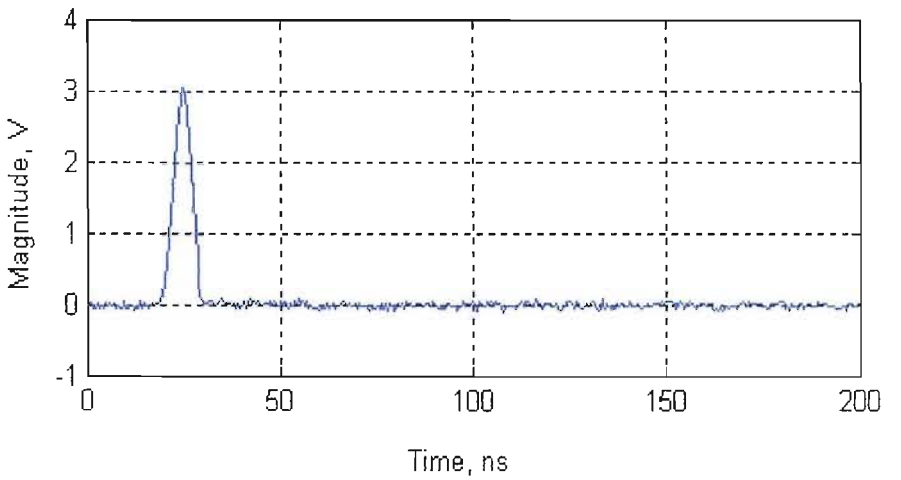

Figure 6.26 A triangle pulse

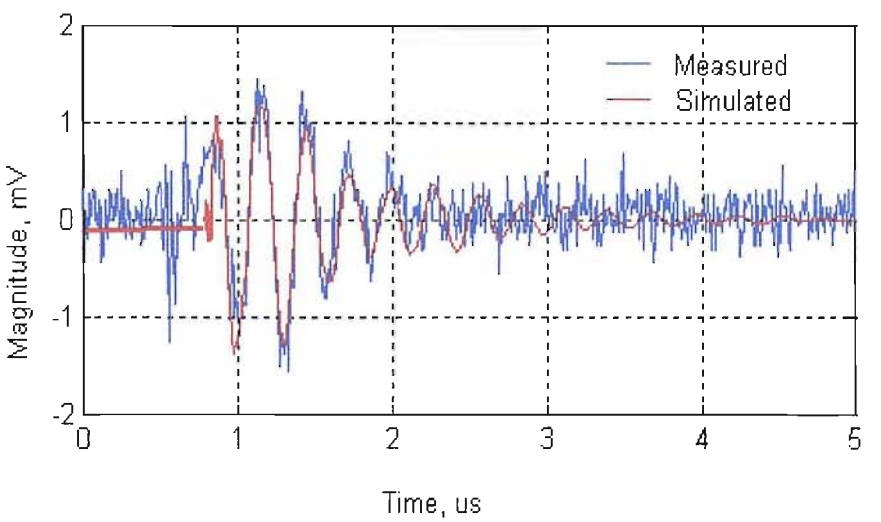

Figure 6.27 Measured and simulated signals

6.7 Conclusions

In this chapter, a principle of measurement and monitoring of partial discharge within oil-filed power transformers is introduced. This principle is based on the fact that partial discharges within a transformer may transfer along a winding and its lead to a bushing core bar. Furthermore, the partial discharge signal may pass through the insulation layers of the bushing to the bushing tap point. In the system, a sensor, for example, a RFCT, can be used to detect output signals at bushing tap point, digital equipment can be used to store, analyze and display measured data.

In order to distinguish partial discharge signals from measured signals, a few software tools based on Matlab programming environment have been developed. By application of the frequency filter functions of these software tools in either time domain or frequency domain, the high frequency components of partial discharge signals can be recognized from a measured signal.

Based on mathematic analysis, frequency domain signal measurements and Matlab/Simulink programming environment, a Black Box Model method to build up a transfer function of a transformer model has been developed. The result indicates that the frequency range of the transfer function constructed by using this method can reach 200 MHz or more. This is an important development as it may allow PD analysis (location, magnitude) based on a frequency response measurement to develop a transfer function combined with sensor-based measurements to detect internal partial discharges.

Chapter 7

Partial Discharge Measurement on the Power Auto-Transformer SGT3A at the Northfleet Substation

Having established the validity of using wide-band RFCTs to measure internal discharges within a high frequency transformer, field trials have been undertaken on the SGT3A transformer. The purpose of there trials was to establish if PD could be detected and discriminated from external sources of noise and then to establish whether the source of any PD activity could be identified.

7.1 Test Object and Measurement Method

Rated Power (MVA)	500/250
Rated Voltage (kV)	400/275/(13)
Vector Symbols	Yy0
Age(yrs)	37

Table 7.1 SGT3A properties

The auto-transformer SGT3A (Photo 7.1) on Northfleet substation was made in 1965. Its relevant properties are shown in Table 7.1.

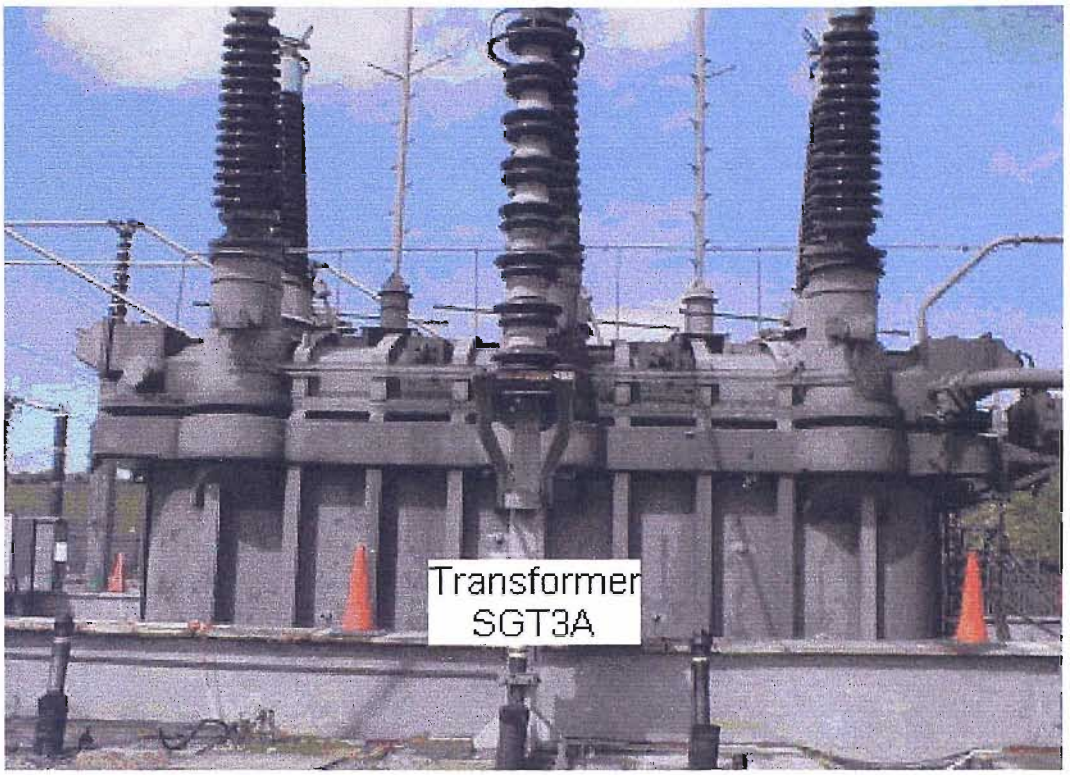

Photo 7.1 the auto-transformer SGT3A

From dissolved gas analysis it has been apparent that the transformer had been producing discharges or partial discharges for some time. From December 1992 to August 1993, there were serious internal discharges with power follow-through. It was possible that the breakdown of oil has occurred between the windings or coils or between the coils and earth. The DGA analysis for data from November 1993 to February 2002 showed evidence of internal partial discharge activity with a high energy density. During this time, a great deal of carbon dioxide (CO2) and monoxide (CO) had been generated. This indicates that cellulose materials (insulation materials in the transformer) were damaged due to the discharge or partial discharge activity [40].

The measurements were carried out using the schematic diagram of the measurement circuit shown in Figure 6.1, Chapter 6. Figure 7.1 shows the measurement circuit applied on-site.

On-site, a 30 meter ethernet cable was used to connect RFCTs contained in metal boxes to the shielded box. Figure 2.5 illustrates the frequency response of the RFCT with a 30 meter cable attached. For on-site measurements, RFCTs with 3 turns on the primary were used at the 275kV bushing taps of a, b and c-phases. The other ends of the primary coils were connected to earth via the metal box that contained the RFCTs and were fixed on to the bushing flanges. Photo 7.2 shows the connections. In addition, a RFCT was placed around the neutral to earth point.

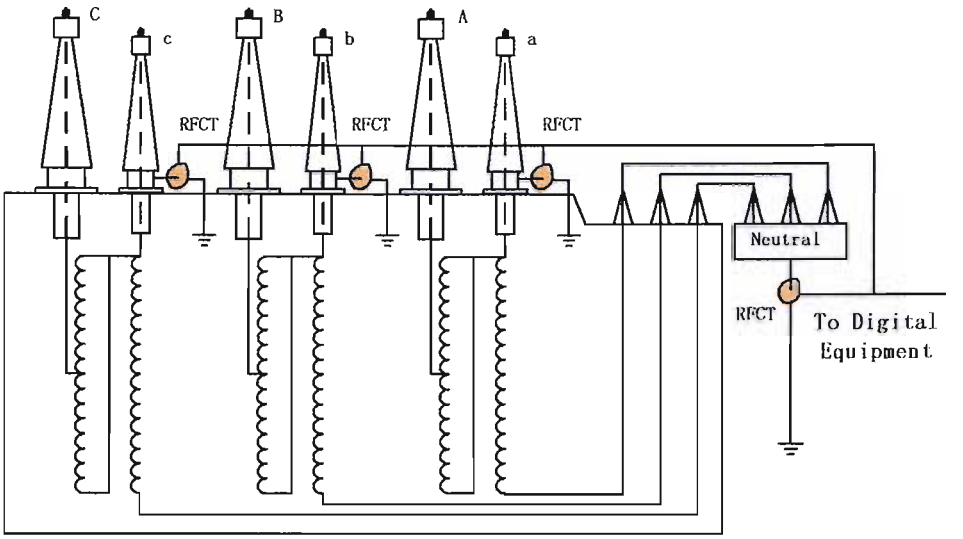

Figure 7.1, the measurement on Northfleet SGT3A auto-transformer

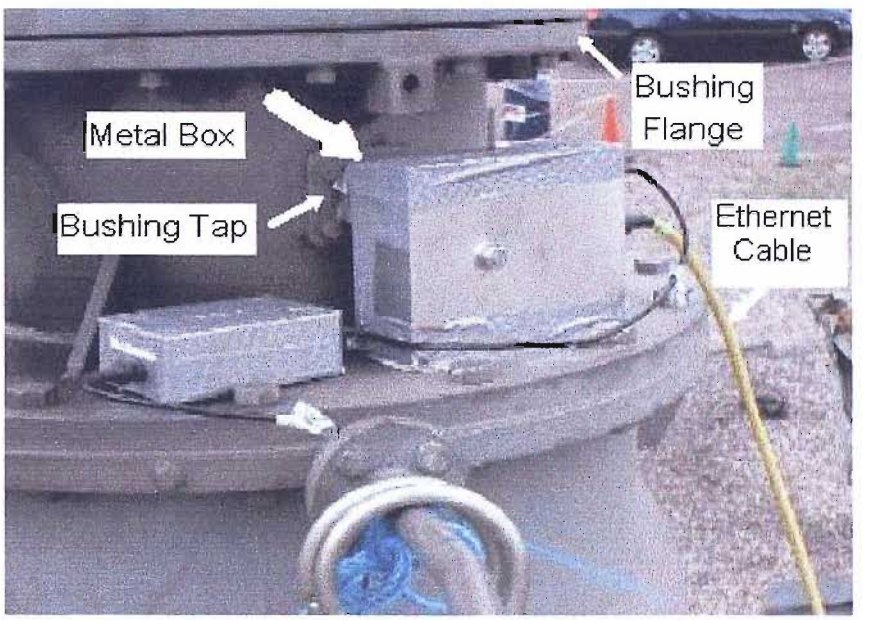

Photo 7.2 the RFCT Box with a RFCT

The capacitance of the 275kV bushing on the auto-transformer is 900pF. Figure 2.1 compares of the simulated frequency response of the 275kV bushing with those of a 60kV bushing and three other capacitors. The results indicate that the 275kV bushing has low impedance at high frequency. Signals above 2 MHz can pass through the bushing to its tap.

7.2 Background Noise Measurements at Northfleet Substation

During the period when the background noise measurements were undertaken the transformer was not energised using the schematic diagram shown in Figure 6.1, Chapter 6 and the measurement circuit shown in Figure 7.1.

7.2.1 Spectra of Background Noise

Spectra of background noise obtained at 6pm on 21 May 2002 are shown in Figure 7.2. The curves are the averaged results of 200 continuous sample sweeps measured using the Spectrum Analyzer. In this test, no external hardware filtering was applied.

There are significant noise signals below 20MHz and between 88MHz and 105 MHz. The noise below 20 MHz may include corona signals induced by the bushings or the busbars connected to them, which act like antennas. The corona might be produced by the neighbouring energized transformers or high voltage equipment on on-site. The signals between 88MHz to 105MHz are FM radio signals.

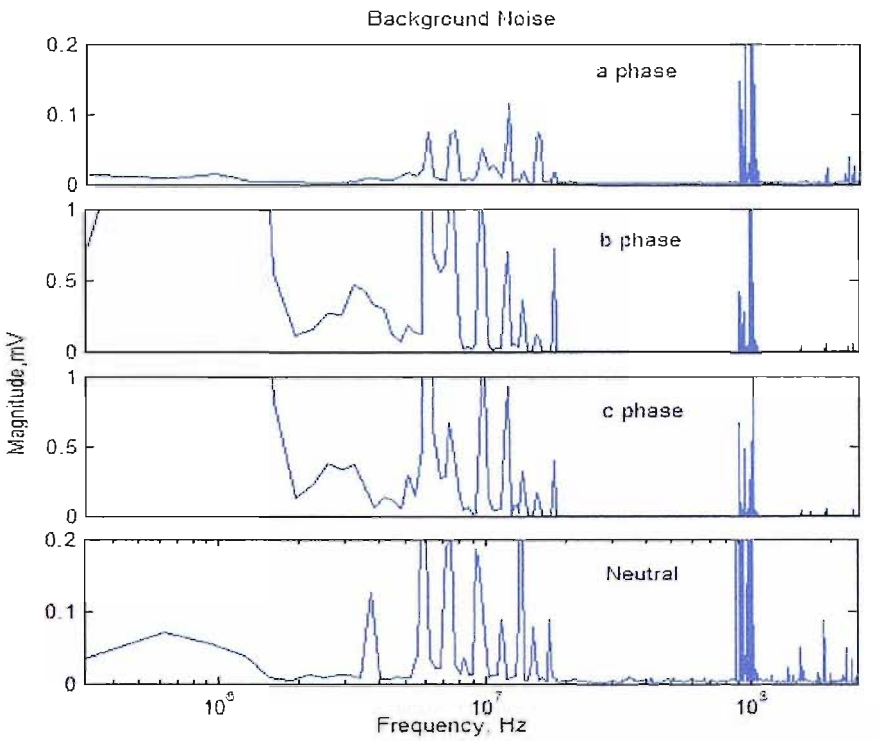

Figure 7.2, Background noise obtained when the transformer was de-energised

7.2.2 Time-based Background Noise Measurements

Time-based measurements of background noise were obtained using the oscilloscope. A zero crossing detector was used as an external trigger which was set 12 degrees (0.67ms) in advance of the 50 Hz waveform of the c-phase of the transformer. The sample rate of the oscilloscope was 250M/s; the signals of all phases were detected separately. Figure 7.3 shows the results merged into the same figure. In this test, no external hardware filtering was applied.

Although there was much noise (induced corona and radio signals, Figure 7.2), Figure 7.3 indicate there is no significant pulses on the time-based waveforms. This means that the noise signals cover the whole cycle and have limited magnitudes throughout the cycle.

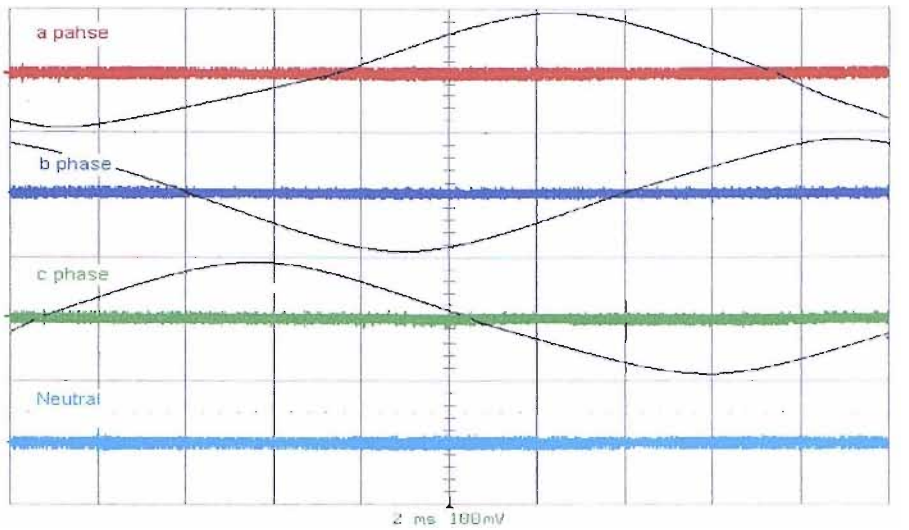

Figure 7.3, Background noise measurements

7.3 On-line Measurements

7.3.1 Spectra of Signals and Analysis

Figure 7.4 shows the measured frequency spectra of signals obtained from the energized transformer using the Spectrum Analyzer. In this case there are significant frequency components below 20 MHz. there are some signals between 20MHz and 100 MHz.

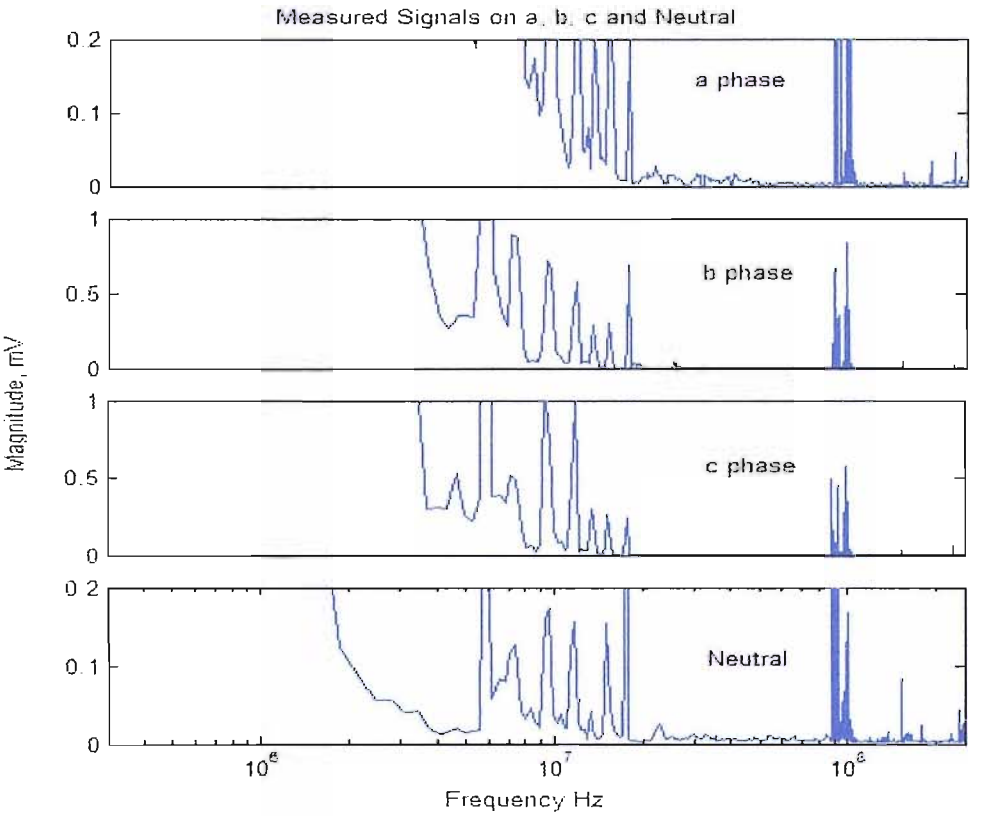

Figure 7.4 Spectra of signals; when the transformer was energized

Figure 7.5 compares the spectra between measured signals (Figure 7.3) and the background noise (Figure 7.4). The scale of magnitudes is in "μV". From Figure 7.5, there are obvious signals between below 50 MHz on a, b and c-phase and the neutral that were produced after the transformer was energized. Some signals between 50MHz and 88MHz were detected for b and c-phases. Some signals on the same frequency range were obtained from the Neutral and were induced or transferred from a, b or c-phases. If the signals below 50 MHz were considered as the corona or external surface discharge, the signals beyond 50 MHz on b or c-phase could be considered as internal PD signals.

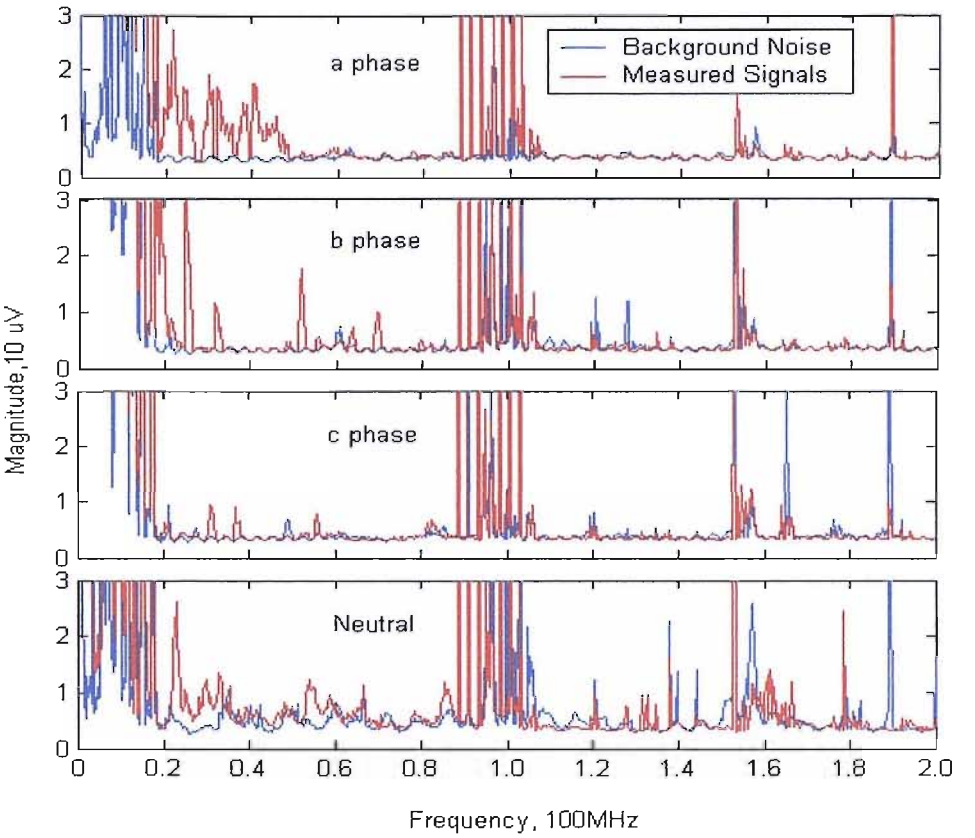

Figure 7.5 Spectra comparison between measured signals (red curves) and background noise (blue curves)

7.3.2 Time-based Signal Measurements and Analysis

Figures 7.6 and 7.7 are the time-based signals obtained for one 50 Hz cycle (20 ms) of the operating voltage of the transformer. They are persistence figures measured over 1000 cycles, detected using the LC684DXL oscilloscope. Figure 7.6 is for c and a-phases, Figure 7.7 is for c and b-phases. The signals were pre-filtered using a 500 kHz high pass, 540 kHz-1.6MHz band stop and 88MHz-108MHz band stop filter. The Oscilloscope filter was set to 200MHz low pass. Amplifiers were not used. A zero crossing detector was used as an external trigger, the trigger leading the c-phase of the transformer by 12 degrees.

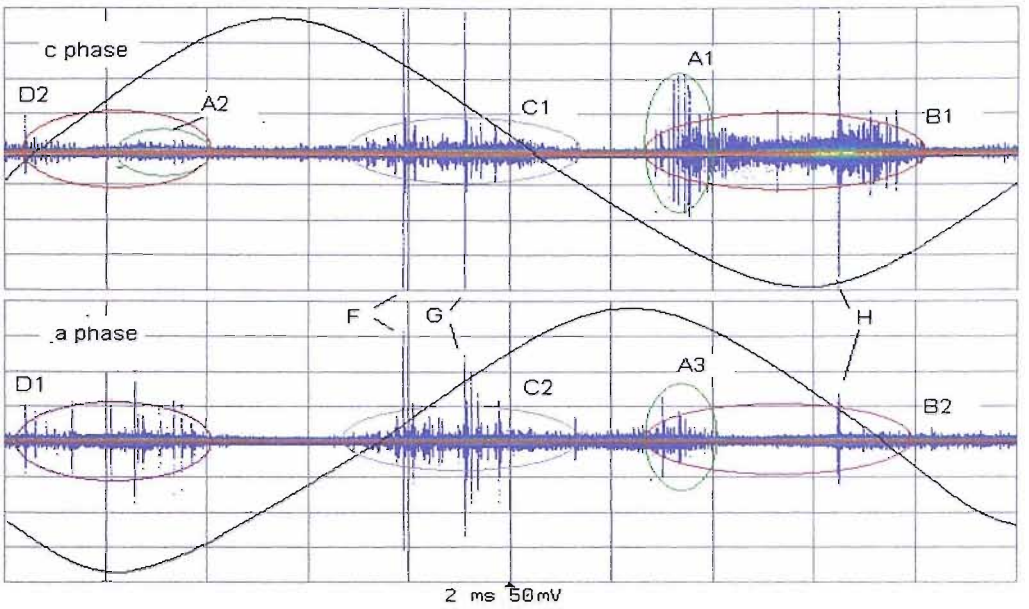

Figure 7.6 Persistence plots for phases c and a

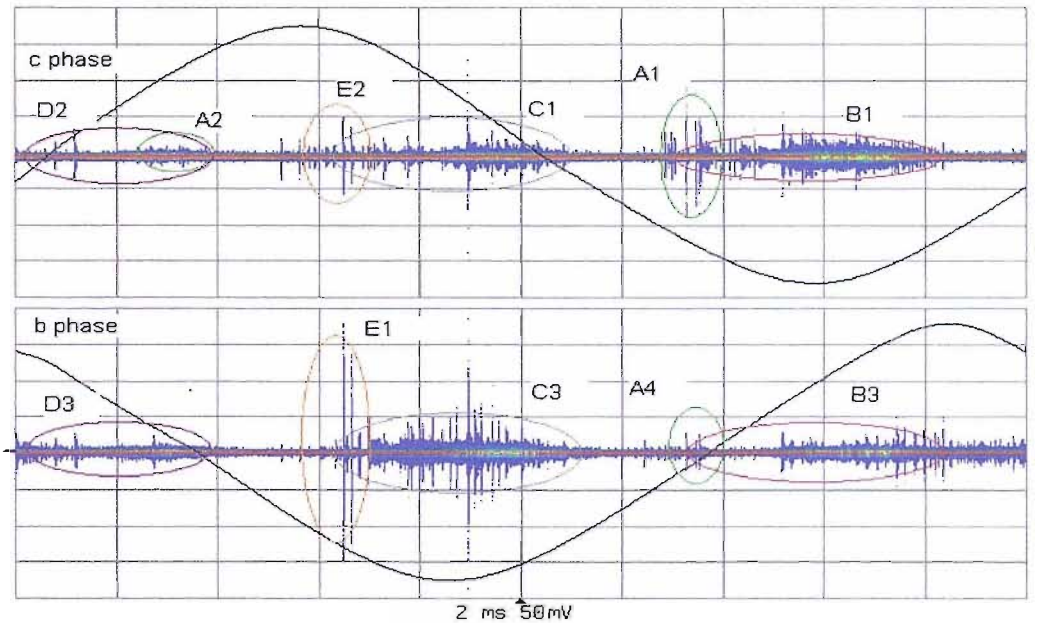

Figure 7.7 Persistence plots for phases c and b

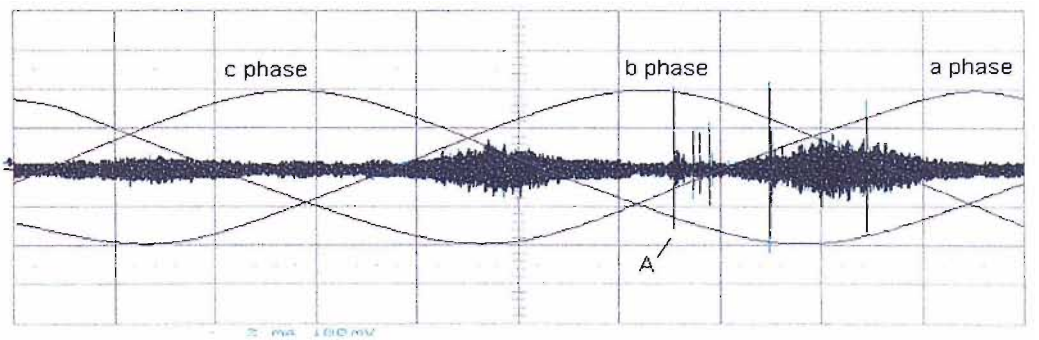

Figure 7.8 Measured signals on the neutral

7.3.2.1 Analysis for the a-phase

With reference to Figures 7.6 and 7.7, the signal D1 on a-phase pattern was a typical corona occurred on the a-phase bushing or the equipment connected to it. The D2 and D3 were the induced or transferred signals of the signal D1 respectively on the c-phase and b-phase. The signal C2 was induced or transferred from corona C3 of b-phase. The signals A3 and B2 were induced or transferred from signal A1 and B1 of c-phase. The signals F, G and H in Figure 7.6 had greater magnitude with smaller number, and might obviously occurred on c-phase due to the magnitudes of them on c-phase are greater.

These signals F, G and H have similar properties to the needle-plane discharge measured in the laboratory. Possibility is that these signals were not surface discharges or corona, (refer to the analysis for the c-phase data) because they do not have the properties of the both external discharges. So they should be internal partial discharges occurring between the high voltage electrode and earth electrode or a lower potential electrode

7.3.2.2 Analysis for the b-phase

The analysis method used for a-phase can be used to analyse the b-phase. In Figure 7.7 the signal D3 was transferred or induced from the corona signal D1 on the a-phase. The signal C3 was the corona occurring on the b-phase. The signals A4 and C3 were from the corona signals on the c-phase. As there was no shielding between the b-phase bushing and the c-phase bushing, also between the b-phase bushing and the a-phase bushing, the coupled signals on phases a and c were almost as large.

The signals E1 and E2 in Figure 7.6 are similar to signals F G and H, but they were produced on the b-phase. Its sporadic and unsteady properties correspond to the needle-plane discharge measured in the laboratory. It is not likely that this is discharge signals produced outside of the transformer; it is more likely that it is an internal PD signal.

7.3.2.3 Analysis for the c-phase

With reference to Figures 7.6 and 7.7, the signal B1 is a typical of a corona discharge. It was produced by an external high voltage electrode onto the transformer either on the 275kV bushing head of the c-phase or on some neighbouring equipment connected to the 275 kV busbar of c-phase. The signal B2 in Figure 7.6 and B3 in Figure 7.7 were induced or propagated from B1. Comparing these two wave shapes, B2 is smaller than B3; this is because the b-phase bushing is between the c-phase and the a-phase. The b-phase bushing not only induced the B1 signal, but also shielded the B1 signal from its reaching the a-phase bushing. Another possible way for signal B1 to travel to the

b-phase bushing or the a-phase bushing is inside the transformer, along the bushing core-lead-winding-lead-neutral-lead-winding-lead-bushing core. For phases b and a, the routes are roughly equivalent for a high frequency signal. The high frequency signal propagating along these two paths should experience attenuation [40]. The similar analysis for signals D2, A2, A1 and C1 can be made, and they were all induced or transferred from the other two phases.

The signal F, G and H in Figure 7.6 do not belong to the any corona signal group, although there is some crosslinking between them, their sporadic and unsteady properties corresponded to an needle-plane discharge Therefore these signals could be internal PD signals.

7.4 Conclusions

There are evidences of PD activities in all three phases of the auto-transformer. The spectrum analysis shows that on the all three phases and the Neutral there were obvious discharge signals below 88 MHz. If the signals below 50 MHz were considered as the external corona or surface discharges, these signals between 50 MHz and 88 MHz on the b-phase and c-phase could be the evidences of PD activity. It is most likely that there are PD sources in c-phase or b-phase or somewhere near to them inside the transformer.

The analysis for the time-based waveforms of a, b and c phase also found that the typical internal discharge signals (the needle-plane discharge in oil) occurred on b-phase and c-phase, and the typical external corona occurred on all three phases. All these signals could be transferred or induced between them and the Neutral.

The measured results had shown that the measurement principal and system shown in Figure 6.1 and Figure 7.1 can detect PD signals on-site. The bushing taps can be considered as the available points to obtain the PD signals within power transformers. Wideband RFCTs can be used as sensors to detect PD signals at transformer bushing taps.

In this measurement, only the 275kV bushing taps and neutral were detected via RFCTs. Future measurements should also monitor the 400kv bushing taps. Then more accurate judgements and conclusions can be deduced.

There is a need to further develop data processing tools, so that data can be efficiently analysed on-site.

Chapter 8

Measurements of High Frequency Signal Propagation within the Transformer Model at UMIST

From 4^{th}-6^{th} of August, 2002, an investigation into the propagation characteristics of high frequency signals within a transformer model was carried out at the High Voltage Laboratory of UMIST.

The transformer model used for the test is a single-phase, dry-type, distribution transformer. It has a capacity of 1600kVA and a high voltage rating of 11kV. The transformer model includes whole construction parts of a real dry-type distribution transformer. The only difference from a real transformer is that its low voltage winding is an earthed metal cylinder instead of a wound conductor. The H.V winding is a plain disc arrangement. No bushing is required as the model operates at low voltage and is a dry-type transformer. The transformer model was designed and manufactured in 1987 at GEC Distribution Transformers Ltd. In the test, the model transformer was considered as a normal power transformer

The aim of the test was to understand the propagation characteristics of high frequency signals (including PD signals) within the transformer model (winding) and to verify the measurement principle developed in Chapter 6.

Photo 8.1 Transformer model

Photo 8.2 Transformer model

8.1 Schematic Diagram of Measurement Circuit

Figure 8.1 shows the main schematic diagram of the measurement circuit. In the circuit, a 50kV, 330pF capacitor (C) was used to simulate a transformer bushing. As sensors, two RFCTs, each with a 3 turn primary coil, were used to detect the transferred signals at the two ends of the high voltage winding as shown in Figure 8.1.

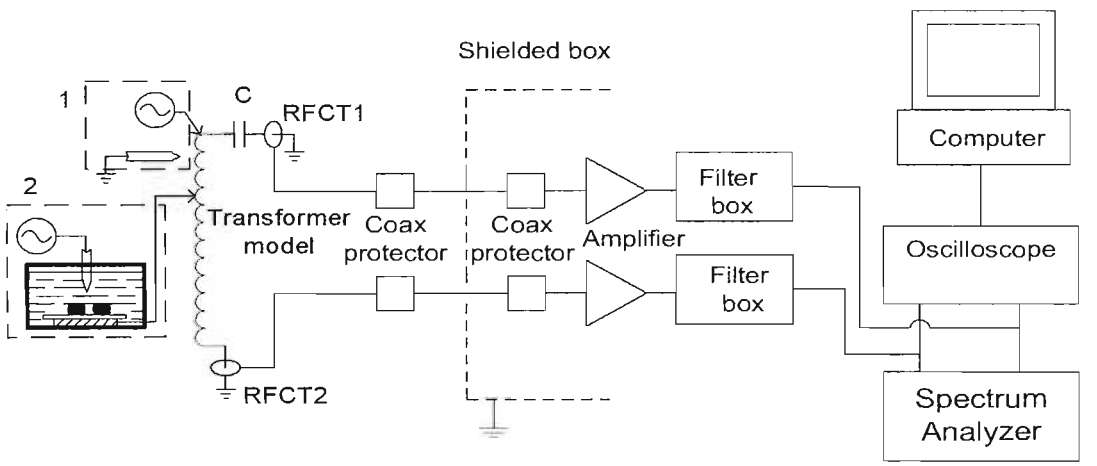

Figure 8.1 Schematic diagram of the measurement circuit

In theory, the PD signals injected into the winding of the transformer model may propagate along the winding and its end leads to reach the measurement points; the RFCTs detect the signals and

pass them via ethernet cables to the oscilloscope, spectrum analyzer and computer contained in a shielded box.

An Agilent 4395A Network/Spectrum/Impedance Analyzer was used to analyze the frequency spectrum of the signals obtained via RFCTs. It can determine the frequency range from 10Hz to 500MHz. Signal amplifiers with a frequency range from 0.01 to 1000MHz and an amplification gain of 20dB were used to amplify the obtained signals. A digital Oscilloscope, LC684DXL, was used to display time-based waveforms and store raw data. A Pentium III 450 MHz computer was used to process measured data. During the test, a zero crossing detector was used as an external trigger. The trigger was considered as having near synchronization with the 50 Hz waveform of the test voltage.

Two kinds of PD sources were used in the test. PD source "1" was used to produce corona. In this discharge system, there was an earth needle point aimed at a disc of the winding of the transformer model with about 3 mm of air gap. A high voltage was applied to the top end of the winding during test. PD source "2" was a discharge system designed to produce floating partial discharges in oil. During tests, a high voltage was applied to the needle point of the set. Another electrode (low potential) of the system was connected to the measuring point within the winding to inject the PD signals into the winding.

8.2 Background Noise

When the transformer model and PD sources were not energized, the circuit shown in Figure 8.1 was used to measure the background noise in both the frequency and time domains. The amplifiers were not used in the test.

8.2.1 Frequency Spectrum

The frequency spectrum of the background noise in the High Voltage Laboratory of UMIST is shown in Figure 8.2, and was obtained using the Spectrum Analyzer.

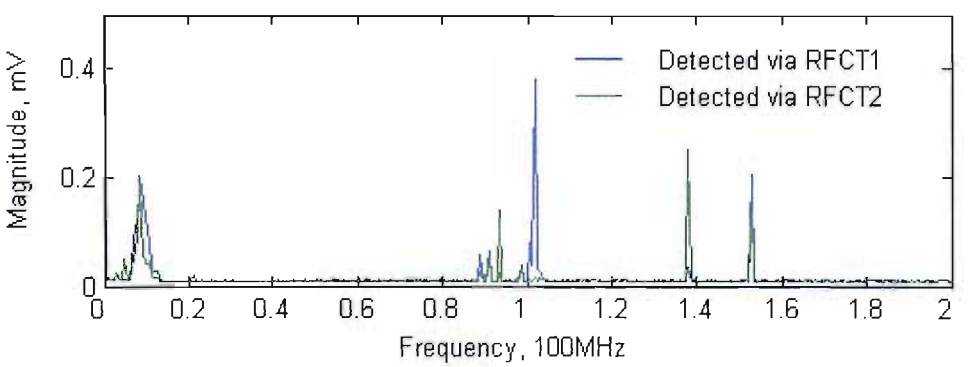

Figure 8.2 Frequency spectra of background noise

The signal around 1 MHz is AM radio; the signals between 4-12 MHz, around 138MHz and 153MHz are noise signals; the signals between 88-102MHz are FM radio signals. During the test the Spectrum Analyzer was set with 10Hz-200MHz ranges; a sample bandwidth of 30Hz and a 16 average sample

8.2.2 Time-based Waveform

The time-based measurements of background noise were obtained using the oscilloscope, LC684DXL. The sample rate of the oscilloscope was 250M/s. The measurement results are shown in Figure 8.3. Figure 8.3 indicates that although there is the background noise of Figure 8.2, there are no significant pulses within the time-based waveforms.

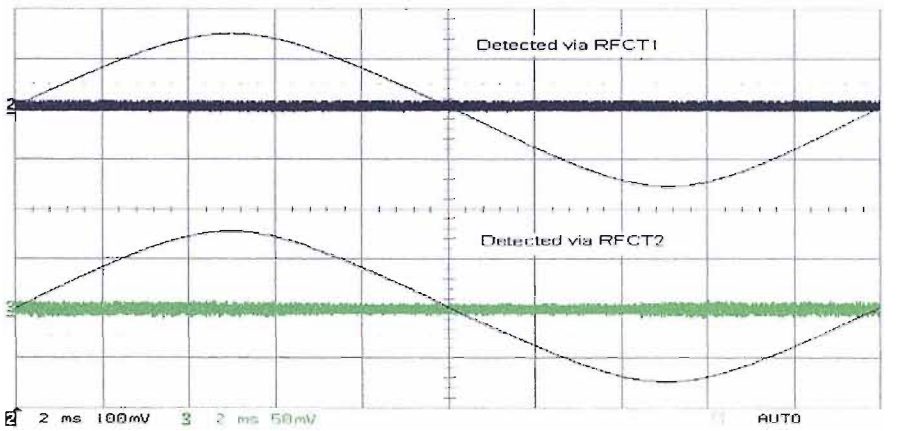

Figure 8.3 Time-based waveform of background noise

8.3 Measurements of the Propagation Characteristics of Signals

Due to the electrical parameters of a transformer winding, the magnitude of a high frequency signal travelling within the winding must be reduced by attenuation, and the high frequency components of the signal could have a loss. This section describes the investigation into the propagation characteristics of a high frequency signal within a transformer winding.

8.3.1 The Propagation of a Single Pulse

Before the test a calibrated measurement for a pulse was undertaken using the following method: A very fast pulse (as shown in Figure 8.5) was generated using the 8082A Pulse Generator. The frequency response of the pulse is shown in Figure 8.6. The measurement was obtained by injecting the pulse directly into the oscilloscope. Figure 8.6 shows that the bandwidth of the input pulse is approximately 500MHz.

This test was carried out using the circuit shown in Figure 8.4. In the circuit a 220pF capacitor was used to simulate the transformer bushing. A digital oscilloscope, LC684DXL, was used to display, analyse and store the pulse output obtained at different measuring points. The pulse shown in Figure 8.5 was injected into the transformer model winding at the upper end of the capacitor. The measuring points were at the 1st, 2nd, 4th, 8th, 16th, 64th and 68th discs of the model winding.

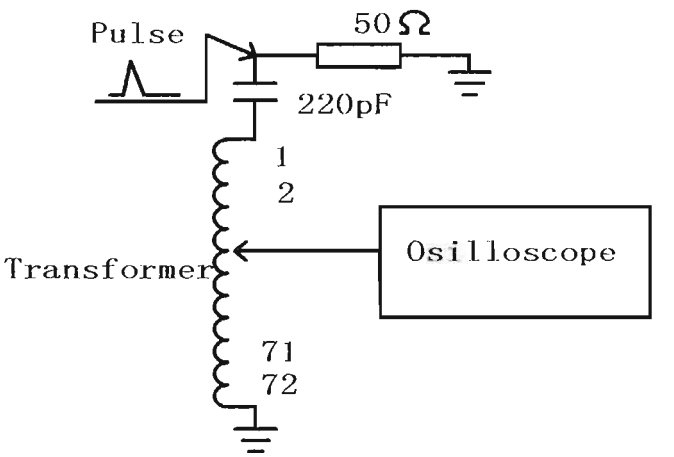

Figure 8.4 Measurement circuit for a single pulse injected into the model

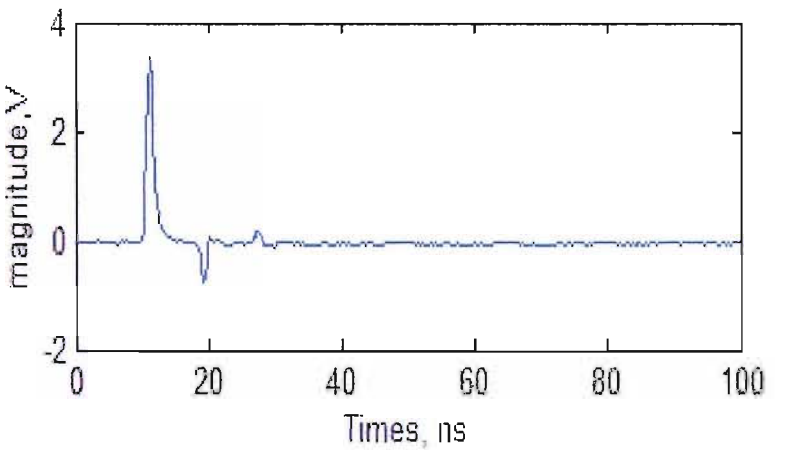

Figure 8.5 a single pulse injected into the model

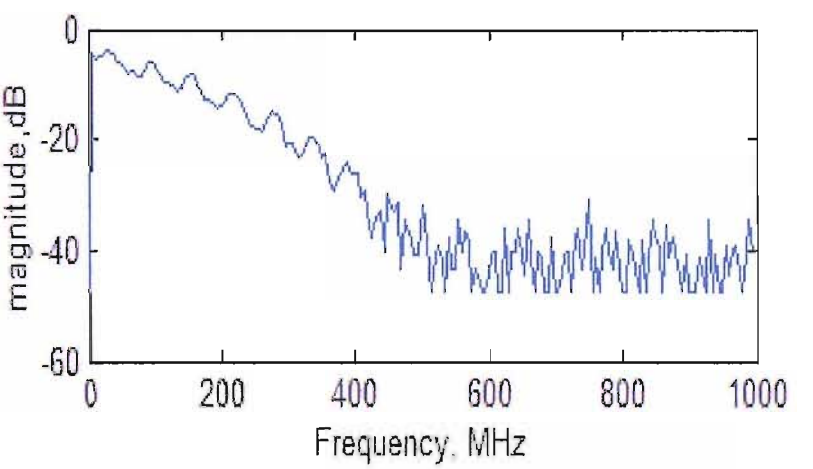

Figure 8.6 Frequency spectrum of the single pulse shown in Figure 8.5

The Figures 8.7 and 8.8 show the measured wave shapes and the frequency responses at each measurement point.

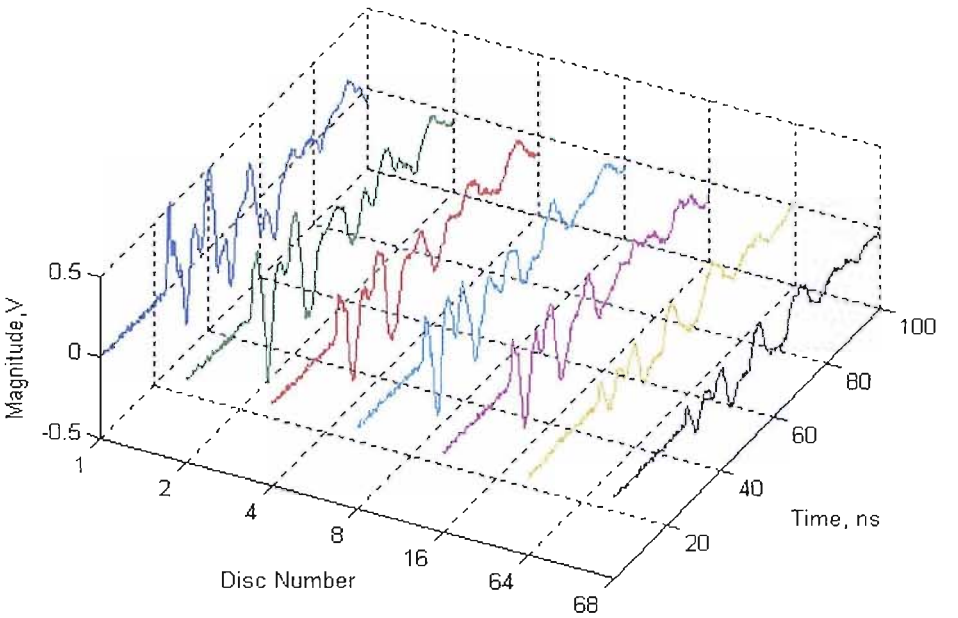

Figure 8.7 Time domain waveforms at various measurement points

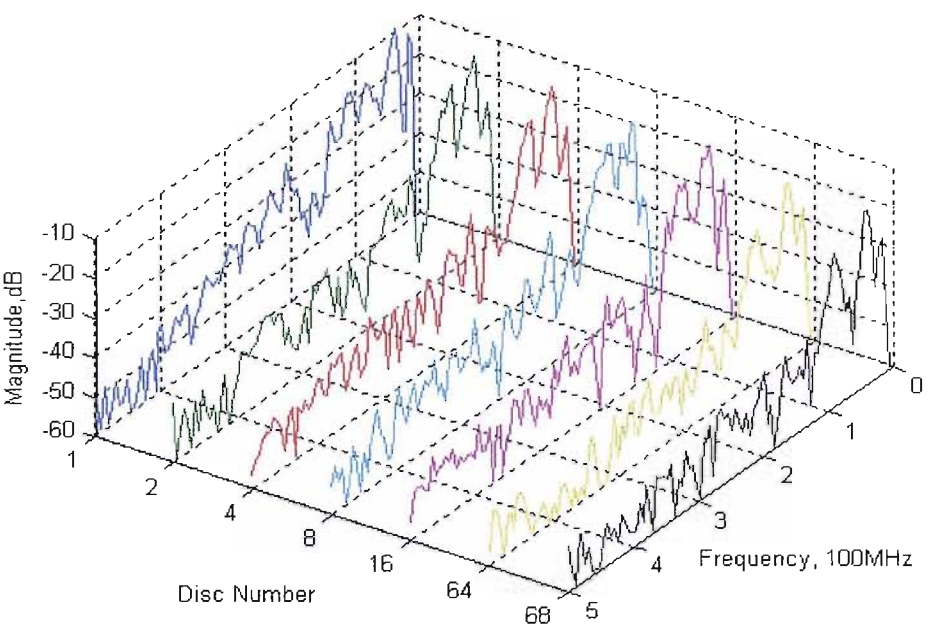

Figure 8.8 Frequency spectra at various measurement points

The measured waveforms in Figure 8.7 indicate that with changes of measuring position the output is attenuated. The more discs between the point of injection and the point of measurement, the greater the attenuation. There is a time lag between the first and last output signals. But for frequency spectra shown in Figure 8.8, all are very similar. It is therefore likely that high frequency signals pass through the winding of the transformer model whereas lower frequency signals are more attenuated.

8.3.2 The propagation of corona signals

In the section the propagation characteristics of simulated corona within the transformer winding at UMIST is introduced. An earthed copper bar with a needle point was used as a corona source.

8.3.2.1 Frequency Spectra

This test was carried out using the corona source and Spectrum Analyzer in the circuit shown in Figure 8.1. When a 3.2kV voltage was applied to the top of the winding, corona discharge occurred around the needle point of the corona source. The corona signals were transferred to another electrode of the discharge system (respectively the 10^{th} disc and the 24th disc of the winding). High frequency components of the corona propagated along the winding and its leads, reaching RFCT1 and RFCT2 where data was captured using digital equipment contained within a shielded box. Figures 8.9 and 8.10 compare of the frequency spectra of the background noise with the corona signals detected via RFCT1 and RFCT2. In this test no hardware filters and amplifiers were used.

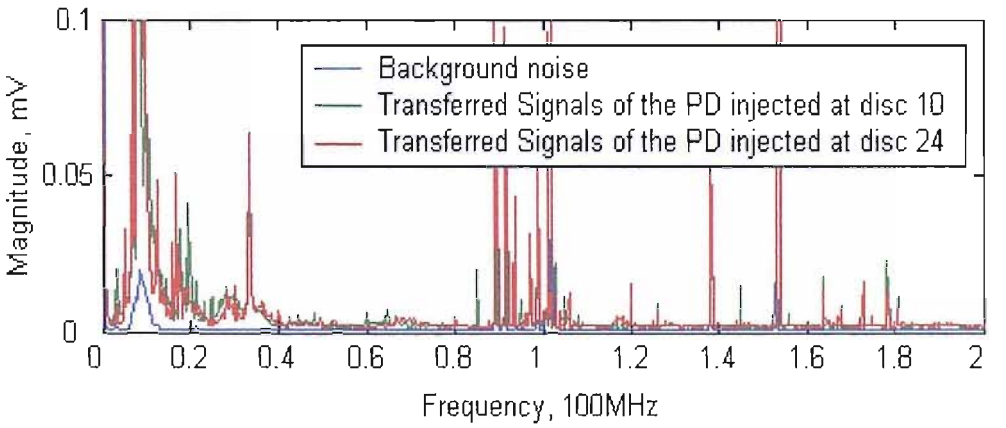

Figure 8.9 Frequency spectra of background noise and transferred corona at discs 10 and 24, measured via RFCT1

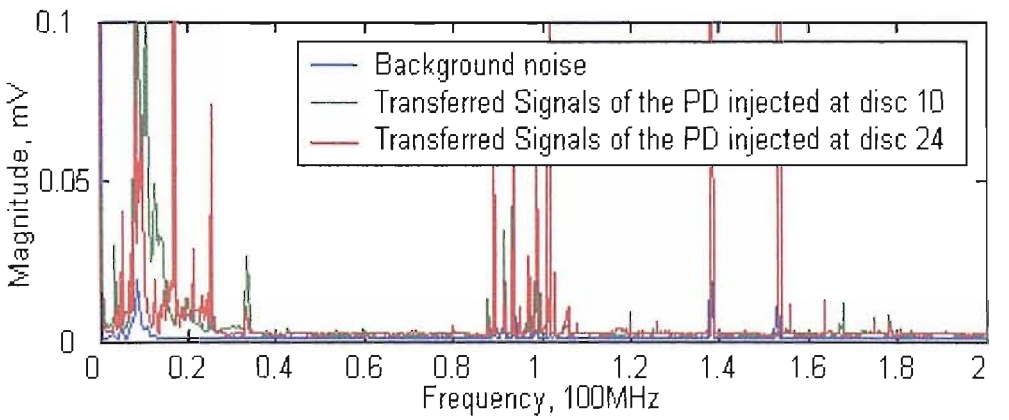

Figure 8.10 Frequency spectra of background noise and transferred corona at discs 10 and 24, measured via RFCT2

All signals over 40MHz can be considered as external noise. The signals from 88 to 108MHz are FM radio signals. The signals below 40MHz are from the corona signals transferred from the injected positions, as well as some background noise.

8.3.2.2 Time-based Waveforms

Time-based waveforms as shown in Figure 8.11 were measured via RFCT1 and RFCT2 and were stored using the oscilloscope. . Figure 8.12 shows a persistence figure over 1000 cycles for the two measured signals.

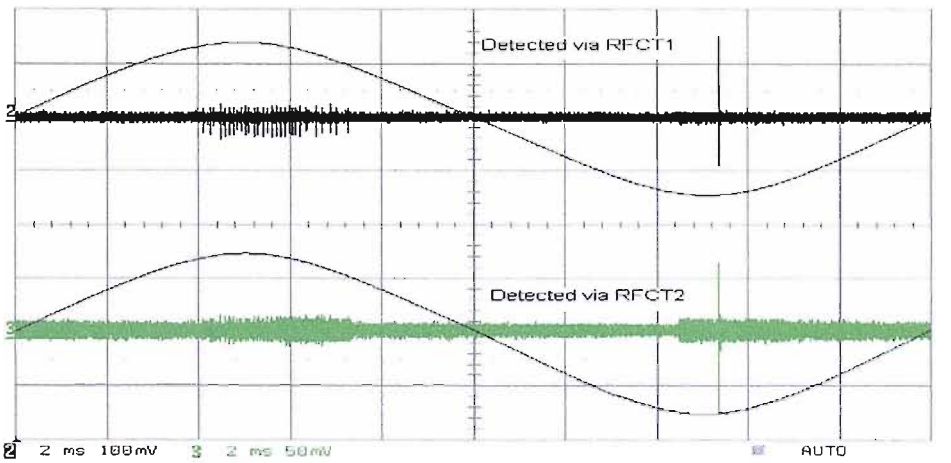

Figure 8.11 Corona discharges, the discharge signals were injected at disc 10

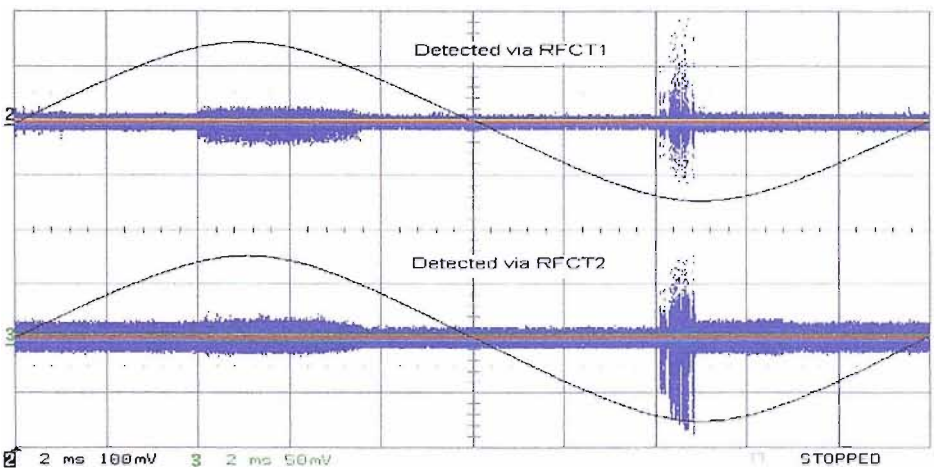

Figure 8.12 Persistence figures of corona discharges,
the discharge signals were injected at disc 10

During the test the applied voltage was 3.2kV and a zero crossing detector was used as an external trigger. The trigger was considered as being in synchronization with the 50 Hz ac test voltage. The sample rate of the oscilloscope was set to 250M/s. The obtained signals were the attenuated signals from the corona discharge source injected into the winding at disc 8. The signal detected was typical of corona discharge generated from a low potential electrode (the earthed needle point in

the discharge system). Its typical characteristic is that discharges appear not only when the needle point is of positive polarity, but also when it is of negative polarity. However, when the needle point is of positive polarity the discharge magnitudes are greater and there are fewer discharges. When the needle point is of negative polarity the discharge magnitude is small but there are more discharges. Corona discharge pulses are observed around the peaks of the test voltage. Comparing the two waveforms detected via the RFCTs, it can be seen that the magnitudes of the pulses detected via RFCT1 are about twice that detected via RFCT2. Also, at the bottom end of the model winding, the PD signals in the positive half cycle are almost obscured by noise

Figure 8.13 shows the measured time-based waveforms when the corona signals were injected into the 24th disc of the model winding. In the test a 3.2kV voltage was applied. Figure 8.14 shows the persistence figure of 1000 cycles of the transferred signals.

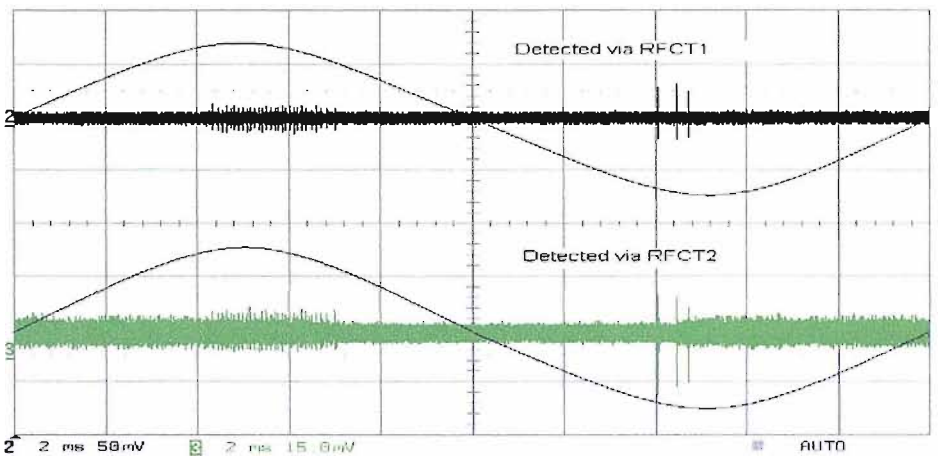

Figure 8.13 Corona discharges, the discharge signals were injected at disc 24

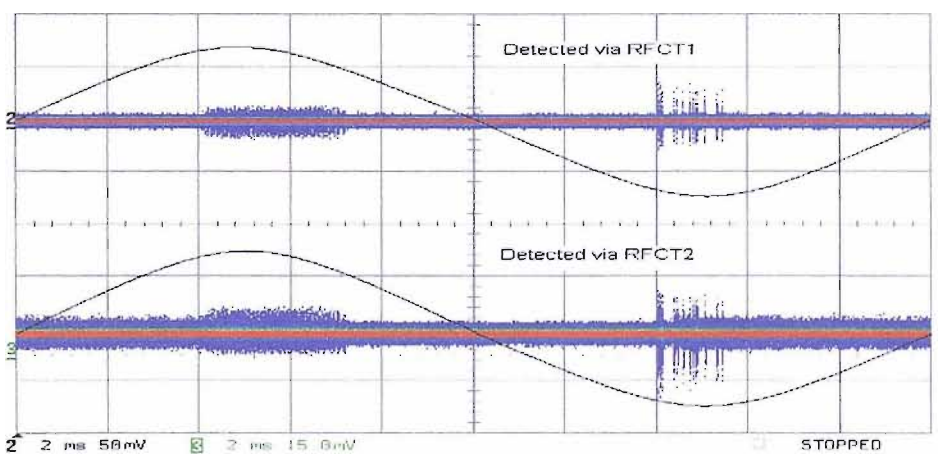

Figure 8.14 Persistence figures of corona discharges,
the discharge signals were injected at disc 24

In Figure 8.15 a single pulse and its frequency spectrum, sampled during negative half cycle, are

shown. The frequency spectrum indicates that the bandwidth of the measured signal is about 50MHz.

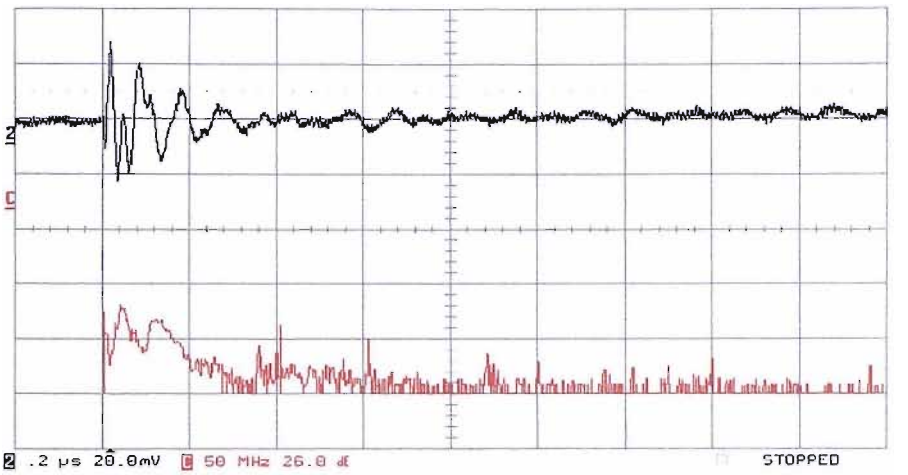

Figure 8.15 a single pulse and its frequency spectrum of corona discharge, sampled during negative half cycle as shown Figure 8.13

8.3.3 The Propagation of Floating Discharge Signals

In the section the propagation characteristics of simulated floating discharge signals within the transformer winding at UMIST is introduced. A earthed copper bar with a needle point was used as a corona source

8.3.3.1 Frequency Spectra

This test was carried out using the floating discharge source and the Spectrum Analyzer as shown in Figure 8.1. When a 9kV voltage was applied to the needle point electrode of the floating discharge source, floating discharge occurred due to the metal particles immersed in oil. The floating discharge signals then transferred to the low potential electrode of the discharge system, which was connected to the 10^{th} or 24^{th} disc of the model winding

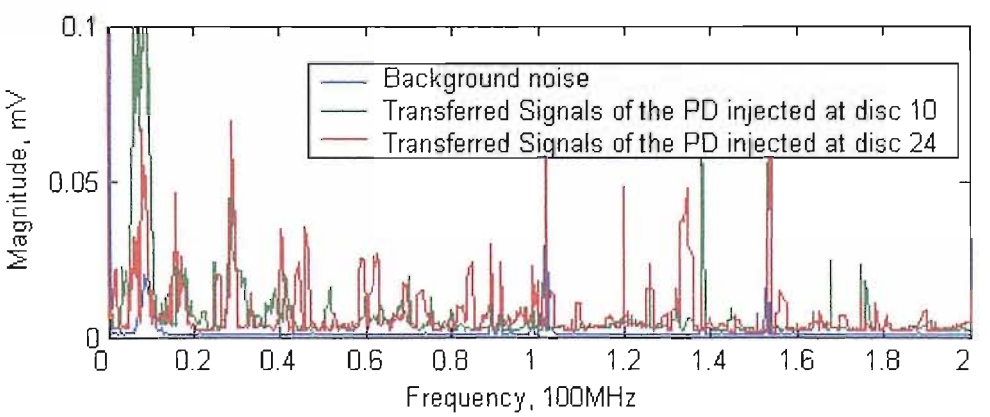

Figure 8.16 Frequency spectra of background noise and transferred floating discharges at discs 10 and 24, measured via RFCT1

The high frequency components of the floating discharge signals propagated along the winding and its leads to RFCT1 and RFCT2, and were detected by digital equipment contained within the Faraday box. In this measurement the signals were pre-filtered using hardware filters of 500 kHz high pass, 540 kHz-1.6MHz band stop and 88MHz-108MHz band stop. The Oscilloscope filter was set to 200MHz low pass. Figures 8.16 and 8.17 compare the frequency spectra of the background noise and floating discharge signals detected via RFCT1 and RFCT2.

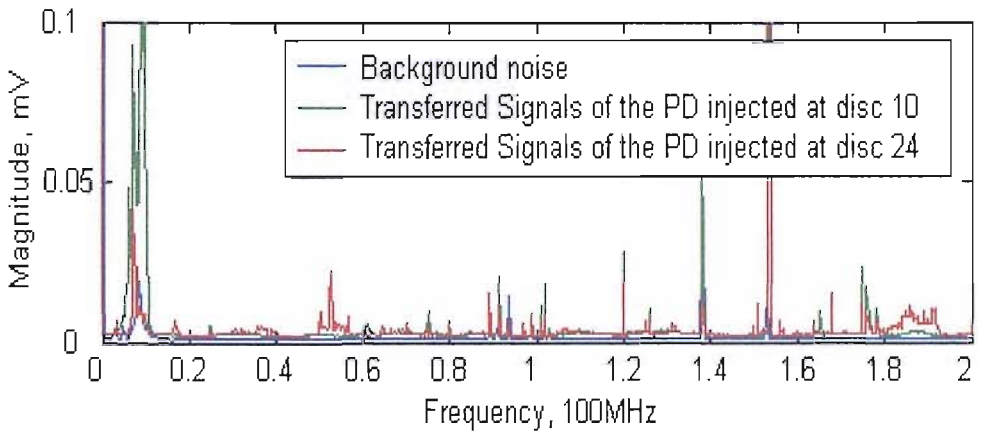

Figure 8.17 Frequency spectra of background noise and transferred floating discharges at discs 10 and 24, measured via RFCT2

8.3.3.2 Time-based Waveforms

Using the floating discharge source and oscilloscope in the measurement circuit shown in Figure 8.1, the time based waveforms as shown in Figures 8.18 were measured via RFCT1 and RFCT2. The test voltage applied to the floating discharge source was 9kV. The sample rate of the oscilloscope was set to 250M/s. During the test the floating discharge signals were injected into the winding at disc 8.

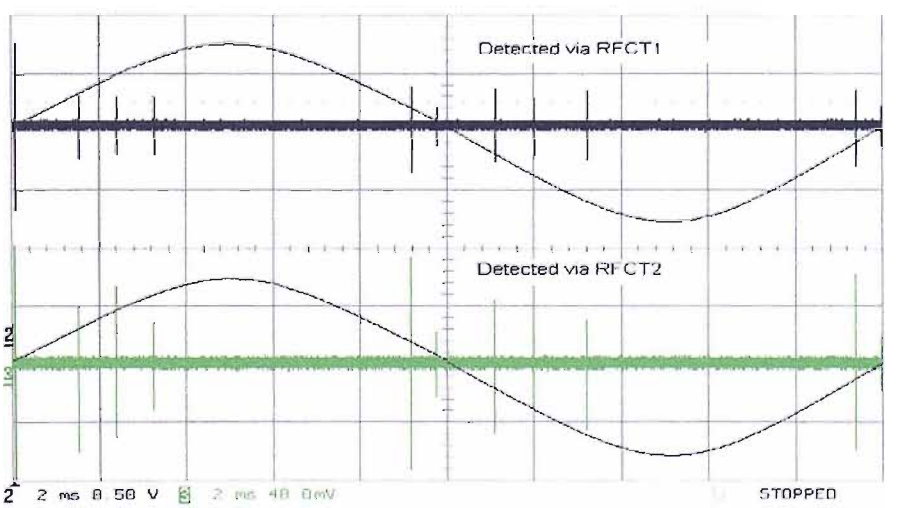

Figure 8.18 Floating discharges, the discharge signals were injected at disc 10

A persistence figure over 1000 cycles is shown in Figure 8.19. In Figure 8.20 a single pulse and its frequency response, sampled during negative half cycle, are shown. The bandwidth of the measured signal is greater than 500MHz.

Results obtained from injecting the PD signals into the 24th disc of the model winding are shown in Figures 8.21. During the test the applied voltage was 10kV.

A persistence figure over 1000 cycles of data is shown in Figure 8.22. In Figure 8.23 a single pulse and its frequency response sampled in the negative half cycle of the applied test voltage are shown.

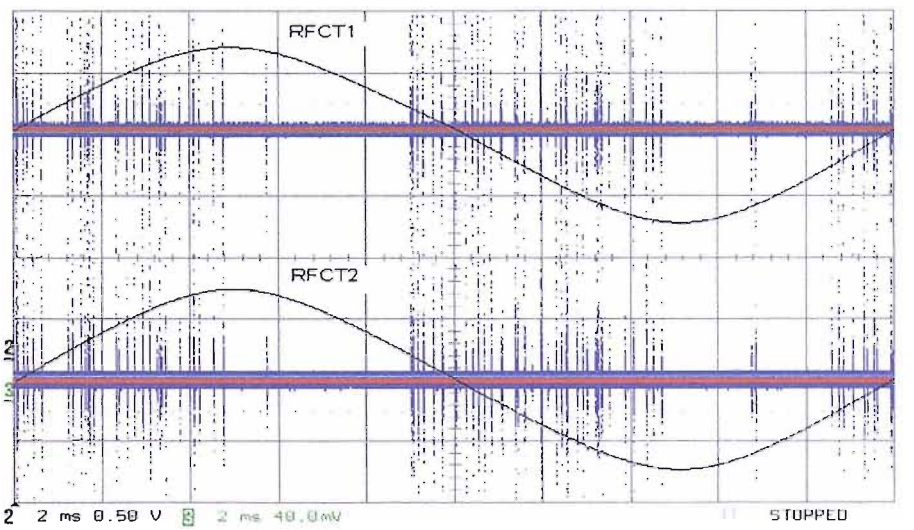

Figure 8.19 Persistence figures of floating discharges,
the discharge signals were injected at disc 10

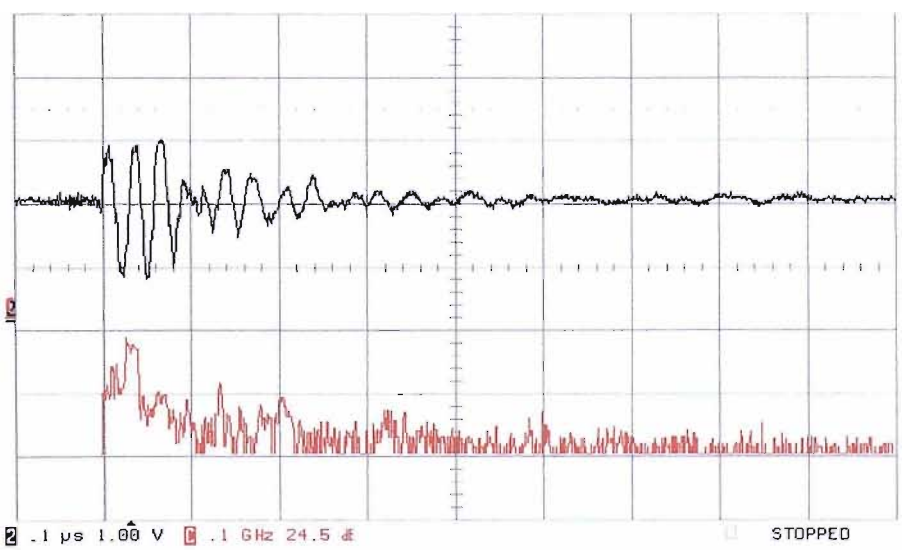

Figure 8.20 a single pulse and its frequency spectrum of floating discharge,
sampled during negative half cycle as shown Figure 8.18

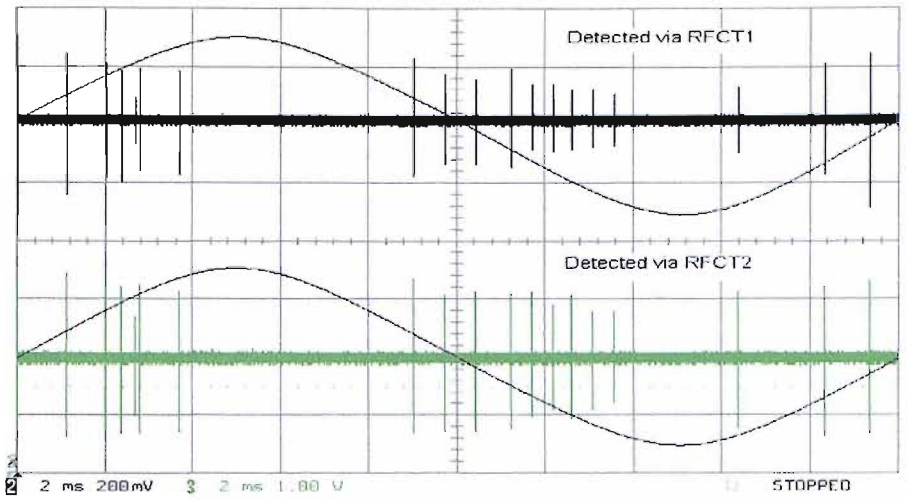

Figure 8.21 Floating discharges, the discharge signals were injected at disc 24

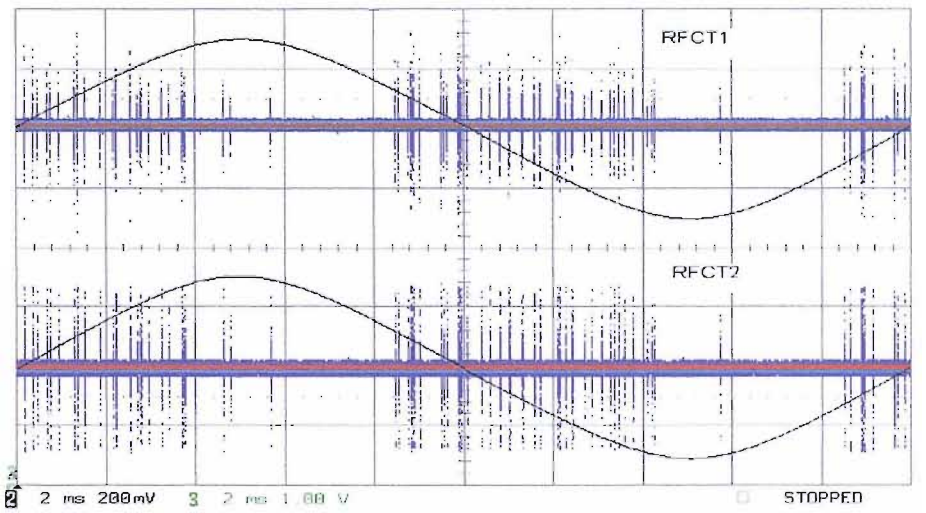

Figure 8.22 Persistence figures of floating discharges, the discharge signals were injected at disc 24

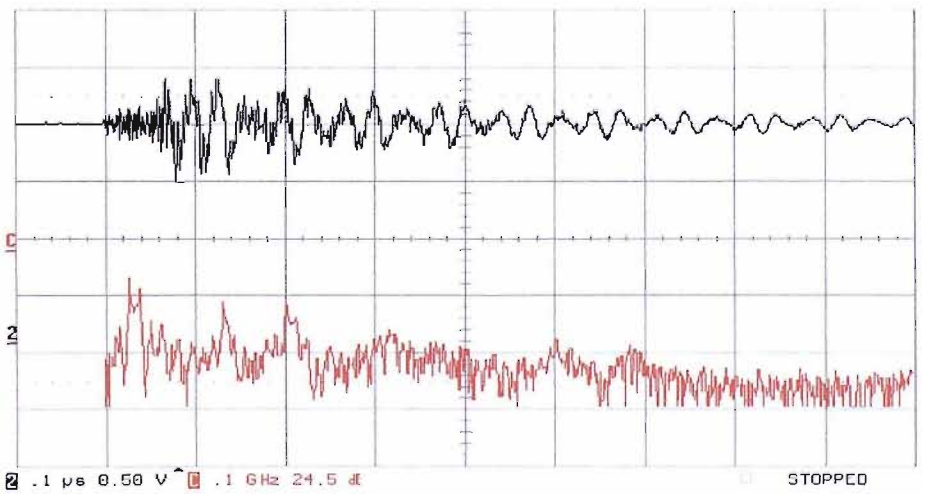

Figure 8.23 a single pulse and its frequency spectrum of floating discharge, sampled during negative half cycle as shown Figure 8.21

8.4 Frequency Response Analysis of the Transformer Model

The measurement circuit as shown in Figure 8.1 includes a winding, a capacitor (simulating a bushing) and two RFCTs. The previous investigation indicates that they have very different influence to propagation characteristics of a high frequency signal or a PD signal. The measurement result using the circuit shown in Figure 8.1 is a common function of the above three parts. This section introduces the test research on propagation characteristics of high frequency signals within the three parts and the relationship between them. The tests were undertaken using the Network Analyzer

8.4.1 Frequency Response Analysis of the Transformer Model Winding

Using the circuit shown in Figure 8.24 a frequency response measurement for the model winding was undertaken. The Network Analyzer was set with a 10Hz-500MHz gain range; a sample bandwidth of 30Hz and a 16 average sample. The result is shown (red curve) in Figure 8.28.

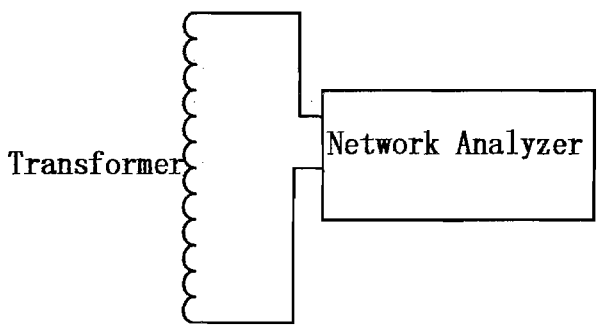

Figure 8.24 Frequency response measurement circuit for the model winding

8.4.2 Frequency Response Analysis of the Capacitor

Using the circuit shown in Figure 8.25 the frequency response measurement for the capacitor (330pF, 50kV) was carried out. The Network Analyzer was set with a 10Hz-500MHz gain range; a sample bandwidth of 30Hz and a 16 average sample. The result is shown (blue curve) in Figure 8.28. Results obtained below 200Hz are distorted by measurement noise.

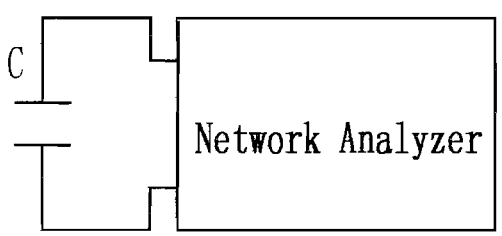

Figure 8.25 Frequency response measurement circuit for the capacitor

8.4.3 Frequency Response Analysis of Two RFCTs in Series

Using the circuit shown in Figure 8.26 the frequency response measurement for the two RFCTs connected in series (each has a three turn primary coil) was undertaken. In the test the Network Analyzer was set with a 10Hz-500MHz gain range; and a sample bandwidth of 30Hz and a 16 average sample. The result is shown (black curve) in Figure 8.28. Again results obtained below 200Hz are distorted.

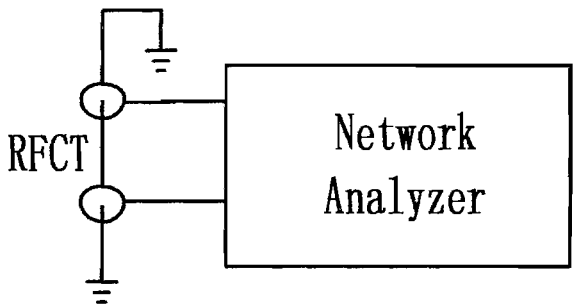

Figure 8.26 Frequency response measurement circuit for the RFCTs

8.4.4 Frequency Response Analysis of the Whole Transformer model

Using the circuit shown in Figure 8.27 the frequency response measurement for whole transformer system was undertaken. The Network Analyzer was set with a 10Hz-500MHz gain range; a sample bandwidth of 30Hz and a 16 average sample. The result is shown (green curve) in Figure 8.28.

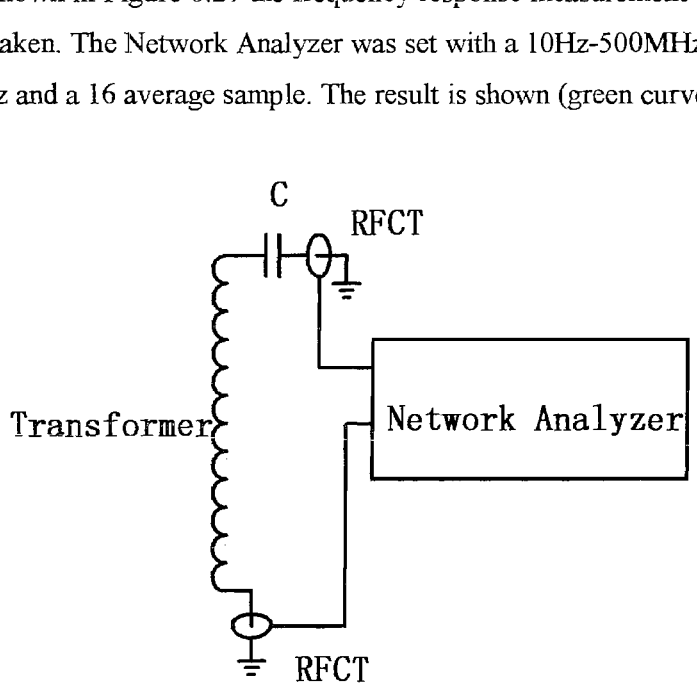

Figure 8.27 Frequency response measurement circuit for the whole transformer model

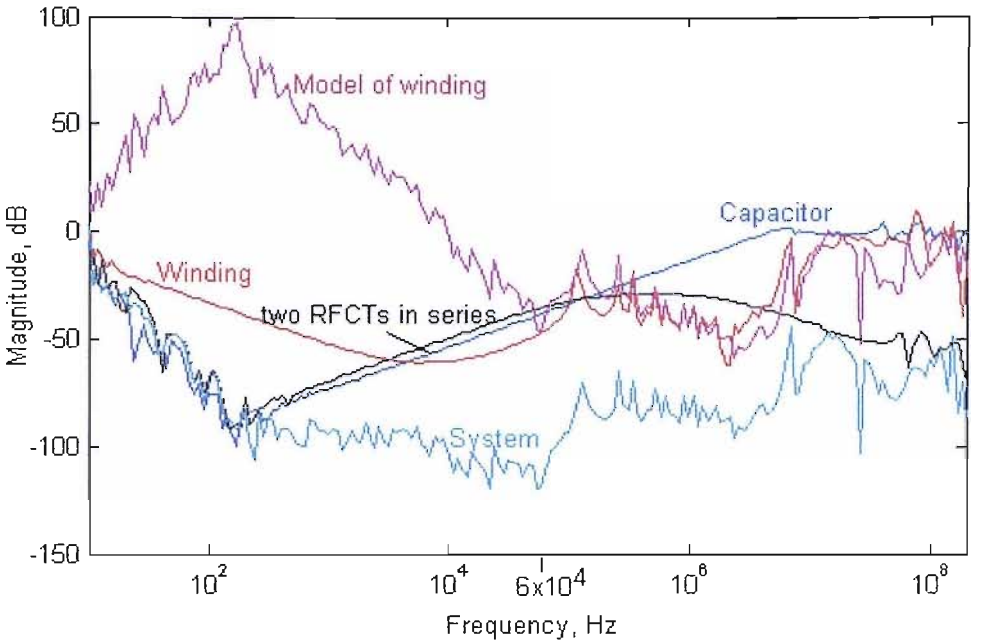

Figure 8.28 Comparison of frequency spectra

In Figure 8.28, the model of winding (pink curve) was obtained by using the frequency response of the whole system (green curve) minus the sum of the frequency response of the capacitor (blue curve) and the frequency response of the two RFCTs in series (black curve). From Figure 8.28, the modelled curve and the measured curve of the winding have a good agreement over 60kHz.

8.5 Comparison of the Frequency Response at Various Points within the Transformer Model

Using the circuit shown in Figure 8.29, multi-point measurements of the frequency response of the model winding were undertaken. The Network Analyzer was set with a 10Hz-500MHz gain range; a sample bandwidth of 30Hz and a 16 average sample. The measured positions were at the 2nd, 4th, 8th, 16th, 64th and 68th discs of the model winding. Results were obtained as shown in Figure 8.30.

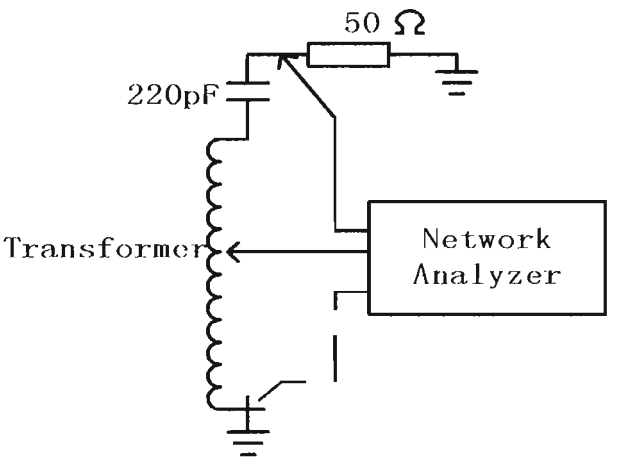

Figure 8.29 Measurement circuit for frequency response at various points

The frequency response below 200Hz is distorted due to the measurement noise and inaccuracy. The frequency response for discs near to the capacitor (2-16) is strongly influenced by the capacitor characteristic. Measurements from more distant discs (64, 68) show a significant effect due to the presence of the winding.

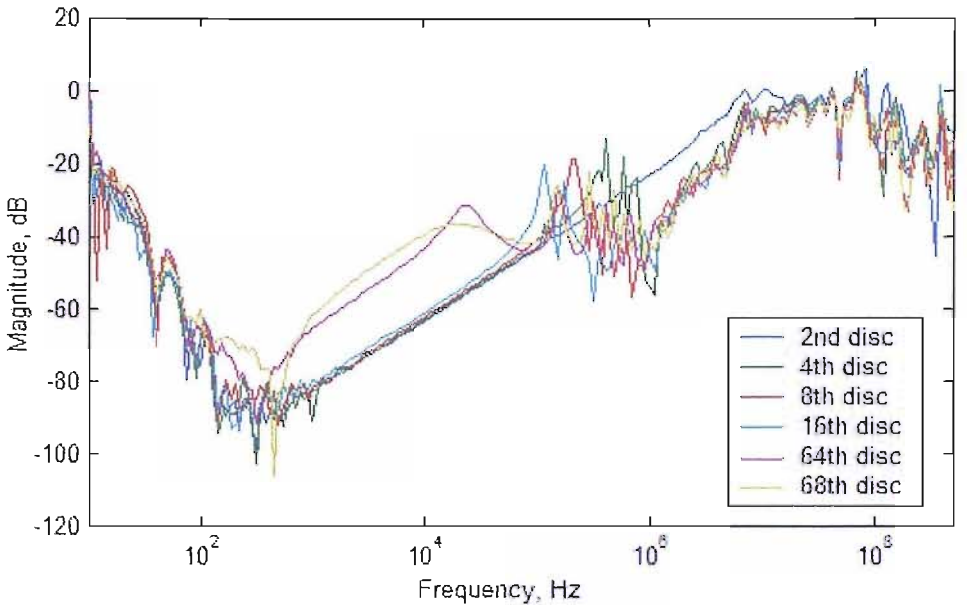

Figure 8.30 Frequency spectra measured at various points, the calibration signal was injected at the far end of capacitor

When the calibration signal was injected into the winding at the end furthest from the capacitor, responses were obtained as shown in Figure 8.31. Above 500 kHz, the frequency responses were similar at all the measurement points. This means that the winding readily transfers signals over 500 kHz.

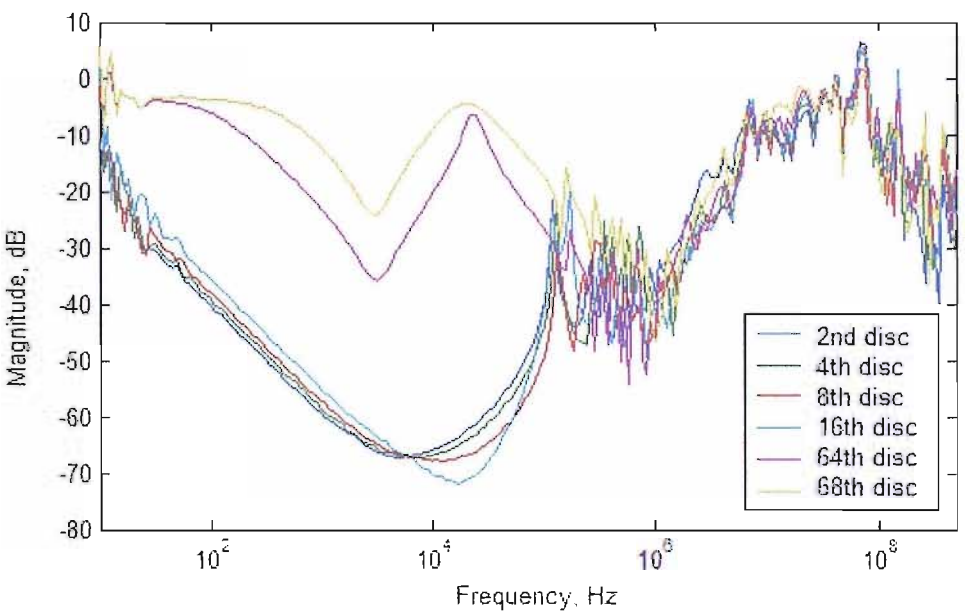

Figure 8.31 Frequency spectra measured at various points, the calibration signal was injected at the bottom end of the winding

8.6 Conclusions

Experiments have shown that the high frequency components of a pulse can propagate through the UMIST transformer model. Propagation is dependent on the magnitude of the pulse and the impedance characteristics of the transfer path. The results shown in Figure 8.8 reveal that every part of the model winding has a similar ability for propagating high frequency components of the injected pulse. This has been verified using frequency response analysis as shown in Figure 8.8. Results for PD injection (Figure 8.7) show that the further the pulse travels before detection the greater the attenuation and propagation time.

Background noise can be detected using the measurement system shown in Figure 8.1. Generally, background noise can be isolated using the frequency spectrum measurement method. As shown in Figure 8.2, results indicate that the noise frequency spectra have obvious properties which can be filtered using a hardware filter on-site or a software filter in the data analysis system. Measurements indicate (Figure 8.3) that the noise bandwidth is very large, but there are distinct pulses appearing in the time-based waveform. This characteristic can be used to distinguish noise from other signals.

In Figures 8.9 and 8.10, the comparisons of the frequency spectra of the propagation characteristics of corona are shown. Combined with results shown in Figure 8.15, the following conclusion can be made: the bandwidth of corona is about 50MHz under these experimental conditions.

In Figures 8.11, 8.12, 8.13 and 8.14 typical time-based waveforms of corona discharges are shown. These discharges occurred at a low potential electrode (the needle point was earthed) and with a near electrode system.

In Figures 8.16 and 8.17, the frequency spectra comparisons between the propagation characteristics of floating discharges in oil are shown. Combined with results shown in Figures 8.20 and 8.23, the following conclusion can be made: The bandwidth of floating discharge is about 200 MHz under these experimental conditions.

In figures 8.18 and 8.19 and 8.21 and 8.22, typical time-based waveforms of floating discharges in oil are shown. The obtained results are as expected for this discharge source.

A frequency spectrum comparison has been completed as shown in Figure 8.28. For the transformer model system, the influence of the capacitor and RFCTs on signal attenuation is significant. The winding also influences signal propagation, but its influence depends on winding construction and the distance that the signal has to travel.

Chapter 9

Discussion, Conclusion and Future Work

9.1 Discussion

The ability of a bushing to pass high frequency signals from its core bar to its bushing tap point has been investigated experimentally. The bushing contains concentric stress relieving foils that act capacitively, providing a graded electric stress across the bushing at power frequency. Very high frequency signals on the bushing core effectively see a low impedance path to ground. It is possible detect these signal components at the bushing tap either by placing an impedance between the tap point and the earth and measuring the voltage dropped across it or by using a current sensor to detect the current flowing from the bushing tap point to ground. The latter choice is preferable because under fault conditions the impedance between the bushing tap point and earth must be as small as possible.

Thus, if the bushing tap point is a suitable location for VHF PD detection, it is important to establish whether high frequency components from an internal discharge can propagate to the bushing core bar and hence be detected. Using a model of a HV transformer winding (having two possible configurations; a plain disc winding and an interleaved disc winding) this has been investigated experimentally. Different PD sources have been applied to the model and measurements obtained. These measurements have been compared to those obtained using conventional electrical detection (to IEC 270) and generally indicated that a suitable sensor placed at the bushing tap can detect some of the frequency components present in the discharge signals.

The frequency spectrum of the winding shows that at fre4quency above 20 MHz the inter-winding capacitance dominates, and consequently, there is little attenuation as the number of winding discs between the PD source and measurement point increases. Below 20 MHz signals propagate through the winding and are attenuated by each additional winding disc.

This property of the winding may be utilized to determine PD location providing that it is possible to detect the coupled signals at the bushing tap point and the neutral to earth point simultaneously.

Having experimentally established in the laboratory that the measurement technique is feasible, possible application in the field has been considered. This has led to the initial development of some software tools for post processing of measured data. From this work it has been established that the use of software filtering is limited. However, wavelet analysis has some potential.

The feasibility of developing a transfer function to describe the whole model used in laboratory tests has also been undertaken. Results obtained are highly promising. The model has a relative degree of 5 and 69 poles. Linear system theory can be applied because this transfer function accurately represents the system (no non-linearities, or time delays). A block diagram of the system is shown in Figure 9.1. Frequency response analysis measurements are routinely used by utilities to assess the condition of transformer windings, and consequently this data may be used to generate a suitable transfer function. In the case of an in internal discharge the sensors placed at the neutral-earth point and bushing tap point provide time-based signals that represent the propagated PD signal.

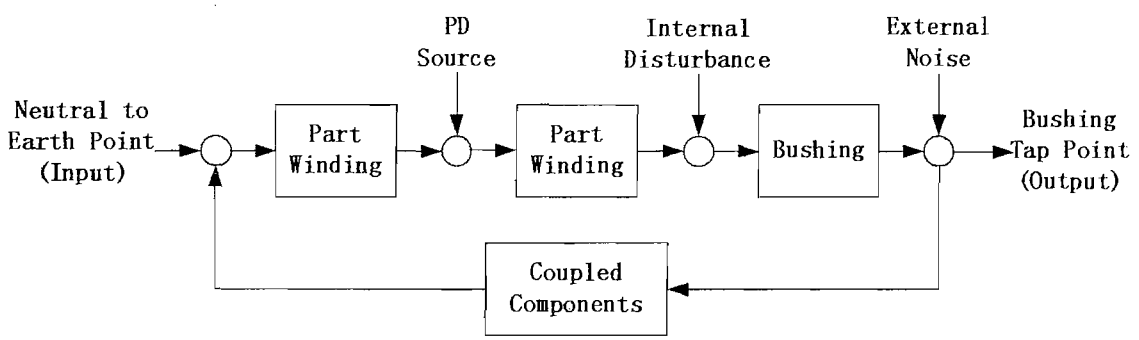

Figure 9.1 A block diagram of a linear system for a transfer function

It is possible that these signals may be used in conjunction with the transfer function to determine PD location and magnitude, by using a least means squares recursive algorithm or possibly applying genetic algorithms. This is a possible direction for future research.

Field measurements undertaken at NGT Northfleet and UMIST have further validated the measurement approach. The major limitation is that assessment of PD activity is largely determined by the analysis of persistence figures. This allows immediate identification of possible internal partial discharge, but has limited value off-site.

9.2 Conclusion of this thesis

The previous investigations described in Chapter 2 indicate that the partial discharges within oil-filled power transformers have special properties. These properties can be expressed in pattern charts of discharge parameters including quantities of partial discharges, energy of partial discharges, inception and extinction voltage of partial discharges. Usually, in the identification of partial discharges these parameters are illustrated in the time or frequency domains. Relying on modern digital technologies, the monitoring, measurement, localization and recognition techniques for partial discharges within transformers have greatly improved. These techniques include the applications of new materials and devices and the development of new analytical techniques.

Based on the summary and analysis for previous work, this thesis provides a new and more closely practical technique to realize partial discharge on-line measurement and monitoring of power transformers. The essential principle of the technique is:

Considering the transformer bushing taps as available measuring points and using high frequency sensors (for example, RFCTs) to detect signals transferred from transformers at these points, then using digital equipment to analyse the collected data to distinguish possible partial discharge signals from noise, furthermore to allow PD diagnosis and localization.

The relevant properties of different partial discharges (such as corona, surface discharge floating discharges etc.) detected at transformer bushing taps were investigated in this project. Different partial discharges have very different bandwidths and very different patterns of pulse groups in the time domain. For example, floating discharges and corona discharges in oil have bandwidths greater than 50 MHz and external corona always occurs at the middle of the half cycles of the 50 Hz test voltage. Consequently, these properties can be used to distinguish internal partial discharges from external partial discharges.

The investigation into a 60kV transformer bushing indicates the bushing is capacitive between its core bar and its tap. The high frequency components of a partial discharge signal can readily pass through it. The properties of transferred partial discharge signals in the frequency and time domains can reflect the situation of the partial discharge on the bushing core bar. A transformer bushing tap can be considered as a reliable position to make measurements and to monitor partial discharges within transformers in the high frequency region.

The investigations into the frequency and impulse responses of transformer windings shows that partial discharge signals can transfer within them. The main properties of the partial discharges in the frequency and time domains can be preserved during this transfer. This was verified by injecting real partial discharges into the windings.

The frequency responses of the transformer model system (including bushing and RFCT) of Figure 5.9 or Figure 5.10 show that it is easier for signals with frequency between 1 MHz to 10 MHz to transfer from a point on a winding to a bushing tap. This was verified in most of the tests in which pulse and real PD signals were injected into the model (see Chapter 5). For this reason the main waveforms of the responses to the injection pulse and real PD signals within the transformer model system were dominated by the waveforms extending not only over several MHz but several tens of MHz.

The measurement and monitoring principle for oil-filled power transformers, proposed in Chapter 6, is feasible. The on-site application of this method on to the auto-transformer SGT3A at Northfleet Substation West London has proved its practicality. The tests on a transformer model in UMIST (Chapter 8) also gave good verification results. The main advantage of this principle is that no alterations to the transformer are required. It is therefore a very valuable method for assessing transformers actually in operation.

9.3 Recommendations for Future Work

In Chapter 6 a method using a transfer function to simulate a transformer system was suggested. The method of "designing" a black box with the required measured frequency spectrum builds up a transfer function of a transformer system and brings a prospect of locating PD sites within a winding. This is by combining the transfer function with that of a winding. The location of a partial discharge on the winding can then be formed (in principal at least) from measurements at a bushing tap.

To combine this approach with some simulation algorithms for transformer windings, the localization of PD within windings may be resolved. But up until now, the resolution of the simulation algorithms of the transfer function of transformer windings is limited to no more than a 2MHz bandwidth. To investigate and develop new algorithms to simulate a winding in the high frequency region up to 200MHz or more is necessary.

Figures 4.12, 4.17, 4.30 and 7.8 show that the PD components over 50MHz may have very smaller magnitudes and even less than that of background noise. On a time-based pattern chart they may therefore be buried in the background noise signals. Therefore, it is necessary to develop software programs to remove background noise and preserve valuable signals in the time domain. A good resolution of this problem will lead to a software tool which can automatically distinguish PD signals from noise.

The PD measurement principle mentioned in this thesis is viable, but the cost of the digital equipment required is high and unacceptable. Considering that they are all laboratory devices and

have many functions surplus to this application, a new specialized measurement tool could be developed in the future. This device must preserve the necessary functions for PD measurement, but its cost could be much reduced.

The wavelet analysis for the multi-PD waveform can be extended to the three-Dimension statistical analysis. The 3-D wavelet analysis in the PD recognition on the multi-cycle-waveforms must be more efficient and directly. But at present it is difficult due to the huge computation as overhead. For example, a single cycle data file sampled at 250 MHz components is 80 Mb long. If a thousand cycles of data are collected a hard drive of over 80 Gb must be used. If considering the computation process this is unacceptable. So, new calculation methods for statistical analysis and data mining should be developed.

References:

1. J. P. Zondervan, E. Gulski, J. J Smit, R. Brooks, "PD Pattern Analysis of On-line Measurements on Rotating Machines" IEEE, Conference on Electrical Insulation and Dielectric Phenomena, (CEIDP), Minneapolis, 1997, pp242-245

2. J. P. Zondervan, E. Gulski, J. J Smit, R. Brooks, "Use of the VHF Detection Technique for PD Pattern Analysis on Tubo-generators", International Symposium on Electrical Insulation (ISEI), Washington, 1998, pp274-277

3. S. Meijer, E. Gulski, W. R. Rutgers, "Acquisition of Partial Discharge in SF6 Insulation IEEE, Conference on Electrical Insulation and Dielectric Phenomena, (CEIDP),, San Fransisco, 1996, pp581-584

4. J. P. Zondervan, E. Gulski, J. J Smit, T. Grun, "Comparison of Conventional and VHF Partial Discharge Detection Methods for Power Transformers", International Symposium on High Voltage Engineering, (ISH), London, 1999 Vol.5, pp348-351

5. S. Meijer, E. Gulski, J. J Smit, F. J. Wester, T. Grun, " Interpretation of PD in GIS Using Special Analysis, International Symposium on High Voltage Engineering, (ISH), London, 1999

6. K. Raja, F. Devaux, S. Lelaidier, " Recognition of Discharge Sources Using UHF PD Signatures", IEEE Electrical Insulation Magazine, September/October 2002, Vol. 18, No5, pp8-14

7. H. Borsi, "A PD Measuring and Evaluation System Based Digital Signal Processing", IEEE Transaction on Dielectrics and Electrical Insulation", Vol 7, No1, February 2000, pp21-29

8. R, Candela, G. Mirelli, R. Schifani, "PD Recognition by Means of Statistical and Fractal Parameter and Neural Network", IEEE Transaction on Dielectrics and Electrical Insulation", Vol. 7, No1, February 2000, pp87-94

9. E. M. Lalitha, L. Satish, "Wavelet Analysis for Classication of Multi-source PD patterns", IEEE Transaction on Dielectrics and Electrical Insulation", Vol. 7, No1, February 2000, pp40-47

10. M. M. A. Salama, R. Bartnikas, "Fuzzy Logic Apllied to PD Pattern Classification", IEEE Transaction on Dielectrics and Electrical Insulation", Vol 7, No1, February 2000, pp118-123

11. P. Werle, V. Wasserberg, H. Borsi, E. Gockenbach, "New Devices for a Dry Type Transformer Protection and Monitoring System" IEEE, transaction on dielectrics and electrical insulation, Feb 2002, volume 7, pp. 21-29

12. Z. D. Wang, P. A. Crossley, K. J. Cornick, D. H. Zhu. "An algorithm for partial discharge location in distribution power transformers", IEEE Power Engineering Society Winter Meeting 2000, 23rd Dec-27th January 2000, Singapore

13. S. N. Hettiwatte, P. A. Crossley, Z. D. Wang, A. Darwin, G. Edwards: "Simulation of a transformer winding for partial discharge propagation studies". IEEE power engineering society winter meeting 2002, paper 105, 27th Dec- 31st January 2002, New York, USA

14 Asghar Akbari, Peter Werle, Hossein Borsi, Ernst Gockenbach, "A Continue Parameter High Frequency Model based on Travelling Waves for Transformer Diagnostic Purposes" IEEE Electrical Insulation Magazine, Vol. 18, No. 5, 2002, pp19-27.

15. T. R. Blackburn, Z. Liu, B. T. Phung and R. Morrow, "Investigation of partial discharge mechanisms in a void under ac electric field", High Voltage Engineering Symposium, 22-27 August 1999 Conference Publication No. 467, IEE 1999

16. "Partial Discharge Measurements", IEC 60270-99, 1999

17. Qui Changrong, Wang Naiqing; "Partial discharge and its Measurements on Electrical Apparatus", 1993, Mechanical Industry Publishing Agency (in Chinese)

18 Franklin, D. P. Franklin, The J & P Transformer Book, 1983, Butterworth & Co.(publishers) Ltd.,

19 A. Nesbitt, BG Stewart, "Condition monitoring of power transformers through partial discharge measurement: problems associated with pulse distortion in the winding", IEEE Transactions on Power Delivery, Vol. 10. No. 3. July 1997. pp1171-1176

20. M. D. Judd, B. M. Pryor, S. C. Kelly and B. F. Hampton, "Transformer monitoring using the UHF technique"; International Symposium on High-Voltage Engineering (ISH), London, 22-27 August 1999; Conference Publication No. 467, IEE 1999

21. Z. D. Wang, P. A. Crossley, K. J. Cornick, "Partial discharge location in power transformer"; High Voltage Engineering Symposium, 22-27 August 1999

22 H. Lamela-Rivera, C. Maci`a-Sanahuja and J. A. Garc´ıa-Souto, "Detection and wavelet analysis of partial discharges using an optical fibre interferometric sensor for high-power

transformers", Journal of Optics a: Pure and Applied Optics, 5 (2003) pp66–72

23 H. Borsi, "A PD measuring and evaluation system based on digital signal processing", IEEE, transaction on dielectrics and electrical insulation, Feb 2000, volume 7, pp. 21-29

24 C. Bengtsson, "Status and Trends in Transformer Monitoring"; IEEE Transactions on Power Delivery, Vol. 11. No. 3. July 1996. pp1379-1384

25 Jones SL, "The detection of partial discharge activities within power transformers using computer aided acoustic emission techniques", IEEE International Symposium On Electrical Insulation, Toronto, Canada, 1990, pp.106-110

26 Zhu Deheng, Yan Zhang, "High Voltage Insulation"; 1992, Qtinghua University Publisher (in Chinese)

27 Su Q and James RE, 1992, "Analysis of partial discharge pulse distribution along transformer windings using digital filtering techniques", Generation, Transmission and Distribution, IEE Proceedings C Publication Date: Sep 1992, Volume: 139, Issue: 5, pp 402-410;

28 R. Candela, G. Mirelli, "PD Recognition by Means of Statistical and Fractal Parameters and a Neural Network"; IEEE Transaction on Dielectrics and Electrical Insulation, Vol. 7 no. 1, Feb. 2000, pp87-94.

29 Gao wengsheng, Tan kexiong; "Study on the influence of pulse propagation in transformer winding on partial discharge recognition"; Proceeding of the 6th international conference on properties and applications of dielectric materials; June 21-26, 2000, Xi'an Jiaotong University, Xi'an China

30 C. Chang; Q. Su; "Partial discharge Distribution pattern Analysis Using Combined Statistical Parameters"; IEEE Power Engineering Society Winter Meeting, Singapore, January 24-28, 2000

31 A. Contin, G. C. Montanari, C. Ferraro; "PD Source Recognition by Weibull Processing of Pulse Height Distributions; IEEE, transaction on dielectrics and electrical insulation, Feb 2000, volume 7, pp. 48-58

32 M. M. A. Salama, R. Bartnikas. "Fuzzy Logic Applied to PD Patterns Classification"; IEEE Transactions on Dielectrics and Electrical insulation, Vol.7, No.1, Feb 2000. ISSN 1070-9878

33 Z. D Wang, P. A. Crossley, K. J. Cornick, "Partial discharge location in power

transformer"; High Voltage Engineering Symposium, 22-27 August 1999 Conference Publication No. 467, IEE 1999

34 P. Werle, H. Borsi, E. Gockenbach; "A New Method for Partial Discharge Location on Power Transformers Based on a system Theoretical Approach"; Proceeding of the 6th international conference on properties and applications of dielectric materials; June 21-26, 2000, Xi'an Jiaotong University, Xi'an China; pp831-834

35 S. Birlasekaran, Yu X., F. Fetherstone , R. Abel, and R.H. Middleton, L. Wang and, "Diagnosis and Identification of transformer Faults from Frequency Response Data", IEEE Power Engineering Society Winter Meeting, Singapore, January 24-28 2000

36 K. Karisai, D. Kerenyi, L. Kiss, "Large Power Transformer", 1987, Elsevier Science Publishers, Amsterdam, Netherlands and Aksdemidai Kiado Budapest, Hungary

37 Asghar Akbari, Peter Werle, Hossein Borsi, and Ernst Gockenbach, "Transfer function-based Partial discharge localization in power transformer: a feasibility study" , IEEE Electrical Insulation Magazine, September/October 2002, Vol. 18, No, 5, pp22-32

38 S. N. Hettiwatte, P. A. Crossley, Z. D. Wang, A. Darwin, G. Edwards. "Simulation of a transformer winding for partial discharge propagation studies"; IEEE power engineering society winter meeting 2002, paper 105, 27th Dec- 31st January 2002, New York, USA

39 H. Tenbohlen, H. Borsi, P. Werle, and S. Tenbohlen, "Enhanced diagnosis of power transformer using on- and offline methods: Results, example and future trends", presented at the International Council on Large Electric System (CIGRE) Paper 12-204, Paris France, 2000

40 A. C. Franklin, D. P. Franklin, "The J&P Transformer Book", 1983, Butterworth & Co.(Publishers) Ltd.;

41 Jan. Peter Bolhuis, E. Gulski, J. J. Smit "On-line VHF Measurements on Transformers", the 1ST International Conference on Insulation Condition Monitoring of Electrical Plant , Sep.24-26, Wuhan University, Wuhan China

42 F. H. Kreuger, "Discharge, Electra", No11, 1995, CIGRE Working Group 21.03

43 P. Werle, V. Wasserberg, H. Borsi, E. Gockenbach: "Comparison of different Partial Discharge measurement Methods on Dry Type Transformers in Operation", 2nd International Conference on Dielectrics and Insulation (ICDI), Stara Lesna, Czech Republic, June 2000

44 H. Borsi, P. Werle: "Various Partial Discharge Measurement and evaluation techniques Adapted to different transformer types", 5th Volta Colloquium on Partial Discharge Measurement, Como, Italy, September 2001

45 J. P. Zondervan, E. Gulski, "A New Multi-Purpose Partial Discharge Analyser for On-site and on-line Diagnosis of High Voltage Components", Proceedings of the International Symposium of High Voltage Engineering, London, 1999, Vol.5 pp 49-52

46 Th. Aschwanden, M. Hassig, V. Der. Houhanessoan, Development and Application of New Condition Assessment Methods for Power Transformers, CIGRE Session 1998, Paris, Paper 12-207

47 B. Han, P. L. Lewin, Y. Tian, P. Jarman and S. G. Swingler: "Propagation Characteristics of Discharges signals of high frequency within Transformer Bushing", In Proceedings of 2nd International Conference on Insulation Condition Monitoring of Electrical Plant (ICMEP-ACEID'2003), pp.179-182, Chongqing China, 27-30th 10 2003

48 B. Han, P. L. Lewin, Y. Tian, P. Jarman and S. G. Swingler: "Distinguishing the Corona and Surface Discharge within Transformer Bushing", In Proceedings of 2nd International Conference on Insulation Condition Monitoring of Electrical Plant (ICMEP-ACEID'2003), pp. 301-304, Chongqing China, 27-30th 10 2003

49 B. HAN, P. L. Lewin, "Partial Discharge On-line Testing of Northfleet SGT3A", Report Ref No BH/1, National Grid Company Project Report, 2001

50 R. Candela, P. Romano and R. Schifani: "Separation of Multiple and Concurrent Partial Discharge Phenomena"; IEE Conference on Dielectric Materials, Measurements and Applications (DMMA), Edinburgh University 17-21 September, 2000.

51 Hepburn DM, Shields AJ & Kemp IJ, "High voltage plant monitoring through oil/paper analysis", 8th IEE Conference on Dielectric Materials Measurements and Applications, Heriot-Watt University, Edinburgh, UK, 17-21 Sept. 2000, pp.218-223

52 Donald Chu, Abdre Lux, "On-line Monitoring of Power Transformers and Components: A Review of Key Parameters"; IEEE Electrical Insulation Conference & Electrical Manufacturers and Coil Winding Explosion, Cincinnai, Ohio, Oct 25, 1999

53 Zhong Zheng and Kexiong Tan. "Partial Discharge Recognition Based on Pulse Shape Characteristic Analyses Using Artificial Neural Network as a Tool"; In Proceeding of IEEE 6th International Conference on Properties and Application of Dielectric Materials (ICPADM) 2000, Xi'an, China. June 21~26 2000, pp. 483~486

54 Zhong Zheng, Kexiong Tan, and Kai Gao; "Pulse Shape Characteristic Analysis of Partial Discharge Signals"; High Voltage Engineering, December, 1999. Vol. 25, No. 4, Pages: 15~17(in Chinese)

55 Meunier, R.; Vaillancourt, G.H., "Propagation Behaviour of Acoustic Partial Discharge Signals in Oil-Filled Transformers", 12th International Conference on Conduction and Breakdown in Dielectric Liquids, ICDL '96, Roma, Italy, 15-19 July 1996.

56 Gulski, E.; Burger, H.P.; Vaillancourt, G.H.; R. Brooks, "PD Data Base for Power Transformers and Reactors", 10th International Symposium on High Voltage Engineering, Montreal, Canada, August 25-29, 1997

57 Gulski, E.; Burger, H.P.; Vaillancourt, G.H.; R. Brooks, "PD Pattern Analysis During Induced Tests of Large Power Transformers", IEEE Transactions on Dielectrics and Electrical Insulation, Vol. 7, No. 1, February 2000, pp. 95-101

58 Philippe Guunic, "CIGRE's Work on Insulation Monitoring of Power Transformers", Proceedings of the 1st International Conference on Insulation Condition Monitoring of Electrical Plant; Sept.24-26, Wuhan University, Wuhan, China

59 Fyed Mofizui Islam, Tony Wu, Gerard Ledwich, "A Novel Fuzzy Logic Approach to Transformer Fault Diagnosis"; IEEE Transactions on Dielectrics and Electrical Insulation, Vol. 7 No.2, April 2000, pp 177-185

60 Z. D. Wang, P. A. Crossley, K. J. Cornick. "Partial discharge location in power transformers using the spectra of the terminal current signals". Proceeding of the 11th International Symposium on High Voltage Engineering (ISH), August 23-27, 1999, London. pp. 5.58.S10-5.61.S10

61 Z. D. Wang, P. A. Crossley, K. J. Cornick, D. H. Zhu. "An algorithm for partial discharge location in distribution power transformers", IEEE Power Engineering Society Winter Meeting 2000, 23rd Dec- 27th January 2000, Singapore

62 J. Wang, F. Li, Z. D. Wang. "Experiment analysis of influence of external coupling network on partial discharge monitoring of transformers". Proceedings of the 6th International Conference on Properties and Application of Dielectric Materials (ICPADM), pp. 672-675, 21st - 26th June 2000, Xi'an, China

63 Z. D. Wang, P. A. Crossley, K. J. Cornick, D.H. Zhu. "Partial discharge location in power transformers", IEE Proceedings of Science, measurement and technology, Vol.47, No.5,

September 2000, pp. 249- 255.

64 S. N. Hettiwatte, Z.D. Wang, P.A. Crossley, A. Darwin, G. Edwards. "Experimental investigation into the propagation of partial discharge pulses in transformers". IEEE Power Engineering Society Winter Meeting 2002, paper 104, 27th Dec-31st January 2002, New York, USA.

65 Y. Tu, Z. D. Wang, P. A. Crossley. "Partial Discharge Pattern Recognition based on 2-D Wavelet Transform and Neural Network Techniques". Submitted to IEEE power engineering society summer meeting 2002, 21st - 25th July, Chicago, USA.

66 D. J. Wilcox, T. P. Mchale, "Development in the Theory and Application of Model 31 Analysis in the Modelling of Power Transformers"; 13th the University Power Engineering Conference, UPEC 1991, pp. 494-497.

67 Li jian, Tang ju, Sun Caixin, "Pattern Recognition of Partial Discharge with Fractal Analysis to Characteristic Spectrum", proceedings of the 6th international conference on properties and applications of dielectric materials, June 21-26, 2000, Xi'an Jiaotong University, Xi'an, China.

68 R. Candela, G. Mirelli, "PD Recognition by Means of Statistical and Fractal Parameters and a Neural Network"; IEEE Transaction on Dielectrics and Electrical Insulation; Vol. 7 no. 1, Feb. 2000, pp.87-94.

69 Lu Changbai, "Insulation Technology for Power Transformer"; PublInterbational Symposium on High Voltage Engineering agency of Herbin Industry, 1997 (in Chinese).

70 I. J. Kemp, "Development in Partial Discharge Plant –Monitoring Technology", International Conference on Partial discharge, IEE, 1993, Conference proceedings No 378, p52- 55.

71 R. Morrow and T.R. Blackburn, "Theory of Discharges in Air-filled Insulation Voids", High Voltage Engineering Symposium, 22-27 August 1999 Conference Publication, No 467, IEE 99, 4th Volume p.228-230.

72 K. Karsai, D. Kerenyi, L. Kiss, "Large Power Transformers", 1987, Elsevier Science Publishere. Amsterdam, Netherlands and Aksdemiai Kiado Budapest, Hungary.

73 Adrian Biran, Moshe Breiner, "MATLAB for Engineers", 1995, Addison-Wesley Publishers Ltd

74 E. Lemke, P. Schmiegel, "Introduction to Fundamentals of PD Diagnostics", Lemke Diagnostics GmbH, Dresden, Germany, 1993

75 A. Kelen, M. G. Danikas, "Evidence and Presumption in PD Diagnostics", IEEE Transaction on Dielectrics and Electrical Insulation, Vol. 2 No5 October 1995, pp780-795.

76 Steven A. Boggs, "Partial Discharge-Part II: Detection Sensitivity"; IEEE Electrical Insulation Magazine, September/October 1990-Vol.6 No 5, pp35-42.

77 J. P. Steiner, "Partial Discharge-Part IV: Commercial PD Testing"; IEEE Electrical Insulation Magazine, Jan/Feb. 1991-Vol.7 No 1, pp20-33.

78 C. Laurent, C. Mayoux, "Partial Discharge-Part XI: Limitations to PD as a Diagnostic for Deterioration and Remaining Life"; IEEE Electrical Insulation Magazine, March/April 1992-Vol.8 No 2, pp14-17.

79 C. Stone, "Partial Discharge-Part VII: Practical Techniques for Measuring PD in Operation Equipment"; IEEE Electrical Insulation Magazine, July/August 1991-Vol.7 No 4, pp9-16

80 David A. Nattrass, "Partial Discharge-Part XVII: The Early Histry of Partial Discharge Research"; IEEE Electrical Insulation Magazine, July/August 1993-Vol.9 No 4, pp27-31.

81 Bartnikas, "A Commentary on Partial Discharge Measurement and Detection"; IEEE Transaction on Dielectrics and Electrical Insulation, Vol. EI-22 No5 October 1987, pp629-651.

82 Chen-Xiang-hui, WANG Zan-ji, "A Novel Simulation Method in Frequency Domain for Locating Faults in Power Transformer Windings under Impulse Voltage Test"; Transformer, Vol. 37 No.8 2000, pp27-32 (in Chinese).

83 Robert M. Del Vecchio, Bertrand Poulin, Pieere T. Feghali, "Transformer Design Principles: with application to core-form power transformer"; published in 2002 by Taylor & Francis, New York.

84 P. T. M Vaessen, E. Hanique, " A New Frequency Analysis Mathod for Power Transformer"; IEEE, Tansaction on Power Delivery, Vol. 7 No.1 January 1992, pp384-391.

85 E. P. Dick, C. C. Erven, " Transformer Dianostic Testing by Frequency Response Analysis"; IEEE, Transactions on Power Apparatus and System, Vol. PAS-97. No. 6, Nov/Dec. 1978.

86 P. Werle, A. Akbari, H. Borsi, E. Gockenbach; " Partial Discharge Localization on Power Transformers using Neural Networks combined with Section Winding Transfer Function as Knowledge Base"; 3rd International Symposium on Electrical Insulating Materials (ISEIM), Himeji, Japan.

87 Shigemitsu Okabe, Masannori Koutou,"A High Frequency Model of an Oil-immersed Transformer, and Its use in Lightning Surge Analysis"; Electrical Engineering in Japan, Vol. 134, No 1, 2001. Translated from Denki Gakkai Ronbunshi, Vol. 119-B, No 8/9, August/September 1999, pp925-930.

88 M. Aro, S. M. Berlijn, K. Feser, B.I. Guruaj, T.Kato, etc.; "Comparison of Processed Results of Test Data for Evaluation of Transformer Transfer Function Analysis Software"; CIGRE 33-96(WG03).

89 A. Akbari, P. Werle, H. Borsi, E. Gockenbach; "A Continuous Parameter High Frequency Model based on Travelling Waves for Transformer Diagnostic Purposes";14th International Symposium on Electrical Insulation (ISEI), Boston, USA, April 2002.

90 O. Moreau, P. Guuinic, R. Door, Q, Su; "Comparison Between the High Frequency Characteristics of Transformer Interleaved and Ordinary Windings"; IEEE, Transactions on Power Apparatus and System, Vol, 4. No. 6, Nov. 2000.

91 B. Han, P. L. Lewin, Y. Tian, P. Jarman and S. G. Swingler: "PD On-line Measurement of Oil-filled Power Transformers"; XIIIth International Symposium on High Voltage Engineering (ISH), 2003, Delft University of Technology, August 25-29th 2003

92 "User's Guide on Signal Processing Toolbox for use with Matlab", The Mathworks, Inc. 1998.

93 Matlab Release 13", 2002, The Mathematic Works Inc.

94 Dutton K., Thompson S. and Barraclough B., "The Art of Control Engineering"; England: Addison-Wesley 1997

95 Wavelet Toolbox User's Guide, The Mathworks, 1996.

96 Frequency response of integrated circuits, Sony Brook, State university of New York, ESE516, pp 24-30

Appendix A

Transformer Model Construction

The windings of the transformer model was designed and produced by Alstom Transformer and National Grid Company. In order to more accurately reveal PD characteristics, the windings were re-designed and rebuilt into a transformer model.

The IEC 27260 was carried out during the remould. The final power frequency withstanding voltage for the oil-filled model is 20Kv, below this voltage the transformer model is partial discharge free.

Core Design

A core of a transformer is generally constructed using ferromagnetic materials, for example, silicon steel plates. The existence or not of a core in a transformer must seriously influence the capacitance of a winding to ground, and also influence other winding parameters, such as inductance. But for a research project focusing on propagation characteristics of high frequency signals within in a transformer model the core can be considered using a metal cylinder, the negative influence due to the use of the metal cylinder can be neglected. Under this consideration, a core made of a metal cylinder was designed to support the windings. .

Winding design

The windings provided by Alstom had a plain disc winding and an interleaved disc winding. But the four shield rings were all made of alumina foil. This will lead to discharges even when a low voltage was applied to them. Four new shield static rings were used instead of the foil static rings in the model. The new rings made of metal plates; and the metal plates were rounded and wrapped with crepe insulation paper to guarantee that they were PD free under high voltage. The overall dimensions of the windings were unaltered.

Tank design

A plastic tank was used. To simulate the state of a real transformer tank, the top, bottom, inner-wall inside the barrel tank is screened using metal plates. So the parameters of the

transformer model, such as, capacitance of a winding to tank wall, capacitance of the ends of windings to ground are similar those for a real transformer.

Construction Parameters

Number of discs per winding	14
Number of turns per disc	14
Total number of turns per winding	24
Mean length of per turn	1810 mm
Width of spacers	40 mm
Radial depth of disc	85 mm
Physical axial length of per winding	150 mm
Width of the conductor	3.0 mm
Height of the conductor	7 mm
Duct dimension between two adjacent discs	3.0 mm
Thickness between the end disc and static ring	3.0 mm
Thickness of static ring	5.0 mm
Turn insulation	1.0 mm
Inside diameter of winding	475 mm
Outside diameter of winding	650 mm
Distance from winding to the outer wall of tank	100 mm
Distance from winding to the inner core	50 mm
Distance from upper static ring to bottom	50 mm
Distance from lower static to top pressure plate	50 mm
Total mass	730 kg

Appendix B

Construction Data of the UMIST Transformer Model

1. H.V. winding data

Length of means turn	1709 mm
Width of spacers	38 mm
Radial depth of disc	23 mm
Physical length of winding axially	949 mm
Width of the conductor	2.5 mm
Height of the conductor	6.5 mm
The thickness of the terminal disc to ground	6.35 mm
The thickness of two adjacent discs	6.35 mm
Interturn insulation thickness	0.5 mm
Number of discs per winding	72
Number of turns per winding	8
Total turns:	558

Arrangement of turns and discs: $7\frac{11}{12}$ turn per disc for 1^{st}–28^{th} and 45^{th}–72nd;

$7\frac{10}{12}$ turn per disc for 29^{th}–32^{nd} and 41^{st}–44^{th};

$6\frac{6}{12}$ turn per disc for 33^{rd}–40^{th}.

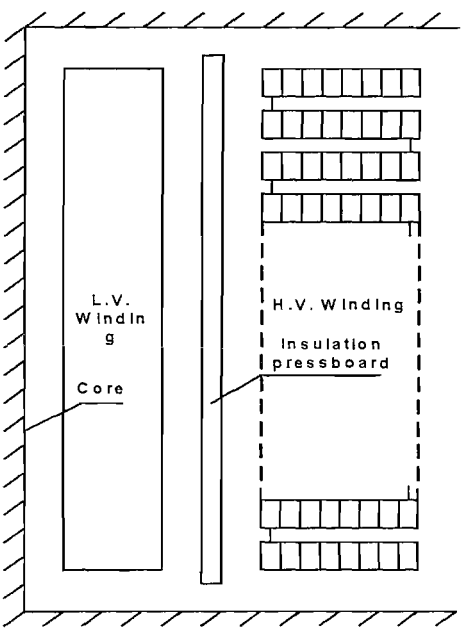

Appendix C

Matlab Code

```
%%%%%%%%%%%%%%%%%%%%%%%%%%%%%%%%%%%%%%%%%%%%%%%%%
%                    Simple Plot in Time Domain                    %
%%%%%%%%%%%%%%%%%%%%%%%%%%%%%%%%%%%%%%%%%%%%%%%%%

% this program can be used to illustrate
% a plot constructed with ascii codes.

clear all; close all;

load filename.txt(dat) -ascii;      % Load data file;
[n,m]=size(filename);               % Calculate sizes of the data file;
x=samplerate*(1:n)/n;               % Scale of x axis;
                                    % samplerate: sample rate of the data file;
figure(1);
plot(x,filename);                   % Plot "filename";
xlabel('Time, ns');
ylabel('Magnitude, V');
title('Pulse');

%%%%%%%%%%%%%%%%%%%%%%%%%%%%%%%%%%%%%%%%%%%%%%%%%


%%%%%%%%%%%%%%%%%%%%%%%%%%%%%%%%%%%%%%%%%%%%%%%%%
%                    Simple Plot in Frequency Domain                    %
%%%%%%%%%%%%%%%%%%%%%%%%%%%%%%%%%%%%%%%%%%%%%%%%%

% this program can be used to illustrate
% a plot constructed with ascii codes.

clear all;
close all;

load filename.txt(dat) -ascii;      % Load data file;
[n,m]=size(filename);               % Calculate sizes of the data file;
x=samplerate*(1:n)/n;               % Scale of x axis;
                                    % samplerate: sample rate of the dat file;
figure(1);
semilogx(x,filename);               % Plot "filename";
xlabel(Frequency, Hz);
ylabel('Magnitude, dB');
title('Spectrum');

%%%%%%%%%%%%%%%%%%%%%%%%%%%%%%%%%%%%%%%%%%%%%%%%%
```

```
%%%%%%%%%%%%%%%%%%%%%%%%%%%%%%%%%%%%%%%%%%%%%%%%%%%%
%                    FFT Plot (Power spectrum)                    %
%%%%%%%%%%%%%%%%%%%%%%%%%%%%%%%%%%%%%%%%%%%%%%%%%%%%
% this program can be used to calculate FFT of a ascii file
% and to plot it in power spectrum.
%%%%%%%%%%%%%%%%%%%%%%%%%%%%%%%%%%%%%%%%%%%%%%%%%%%%

clear all; close all;
load filename.txt(dat) -ascii;      % Load data file;
[n,m]=size(filename);               % Calculte sizes of the data file;
f=samplerate*(1:n/2)/n;             % Scale of x axis;
                                    % samplerate: sample rate of the dat file;
y=fft(filename);                    % FFT Calculation
yy=(y.*conj(y))/n;
figure(1);
plot(f,yy(1:n/2));
title('Power spectrum');
xlabel('Frequency,MHz');
ylabel('Magnitude, uW');

%%%%%%%%%%%%%%%%%%%%%%%%%%%%%%%%%%%%%%%%%%%%%%%%%%%%
```

```
%%%%%%%%%%%%%%%%%%%%%%%%%%%%%%%%%%%%%%%%%%%%%%%%%%%%
%                    FFT Plot (magnitude in dB)                    %
%%%%%%%%%%%%%%%%%%%%%%%%%%%%%%%%%%%%%%%%%%%%%%%%%%%%
% this program can be used to calculate FFT of a ascii file
% and to plot it magnitude in dB.
%%%%%%%%%%%%%%%%%%%%%%%%%%%%%%%%%%%%%%%%%%%%%%%%%%%%

clear all; close all;
load filename.txt(dat) -ascii;      % Load data file;
[n,m]=size(filename);               % Calculte sizes of the data file;
f=samplerate*(1:n/2)/n;             % Scale of x axis;
                                    % samplerate: sample rate of the dat file;
y=fft(filename);                    % FFT Calculation
yy=(y.*conj(y)).^0.5/n;
dByy=yy/yy(max);
figure(1);
plot(f,dByy(1:n/2));
title('spectrum');
xlabel('Frequency,MHz');
ylabel('Magnitude, dB');

%%%%%%%%%%%%%%%%%%%%%%%%%%%%%%%%%%%%%%%%%%%%%%%%%%%%
```

```
%%%%%%%%%%%%%%%%%%%%%%%%%%%%%%%%%%%%%%%%%%%%%%%%
%%%%%%%%%%%%%%%%%%%%%%%%%%%%%%%%%%%%%%%%%%%%%%%%
%        Transfer Function and Bode plots Creater                %
%          for a transformer model system                        %
%        (the circiut cable is not calibrated)                   %
%%%%%%%%%%%%%%%%%%%%%%%%%%%%%%%%%%%%%%%%%%%%%%%%
%%%%%%%%%%%%%%%%%%%%%%%%%%%%%%%%%%%%%%%%%%%%%%%%

%This program can be used to create two bode plots (amplitude and phase)
%You can refer to measured bode plots to edit and adjust follow file to
%produce a simulation transfer function, therefore get bode plots

%    Witten by Baojia Han for his PhD project
%%%%%%%%%%%%%%%%%%%%%%%%%%%%%%%%%%%%%%%%%%%%%%%%
%%%%%%%%%%%%%%%%%%%%%%%%%%%%%%%%%%%%%%%%%%%%%%%%

clear all; close all;
load f:/temp/SIMULATION/EEEEE.txt -ascii;
load f:/temp/SIMULATION/EEEEA.txt -ascii;

K=10^-4.895;
p0=10e3*2*pi;
p1=44.1e3*2*pi;  p2=16.6e4*2*pi;  p3=28.7e4*2*pi;  p4=14.2e5*2*pi;
p5=17.3e5*2*pi;  p6=21.0e5*2*pi;  p7=27.0e5*2*pi;  p8=35.8e5*2*pi;
p9=59.4e5*2*pi;  p10=88.3e5*2*pi; p11=12.3e6*2*pi; p12=16.0e6*2*pi;
p13=17.9e6*2*pi; p14=28.5e6*2*pi; p15=33.8e6*2*pi; p16=39.9e6*2*pi;
p17=50.5e6*2*pi; p18=65.0e6*2*pi; p19=74.7e6*2*pi; p20=87.2e6*2*pi;
p21=12.3e7*2*pi; p22=15.6e7*2*pi;

z0=10.0e3*2*pi;
z1=62.9e3*2*pi;  z2=17.3e4*2*pi;  z3=28.9e4*2*pi;  z4=14.9e5*2*pi;
z5=18.3e5*2*pi;  z6=21.4e5*2*pi;  z7=29.7e5*2*pi;  z8=48.8e5*2*pi;
z9=75.5e5*2*pi;  z10=10.8e6*2*pi; z11=13.9e6*2*pi; z12=17.8e6*2*pi;
z13=26.0e6*2*pi; z14=30.6e6*2*pi; z15=37.1e6*2*pi; z16=45.2e6*2*pi;
z17=61.2e6*2*pi; z18=71.0e6*2*pi; z19=78.3e6*2*pi; z20=95.9e6*2*pi;
z21=13.8e7*2*pi; z22=19.1e7*2*pi;  zz10=97.9e5*2*pi;

qp1=0.08;   qp2=0.09;   qp3=0.075;  qp4=0.090;  qp5=0.17;   qp6=0.055;
qp7=0.23;   qp8=0.093;  qp9=0.225;  qp10=0.05;  qp11=0.105; qp12=0.21;
qp13=0.610; qp14=0.52;  qp15=0.19;  qp16=0.08;  qp17=0.53;  qp18=0.37;
qp19=0.175; qp20=0.14;  qp21=0.27;  qp22=0.16;

qz0=0.28;
qz1=0.075;  qz2=0.085;  qz3=0.067;  qz4=0.063;  qz5=0.22;   qz6=0.064;
qz7=1.12;   qz8=0.40;   qz9=0.37;   qz10=0.09;  qz11=0.080; qz12=0.17;
qz13=0.085; qz14=0.058; qz15=0.036; qz16=0.05;  qz17=0.08;  qz18=0.055;
qz19=0.073; qz20=0.04;  qz21=0.047; qz22=0.29;
qzz10=0.19;
```

```
%%%%%%%%%%%%%%%%%%%%%%%%%%%%%%%%%%%%%%%%%%
N=[];X=[];y=[];x=10^4;

while x<=2*10^8,
  s=i*x*2*pi;

  y=K*(s/z0)^2....
    *((s/z1)^2+qz1*s/z1+1)....
    *((s/z2)^2+qz2*s/z2+1)....
    *((s/z3)^2+qz3*s/z3+1)*(s/z3+1)^1....
    *((s/z4)^2+qz4*s/z4+1)....
    *((s/z5)^2+qz5*s/z5+1)....
    *((s/z6)^2+qz6*s/z6+1)....
    *((s/z7)^2+qz7*s/z7+1)....
    *((s/z8)^2+qz8*s/z8+1)....
    *((s/z9)^2-qz9*s/z9+1)*(s/z9-1)....
    *((s/z10)^2+qz10*s/z10+1)....
    *((s/zz10)^2+qzz10*s/zz10+1)....
    *((s/z11)^2+qz11*s/z11+1)....
    *((s/z12)^2+qz12*s/z12+1)....
    *((s/z13)^2+qz13*s/z13+1)....
    *((s/z14)^2+qz14*s/z14+1)....
    *((s/z15)^2+qz15*s/z15+1)....
    *((s/z16)^2+qz16*s/z16+1)*(s/z16-1)^2....
    *((s/z17)^2+qz17*s/z17+1)*(s/z17-1)^2....
    *((s/z18)^2+qz18*s/z18+1)*(s/z18-1)^2....
    *((s/z19)^2+qz19*s/z19+1)*(s/z19-1)^2....
    *((s/z20)^2+qz20*s/z20+1)*(s/z20-1)^2....
    *((s/z21)^2+qz21*s/z21+1)*(s/z21-1)^2....
    *((s/z22)^2+qz22*s/z22+1)*(s/z22-1)^2....
    *exp(-s/z10*2*pi)*exp(s/z11*2*pi)*exp(-s/z13*2*pi)*exp(s/z14*2*pi)....
    /(((s/p1)^2+qp1*s/p1+1)....
    *((s/p2)^2+qp2*s/p2+1)*(s/p2+1)^1....
    *((s/p3)^2+qp3*s/p3+1)*(s/p3+1)^1....
    *((s/p4)^2+qp4*s/p4+1).....
    *((s/p5)^2+qp5*s/p5+1)....
    *((s/p6)^2+qp6*s/p6+1)....
    *((s/p7)^2+qp7*s/p7+1)....
    *((s/p8)^2+qp8*s/p8+1)....
    *((s/p9)^2+qp9*s/p9+1)....
    *((s/p10)^2+qp10*s/p10+1)....
    *((s/p11)^2+qp11*s/p11+1)*(s/p11+1)^1....
    *((s/p12)^2+qp12*s/p12+1)*(s/p12+1)^1....
    *((s/p13)^2+qp13*s/p13+1)....
    *((s/p14)^2+qp14*s/p14+1)*(s/p14+1)^1....
    *((s/p15)^2+qp15*s/p15+1)*(s/p15+1)^2....
    *((s/p16)^2+qp16*s/p16+1)*(s/p16+1)^2....
    *((s/p17)^2+qp17*s/p17+1)*(s/p17+1)^2....
    *((s/p18)^2+qp18*s/p18+1)*(s/p18+1)^2....
```

```
        *((s/p19)^2+qp19*s/p19+1)*(s/p19+1)^2....
        *((s/p20)^2+qp20*s/p20+1)*(s/p20+1)^2....
        *((s/p21)^2+qp21*s/p21+1)^2*(s/p21+1)^2....
        *((s/p22)^2+qp22*s/p22+1)^2*(s/p22+1)^2....
        );


    X=[X,x];
    N=[N,y];
    x=x*1.01;

end
    Yang=unwrap(angle(N))*180/pi;
    figure(1);
    semilogx(X,Yang,EEEEA(:,1),EEEEA(:,2));
    grid;
    Ymag=20*log10(abs(N));
    figure(2);
    semilogx(X,Ymag,EEEEE(:,1),EEEEE(:,2));
    grid;
%%%%%%%%%%%%%%%%%%%%%%%%%%%%%%%%%%%%%%%%%%%%%%%%%%%%%%%%%%%%%%%%%%%%%%%%%%%%%%%%
%%%%%%%%%%%%%%%%%%%%%%%%%%%%%%%%%%%%%%%%%%%%%%%%%%%%%%%%%%%%%%%%%%%%%%%%%%%%%%%%
%                Calculation Numerator and Denominator                            %
%%%%%%%%%%%%%%%%%%%%%%%%%%%%%%%%%%%%%%%%%%%%%%%%%%%%%%%%%%%%%%%%%%%%%%%%%%%%%%%%
%%%%%%%%%%%%%%%%%%%%%%%%%%%%%%%%%%%%%%%%%%%%%%%%%%%%%%%%%%%%%%%%%%%%%%%%%%%%%%%%

%  G1(s)=(s/z0)^2/((s/p1)^2+qp1*s/p1+1)
numg1=10^4*[1/z0^2 0 0];deng1=10^4*[(1/p1)^2 qp1/p1 1];
%  G2(s)=((s/z1)^2+qz1*s/z1+1)/((s/p2)^2+qp2*s/p2+1)
numg2=10^4*[(1/z1)^2 qz1/z1 1];deng2=10^4*[(1/p2)^2 qp2/p2 1];
%  G3(s)=((s/z2)^2+qz2*s/z2+1)/((s/p3)^2+qp3*s/p3+1)
numg3=10^5*[(1/z2)^2 qz2/z2 1];deng3=10^5*[(1/p3)^2 qp3/p3 1];
%  G4(s)=((s/z3)^2+qz3*s/z3+1)/((s/p4)^2+qp4*s/p4+1)
numg4=10^5*[(1/z3)^2 qz3/z3 1];deng4=10^5*[(1/p4)^2 qp4/p4 1];
%  G5(s)=((s/z4)^2+qz4*s/z4+1)/((s/p5)^2+qp5*s/p5+1)
numg5=10^5*[(1/z4)^2 qz4/z4 1];deng5=10^5*[(1/p5)^2 qp5/p5 1];
%  G6(s)=((s/z5)^2+qz5*s/z5+1)/((s/p6)^2+qp6*s/p6+1)
numg6=10^5*[(1/z5)^2 qz5/z5 1];deng6=10^5*[(1/p6)^2 qp6/p6 1];
%  G7(s)=((s/z6)^2+qz6*s/z6+1)/((s/p7)^2+qp7*s/p7+1)
numg7=10^5*[(1/z6)^2 qz6/z6 1];deng7=10^5*[(1/p7)^2 qp7/p7 1];
%  G8(s)=((s/z7)^2+qz7*s/z7+1)/((s/p8)^2+qp8*s/p8+1)
numg8=10^5*[(1/z7)^2 qz7/z7 1];deng8=10^5*[(1/p8)^2 qp8/p8 1];
%  G9(s)=((s/z8)^2+qz8*s/z8+1)/((s/p9)^2+qp9*s/p9+1)
numg9=10^5*[(1/z8)^2 qz8/z8 1];deng9=10^5*[(1/p9)^2 qp9/p9 1];
%  G10(s)=((s/z9)^2+qz9*s/z9+1)/((s/p10)^2+qp10*s/p10+1)
numg10=10^5*[(1/z9)^2 qz9/z9 1];deng10=10^5*[(1/p10)^2 qp10/p10 1];
%  G11(s)=((s/zz10)^2+qzz10*s/zz10+1)/((s/p11)^2+qp11*s/p11+1)
numg11=10^6*[(1/zz10)^2 qzz10/zz10 1];deng11=10^6*[(1/p11)^2 qp11/p11 1];
%  G12(s)=((s/z10)^2+qz10*s/z10+1)/((s/p12)^2+qp12*s/p12+1)
```

```
numg12=10^6*[(1/z10)^2 qz10/z10 1];deng12=10^6*[(1/p12)^2 qp12/p12 1];
% G13(s)=((s/z11)^2+qz11*s/z11+1)/((s/p13)^2+qp13*s/p13+1)
numg13=10^6*[(1/z11)^2 qz11/z11 1];deng13=10^6*[(1/p13)^2 qp13/p13 1];
% G14(s)=((s/z12)^2+qz12*s/z12+1)/((s/p14)^2+qp14*s/p14+1)
numg14=10^6*[(1/z12)^2 qz12/z12 1];deng14=10^6*[(1/p14)^2 qp14/p14 1];
% G15(s)=((s/z13)^2+qz13*s/z13+1)/((s/p15)^2+qp15*s/p15+1)
numg15=10^6*[(1/z13)^2 qz13/z13 1];deng15=10^6*[(1/p15)^2 qp15/p15 1];
% G16(s)=((s/z14)^2+qz14*s/z14+1)/((s/p16)^2+qp16*s/p16+1)
numg16=10^6*[(1/z14)^2 qz14/z14 1];deng16=10^6*[(1/p16)^2 qp16/p16 1];
% G17(s)=((s/z15)^2+qz15*s/z15+1)/((s/p17)^2+qp17*s/p17+1)
numg17=10^6*[(1/z15)^2 qz15/z15 1];deng17=10^6*[(1/p17)^2 qp17/p17 1];
% G18(s)=((s/z16)^2+qz16*s/z16+1)/((s/p18)^2+qp18*s/p18+1)
numg18=10^6*[(1/z16)^2 qz16/z16 1];deng18=10^6*[(1/p18)^2 qp18/p18 1];
% G19(s)=((s/z17)^2+qz17*s/z17+1)/((s/p19)^2+qp19*s/p19+1)
numg19=10^6*[(1/z17)^2 qz17/z17 1];deng19=10^6*[(1/p19)^2 qp19/p19 1];
% G20(s)=((s/z18)^2+qz18*s/z18+1)/((s/p20)^2+qp20*s/p20+1)
numg20=10^7*[(1/z18)^2 qz18/z18 1];deng20=10^7*[(1/p20)^2 qp20/p20 1];
% G21(s)=((s/z19)^2+qz19*s/z19+1)/((s/p21)^2+qp21*s/p21+1)
numg21=10^7*[(1/z19)^2 qz19/z19 1];deng21=10^7*[(1/p21)^2 qp21/p21 1];
% G22(s)=((s/z20)^2+qz20*s/z20+1)/((s/p22)^2+qp22*s/p22+1)
numg22=10^7*[(1/z20)^2 qz20/z20 1];deng22=10^7*[(1/p22)^2 qp22/p22 1];

% G210(s)=((s/z21)^2+qz21*s/z21+1)/((s/p21)^2+qp21*s/p21+1)
numg210=10^7*[(1/z21)^2 qz21/z21 1];deng210=10^7*[(1/p21)^2 qp21/p21 1];
% G220(s)=((s/z22)^2+qz22*s/z22+1)/((s/p22)^2+qp22*s/p22+1)
numg220=10^7*[(1/z22)^2 qz22/z22 1];deng220=10^7*[(1/p22)^2 qp22/p22 1];

% Gg21(s)=1/(s/p2+1)
numgg21=10^4*[1];dengg21=10^4*[1/p2 1];
% Gg31(s)=(s/z3+1)/(s/p3+1)
numg31=10^5*[1/z3 1];deng31=10^5*[1/p3 1];
% G111(s)=(s/z9-1)/(s/p11+1)
numg111=10^6*[1/9 -1];deng111=10^6*[1/p11 1];
% G121(s)=1/(s/p12+1)
numg121=10^6*[1];deng121=10^6*[1/p12 1];
% G141(s)=1/(s/p14+1)
numg141=10^6*[1];deng141=10^6*[1/p14 1];
% G151(s)=1/(s/p15+1)
numg151=10^6*[1];deng151=10^6*[1/p15 1];
% G152(s)=1/(s/p15+1)
numg152=10^6*[1];deng152=10^6*[1/p15 1];
% G161(s)=(s/z16-1)/(s/p16+1)
numg161=10^7*[1/z16 -1];deng161=10^7*[1/p16 1];
% G162(s)=(s/z16-1)/(s/p16+1)
numg162=10^7*[1/z16 -1];deng162=10^7*[1/p16 1];
% G171(s)=(s/z17-1)/(s/p17+1)
numg171=10^7*[1/z17 -1];deng171=10^7*[1/p17 1];
% G172(s)=(s/z17-1)/(s/p17+1)
numg172=10^7*[1/z17 -1];deng172=10^7*[1/p17 1];
```

```
% G181(s)=(s/z18-1)/(s/p18+1)
numg181=10^7*[1/z18 -1];deng181=10^7*[1/p18 1];
% G182(s)=(s/z18-1)/(s/p18+1)
numg182=10^7*[1/z18 -1];deng182=10^7*[1/p18 1];
% G191(s)=(s/z19-1)/(s/p19+1)
numg191=10^7*[1/z19 -1];deng191=10^7*[1/p19 1];
% G192(s)=(s/z19-1)/(s/p19+1)
numg192=10^7*[1/z19 -1];deng192=10^7*[1/p19 1];
% G201(s)=(s/z20-1)/(s/p20+1)
numg201=10^7*[1/z20 -1];deng201=10^7*[1/p20 1];
% G202(s)=(s/z20-1)/(s/p20+1)
numg202=10^7*[1/z20 -1];deng202=10^7*[1/p20 1];
% G211(s)=(s/z21-1)/(s/p21+1)
numg211=10^7*[1/z21 -1];deng211=10^7*[1/p21 1];
% G212(s)=(s/z21-1)/(s/p21+1)
numg212=10^7*[1/z21 -1];deng212=10^7*[1/p21 1];
% G221(s)=(s/z22-1)/(s/p22+1)
numg221=10^7*[1/z22 -1];deng221=10^7*[1/p22 1];
% G222(s)=(s/z22-1)/(s/p22+1)
numg222=10^7*[1/z22 -1];deng222=10^7*[1/p22 1];

%%%%%%%%%%%%%%%%%%%%%%%%%%%%%%%%%%%%%%%%%%%%
% Transfer function A
%%%%%%%%%%%%%%%%%%%%%%%%%%%%%%%%%%%%%%%%%%%%
numa=conv(conv(numg1,numg2),numgg21);
dena=conv(conv(deng1,deng2),dengg21);
sysa=tf(numa,dena);
% Transfer function B
numb=conv(conv(numg3,numg4),numg31);
denb=conv(conv(deng3,deng4),deng31);
sysb=tf(numb,denb);
% Transfer function C
numc=conv(conv(numg5,numg6),conv(numg7,numg8));
denc=conv(conv(deng5,deng6),conv(deng7,deng8));
sysc=tf(numc,denc);
% Transfer function D
numd=conv(conv(numg9,numg10),conv(numg11,numg111));
dend=conv(conv(deng9,deng10),conv(deng11,deng111));
sysd=tf(numd,dend);
% Transfer function E
nume=conv(conv(numg12,numg121),numg13);
dene=conv(conv(deng12,deng121),deng13);
syse=tf(nume,dene);
% Transfer function F
numf=conv(numg14,numg141);
denf=conv(deng14,deng141);
sysf=tf(numf,denf);
% Transfer function G
numg=conv(conv(numg15,numg151),numg152);
```

```
deng=conv(conv(deng15,deng151),deng152);
sysg=tf(numg,deng);
% Transfer function H
numh=conv(conv(numg16,numg161),numg162);
denh=conv(conv(deng16,deng161),deng162);
sysh=tf(numh,denh);
% Transfer function I
numi=conv(conv(numg17,numg171),numg172);
deni=conv(conv(deng17,deng171),deng172);
sysi=tf(numi,deni);
% Transfer function J
numj=conv(conv(numg18,numg181),numg182);
denj=conv(conv(deng18,deng181),deng182);
sysj=tf(numj,denj);
% Transfer function K
numk=conv(conv(numg19,numg191),numg192);
denk=conv(conv(deng19,deng191),deng192);
sysk=tf(numk,denk);
% Transfer function L
numl=conv(conv(numg20,numg201),numg202);
denl=conv(conv(deng20,deng201),deng202);
sysl=tf(numl,denl);
% Transfer function M
numm=conv(conv(numg21,numg210),conv(numg211,numg212));
denm=conv(conv(deng21,deng210),conv(deng211,deng212));
sysm=tf(numm,denm);
% Transfer function N
numn=conv(conv(numg22,numg220),conv(numg221,numg222));
denn=conv(conv(deng22,deng220),conv(deng221,deng222));
sysn=tf(numn,denn);
%%%%%%%%%%%%%%%%%%%%%%%%%%%%%%%%%%%%%%%%%%%%%%
numaa=conv(conv(numa,numb),conv(numc,numd));
denaa=conv(conv(dena,denb),conv(denc,dend));
%-----------------------------------------
numbb=conv(conv(nume,numf),conv(numg,numh));
denbb=conv(conv(dene,denf),conv(deng,denh));
%-----------------------------------------
numcc=conv(conv(numi,numj),conv(numk,numl));
dencc=conv(conv(deni,denj),conv(denk,denl));
%-----------------------------------------
numdd=conv(numm,numn);
dendd=conv(denm,denn);
%%%%%%%%%%%%%%%%%%%%%%%%%%%%%%%%%%%%%%%%%%%%%%
num=conv(conv(numaa,numbb),conv(numcc,numdd));
den=conv(conv(denaa,denbb),conv(dencc,dendd));
%%%%%%%%%%%%%%%%%%%%%%%%%%%%%%%%%%%%%%%%%%%%%%
T=(-1/z10*2*pi)+(1/z11*2*pi)+(-1/z13*2*pi)+(1/z14*2*pi)
%%%%%%%%%%%%%%%%%%%%%%%%%%%%%%%%%%%%%%%%%%%%%%s
ys=tf(num,den)
```

%%
Simulink Model of Transfer Function Application

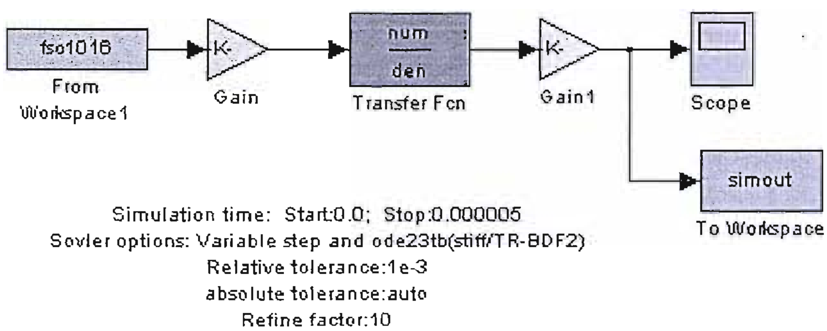


```
%%%%%%%%%%%%%%%%%%%%%%%%%%%%%%%%%%%%%%%%%%%%%%%%
%        Compensator for frequency measurement from Bushing and RFCT          %
%%%%%%%%%%%%%%%%%%%%%%%%%%%%%%%%%%%%%%%%%%%%%%%%

clear all;close all;
load f:\FRCTB020603\ABC.txt -ascii;
load f:\RPDI280503\c38.txt -ascii;
load f:\RPDI280503\c3B.txt -ascii;
[na,ma]=size(ABC);

cc38=[];
cc3B=[];

for q=1:na

    cc38=[cc38;[c38(q,1),c38(q,2)/10^(ABC(q,2)/20)]];
    cc3B=[cc3B;[c3B(q,1),c3B(q,2)/10^(ABC(q,2)/20)]];
 end
figure(1)
plot(c38(:,1),c38(:,2),cc38(:,1),cc38(:,2),c3B(:,1),c3B(:,2),cc3B(:,1),cc3B(:,2));

%%%%%%%%%%%%%%%%%%%%%%%%%%%%%%%%%%%%%%%%%%%%%%%%



%%%%%%%%%%%%%%%%%%%%%%%%%%%%%%%%%%%%%%%%%%%%%%%%
%                    Elliptic filter for time-based signals (Bandpass)              %
%%%%%%%%%%%%%%%%%%%%%%%%%%%%%%%%%%%%%%%%%%%%%%%%
clear all;close all;
load f:\writing\testonsite\ncc.txt -ascii; %in put following prameters
[n,m]=size(ncc);%number of samples
```

```
x1=20*(0:n-1)/n;
[b,a] = ellip(8,0.1,40,[50000000 87000000]*2/500000000);
aa=round(406.65/800*n);bb=round(407.5/800*n);
cc=ncc(aa:bb);
nn=bb-aa+1;
x=(1:nn)/n*20000*0.8;%x=(1:nn)*(nn/n)*20;
figure(2);
plot(x,cc);
xlabel('Time, us');
ylabel('Magnitude, V');
axis([0 17 -0.2 0.2]);

f=500*(0:nn/2)/nn;
y=fft(cc);
yy=(y.*conj(y)).^0.5/nn;
figure(3);
plot(f,yy(1:nn/2+1));
xlabel('Frequency, MHz');
ylabel('Magnitude, V');
axis([0 200 0 0.005]);
%After filtering, we see the signal is a 15 Hz sinusoid, exactly as expected.

sf = filter(b,a,ncc);
clear ncc;
ccc=sf(aa:bb);clear sf;
cccc=filter(b,a,ccc);
figure(5);
plot(x,cccc);
xlabel('Time, us');
ylabel('Magnitude, V');
axis([0 17 -0.1 0.1]);

y=fft(cccc);
yy=(y.*conj(y)).^0.5/nn;
figure(6);
plot(f,yy(1:nn/2+1));
xlabel('Frequency, MHz');
ylabel('Magnitude, V');
axis([0 200 0 0.0005]);

aaa=round(1.7/17*nn);bbb=round(2/17*nn);
nnn=bbb-aaa+1;
ccccc=cccc(aaa:bbb);
xx=(1:nnn)/nn*17;
figure(7);
plot(xx,ccccc);
xlabel('Time, us');
ylabel('Magnitude, mV');
axis([0 0.3 -0.1 0.1]);
```

```
y=fft(ccccc);
yy=(y.*conj(y)).^0.5/nnn;
ff=500*(0:nnn/2)/nnn;
figure(8);
plot(ff,yy(1:nnn/2+1));
xlabel('Frequency, MHz');
ylabel('Magnitude, mV');
axis([0 200 0 0.0005]);
```

```
%%%%%%%%%%%%%%%%%%%%%%%%%%%%%%%%%%%%%%%%%%%%%%%%%%%%%%%%%%%%
%          High Pass Filter to cut off signal of low frequency          %
%                         (time domain)                                 %
%%%%%%%%%%%%%%%%%%%%%%%%%%%%%%%%%%%%%%%%%%%%%%%%%%%%%%%%%%%%
clear;
%in put following prameters
load f:\writing\testonsite\c1713.txt -ascii;
[n,m]=size(c1713);%number of samples
x1=10*(0:n-1)/n;
figure(1);
plot(x1,c1713);
xlabel('Time, ms');ylabel('Magnitude,10mV');
fs=500000000;%sample frequency
fHz0=[0 40000000 40001000 87000000 87010000 fs/2];
mh1=[0 0 1 1 0 0];
%--------------------------------------------------%
f0=fHz0/(fs/2);
[b1,a1]=yulewalk(6,f0,mh1);
ss=filter(b1,a1,c1713);clear c1713;
figure(2);
plot(x1,ss);clear x1;
xlabel('Time, ms');ylabel('Magnitude,10mV');
%%%%%%%%%%%%%%%%%%%%%%%%%%%%%%%%%%%%%%%%%%%%%%%%%%%%%%%%%%%%
```

```
%%%%%%%%%%%%%%%%%%%%%%%%%%%%%%%%%%%%%%%%%%%%%%%%%%%%%%%%%%%%
%                        Wavelet Filter                                 %
%%%%%%%%%%%%%%%%%%%%%%%%%%%%%%%%%%%%%%%%%%%%%%%%%%%%%%%%%%%%
% this program is for filtering time-based waveform using wavelet method
%%%%%%%%%%%%%%%%%%%%%%%%%%%%%%%%%%%%%%%%%%%%%%%%%%%%%%%%%%%%
clear all;close all;
```

```
%load original signal
load f:\needle-plane280503\C3halfcycle.txt -ascii;
[n,m]=size(C3halfcycle);

a=round(209.715/500*n);b=round(209.900/500*n);
ca=C3halfcycle(a:b,:);

[c,l]=wavedec(C3halfcycle,4,'db10');

clear C3halfcycle;

  figure(1);
  cd4=detcoef(c,l,4);
  [xn,xxm]=size(cd4);
  x=10*(1:xn)/xn;
  subplot(4,1,4);plot(x,cd4);xlabel('Times,ms');
  clear cd4;

  cd3=detcoef(c,l,3);
  [xn,xxm]=size(cd3);
  x=10*(1:xn)/xn;
  subplot(4,1,3);plot(x,cd3);
  set(gca,'xtick',[]);
  clear cd3;

  cd2=detcoef(c,l,2);
  [xn,xm]=size(cd2);
  x=10*(1:xn)/xn;
  subplot(4,1,2);plot(x,cd2);ylabel('Magnitude,mV');
  set(gca,'xtick',[]);
  clear cd2;

  cd1=detcoef(c,l,1);
  [xn,xxm]=size(cd1);
  x=10*(1:xn)/xn;
  subplot(4,1,1);plot(x,cd1);title('Wavelet Analysis for PD waveform');
  set(gca,'xtick',[]);
  clear cd1;
  clear c;

 [cc,l]=wavedec(ca,4,'db10');
 clear ca;

 figure(2);

  ccd4=detcoef(cc,l,4);
  [xxn,xxm]=size(ccd4);
  nn=b-a+1;
  xx=(1:xxn)/xxn*nn/n*10*1000;
```

```
subplot(4,1,4);plot(xx,ccd4); xlabel('Times,us');


ccd3=detcoef(cc,l,3);
[xxn,xxm]=size(ccd3);
xx=10*(1:xxn)/xxn;
subplot(4,1,3);plot(xx,ccd3);
set(gca,'xtick',[]);


ccd2=detcoef(cc,l,2);
[xxn,xxm]=size(ccd2);
xx=10*(1:xxn)/xxn;
subplot(4,1,2);plot(xx,ccd2); ylabel('Magnitude,mV');
set(gca,'xtick',[]);


ccd1=detcoef(cc,l,1);
[xxn,xxm]=size(ccd1);
xx=10*(1:xxn)/xxn;
subplot(4,1,1);plot(xx,ccd1);title('Wavelet Analysis for PD waveform');
set(gca,'xtick',[]);

figure(3);
yccd4=fft(ccd4);
yccd4=(yccd4.*conj(yccd4));
[xxn,xxm]=size(ccd4);
yxx=500/16*((1:xxn)/xxn);
subplot(4,1,4);plot(yxx,yccd4);

yccd3=fft(ccd3);
yccd3=(yccd3.*conj(yccd3));
[xxn,xxm]=size(ccd3);
yxx=500/8*((1:xxn)/xxn);
subplot(4,1,3);plot(yxx,yccd3);

yccd2=fft(ccd2);
yccd2=(yccd2.*conj(yccd2));
[xxn,xxm]=size(ccd2);
yxx=500/4*((1:xxn)/xxn);
subplot(4,1,2);plot(yxx,yccd2);

yccd1=fft(ccd1);
yccd1=(yccd1.*conj(yccd1));
[xxn,xxm]=size(ccd1);
yxx=500/2*((1:xxn)/xxn);
subplot(4,1,1);plot(yxx,yccd1);
```

```
%%%%%%%%%%%%%%%%%%%%%%%%%%%%%%%%%%%%%%%%%%%%%%%%%%%%%%%%%
%                          Spectra Figure
%%%%%%%%%%%%%%%%%%%%%%%%%%%%%%%%%%%%%%%%%%%%%%%%%%%%%%%%%
clear all;close all;
load f:/OFRBCW/OIBCW170603/OIBC11.txt -ascii;
load f:/OFRBCW/OIBCW170603/OIBC12.txt -ascii;
load f:/OFRBCW/OIBCW170603/OIBC13.txt -ascii;
load f:/OFRBCW/OIBCW170603/OIBC14.txt -ascii;
load f:/OFRBCW/OIBCW170603/OIBC15.txt -ascii;
load f:/OFRBCW/OIBCW170603/OIBC16.txt -ascii;
load f:/OFRBCW/OIBCW170603/OIBC17.txt -ascii;
load f:/OFRBCW/OIBCW170603/OIBC18.txt -ascii;
OIBC1=OIBC11(1:201,1:2);
OIBC2=OIBC12(1:201,1:2);
OIBC3=OIBC13(1:201,1:2);
OIBC4=OIBC14(1:201,1:2);
OIBC5=OIBC15(1:201,1:2);
OIBC6=OIBC16(1:201,1:2);
OIBC7=OIBC17(1:201,1:2);
OIBC8=OIBC18(1:201,1:2);
semilogx(OIBC1(:,1),OIBC1(:,2),....
      OIBC2(:,1),OIBC2(:,2),....
      OIBC3(:,1),OIBC3(:,2),....
      OIBC4(:,1),OIBC4(:,2),....
      OIBC5(:,1),OIBC5(:,2),....
      OIBC6(:,1),OIBC6(:,2),....
      OIBC7(:,1),OIBC7(:,2),....
      OIBC8(:,1),OIBC8(:,2));

grid;
xlabel('Frequncy, Hz');
ylabel('Magnitude, dB');
title('Frequency Responses of the transformer model  filled oil with the Interleaved
disc winding ');
figure(2);
grid on;
A1(1:201)=1;B1=A1(:);
A2(1:201)=2;B2=A2(:);
A3(1:201)=3;B3=A3(:);
A4(1:201)=4;B4=A4(:);
A5(1:201)=5;B5=A5(:);
A6(1:201)=6;B6=A6(:);
A7(1:201)=7;B7=A7(:);
A8(1:201)=8;B8=A8(:);
plot3(OIBC1(:,1),B1,OIBC1(:,2),OIBC2(:,1),B2,OIBC2(:,2),....
   IBC3(:,1),B3,OIBC3(:,2),OIBC4(:,1),B4,OIBC4(:,2),OIBC5(:,1),B5,OIBC5(:,2),....
   OIBC6(:,1),B6,OIBC6(:,2),OIBC7(:,1),B7,OIBC7(:,2),OIBC8(:,1),B8,OIBC8(:,2));
```

Appendix D

List of Publications

1. B. Han, P. L. Lewin, Y. Tian, P. Jarman and S. G. Swingler: "Propagation Characteristics of Discharges signals of high frequency within Transformer Bushing", ICMEP-ACEID'2003, Chongqing China, 27-30th 10 2003

2. B. Han, P. L. Lewin, Y. Tian, P. Jarman and S. G. Swingler: "Distinguishing the Corona and Surface Discharge within Transformer Bushing", ICMEP-ACEID'2003, Chongqing China, 27-30th 10 2003

3. B. Han, P. L. Lewin, Y. Tian, P. Jarman and S. G. Swingler: "PD On-line Measurement of Oil-filled Power Transformers"; XIIIth International Symposium on High Voltage Engineering (ISH2003) at Delft University of Technology, August 25-29th 2003

4. B. Han, P. L. Lewin, P Jarman: "ON-line Partial Discharges on a Power Transformer Using Bushing tap Measurements", to be published

5, B. Han, P. L. Lewin, P Jarman: "Partial Discharge behaviour with in a Transformer model", to be published

Appendix E

Main test equipment used

- **Agilent 4395A Network/Spectrum/Impedance Analyzer**

As a vector network analyzer, the Agilent 4395A operates from 10Hz to 500MHz with 1 MHz resolution; and its integrated synthesized source provides -50 to + 15dBm of output power with 0.1 dB resolution. The dynamic magnitude and phase accuracy are +/-0.05dB and +/-0.3deg. As a spectrum analyzer, the Agilent 4395A operates from 10 Hz to 500 MHz with resolution bandwidths (RBWs) spanning 1 Hz to 1 MHz in a 1-3-10 steps. A fully-synthesized local oscillator allows stable and accurate frequency analysis. Direct A/D conversion (no LOG amplifier is used) results in +/-0.8 dB level accuracy (50 MHz, -20 dBm). Noise sidebands fall below 100dBc/Hz at 100 kHz offset from carriers, while sensitivity is -145dBm/1Hz at 10 MHz.

- **LC684DXL, Digital Oscilloscope**

The oscilloscope has a 1.5 GHz bandwidth for high accuracy and signal fidelity. Its sample rate is 8 GS/s, 10 ppm time base accuracy, and its 5 ps interpolator resolution delivers the signal detail and stability needed to identify and characterize critical signal transitions and delays. The long memory is 16 million data points at 8 GS/s. Its analog persistence function can visually explore the full depth of signal information and get the complete picture of waveform activity.

HP 8082A Pulse Generator

The HP 8082A is a fast pulse generator with all pulse parameters variable. With repetition rates up to 250 MHz, transition times down to 1 nsec, and amplitudes to 5V, the HP 8082A is ideally suited for TTL and ECL logic designs. HP 8082A is easy to use because of its logical front panel layout, and switch selectable ECL output levels. Another feature that contributes to easy operation is the square wave mode. One can, for example, carry out toggle rate tests in this mode up to 250 MHz without having to worry about pulse duty cycle.